The effect of oxidative stress and hypoxic conditioning on mesenchymal stem cell differentiation

By

Danielle de Villiers

Submitted in partial fulfillment of the requirements for the degree

Master of Science (Medical Immunology)

In the faculty of Health Sciences
Department of Immunology
University of Pretoria
South Africa

Supervisor:

Prof. M S Pepper
Department of Immunology, ICMM, University of Pretoria, South Africa

Co-supervisor:

Dr. M Potgieter
Department of Immunology, ICMM, University of Pretoria, South Africa

2015

Statement of original authorship

I declare that this dissertation, which I hereby submit in fulfillment of part of the requirements for the degree Master of Science (Medical Immunology) at the University of Pretoria, is my own work that has not been previously submitted for a degree at this or any other University.

Danielle de Villiers

Abstract

Introduction

South Africa is ranked the third most obese country after the United States of America and Great Britain. According to a study conducted by the South African Medical Research Council, 61% of the South African population is overweight, obese, or severely obese. Research into obesity and its contributing factors has increased as the problem continues to increase on a global scale. Adipose-derived stromal/stem cells (ASCs), formerly known as mesenchymal stem cells (MSCs), are obtained from adipose tissue and have self-renewal properties and multipotential capabilities. A subpopulation of these cells with stem cell characteristics has the potential to differentiate down the adipogenic lineage. This provides a human primary cell model to study the mechanisms of adipogenesis including hyperplasia (cell number proliferation and/or differentiation) and hypertrophy (cell size increase due to lipid droplet accumulation). The stromal/stem cells are said to reside in hypoxic niches where the physiological O_2 tension is lower than ambient O_2 tension (21% O_2) and thus oxidative stress may be reduced. Obesity is correlated with increased oxidative stress and chronic inflammation. Inflammation is associated with the generation of ROS and the accumulation of ROS leads to oxidative stress. ROS is also important in signal transduction pathways. Adipogenesis is triggered by signaling molecules leading to the conversion of a subpopulation of ASCs to preadipocytes, which further differentiate into mature adipocytes. Differentiation down specific lineages coincides with the migration of these stromal/stem cells out of the hypoxic niche. This motivated the assessment of the effect of oxidative stress and a hypoxic mimetic, Dimethyloxalylglycine (DMOG) on adipogenesis *in vitro*.

Methods

ASCs were induced to differentiate into adipocytes using adipogenic-inducing medium. The use of the pro-oxidant, H_2O_2, and the antioxidants, Trolox and CoQ10 allowed for the modulation of ROS in the ASC cultures. Hypoxia was mimicked by the addition of DMOG to ASCs that were induced to differentiate into adipocytes. The adipogenic differentiation was quantitatively detected using flow cytometry and the emission profiles of Nile Red.

Results

It was demonstrated that ROS added exogenously to adipogenic-induced ASCs enhanced adipogenesis. It was also observed that H_2O_2 added to non-induced ASCs caused lipid accumulation. Trolox and CoQ10 attenuated the increase in ROS and thus a decrease in adipogenesis was seen. Removal of pyruvate, a ROS scavenger, was necessary to see these

effects. The addition of DMOG resulted in a trend towards the reduction in adipogenesis over the 14 and 21-day induction periods.

Conclusion

ASCs provide a primary cell model for investigating adipogenesis and the effects of oxidative stress and hypoxia on this process. This is relevant for many diseases and therapeutic options. The study also showed that flow cytometry is a powerful technique that can aid in the quantitative detection of adipogenesis and the cell sub-populations that make up this process. This research underscores the importance of assessing the effects of both oxidative stress and hypoxia on adipogenesis at a gene and protein level in the future.

Key words

Adipose derived-stromal cells (ASCs); Reactive oxygen species (ROS); Hydrogen peroxide (H_2O_2); Coenzyme Q10 (CoQ10); Trolox; Artificial hypoxia; Dimethyloxalylglycine (DMOG); Adipogenic differentiation; Flow cytometry; Nile red

Research outputs

Conferences Oral Presentations

de Villiers D, Durandt C, Potgieter M, Pepper MS. The effect of oxidative stress on adipogenic differentiation in adipose-derived stromal cells. Pathology Research and Development (PathReD) Congress, Johannesburg, South Africa, 2015.

de Villiers D, Potgieter M, Durandt C, Pepper MS. The effect of induced oxidative stress and antioxidant supplementation on the adipogenic differentiation potential of adipose-derived mesenchymal stem cells. International Conference on Tissue Engineering and Regenerative Medicine *(*ICTERM*)*, Pretoria, South Africa, 2014.

Posters

de Villiers D, Potgieter M, Durandt C, Pepper MS. The effect of coenzyme Q10 on adipogenic differentiation in adipose-derived stromal cells. Faculty Day, Faculty of Health Sciences, University of Pretoria, Pretoria, South Africa, 2015.

de Villiers D, Potgieter M, Durandt C, Pepper MS. The effect of artificial hypoxia on adipogenic differentiation in adipose-derived stromal cells. Faculty Day, Faculty of Health Sciences, University of Pretoria, Pretoria, South Africa, 2015.

de Villiers D , Durandt C, Potgieter M, Pepper MS. The effect of induced oxidative stress and antioxidant supplementation on the adipogenic differentiation potential of adipose-derived mesenchymal stromal cells. Pathology Research and Development (PathReD) Congress, Johannesburg, South Africa, 2015.

de Villiers D, Potgieter M, Durandt C, Pepper MS. The effect of oxidative stress and antioxidants on the adipogenic differentiation potential of adipose-derived mesenchymal stem cells. Faculty Day, Faculty of Health Sciences, University of Pretoria, Pretoria, South Africa, 2014.

de Villiers D, Potgieter M, Durandt C, Pepper MS. The effect of oxidative stress on adipose-derived mesenchymal stem cells. Faculty Day, Faculty of Health Sciences, University of Pretoria, Pretoria, South Africa, 2013.

de Villiers D, Potgieter M, Durandt C, Pepper MS. The effect of oxidative stress on adipose-derived mesenchymal stem cells. NRF Research Day, Johannesburg, South Africa, 2013.

Potgieter M, Durandt C, de Villiers D, Pepper MS. The effect of light activation on mesenchymal stem cell phenotype. Faculty Day, Faculty of Health Sciences, University of Pretoria, South Africa, 2012.

Acknowledgements

A special thank you goes to my supervisor, Prof Michael S Pepper. Thank you so much for this opportunity and everything you have done for me. Your wisdom, boundless knowledge, advice, concern and unwavering support helped me to complete this degree. It is a great privilege to have been mentored by someone that is held in such high esteem in the field of stem cell research.

Thank you to Dr Marnie Potgieter, my co-supervisor, for introducing me to the world of mesenchymal stem cells! Your unwavering assistance and support, even into the early hours of the morning, will always be appreciated. Thank you for not only being my co-supervisor but for also becoming a friend.

Thank you to the following organizations for the funding which enabled me to complete this MSc: the National Research Foundation (NRF) and the Department of Science and Technology (DST) for the DST-NRF internship, the Faculty of Health Sciences of the University of Pretoria for the research assistant post, the Institute for Cellular and Molecular Medicine (ICMM) and the Medical Research Council (MRC) University Flagship Programme.

Thank you to Prof Riana Cockeran, head of the Department of Immunology for granting me the opportunity to conduct and complete my MSc in the department.

Thank you to Dr Marnie Potgieter, Mrs Fiona Anastasia van Vollenstee and Ms Karlien Kallmeyer for the previously isolated samples and for showing me how to carry out this useful technique.

Thank you to Dr Chrisna Durandt for showing me the art of flow cytometry. Thank you for your assistance with Nile red and the flow cytometer. Teaching me how to use the Kaluza® Analysis Software is an invaluable asset to my research career.

Thank you to my fellow researchers in the Pepper group in the Department of Immunology of the University of Pretoria for their empathy, assistance, laughter and friendship. Each person has enriched my life. I want to thank in particular: Mrs Candice Murdoch (#Captain), thank you for managing a stellar lab! Ms Carla Dessels (#Relentless), thank you for your

advice, support, and humour. Ms Elize Wolmerans (#RealLifeDisneyPrincess), thank you for your kindness, your encouraging hugs, advice and singing that got us through tough days. Dr Cheryl Stewart (#Yoda), thank you for your nuggets of wisdom.

A very special thank you goes to my amazing parents; for your combination of genetics that gave me a modicum of intelligence and the opportunity to complete anything I set my mind to. Thank you to my Dad for always challenging me and pushing me to be better at everything in life. Thank you to my Mom for her constant enthusiasm and encouragement.

Graphical representation

All graphical figures represented within this dissertation were designed by Danielle de Villiers using Microsoft® PowerPoint® for Mac 2011, version 14.4.3 (140616).

Table of Contents

List of figures

List of tables

List of abbreviations and symbols

ABCG2	ATP-binding cassette sub-family G member 2
AdMSCs	Adipose-derived mesenchymal stem cells
ADP	Adenosine diphosphate
AIDS	Acquired immunodeficiency syndrome
ALCAM	Activated leukocyte cell adhesion molecule; CD166
aP2	Adipocyte fatty acid binding protein
APCs	Antigen-presenting cells
APN	Aminopeptidase; CD13
ARNT	Aryl hydrocarbon receptor nuclear translocator
ASC	Adipose tissue-derived stromal cell
ATP	Adenosine triphosphate
bFGF	Basic fibroblast growth factor
bHLH	Basic helix–loop–helix
BMDACs	Bone-marrow-derived angiogenic cells
BMPs	Bone matrix proteins
BP	Band pass
c-MYC	Cellular-myelocytomatosis
C/EBP	CCAAT/enhancer-binding protein
$CaCl_2$	Calcium chloride
CALLA	Common acute lymphocytic leukemia antigen; CD10
cAMP	Cyclic adenosine monophosphate
CAT	Catalase
CBP	p300/cyclic AMP response element-binding protein
CCK-8	Counting Kit-8
CD	Cluster of differentiation
CFU-F	Colony forming units-fibroblastic
cm^2	Centimetre squared
CO_2	Carbon dioxide
$CoCl_2$	Cobalt chloride
CODD	C-terminal oxygen-dependent degradation domain
CoQ/10	Coenzyme Q/10; Ubiquinone
$CoQH_2$	Ubiquinol
CREB	cAMP response element-binding protein
CRP	C-reactive protein
CTAD	C-terminal activation domain
CTLs	Cytotoxic T-cells
CuZnSOD	Copper-zinc superoxide dismutase
CXCR4	Cysteine-X-cysteine receptor 4

DAMPs	Damage-associated molecular patterns; alarmins
DAPI	4',6-diamidino-2-phenylindole
ddH_2O	Double distilled water
DFO	Desferrioxamine
dH_2O	Distilled water
DMEM	Dulbecco's modified Eagle's medium
DMOG	Dimethyloxalylglycine
DMSO	Dimethyl sulfoxide
DNA	Deoxyribonucleic acid
DPI	Diphenyleneiodonium
EDTA	Ethylenediaminetetraacetic acid
EPAS	Endothelial PAS domain-containing protein 1
ERK-1/2	Extracellular signal-regulated kinase
ESC	Embryonic stem cell
EtOH	Ethanol
FABP4	Fatty acid binding protein 4
FBS	Fetal bovine serum
Fe^{2+}	Ferrous iron
FIH-1	Factor Inhibiting HIF-1
FITC	Fluorescein isothiocyanate
FMN	Flavin mononucleotide
FS	Forward-scatter
g	Gravity /gravitational force
GFP	Green fluorescent protein
GMP	Good Manufacturing Practice
GPIIIb	Glycoprotein IIb; CD36
GPx	Glutathione peroxidase
GVHD	Graft-versus-host disease
h	Human
H^+	Proton
H_2O	Water
H_2O_2	Hydrogen peroxide
HIF	Hypoxia-inducible factor
HIV	Human immunodeficiency virus
HLA	Human leukocyte antigen
HREs	Hypoxia-response elements
ICAM-1	Intercellular adhesion molecule 1; CD54
IDO	Indoleamine 2,3-dioxygenase
IFATS	International Federation for Adipose Therapeutics and Science
IFN	Interferon
IL-1R	Interleukin-1 receptor

IL-1RA	IL-1R antagonist
IPC	Insulin-producing cells
iPS	Induced pluripotent stem
IRAK1	IL-1R-associated kinase
IRAK4	IL-4R-associated kinase
IRF3	Interferon regulatory factor 3
ISCT	International Society for Cytotherapy
ITGA4	Integrin alpha-4; CD49d
ITGA6	Integrin alpha-6; CD49f
ITGB1	Integrin beta 1; CD29
IκK	Inhibitor of NF-κβ-kinase complex
JNK	c-Jun N-terminal kinase
KLF4	Kruppel-like factor 4
KO	Krome orange
L-VAP-2	Lymphocyte-vascular adhesion protein-2; CD73
lin	Linear
LMD	List mode data
log	Logarithmic
LP	Long pass
LPS	Lipopolysaccharide
M	Molar
m	Murine
MAP	Mitogen-activated protein
MAPK	Mitogen-activated protein kinases
MCAM	Melanoma cell adhesion molecule; CD146
MCP-1	Monocyte chemoattractant protein-1
MEFs	Murine embryonic fibroblasts
$MgCl_2$	Magnesium chloride
MHC	Major histocompatibility complex
ml	Milliliter
mM	Milimolar
mm Hg	Millimeter of mercury
MnSOD	Manganese superoxide dismutase
MnTBAP	Manganese(III)tetrakis(4-benzoic acid)porphyrin chloride
mtDNA	Mitochondrial DNA
MyD88	Myeloid differentiation primary response gene 88
n	Population number
N	Asparaginyl
NAC	N-acetyl-L-cysteine
NaCl	Sodium chloride
NADH	Nicotinamide adenine dinucleotide

NADPH	Nicotinamide adenine dinucleotide phosphate
NAT	Nucleic acid amplification test
NF-κβ	Nuclear factor-κβ
NK	Natural killer cells
nm	Nanometer
NO	Nitric oxide
NODD	N-terminal oxygen dependent degradation domain
NOS	Nitric oxide synthase
Nox	NADPH oxidase
NT-ESC	Nuclear transfer embryonic stem cell
O_2	Oxygen
O_2^-	Superoxide
OCT4	Octamer-binding transcription factor 4
OD	Optical density
P	Prolyl
P#	Passage number
P#F#	Passage number and thawing number
PAMPs	Pathogen-associated molecular patterns
PAT	Perilipin–adipophilin-TIP47
PBS	Phosphate buffered saline
PC5	Phycoerythrin-cyanine 5.1
PC7	Phycoerythrin-cyanine 7
PCR	Polymerase chain reaction
PE	Phycoerythrin
Pen/Strep	Penicillin-Streptomycin
PER	Period clock protein
Pgc1α	Coactivator 1 alpha
PGE2	Prostaglandin E2
pH	Potential of hydrogen
PHD	Prolyl hydroxylase domain-containing protein
PI	Propidium iodide
PLA	Processed lipoaspirate
PlGF	Placental growth factor
pO_2	Partial pressure of oxygen
PPARγ	Peroxisome proliferator-activated receptor-γ
Pref-1	Preadipocyte factor-1
Pro	Proline
PROM1	Prominin-1
PRRs	Pattern-recognition receptors
pVHL	von Hippel–Lindau protein
qPCR	Real-time PCR

RNA	Ribonucleic acid
RNS	Reactive nitrogen species
ROS	Reactive oxygen species
SAECs	Small airway epithelial cells
SANBS	South African National Blood Services
SD	Standard deviation
SDF-1	Stromal-derived factor-1; CXCL12
SEM	Standard error of the mean
SIM	Single-minded protein
SOD	Superoxide dismutase
SOX2	Sex determining region Y-box
Spi-1	Spleen focus-forming virus proviral integration 1
SRY	Sex determining region Y
SS	Side-scatter
SVF	Stromal vascular fraction
T-cells	T-lymphocytes
TAB1	TGF-β-activated kinase-binding protein 1
TAB2	TGF-β-activated kinase-binding protein 2
TAK1	TGF-β-activated kinase
tBHP	tert-Butyl hydroperoxide
TGF	Transforming growth factor
TGF-β	Transforming growth factor-β
Thy-1	Thymocyte antigen 1; CD90
TIP47	Tail-Interacting Protein of 47
TIR	Toll/interleukin-1 receptor homologous region
TIRAP	TIR-domain containing adaptor protein
TLRs	Toll-like receptors
TNFR	Tumor necrosis factor receptor
TRAF6	TNFR-associated factor 6
TRAM	TRIF-related adaptor molecule
TRIF	TIR-domain-containing adaptor protein inducing IFN-β
Tris	Tris(hydroxymethyl)aminomethane
TSG-6	TNF stimulated gene 6 protein
Ub	Ubiquitination
UCP1	Uncoupling protein-1
UCP2	Uncoupling protein-2
VCAM-1	Vascular cell adhesion molecule 1; CD106
VEGF	Vascular endothelial growth factor
WAT	White adipose tissue
Wnt	Wingless-type mouse mammary tumor virus integration site
α	Alpha

α-MEM	Minimum Essential Medium-alpha
β	Beta
γ	Gamma
δ	Delta
κ	Kappa
μ	Micro
μm	Micrometer
μM	Micromolar
%	Percentage
•OH	Hydroxyl radical
°C	Degrees Celsius
3D	Three-dimensional

Be curious.

- Stephen Hawkings

Chapter 1

Literature review

An introduction to stem cells

Stem cells have gained attention because of the potential benefits to human health. These cells can become different cell types and this is exciting because developmental processes, disease models, and drug discovery can be studied. There are also great expectations posed by the prospects of using these cells for therapeutic purposes. The reason stem cells have become so popular is their potential in the regeneration of tissues. The idea that stem cells could be manipulated to specialize (differentiate) into other cell types that are needed and are immunologically matched to a patient is a great source of hope for treating a wide range of diseases. The term "stem cell" elicits debate of an ethical nature. There has even been fraudulent research published due to the popular and competitive nature of this field (1-3). The South Korean and more recent Japanese debacle renewed the public's ethical concerns about stem cell research. However, most of this stem cell sensationalism surrounds embryonic stem cell (ESC) research. Stem cells have been identified from a myriad of regions within the body and are not just produced from preimplantation-stage embryos (the commonly associated ESCs).

Stem cells are difficult to describe morphologically and phenotypically. However, a few stem cell definitions have emerged. Stem cells are defined by an ability to extensively self-renew, and the capacity to undergo multi-lineage differentiation and generate terminally differentiated cells (4, 5). A third definition of stem cells is their capability of repopulating a tissue *in vivo* (6). The ability to self-renew and expand cell numbers is a process known as symmetrical cell division. Another division process, asymmetric cell division, generates one daughter cell and another daughter cell that undergoes differentiation. As the basic definition of a stem cell suggests, stem cells can undergo both types of cell division (7). Differences are found between stem cells, which can be ascribed to their tissue of origin, their bias in differentiation potential, and their gene expression patterns. Despite the existence of said differences there must be an overlap in the properties of different stem cells, which has led to the concept of "stemness". Stemness, now a key term in stem cell biology, describes the

ability of the stem cells to self-renew but still retain the capability to differentiate. A number of studies attempting to identify common stem cell markers and define stemness more stringently were unsuccessful, resulting in the finding of only the expression of one common gene, integrin alpha-6 (ITGA6 or CD49f) (8-10).

There are two main categories of stem cells, pluripotent stem cells and adult or somatic stem cells. A zygote can also be considered a type of stem cell, totipotent in nature, which has the ability to create all the cells of the human body and the extraembryonic tissues. Pluripotency pertains to the ability to produce any somatic cell lineage of the body. Pluripotent stem cells include ESCs, induced pluripotent stem (iPS) cells, and nuclear transfer (NT)-ESCs. Embryonic stem cells are cultured from a group of cells termed the epiblast contained within the inner cell mass of the blastocyst of a preimplantation-stage embryo (11). The epiblast gives rise to the three germ layers. Embryonic stem cells are capable of differentiating into the cells of the three germ layers, the ectoderm, mesoderm, and endoderm. Induced pluripotent stem cells are differentiated somatic cells that have been genetically reprogrammed to an embryonic-like state. The 2012 Nobel Laureate, Shinya Yamanaka, illustrated the successful derivation of iPS cells from embryonic and adult mouse fibroblasts through the ectopic co-expression of four genes, which produce the transcription factors octamer-binding transcription factor 4 (OCT4), SRY (sex determining region Y)-box (SOX2), Kruppel-like factor 4 (KLF4) and cellular-myelocytomatosis (c-MYC) (12).

Induced pluripotent stem cells are similar to ESCs in morphology and their ability to form teratomas, which are tumours that can contain cells of all three germ layers (12). Yet, iPS cells cannot be considered the same as embryonic stem cells as there are numerous epigenetic differences. An example of the epigenetic differences was demonstrated by Bar-Nur and colleagues (13). The researchers reprogrammed human pancreatic islet beta cells. These cells acquired pluripotency markers and differentiated into the three germ layers but interestingly maintained an open chromatin structure at important beta-cell genes. It is thought that somatic DNA that is reprogramed to an embryonic-like state maintains a unique DNA methylation signature characteristic of the somatic tissue of origin. This favours the differentiation of a cell along the lineages related to the donor cell (14). Forced expression of the gene, *Nanog*, resulted in iPS cells with similar DNA methylation patterns to ESCs (15). Conditions that contribute to the formation of stem cells more primal in nature, that have the

plasticity to differentiate into any somatic cell lineage, constitute one of the main goals in stem cell research.

Nuclear transfer (NT)-ESCs are an area of recent endeavor (16). Infamously associated with the fabricated results of Woo Suk Hwang in the years 2004 and 2005, this research involves transferring a somatic cell nucleus into an enucleated oocyte. What follows is the reprograming of the somatic DNA to an embryonic-like state and the oocyte divides until the blastocyst stage is reached. The cells from the inner cell mass are isolated and cultured resulting in the generation of NT-ESCs. The afore-mentioned stem cells are all pluripotent in nature but there are a few pitfalls. They produce teratomas, which is a defining characteristic of ESCs but is detrimental in terms of their transplantation potential (17). These stem cells are technically difficult to isolate or generate and culture. Embryonic stem cells and NT-ESCs are shrouded in ethical controversy due to the belief by some that this constitutes the destruction of potential life, which is overcome with the use of iPS cells. These concerns do not apply to adult stem cells, thus, encouraging research in this area (18, 19).

Adult stem cells are present in multiple tissues and are generally considered as either multipotent stem cells or unipotent stem cells. Unipotent stem cells are in all probability better known as progenitor cells, however this is not well defined. Numerous adult stem cells have been identified, such as neural stem cells (NSCs) of ectodermal origin (20-22), pancreatic islet stem cells of endodermal origin (23) as well as hematopoietic stem cells (HSCs) (24, 25) and mesenchymal stem cells (MSCs), both of mesodermal origin (26). These stem cells are all classified as multipotent stem cells and are considered to be more limited in their differentiation potential than pluripotent stem cells. Multipotent stem cells are classified as antecedents of specialized cells in particular tissues and are supposedly limited to generating cells of the specific germ layer of their origin. Adult stem cells such as spermatogonial, corneal and endothelial stem cells have been identified as unipotent stem cells because they only differentiate along one cell lineage to produce one cell type (27). A schematic depicting the above-mentioned ESCs, iPS cells, NT-ESCs and adult stem cells is presented in Figure 1.1. Adult stem cells, particularly MSCs, have come to center stage in light of the fact that they can undergo a rather unorthodox differentiation or transdifferentiation into cells that are not of the same lineage. This discovered plasticity has generated much excitement over possible uses in treating multiple pathological conditions

such as Parkinson's disease and cardiovascular disease, for rejuvenation of tissues that the body cannot repair naturally such as in age-related osteoporosis, and even possibly for use in anti-aging (28-30).

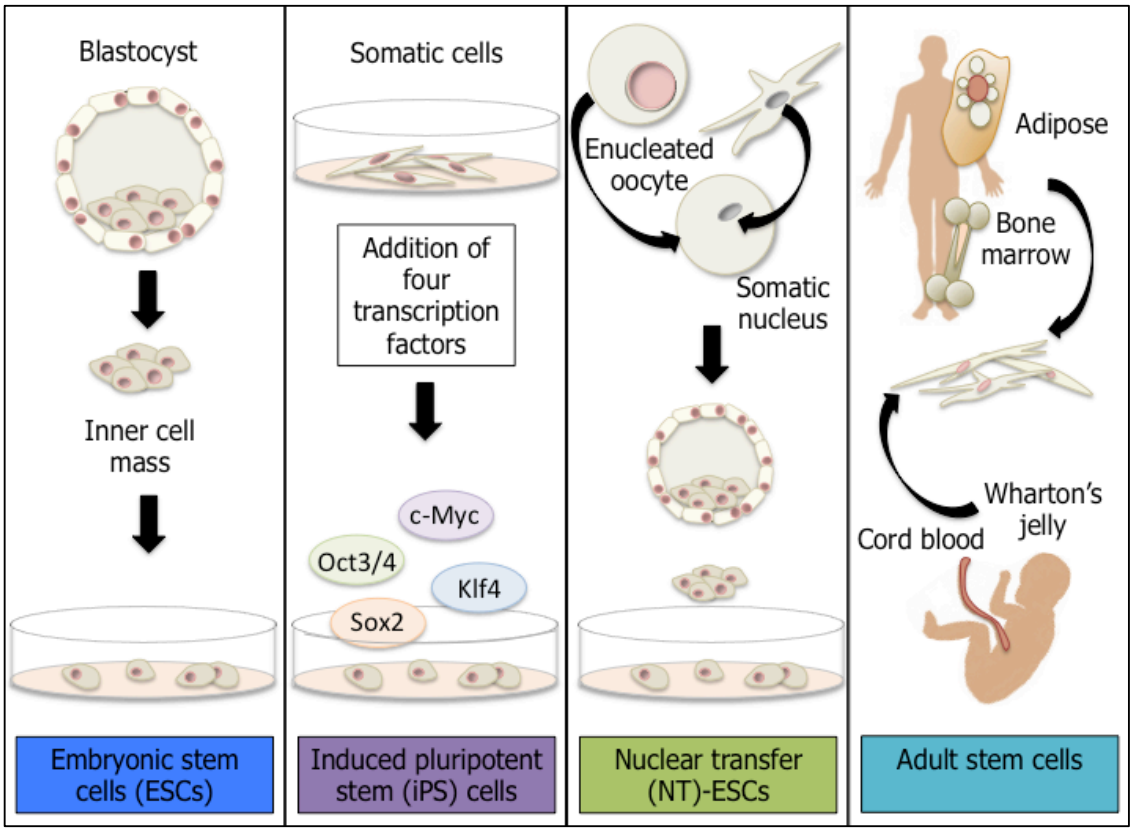

Figure 1.1. Pluripotent and adult stem cells. Schematic diagram depicting human embryonic stem cells (ESCs), induced pluripotent stem (iPS) cells, nuclear transfer (NT)-ESCs, and adult stem cells.

Defining stromal cells; their procurement and characterization

Mesenchymal stromal cells (31) are a population of heterogeneous multipotential cells. Caplan coined the term "mesenchymal stem cell". The choice between the terms "mesenchymal stem cell" and "mesenchymal stromal cell" is an important one. Use of the term "stromal cell" instead of "stem cell" is more appropriate. It is now consensus that only a minor proportion of the heterogeneous population constitutes true stem cells. The International Society for Cytotherapy (ISCT) suggested the following name: multipotent mesenchymal stromal cells (31, 32). Literature originally stated that these adult stromal cells were commonly found in several adult and neonatal tissues. These sources included bone

marrow, Wharton's jelly of the umbilical cord as well as the umbilical cord blood and adipose tissue. Adherent cells isolated from adipose tissue are an important source of MSCs (33). The adult stromal cells isolated from adipose tissue were originally termed processed lipoaspirate (PLA) cells and are still widely known as adipose-derived MSCs (AdMSCs) (34). In February of 2013 a joint statement of the ISCT and the International Federation for Adipose Therapeutics and Science (IFATS) was released. It was proposed that adherent cell populations isolated from adipose tissue should from now on be termed adipose-derived stromal cells (ASCs) and not considered AdMSCs or PLA cells (35). The ISCT defines MSCs as being isolated from bone marrow.

A large proportion of adult stromal cell research has concentrated on bone marrow-derived MSCs. However, it was found that there was a strong resemblance between cultured stromal cells isolated from bone marrow and those isolated from adipose tissue. This is in terms of their differentiation capacity, growth kinetics, gene expression profiles, and surface markers (36). Human MSCs derived from bone marrow and human ASCs derived from adipose tissue thus far appear to be safe to use in patients and circumvent the ethical issues associated with ESCs. De Ugarte and colleagues as well as Kern and colleagues mentioned that cell yields are not significantly different when comparing the two different adult stem cells (36, 37). Fraser and colleagues, however, suggested that adipose tissue yields a larger number of stem cells, around 500-fold more, than bone marrow (38). Adipose-derived stromal cells have shown similar morphology (37) and immunosuppressive capabilities to those of MSCs (39) and both MSCs and ASCs display common expression profiles for many cell-surface markers with some exceptions (40). However, both bone marrow aspiration and adipose tissue liposuction are invasive and painful procedures.

Adipose tissue specifically, is becoming plentiful due the increased incidence of obesity, and liposuction procedures being the most popular cosmetic surgical procedure in the United States according to The American Society for Aesthetic Plastic Surgery (2014). This is apparently the trend that exists in South Africa as well; however, no official statistics have been released. Adipose tissue is derived from the mesenchyme and is composed mainly of mature adipocytes that contain lipid droplets and a supportive stroma. This stromal vascular fraction (SVF) contains an abundant heterogenous cell population. This heterogenous population consists of, amongst others, a minor proliferative, multipotential stem cell population (33, 41, 42). Similarly to ASCs, MSCs are isolated from the stroma within the

mononucleated fraction of the bone marrow, which is also derived from the mesenchyme. A number of scientists have reported that the existence of ASCs within adipose tissue is supported by the rare genetic disorder known as progressive osseous heteroplasia. This disorder presents with heterotopic bone and cartilage formation, found within lesions, in subcutaneous adipose and dermis layers of the skin (43). Spalding and colleagues showed that there was a high fat cell turnover in adults, which would require the presence of adipocyte precursor cells such a ASCs (44). This provides evidence that adipose tissue contains cells that have the potential to differentiate into multiple cell types, a main characterizing factor of multipotential stem cells.

There are many ways of harvesting adipose tissue, from using different cannulas to using dry (45), wet, or ultrasound-assisted techniques. Excising abdominoplasty tissue is another option (46). The size of the adipose tissue fragments obtained depends on the diameter of the cannula. Tumescent liposuction, a wet-assisted technique, involves infusing the subcutaneous tissues with a saline solution containing anaesthetic and/or epinephrine and removing both the liquid and adipose tissue under suction. Conventional high-pressure liposuction, which is suction-assisted, causes most of the adipocytes to rupture upon removal (47). A gentler lipoaspiration method known as the Coleman technique, is a popular method used for the isolation of ASCs. Sydney Coleman developed the technique for obtaining fat grafts. Pu and colleagues compared the two methods of isolation and found that the Coleman method yielded a greater number of viable adipocytes (48). Although they were not looking at ASC viability, it is likely that if the adipocytes were viable, the ASCs would also remain viable. Ultrasound-assisted liposuction is the least favourable adipose tissue harvesting procedure, as the number of ASCs recovered is reduced (49). The standard protocol for ASC isolation involves collagenase digestion of isolated white adipose tissue (WAT). The common deposits of WAT are located around the abdomen, buttocks, and thighs. The most popular harvest site being the abdomen (50). Collagenase digestion of the lipoaspirate of WAT and centrifugation separates the mature adipocytes from the pelleted SVF. This isolation process involving digestion and centrifugation of the adipose tissue incorporates a method pioneered by Rodbell (51). However, this method was specialized for the isolation of ASCs by Zuk and colleagues in 2001 (33).

The harvesting method, ASC isolation method, as well as the location of the adipose tissue could have an effect on the composition and heterogeneity of the ASC population. There is

insufficient data describing the outcome of the adipose tissue location and isolation procedures on the ASC properties, as there is no single characteristic that can be used to describe an ASC, or MSC for that matter. The initial steps of the standard procedure for characterizing MSCs and their adipose-derived counterparts are by their tendency to adhere to plastic upon seeding in culture and their fibroblast-like morphology (31, 35, 52). Another feature used to determine whether the obtained cells are ASCs, or similarly MSCs, is their ability to form colonies upon low-density seeding of the cells. The MSC colonies as described by Owen and Friedenstein are derived from a single colony-forming unit that is fibroblastic in nature (CFU-F) (53, 54). The CFU-F assay used for MSCs is also applicable to ASCs. A higher colony-forming efficiency, when larger colonies were produced, is said to be characteristic of a more prominent replicative potential of the cells (55). In contrast to embryonic stem cells, adult stem/stromal cells in general have a lower replicative/self-renewal capacity. Cultures expanded over longer periods begin to lose their multipotentiality. This should be kept in mind when expanding ASCs and for the use of ASCs in clinical trials.

The phenotype of the stromal cell population is also used as a distinguishing characteristic. The phenotype of the human ASCs is generally similar to that of human bone marrow-derived MSCs with the exception of a few surface markers. Isolated stromal cell populations in a heterogenous cell culture can be distinguished from other cell populations by selecting against the endothelial and hematopoietic characteristic markers, cluster of differentiation 14 (CD14), CD31, CD34, and CD45 (leukocyte common antigen). Surface marker CD45 has been commonly used and is considered a classic marker to identify cells of the hematopoietic lineage. Surface marker CD34 has generally been used as a negative marker for MSC and ASC populations because HSCs and endothelial cells express it. However, there have been a few studies stating that it can be used to identify stromal cell precursors and ASCs and that a lack of $CD34^{+}$ on MSCs and ASCs is the result of cell culturing (56-60). Surface marker CD31 is an endothelial marker and monocytes/macrophages and granulocytes express CD14. The marker STRO-1 is expressed on MSCs but ASCs can be STRO-1 negative (56, 61).

The surface enzymes CD13 (aminopeptidase; APN) and CD73 (nucleotidase also known as lymphocyte-vascular adhesion protein-2; L-VAP-2), the integrin beta 1 (ITGB1) CD29, the glycoprotein CD90 (thymocyte antigen 1; Thy-1) and the adhesion molecules CD105 (Endoglin), and CD166 (activated leukocyte cell adhesion molecule; ALCAM) are usually indicative of positive markers in the identification of stromal cells (62). Unfortunately there

are no MSC- or ASC-specific cell-surface markers, and even combinations of cell-surface markers that can define ASCs, are elusive. This is seen with the cell-surface markers CD73 and CD105, which cannot definitively prove that the cultured cells are stromal cells because skin fibroblasts also express these markers (63). Surface marker CD90 has a similar situation and is also expressed on endothelial cells. Bourin and colleagues suggested using CD36 (glycoprotein IIb; GPIIIb) and another adhesion molecule CD106 (vascular cell adhesion molecule 1; VCAM-1) as markers to distinguish ASCs from MSCs. The ASCs, interestingly, are said not to express CD106 but express CD36, which is in juxtaposition to MSCs. Discrepancies have arisen between ASC populations as well, with Gronthos and colleagues detecting CD106 expression on ASCs, while Zuk and colleagues did not detect positive expression of this marker on ASCs (61, 64). The integrin CD49d (ITGA4) has been considered a positive stromal cell marker. However, De Ugarte and colleagues found CD49d to be expressed on ASCs but not expressed and thus negative in MSC populations (62). Surface markers that can be considered positive stromal cell markers are the neutral endopeptidase CD10 (common acute lymphocytic leukemia antigen; CALLA) and CD54 (intercellular adhesion molecule 1; ICAM-1) (65). It was observed that CD54 was highly expressed in ASCs but only minimally expressed in MSCs (62). Surface marker CD146 (melanoma cell adhesion molecule; MCAM) is considered a positive stromal cell marker and pericyte marker. The present "gold standard" for identifying ASCs in a cell population still consists of greater than 95% of the cell population expressing CD105, CD90, CD73, and less than 2% of the cell population expressing CD14, CD34, and CD45 (31).

A shared characteristic of both stromal cell types is their multilineage differentiation potential. Mesenchymal stromal cells have the potential to differentiate towards lineages of mesenchymal tissues, including osteogenic, adipogenic, chondrogenic and myogenic lineages *in vitro* (66-72). Adipose-derived stromal cells, similarly, have been shown to differentiate into the osteogenic (73) adipogenic, (33), and chondrogenic (74) lineages as well as the myogenic (75) lineages under *in vitro* differentiation conditions. The ISCT and IFATS have proposed a set of standards to define ASCs and MSCs (indicated in Table 1.1) and a main criterion is their ability to differentiate into bone, fat, and cartilage *in vitro* (31, 35). It has also been demonstrated that ASCs and MSCs have the potential to differentiate *in vivo* (76, 77).

Table 1.1. Minimal criteria defining adipose tissue-derived stromal cells and mesenchymal stromal cells.

1	Adherence to plastic in standard culture conditions				
2	Immunophenotype	ASCs		MSCs	
		Positive (≥95%)	Negative (≤2%)	Positive (≥95%)	Negative (≤2%)
		CD105		CD105	
		CD90		CD90	
		CD73		CD73	
		Unstable positive marker: CD34	CD34		CD34
			CD45		CD45
			CD14		CD14
			CD31		CD31
		CD36			CD36
			CD106	CD106	
			STRO-1	STRO-1	
3	*In vitro* multipotent differentiation potential: osteogenic, adipogenic, chondrogenic				

Adapted from Dominici *et al*. and Bourin *et al*. The minimal criteria required to define ASC and MSC populations (31, 35).

A paradigm shift also resulted from some studies suggesting that these stromal cells have the ability to transdifferentiate into cells of non-mesodermal origin giving rise to cells of the endoderm including hepatocytes and even ectoderm shown by the differentiation into neuronal cells (78-83). Planat-Bernard carried out a study in which ASCs where plated into methylcellulose and spontaneously beating cells, cardiomyocyte in nature, were eventually observed (84). Cardiovascular disease in particular has been one of the most studied applications for future stem cell therapy. There is a controversial therapeutic application involving type I diabetes regarding the ability of the MSCs to differentiate into insulin-producing cells (IPCs) that are able to release insulin in a glucose-dependent manner (85). The differentiation potential of ASCs puts them on par with bone marrow-derived MSCs; however, it is thought that the proliferation of ASCs is less affected by age and multiple passages than MSCs (86). Another aspect is that ASCs appear to have a disposition to differentiate, more readily than the MSCs, into adipocytes (40). They also appear to be more prone to differentiating into the myogenic lineage compared to MSCs (87). Further evidence suggests that ASCs are of inferior osteogenic and chondrogenic differentiation potential when compared to MSCs (88).

The appearance of a broader differentiation capacity than previously expected has generated much excitement over the wider regenerative potential these cells may now present. The therapeutic potential of MSCs and now ASCs has been and is still being examined and as yet their clinical potential is still being assessed. To date, no ASC or MSC therapy is used routinely as a clinical therapy. Even with the discovered potency, MSCs and ASCs are not considered pluripotent cells, as they supposedly do not express any markers for pluripotency or "stemness" such as telomerase, CD133 also known as prominin-1 (PROM1), ATP-binding cassette sub-family G member 2 (ABCG2), and OCT4 (89). Only ESCs were thought to express OCT4 but interestingly, postembryonic stromal cells, such as those in second-trimester amniotic fluid have also been shown to express OCT4 (90, 91). Thus neonatal stromal cells in humans may have a different growth potential to that of adult stromal cells (92). In two separate studies the stromal cells derived from umbilical cord blood and third-trimester fetal bone marrow from primates were shown to have superior expansion capabilities and plasticity compared to adult MSCs (37, 93). The different growth potentials of the stromal cells may be relevant when considering the long-term aim, namely cell therapy. These cells can be isolated from numerous organisms and tissues and there are multiple isolation methods used to obtain them. To add to this variation there are different culture media used and multiple growth conditions. Thus, comparing related studies tends to be difficult. In the context of cellular therapies, ASCs will need to be expanded to obtain large-scale numbers and it will be important to use standardized isolation procedures and growth media, particularly without xenogeneic factors, such as fetal bovine serum (FBS) for expansion.

Adipose tissue-derived stromal cells and MSCs are mainly classified by the above-mentioned *in vitro* characteristics. An interesting property of both stromal cell populations is that they are considered hypoimmunogenic because they have been shown to exhibit low major histocompatibility complex (MHC) class II and co-stimulatory molecule expression. The outcome is that a proliferative response from autologous or allogeneic (human leukocyte antigen (HLA)-mismatched individuals) T-lymphocytes (T-cells) is not elicited (94-97). Removing MSCs restores the T-cells' proliferative response (98). The immune phenotype of MSCs is considered to be MHC class I^+ and MHC class II^-. However, MHC class II molecules have been found to be situated intracellularly (99). The MHC class I surface receptors may activate T-cells although the lack of the co-stimulatory molecules is thought to render the T-cells anergic. Both sets of stromal cells have a low expression of HLA-ABC, a MHC class I

molecule, and lack the expression of HLA-DR, a MHC class II cell surface receptor, unless stimulated by interferon-γ (IFN-γ). Bone marrow-derived MSCs were found to have a higher expression of HLA-ABC by Rider and colleagues. This finding may make ASCs more favourable for allogeneic transplantation (100). Both ASCs and MSCs are able to actively inhibit mixed lymphocyte reactions (immune response), which is indicative of their immunosuppressive ability. The active inhibition is due to the cells producing soluble factors. Cui and colleagues discovered that ASCs increase their secretion of prostaglandin E2 (PGE2) upon co-culture with mixed lymphocyte reactions (101). Tryptophan depletion due to the expression of the enzyme, indoleamine 2,3-dioxygenase (IDO), was induced by IFN-γ stimulation. This has been shown to also inhibit T-cell proliferation. Mesenchymal stromal cells that were induced with IFN-γ, expressed IDO and thus, tryptophan depletion could be a mechanism of immune suppression used by MSCs (102). Mesenchymal stromal cells have also been shown to escape the lytic effects of cytotoxic T-cells (CTLs) and natural killer (NK)-cells (103). These properties together may account for the low immunogenicity and safety demonstrated during allogeneic transplantation (104). Further evidence was provided when an infusion of allogeneic MSCs following donor bone marrow transplantation did not produce any graft-versus-host disease (GVHD) (105). Another study also demonstrated that allogeneic stem cell co-transplantation with MSCs resulted in the treatment of severe GVHD (106). The use of ASCs and MSCs could have a positive outcome in reducing the incidence of GVHD.

The major limitation in using stromal cells in therapy is finding the least invasive approach to deliver these cells to the patient that will allow effective mobilization and homing of the cells to the appropriate tissue in need. Homing of MSCs or ASCs is not well defined but the term "homing" is associated with the egress of the cells from the vasculature by transmigration across the endothelium to target cells (107). Stem cell homing is an essential part of embryonic development of the blood cell lineage and immune systems. Hematopoietic stem cells originate within fetal liver and migrate to the bone marrow via peripheral blood (108). The cells can be mobilized as a result of inflammation and/or tissue injury (109, 110) and even during strenuous exercise (111). Chemotactic gradients or administered cytokines are suspected to be involved in MSC mobilization and homing to injured sites. There is evidence that this involves α-chemokine stromal-derived factor-1 (SDF-1), also known as CXCL12, and a seven-transmembrane-spanning GαI-protein-coupled receptor, CXCR4, that together form

an axis. The SDF-1/CXCR4 axis may have the primary function of retaining HSCs within bone marrow (112). A small sub-population of MSCs was shown to express cell surface CXCR4s. In a dose-dependent study using a transwell assay to assess migration, the cells that expressed the most CXCR4 migrated the furthest. Anti-CXCR4 antibodies inhibited MSC migration (113). Rat MSCs, transplanted into the cerebrospinal fluid in a hypoglossal nerve injury model, migrated to SDF-1 and fractalkine expressing regions of the brain. The rat MSCs that migrated to the injured region in the brain expressed cell surface CX_3CR1, the receptor for fractalkine, and CXCR4, the receptor for SDF-1, suggesting that these receptors in all probability play a role in stromal cell migration (114).

Looking at stromal cells as a tissue engineering option, they may themselves directly differentiate after transplantation to repair injured tissue. However, evidence is accumulating that during repair, MSCs display trophic activity by releasing paracrine factors and cytokines that, in fact, induce other cells to differentiate into tissue-specific cells (115-117). If one looks back at the clinical trial results published in 1999 by Horwitz and colleagues, only 1% of administered MSCs engrafted in patients. It was noted that there was still improvement in the patients' functions. Paracrine activity was suggested from a study by Tang *et al*. who demonstrated increased expression of vascular endothelial growth factor (VEGF) by administered MSCs, which resulted in increased blood flow and vascular density in a myocardial infarction model (118). Both ASCs and MSCs secrete angiogenic factors including VEGF, transforming growth factor-β (TGF-β), basic fibroblast growth factor (bFGF), placental growth factor (PlGF), and monocyte chemoattractant protein-1 (MCP-1), leading to the stimulation of angiogenesis (119, 120). Another mode of repair by MSCs may be cell fusion. This was observed when MSCs labeled with green fluorescent protein (GFP) were co-cultured with heat-shocked human small airway epithelial cells (SAECs), which resulted in 14% of the MSCs having undergone cell fusion. Although much research on MSCs and ASCs has accumulated over many years and the myriad of proposed repair mechanisms has expanded, our understanding of these stromal cells is still in its infancy.

ASCs can be maintained in an undifferentiated multipotent state and be expanded in culture with relative ease. This in itself opens up many new opportunities to evaluate these cells and the biology behind their use in tissue regeneration. Reviewing the available literature one can see that there is a lack in standardization of donor tissue used, isolation method, *in vitro* cultivation and expansion, immunophenotyping, differentiation along specific cell lineages,

and even in their nomenclature! This remains a major obstacle when comparing results and considering the applications of ASCs for cell therapy. A greater understanding of the complex and multifactorial differentiation pathways of ASCs may make it easier to manipulate ASCs *in vivo*. The potential of cellular therapy lies in its ability to repair damaged tissues *in vivo* as well as generating tissue *in vitro* for future transplantation and subsequent repair. Their attributes and ease of accessibility suggest that ASCs may become an effective therapeutic option for cell-based therapy.

Influence of inflammation and oxidative stress on the therapeutic potential of stromal cells

The therapeutic effect of stromal cells is being assessed globally in clinical trials for many disorders. Their potential use in cellular therapy in numerous human diseases is the driving factor behind most research involving MSCs and ASCs. However, all this on-going research would be thwarted if the survival of these cells after transplantation were compromised. Their survival is crucial for any therapeutic benefit. Following transplantation, MSCs come into contact with a complex milieu *in vivo*, being exposed to numerous factors that may lead to cellular loss. The factors influencing the outcome of MSC transplantation could include frictional loss in the vasculature, oxidative stress, hypoxia, serum and glucose deprivation and inflammation (121).

Inflammation is a unifying mechanism in most diseases, ranging from obesity to myocardial infarction and arthritis. In most of the cases where ASCs will be used therapeutically, there will be underlying inflammation. The behavior of ASCs within a diseased microenvironment is not well understood, although the majority of the literature concentrates on the immunomodulatory effect of ASCs in this context. The events initiating an inflammatory response have been described in great detail. There are two separate known inflammatory triggers. These are infectious triggers, such as a microbial infection, and sterile triggers, which could be instigated by oxidative stress, necrosis (not apoptosis), and injury. The inflammatory response that is pertinent to ASC therapy research occurs during injury and diseased states. Thus, sterile inflammation will be looked at in more detail. Matzinger was the instigator behind what is known as sterile inflammation (122). Inflammation induced by a sterile trigger has been proposed to have numerous similarities to inflammation induced by an infectious trigger; however, the details are less known.

Sterile inflammation involves many innate or primary immune response mechanisms. Sterile inflammation when compared to infectious inflammation still results in the influx of immune cells, swelling, and tissue damage. Antigen-presenting cells (APCs), such as dendritic cells and macrophages, have different receptors collectively known as pattern-recognition receptors (PRRs) on their cell surface. The PRRs, such as the toll-like receptors (TLRs), recognize what is known as pathogen-associated molecular patterns (PAMPs) during an infection. The recognition between these conserved structures found on the surfaces of pathogens and the PRRs, triggers the activation of APCs, stimulating inflammation. Damage-associated molecular patterns (DAMPs), also denoted as alarmins, are non-infectious molecules that are intracellularly located and therefore protected from immune recognition. Upon tissue injury, environmental stress and necrosis, these DAMPs can be released either through degradation of the cell membrane or enzymatic release, and can be recognized by the PRRs on the surface of APCs.

In addition to DAMPs, injured and necrotic cells release pro-inflammatory cytokines and chemokines. These molecules do not have what are considered "molecular patterns". This is how the term alarmin came into use, although many articles also refer to the cytokines and chemokines as DAMPs. To clarify the terminology, DAMPs will refer to any molecule which stimulates PRRs and ultimately produces an inflammatory response. It is also unclear which of the PRRs are specifically involved in the sterile inflammatory response. Evidence is accumulating that TLRs, and in particular heterodimers incorporating TLR4, are involved in sterile inflammation (123). It appears that signal transduction initiated through TLRs mainly involves the interaction of the Toll/interleukin-1 receptor (IL-1R) homologous region (TIR) of the receptor with TIR signaling adaptor proteins of the myeloid differentiation primary response gene 88 (MyD88)-adaptor family.

To date, there have been 10 functional TLRs discovered in humans. The TLRs can be categorized into two groups. Toll-like receptor 1, TLR2, TLR4, TLR5, TLR6 and TLR11 are all expressed on cell surfaces and are grouped together. Toll-like receptor 3, TLR7, TLR8 and TLR9, which are expressed intracellularly comprise the second group (124). It was demonstrated that hASCs and hMSCs express the cell surface TLRs, TLR1, TLR2, TLR4, TLR5 and TLR6 as well as the intracellular TLRs, TLR3 and TLR9. Human ASCs and hMSCs express particularly high levels of TLR3 and TLR4 (125, 126). The specific components that a

particular TLR recognizes and the pathways that are involved are extremely complicated. To simplify the situation, the binding of a ligand to most TLRs, except TLR3, activates the MyD88-dependent pathway. In the case of a ligand binding to TLR3, another pathway is activated, the TRIF-dependent pathway, which is also used by TLR4.

The signal transduction that occurs following TLR activation, is mediated by the molecules MyD88, TIRAP, TRIF and TRAM. Stimulation of MyD88 in the MyD88-dependent pathway for example facilitates the phosphorylation of IL-1R-associated kinase (IRAK1) by the recruitment of IRAK4. Activation of IRAK1 results in the association and activation of tumor necrosis factor receptor (TNFR)-associated factor 6 (TRAF6). Protein kinase C and extracellular signal-regulated kinase (ERK)-1/2 are activated by TRAF6. A complex is formed consisting of TRAF6, transforming-growth-factor (TGF)-β-activated kinase (TAK1), TAK1-binding protein 1 (TAB1) and TAB2 (with IRAK1 being degraded). The complex associates with ubiquitin ligases resulting in the subsequent ubiquitylation of TRAF6. This activates TAK1. Activated TAK1 phosphorylates mitogen-activated protein (MAP) kinases, c-Jun N-terminal kinase (JNK), and I-κ kinase (IκK) complex. Activation of IκK complex leads to the phosphorylation, ubiquitylation and degradation of Iκβ. This mediates the nuclear translocation of the transcriptional regulator nuclear factor κβ (NF-κβ) and results in the expression of pro-inflammatory cytokines. The TRIF-dependent pathway, used by TLR3, involves the activation of IFN-regulatory factor (IRF3) and the production of IFN-β. This also results in the generation of pro-inflammatory cytokines. Findings suggest that TLR4 requires both the MyD88-dependent and MyD88-independent/TRIF-dependent pathways to induce the expression of pro-inflammatory cytokines (123, 127).

Inflammation and oxidative stress are tightly interwoven. The influx of neutrophils and macrophages in response to an inflammatory trigger results in the production and release of reactive oxygen species (ROS), reactive nitrogen species (RNS) and elevated levels of cytokines by these activated immune cells. Excessive ROS or oxidative stress results in tissue destruction and the production of DAMPs. Injured and necrotic cells can also release pro-inflammatory factors. This sets in motion a self-perpetuating series of events. Oxidative stress can activate NF-κβ resulting in the production of pro-inflammatory cytokines, which results in immune cell activation. Activated immune cells produce ROS which in excess cause oxidative stress exacerbating the cycle (128). Liu and colleagues have stated that

senescence is a major factor that negatively affects cell engraftment *in vivo*. The authors found that the senescence of cultured human umbilical cord MSCs was due to increased ROS and activation of the NF-κβ pathway (129).

It is hypothesized that ASCs are able to modulate ROS production in instances of oxidative stress, inflammation, and disease. There are a variety of anti-inflammatory mechanisms produced by ASCs. DAMPs, RNS, and ROS can activate ASCs. An anti-inflammatory mechanism of activated MSCs is their ability to produce and express interleukin-1 receptor antagonist (IL-1RA). This protein antagonist binds to the interleukin-1 receptor (IL-1R) and inhibits the activities of IL-1α and IL-1β thus modulating numerous interleukin 1 cytokine related inflammatory and immune related responses. The activated MSCs also produce tumour necrosis factor (TNF) stimulated gene 6 protein (TSG-6). This protein decreases translocation of NF-κβ to the nucleus in macrophages thus decreasing signaling and impacting on the inflammatory cascade. Another known anti-inflammatory mechanism is PGE2 which in turn increases the secretion of IL-10 (130). The resultant anti-inflammatory effects are the induction of regulatory T-cells and inhibition of T-cell proliferation (131). Intriguingly, ASCs were shown to produce anti-inflammatory and immunomodulating factors in a more potent manner than bone marrow-derived MSCs (132).

Another interesting observation is that MSCs in culture can directly transfer either the mitochondria or mitochondrial DNA (mtDNA) to cells with non-functional mitochondria (133). Wang *et al*. showed that transfer of functional mitochondria to UV-stressed cells via cell-cell connections reversed apoptotic cells in early stages of apoptosis (134). The cell-cell connections called tunneling nanotubes have been observed in multiple cell types (135-137). This is important because damaged mitochondria will be unable to provide the required electrons needed to reduce oxygen, which will result in the production of destructive ROS. A suspected anti-inflammatory and even anti-apoptotic factor that is secreted by MSCs is stanniocalcin-1. Stanniocalcin-1 reduces ROS by increasing the expression of uncoupling protein-2 (UCP2), reducing mitochondrial membrane potential and superoxide generation, and abolishing lipopolysaccharide (LPS)-induced superoxide (O_2^-) generation in macrophages (138). Mitochondrial DNA mutations and mitochondrial dysfunction as well as oxidative stress contribute to disease pathogenesis. The immunosuppressive effect and anti-apoptotic property of these stromal cells, as well as their ability to transfer mtDNA to other cells makes them particularly attractive from a therapeutic perspective.

Reactive oxygen species and antioxidant mechanisms

Inflammation is associated with excess production of ROS and high concentrations of ROS are hazardous for cellular constituents. Oxidative stress results when the generation of ROS exceeds the capacity of antioxidant defense mechanisms. These potentially toxic products are known as "reactive oxygen species", due to their higher reactive states relative to molecular oxygen (O_2). They are highly reactive due to the presence of unpaired outer valence shell electrons. The existence of one or more unpaired electrons in an orbital cloud could lead to electrons being stripped from other molecules in order for the reactive species to gain stability. Examples of ROS include the highly reactive hydroxyl radical (•OH), O_2^-, hydrogen peroxide (H_2O_2), which does not contain a free radical, and nitric oxide (NO), which is also considered a reactive nitrogen species (RNS) (139, 140). Most of the ROS are labile and dissipate shortly after production. The exception is H_2O_2, which is relatively stable (longer half-life) and can diffuse across cell membranes. It is commonly used as a model of exogenous oxidative stress due to its biochemical properties (141, 142).

Reactive oxygen species can be generated exogenously or intracellularly from a number of different sources such as the mitochondrial electron-transport system, nicotinamide adenine dinucleotide phosphate (NADPH) oxidase or Nox, xanthine oxidase**,** cytochrome p450**,** uncoupled NOS and myeloperoxidase. Reactive oxygen species mainly have a negative connotation but they are important secondary messengers in signal transduction pathways. Reactive oxygen species possess the ability to act as both intracellular and extracellular messengers in signal transduction. There have been a number of studies demonstrating that H_2O_2 is a popular candidate for relaying intracellular responses. Exogenously administered H_2O_2 activates kinase enzymes and inactivates phosphatase enzymes (143). The ERK1/2 and p38 MAPK pathways (ERK1/2 and p38 MAPK are kinases) are activated by growth factors and angiotensin II involving H_2O_2 as a messenger. The stimulation of cells by cytokines such as TGF-β1 (144), TNF-α and IL-1 (145) resulted in the production of ROS and once again confirmed their role, particularly H_2O_2, as signaling messengers. Hydrogen peroxide is frequently used as a standard to measure mitochondrial ROS production due to the fact that the mitochondrial electron transport chain produces O_2^-, which is then converted to H_2O_2.

The consensus is that ROS generated from mitochondria are the main source of subcellular ROS. The mitochondrial electron-transport chain consists of multi-enzyme complexes and

cofactors embedded within the inner mitochondrial membrane (Figure 1.2). There are five multi-enzyme complexes (I to V) as well as ubiquinone also known as coenzyme Q10 (CoQ) and cytochrome *c*. Complex I (NADH-ubiquinone reductase) accepts electrons from NADH. Complex II (succinate dehydrogenase) accepts electrons from reduced succinate, a substrate of the Krebs cycle, to produce fumarate. Ubiquinone, the oxidized form of CoQ10, comes into contact with either Complex I or Complex II by random collision as it is mobile within the hydrophobic region of the inner membrane and accepts an electron thus forming the reduced ubiquinol ($CoQH_2$). Ubiquinol subsequently undergoes oxidation via two sequential electron transfers known as the Q cycle. During the Q cycle, the first electron is donated/transferred to a component of Complex III (ubiquinol-cytochrome *c* reductase also known as cytochrome bc_1 complex), the iron-sulphur Rieske protein, while the second electron is donated to cytochrome *b* of Complex III. The unstable intermediate in the Q cycle, semiquinone, can lead to O_2^- formation by transferring electrons directly to O_2 (146).

Electrons move down an electrochemical gradient through ubiquinone to Complex III. Another mobile electron carrier, cytochrome *c*, picks up electrons from Complex III. When the oxidized form of cytochrome *c* makes contact with Complex III through a random collision, its own heme group can accept an electron from the heme group of the cytochrome c_1 subunit in Complex III. Cytochrome *c* then carries this electron until the carrier collides with the final protein carrier in the electron-transport chain, Complex IV (cytochrome oxidase). Complex IV accepts an electron from cytochrome *c* and passes it to O_2, the final electron acceptor in this chain, to form water (H_2O). Water is formed by the reduction of O_2 with a series of four electrons, consecutively. Energy is released by electron transfer, which is used to pump protons (H^+) out of the matrix, through Complex I, III, and IV into the intermembrane space, building up a significant H^+-concentration gradient. The H^+ gradient that is generated provides the energy needed to produce ATP (adenosine triphosphate) by ATP synthase (Complex V) (Figure 1.2). Leakage of electrons to O_2 forming the one-electron reduction of O_2 to O_2^- and thus, its derivative ROS, occurs mainly at Complex I and III (146).

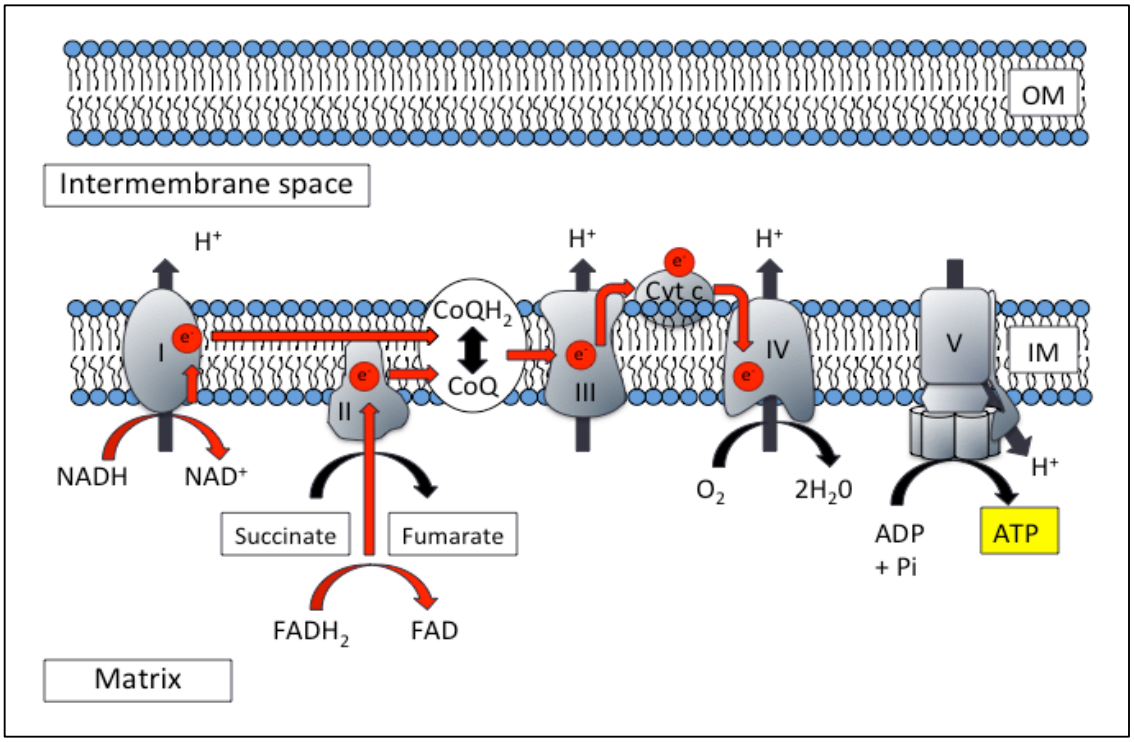

Figure 1.2. The mitochondrial electron transport chain. Electrons are transferred through Complex I to IV resulting in the leakage of electrons and finally the addition of electrons to oxygen (O_2). The proton (H^+) gradient generated by the electron transfer provides the energy needed to generate ATP (adenosine triphosphate) by the final Complex V or ATP synthase. CoQ = oxidised ubiquinone; $CoQH_2$ = reduced ubiquinol.

Superoxide appears to be the first reactive species produced by the electron transport chain. It has emerged from the literature that there are seven key sites within mitochondria that produce O_2^-. The O_2^- that is generated by the electron transport chain is mainly produced through Complex I's ubiquinone-binding site and the flavin mononucleotide (FMN) group and is released into the mitochondrial matrix (147-149). The ubiquinone-binding site of Complex III produces O_2^- and this complex is capable of generating ROS on both sides of the mitochondrial membrane (146, 150). It was discovered that Complex II can also produce ROS, but indirectly, through Complex I (147). It is stated that in the absence of ADP, electrons derived from succinate can instead now flow to Complex I, though the O_2^- that is generated here, is minimal. The O_2^- generated by Complex I and III can undergo dismutation to H_2O_2 by the antioxidant manganese superoxide dismutase (MnSOD) or copper-zinc superoxide dismutase (CuZnSOD) (148). Copper-zinc superoxide dismutase is localized within the mitochondrial intermembrane space and the cytosol. Manganese

superoxide dismutase is localized in the mitochondrial matrix (149). Hydrogen peroxide can be scavenged by another antioxidant, glutathione peroxidase (GPx), in the mitochondrial matrix. Glutathione peroxidase is essential for the conversion of glutathione to oxidized glutathione, resulting in H_2O_2 being converted to H_2O. Hydrogen peroxide can move across the mitochondrial membrane into the cytosol and be scavenged by the antioxidant catalase (CAT) resulting in the production of H_2O and O_2. Superoxide is unable to cross cell membranes in contrast to H_2O_2 which can do this with ease. Hydroxyl radicals are highly reactive and are the result of the Fenton or Haber-Weiss reactions between H_2O_2 and O_2^- (Figure 1.3) (151).

Reactive oxygen species are produced through other mechanisms and not just through the mitochondrial electron transport chain. Mitochondria are not the only organelles to have an electron transport chain; the endoplasmic reticulum also has an electron transport chain. An endoplasmic reticulum NADPH-cytochrome P450 reductase can leak electrons to generate O_2^- from O_2. NADPH oxidase is a membrane associated enzyme complex including a special cytochrome, cytochrome *b558* that catalyzes the reduction of O_2 to O_2^- and thus other ROS, using NADPH or NADH as an electron donor (152, 153). The Nox enzyme was first discovered in the membranes of phagosomes in neutrophils as the initiator of the respiratory burst, which is a key step in the immune defense against bacterial and fungal pathogens. It is now known that Nox homologs are present in virtually every tissue. In particular Nox2 and Nox4 are found in HSCs and MSCs (154-156). Park and Kim have published numerous articles in this field. They found that the expression levels of Nox4 and Nox5 in ASCs were high compared to Nox1, Nox2 and Nox3 (155). The Nox enzymes are reportedly one of the main sources of ROS in stem cells and are activated by growth factors, cytokines, and hypoxia (157). The ROS generated by Nox are said to play an important role in many redox signaling pathways that are involved in stem cell mobilization and proliferation. Kim *et al*. first demonstrated Nox-family-mediated ROS generation in ASCs by showing that the ROS level was reduced by diphenyleneiodonium (DPI), which is a potent Nox inhibitor (156).

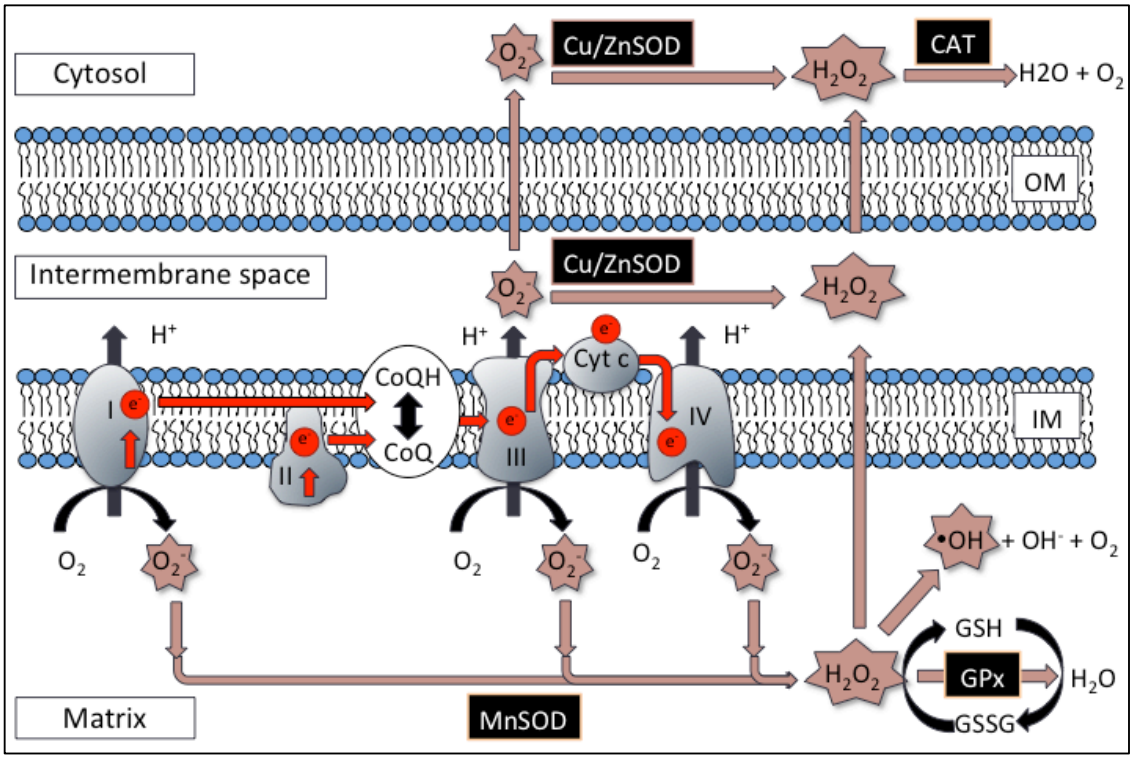

Figure 1.3. An overview of the production of reactive oxygen species (ROS). Molecular O_2 may be reduced to superoxide anion radical, which can be further reduced to hydrogen peroxide either spontaneously, or through the action of superoxide dismutase enzymes, for example MnSOD and Cu/ZnSOD. The transition metals such as Fe^{2+} and Cu^{+} catalyze the conversion of hydrogen peroxide to the hydroxyl radical via the Fenton or Harber–Weiss reactions. The enzymes catalase (CAT) or glutathione peroxidase (GPx) detoxify hydrogen peroxide (H_2O_2) by converting it to water (H_2O). GSSG = glutathione; GSH = oxidized glutathione.

There are several antioxidant enzymes that exist within cells that counteract the potentially damaging effects of ROS. Antioxidants donate electrons to free radicals and thus stabilize them. Coenzyme Q10 (ubiquinone), the electron transporter in the mitochondrial respiratory chain, is a lipid-soluble molecule containing a redox active benzoquinone ring that is connected to a long isoprenoid side chain. This feature allows it to be localized within the inner mitochondrial membrane and to act as an electron and H^{+} transporter within phospholipid bilayers in general. Coenzyme Q10 is found ubiquitously in the human body (hence its original name, ubiquinone) (158). The role of CoQ in the mitochondrial respiratory chain is an obligatory one but CoQ has many other functions. These include the regulation of the physiochemical properties of membranes (159), the modulation of the amount of β2-integrin on the surface of blood monocytes (160) and an endogenously synthesized lipid-

soluble antioxidant (161). It can be regenerated from its oxidized product, it can be produced *de novo*, or it can be acquired through diet, and it has become a popular dietary supplement due to its antioxidant capabilities (162, 163). The antioxidant role of CoQ has sparked interest into its use therapeutically because oxidative damage contributes to many diseases. The success of cellular therapy relies on transplanting viable ASCs. Witort and colleagues demonstrated that CoQ preserved the viability of harvested adipocytes (164).

Appropriate intracellular levels of ROS are essential as an over-production of ROS, or an inadequate production of antioxidants causes oxidative stress resulting in cell-wide damage. The oxidative damage that contributes to disease is the peroxidation of lipids, nucleic acid damage as a result of peroxidation products, and the oxidation and degradation of proteins. Oxidative stress has been implicated in a number of human diseases including cardiovascular disease (165, 166) and many diseases involving neuro-degeneration. Dysfunctional antioxidant enzymes and faulty electron transport chains have been associated with amyotrophic lateral sclerosis (ALS) (167), Alzheimer's disease (168), Parkinson's disease (169), and Huntington's disease (170). Oxidative stress has also been implicated in cancer and aging (171, 172). Reactive oxygen species operating as secondary messengers in signal transduction pathways result in a large number of oxidative stress-responsive transcription factors and genes being expressed. Some of these genes are involved in proliferation, survival and differentiation (173). It will be important to observe the effect that an environment of oxidative stress has on ASCs behaviour and differentiation if they are to be used therapeutically. The ultimate goal of stem cell therapy is the rejuvenation or complete replacement of a defective tissue or organ. What is even more fascinating is that it is thought that MSCs efficiently manage oxidative stress and exhibit high resistance to ROS-induced death due to the constitutive expression of antioxidant enzymes (174). The mechanisms by which ROS affect ASCs are to a large extent still unknown.

Hypoxia and the stem cell niche

The stem cell niche is ill defined and little is known about their *in vivo* properties. This confusion arises due to the fact that stem cells have been isolated from many different regions of the human body and many exhibit similar cell surface markers and differentiation capabilities (89, 175). Scadden has suggested that the simple location of stem cells is not sufficient to define a niche. There are specific cues provided by the niche that regulate cell

number, cell fate and other aspects of stem cell function (176). It appears that supporting cells, the extracellular matrix, and other factors within the stem cell niche largely influence the fate of a stem cell and its progeny (177, 178). One of these factors, O_2, appears to play a role in the stem cell niche and the differentiation of MSCs (179, 180). Common *in vitro* practice is to culture stromal cells under normoxic conditions, the O_2 concentration of ambient or atmospheric air, which is approximately 21% O_2, or the partial pressure of oxygen (pO_2) at sea level which is 159 mm Hg. Humans cannot survive O_2 deprivation; one would consequently think that cell survival is threatened in an environment of reduced O_2. However, the pO_2 within the human body is usually lower than that of the atmosphere and the pO_2 of a niche would depend on the level of vascularization and the position within a tissue.

The pO_2 of oxygenated arterial blood is about 95 mm Hg, and thus percentage-wise, this is approximately 12%. Venous and capillary blood both have a pO_2 of about 40 mm Hg or approximately 5%. The pO_2 within cartilage is around 1% (7.2 mm Hg) and within bone marrow it ranges from 1% to 7% (181, 182). Harrison and colleagues found the mean pO_2 of bone marrow to be 54.9 mm Hg, around 6.6% (183). The pO_2 within adipose tissue is not as clear but has been established to be approximately 55 mm Hg (184). Confocal imaging by Maumus and colleagues confirmed that human ASCs located in the stroma of adipose tissue were not close to capillaries (60). The fetus develops in a low oxygen environment usually around 4% to 5% O_2 and cord blood taken from the umbilical cord vein or arteries (there is one vein and two arteries) of the fetus has a pO_2 of 10% and 13%, respectively (185). Thus, Warton's jelly and cord blood are also obtained from a hypoxic microenvironment. All of the pO_2s indicated certainly show that MSCs and ASCs are not routinely cultivated under physiological conditions.

Oxygen levels regulate stem cell behaviour through hypoxia-inducible factors (HIFs). The hypoxic environment leads to an increase in HIF expression. Hypoxia thus has major transcriptional and post-translational effects that are primarily mediated by the HIFs. These are basic helix–loop–helix (bHLH) transcription factors that contain a PAS domain (named after the three proteins, the *Drosophila* period clock protein (PER), vertebrate aryl hydrocarbon receptor nuclear translocator (ARNT), and *Drosophila* single-minded protein (SIM), first discovered to contain the recognized motifs). PAS domains through the interaction with cofactors can sense O_2, redox potential, chemicals (planar aromatic

hydrocarbons), and light, to name a few stimuli (186). The HIF transcription factors are heterodimers consisting of two subunits, HIF-α and HIF-β also known as ARNT. There are a number of isoforms for the HIF-α and HIF-β subunits: HIF-1α, Endothelial PAS domain-containing protein 1 (EPAS or formerly known as HIF-2α), and HIF-3α as well as HIF-1β. HIF-1α is a ubiquitously expressed subunit. HIF-2α is expressed in embryonic vasculature (187) and Weisener and colleagues discovered that it is also extensively expressed in different organs with accumulation in the kidney, pancreas, brain, liver, intestine and myocardium (188). HIF-3α is expressed in adult thymus, lung, brain, heart and kidney (189). HIF-1β is constitutively expressed and is situated in the nucleus. The importance of HIF-1α and HIF-2α in physiological hypoxia was demonstrated with HIF-1α-null and HIF-2α-null (*Hif-1*$\alpha^{-/-}$ and *Hif-2*$\alpha^{-/-}$) murine embryos. The *Hif-1*$\alpha^{-/-}$ and *Hif-2*$\alpha^{-/-}$ embryos displayed arrested development and lethality. An analysis of the details of the phenotype of *Hif-1*$\alpha^{-/-}$ and *Hif-2*$\alpha^{-/-}$ mouse embryos revealed that mesenchymal cell survival was reduced, and that cardiovascular development, vascularization and neural tube development were defective (190).

With an abundance of O_2, HIF-1α is degraded. The main mediators are prolyl hydroxylases (prolyl hydroxylase domain proteins; PHDs1-3) and asparaginyl hydroxylase (Factor Inhibiting HIF-1; FIH-1). The three human PHDs utilize the cofactors dioxygen, ascorbate and α-ketoglutarate (2-oxoglutarate) under normoxic conditions to catalyze the hydroxylation of two proline residues, Pro402, and Pro564, within the HIF-α subunit. The PHDs hydroxylate the N-terminal oxygen dependent degradation domain (NODD) and the C-terminal oxygen-dependent degradation domain (CODD). One oxygen atom is inserted into the proline and the other oxygen atom is inserted into the co-substrate α-ketoglutarate, resulting in its splitting into carbon dioxide (CO_2) and succinate. The PHDs contain ferrous iron (Fe^{2+}) in their catalyzing centre (191). Hydroxylation of the two residues results in an E3 ubiquitin ligase, known as the von Hippel–Lindau protein (pVHL), being targeted to the HIF-1α subunit. This facilitates in the ubiquitination of HIF-1α, leading to its degradation (192). Additionally, asparagine hydroxylation by FIH-1 hydroxylates the C-terminal activation domain (CTAD) on HIF-1α once again using O_2 and α-ketoglutarate as substrates. This blocks the interaction of HIF-1α with the transcriptional co-activator p300/cyclic AMP response element-binding protein (CBP) leading to inhibition of HIF-1-mediated gene transcription (193). During hypoxia, degradation of HIF-1α does not occur due to abrogation

of both the prolyl and asparaginyl hydroxylases. The HIF-1α subunit can subsequently translocate to the nucleus. Once in the nucleus, HIF-1α can dimerize with HIF-1β and recruit coactivators such as p300 and CBP (194). The HIF-1α/HIF-1β heterodimer binds to hypoxia-response elements (HREs) in the promoter regions of specific genes and drives transcription of NF-κβ, TLRs and VEGF amongst others. Many of these genes are responsible for angiogenesis, glycolysis, and the inhibition of apoptosis.

The inhibition of prolyl and asparaginyl hydroxylases can be mediated by chemical hypoxia. This is accomplished by administering a non-specific α-ketoglutarate antagonist known as dimethyloxalylglycine (DMOG). As mentioned previously, during the hydroxylation of HIF1α by FIH-1 and the PHDs, the oxidative decarboxylation of α-ketoglutarate to succinate and CO_2 is also catalysed. Thus, when the α-ketoglutarate catalysis is competitively blocked, HIF-1α can be stabilized (Figure 1.4). This does not achieve the same exact control that one would obtain *in vivo*; however, Elvidge and colleagues looked at the expression of 22 000 transcripts and they revealed a striking concordance between patterns of gene expression induced by hypoxia and by DMOG (195).

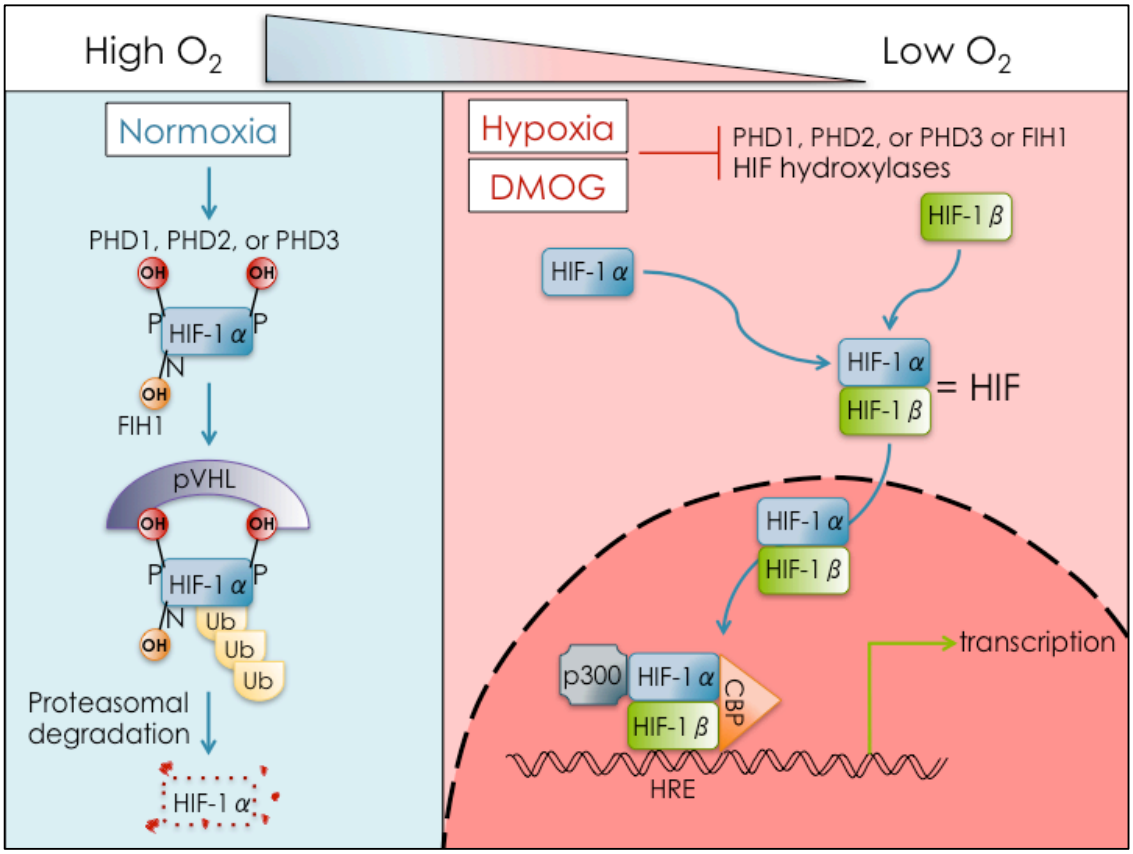

Figure 1.4. The cellular oxygen-sensing system of the body under normoxic and hypoxic conditions. During normoxic conditions, hydroxylation of the prolyl (P) and asparaginyl (N) residues by the PHDs and FIH-1 results in an E3 ubiquitin ligase known as the von Hippel–Lindau protein (pVHL) being targeted to the HIF-1α subunit. This facilitates in the ubiquitination (Ub) of HIF-1α, leading to its degradation. During hypoxic conditions, hydroxylation of HIF-1α does not occur and the HIF-1α subunit can subsequently translocate to the nucleus. Once in the nucleus, HIF-1α can dimerize with HIF-1β and recruit co-activators p300 and CBP. The HIF-1α/HIF-1β heterodimer can now bind to the hypoxia-response elements (HREs) within the promoter regions of specific genes.

The HIF transcription factor targets some of the genes mentioned in the earlier discussion on inflammation. There are two sides to the coin when it comes to the association between hypoxia and inflammation. The first is that hypoxia may induce inflammation (196, 197) and the second is that regions of inflammation may become hypoxic. Hartmann and colleagues demonstrated that C-reactive protein (CRP), the pro-inflammatory cytokine IL-6 and IL-1RA, which are associated with inflammation, are upregulated during hypobaric hypoxic conditions at high altitude (198). Inflamed tissue may become hypoxic as a result of the increased oxygen demand of highly metabolizing cells in inflamed tissue and the number of

inflammatory cells that localize to the inflamed region. A number of the genes induced by hypoxia display a barrier-protective function during mucosal inflammation and are upregulated during colitis (199). The NF-κβ family of transcription factors is activated by a hypoxic environment and by pro-inflammatory cytokines such as TNF-α. The NF-κβ regulates the transcription of inflammatory and anti-apoptotic genes and it can thus be speculated that this transcription factor's activation during hypoxia is due to its conference of anti-apoptotic properties upon the cells allowing them to withstand a low oxygen environment. Mice that lack the IκK complex and thus lack the activation of NF-κβ will not initiate an inflammatory response and promote apoptosis (200). Activity of HIF-1α is increased by the pro-inflammatory cytokines TNF-α and IL-1β. Tumour necrosis factor-α activation of HIF-1α occurs via its stabilization through NF-κβ. Interleukin 1β inhibits pVHL leading to HIF-1α stability and it can also activate NF-κβ. The activation of HIF through numerous pro-inflammatory cytokines shows that that inflammation and hypoxia are intertwined in a disease setting.

The incomplete understanding of ASC parameters *in vivo* may compromise the quality of a stem cell population intended for clinical application. There is a need to replicate various aspects of the supposed *in vivo* niche in order to better maintain the stemness and original characteristics of MSCs. There is also a demand in obtaining clinically relevant cell numbers from the small starting stromal cell population. Cell expansion techniques under normoxic conditions have demonstrated optimal cellular growth although with the gradual loss of their self-renewal properties at late passages (201). These changes may influence the feasibility of using later passage ASCs for cell therapies. Hypoxia could provide a favorable culture environment and one that they are more naturally adapted to. A few studies have shown that hypoxia enhances expansion ability of MSCs (202, 203). Mesenchymal stromal cells were found to produce more colonies, have a longer expansion time, and remain undifferentiated under hypoxic conditions (202, 204-206). However, there is also evidence that HIF-1α acts as a direct inhibitor of DNA replication and increases quiescence (207, 208). Hypoxia preconditioned-MSCs showed enhanced survival upon transplantation (209). The effect of hypoxia on the differentiation of ASCs shows conflicting results but will be expanded on later in the chapter.

Adipogenic differentiation

The two features that define a stem cell are [1] its ability to self-renew and [2] its differentiation capabilities. Harnessing the potential of stem cells to proliferate and form a range of differentiated cell types is ideally what one would want for regenerative applications. A second advantage is that we may advance our understanding of the pathogenesis of a number of diseases. Human ASCs are capable of differentiating down the adipocyte lineage providing a useful human primary cell model of adipogenesis. In order to manage obesity and to understand the role of adipose tissue in this disease it will be necessary to understand the process of adipogenesis in its entirety. A few studies have proposed that impaired adipocyte differentiation contributes to obesity, type II diabetes and its associated complications (210-212).

The full process of adipogenesis involving the commitment of ASCs down the adipogenic lineage resulting in a mature adipocyte is not well defined. In particular, it is the intermediate cellular components during adipogenesis that are not well characterized. Adipogenesis is said to consist of two phases: determination and differentiation. Determination is the commitment of a stem cell, be it an ASC or MSC, towards the pre-adipocyte lineage. This involves the conversion of the stem cell into a pre-adipocyte, an adipocyte progenitor, and the expression of adipogenic transcription factors. These cells, according to Rosen and colleagues, are morphologically indistinct from their predecessors (213). The second phase is differentiation. Pre-adipocytes start producing many small lipid droplets within their cytoplasm. This is followed by the accumulation and aggregation of these lipid droplets to form larger lipid droplets. A hallmark of adipogenic differentiation is the change in morphology from spindle/fibroblastic to spherical (Figure 1.5) (214). The terminally differentiated cell is a mature adipocyte.

Growth arrest upon cell-cell contact precedes the differentiation process, although cell-cell contact is not a prerequisite for adipose differentiation. The adipogenic differentiation process can be thought of as a transition through the expression of different genes. The expression of preadipocyte factor-1 (Pref-1) inhibits adipogenesis and downregulation of Pref-1 occurs during differentiation of adipocytes. Other factors that play a key role in adipocyte differentiation include peroxisome proliferator-activated receptor-γ (PPARγ) and CCAAT/enhancer-binding protein (C/EBP) transcription factors. There are three C/EBP

transcription factors (C/EBPα, C/EBPβ, and C/EBPδ) that can form heterodimers with each other and that bind to C/EBP regulatory elements within promoters. The first transcription factors to be induced during adipogenesis upon exposure to glucocorticoids or insulin are C/EBPβ and C/EBPδ. These two factors then activate C/EBPα, which was the first C/EBP transcription factor to be discovered. C/EBPα is not activated in adipoblasts, a type of pre-adipocyte, but only in the later phase of adipocyte differentiation. It is thought to play a role in establishing terminally differentiated adipocytes (215). Both C/EBPβ and C/EBPδ induce the up-regulation of PPARγ, which coordinates the expression of various adipogenic-specific genes (Figure 1.5) (216, 217). Adipocytes can attain their fully differentiated status approximately one week after induction of confluent ASCs or MSCs, using specific differentiation-inducing medium (218, 219).

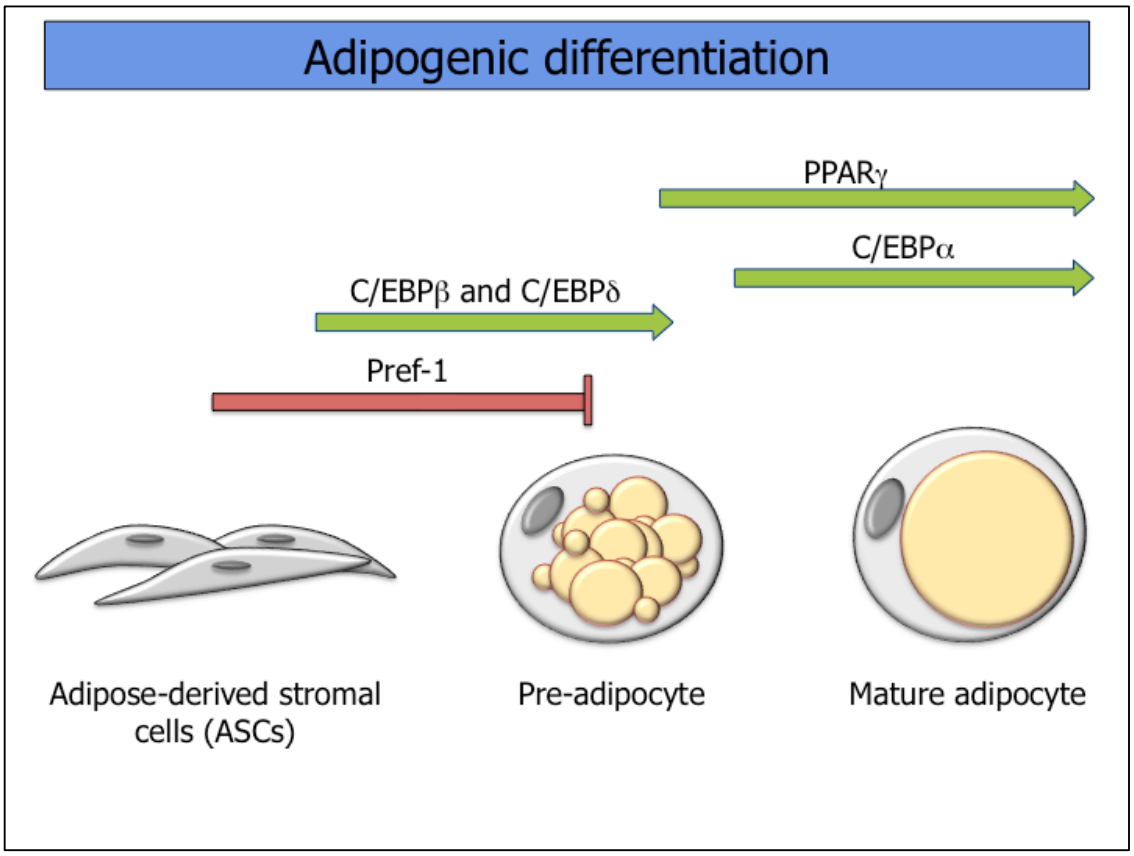

Figure 1.5. Adipogenic differentiation. Adipose-derived stromal cells (ASCs) can be committed to the adipogenic lineage and thus converted to preadipocytes, which further terminally differentiate into mature adipocytes. During the conversion of preadipocytes to adipocytes, growth arrest and the subsequent activation of adipocyte genes by the transcription factors, CCAAT/enhancer-binding

protein (C/EBPα) and peroxisome proliferator-activated receptor-γ (PPARγ) mediates adipogenesis. Changes in morphology include the acquisition of a more spherical shape and the accumulation of lipid droplets.

To initiate the induction of adipogenic differentiation, ASC cultures are incubated with medium containing insulin, dexamethasone, isobutylmethylxanthine, and indomethacin. Induction is followed by the accumulation of lipid droplets, and eventually the lipid droplets combine and fill the cells. A histochemical stain called Oil Red O is commonly used to assay for the accumulation of lipid droplets. Oil Red O mainly detects neutral lipids such as triacylglycerols and cholesteryl esters (220). Intracellular lipid droplets can also be detected via fluorescence microscopy and flow cytometry using 9-diethylamino-5H-benzo[a]phenoxazine-5-one, also known as Nile Red, which is a phenoxazone dye that fluorescently stains lipids. A unique and advantageous property of Nile Red over Oil Red O is that it has a range of emission profiles, changing according to the characteristics of the lipids it has stained. Intracellular lipid droplets are neutral lipids, which are usually triacylglycerols for fatty acid energy reserves or cholesteryl esters, which serve as storage for excess cellular cholesterol. When neutral lipids are stained with Nile Red, the Nile Red emits yellow-gold fluorescence with an emission wavelength greater than 528 nm. Cellular membranes consist of amphipathic lipids, a major component being phospholipids. Nile Red emits deep red fluorescence with an emission wavelength greater than 590 nm when staining amphipathic lipids. Another advantage is that Nile Red only fluoresces in a hydrophobic environment but may be applied to cells in a dilute aqueous medium (221-223). A third advantage of Nile Red compared to Oil Red O is that Nile Red can be quantitatively analyzed via flow cytometry. Oil Red O is a common qualitative analysis of adipocytes used in histochemistry in tissue sections.

Adipose tissue is primarily composed of adipocytes. There are two types of adipocytes, white adipocytes and brown adipocytes. White adipocytes are the more abundant of the two in the human body. White adipocytes are mainly involved in energy storage and mobilization, but they also produce proteins important in homeostasis and blood pressure, and are involved in immune function, angiogenesis, endocrine and secretory functions (224-227). White adipose tissue is located intra-abdominally and subcutaneously. Interestingly, it is also located in the bone marrow and areas such as the face and extremities. Brown adipose tissue was initially considered to be located only in newborns but reports suggest that it is indeed found within

adults and it is most evident in the supraclavicular area. Brown adipocytes are involved in thermogenesis or energy expenditure (228). Mature brown adipocytes are nucleated cells and can be distinguished from their white counterparts by their numerous mitochondria contributing to thermogenesis and also contain fewer lipids. Mature white adipocytes are nucleated cells that contain a large single lipid vacuole consisting of triglycerides (229).

Adipose differentiation is a complex process. It involves a transcriptional cascade, changes in cell morphology and sensitivity towards hormones. All the functions are neatly coordinated and there is still much to be learnt about the intermediate cellular components making up this complex process. Adipogenesis has been primarily studied *in vitro* in murine preadipocyte cell lines (already committed to the adipogenic lineage), such as the 3T3-L1 and 3T3-F442A lines, or on both primary and immortalized murine embryonic fibroblasts (MEFs), as well as murine (m)ESCs and mMSC. An immortalized mMSC line was developed called C3H10T1/2. Murine brown ASCs isolated from mouse fat pads have been used for adipogenic research as well. Very little research on adipogenesis has been done using human primary cell models. One should be wary of translating observations seen in murine experiments to humans as mouse fat distribution and the percentage of white and brown fat differs to that of humans. Observed differences may also be due to heterogeneity: heterogeneity in the locations of adipose tissue, heterogeneity among individual cells and patient heterogeneity. Brown and white adipose tissues are clearly different in their location and metabolic capabilities. The adipose tissue used to isolate ASCs in our research laboratory is WAT from patients mainly undergoing routine liposuction, breast augmentation and abdominoplasty procedures. Adipose tissue from different locations is metabolically different and has different functions (230-232). White adipose tissue is a heterogeneous organ consisting of several cell types and not just adipocytes. These other cell types include cells of the SVF such as ASCs, fibroblasts and macrophages. Adipose-derived stromal cell populations themselves are heterogeneous and any one cell within this population has a variable differentiation capability compared to the other cells in this population. Lastly, the adipose tissue and the cells contained therein are also different between patients. The high variability that we have seen has made it difficult to define stromal cells and as such they are classified by a combination of properties previously described.

Improvement in quantitative detection methods for adipocytes and the differentiation process will assure the way forward for the study of adipogenesis and the intermediate cells

involved in this process, particularly for translation *in vivo*. This would be of particular interest in studies on disease and inflammation as the ratio of pre-adipocytes to mature adipocytes is said to change during inflammation. White adipose tissue releases many pro-inflammatory cytokines such as TNF-α and IL-6 (233). Adipocytes also contain receptors for many of pro-inflammatory cytokines. Adipose tissue, for example, contains both TNF receptors 1 and 2, known as TNFR60 and TNFR80 respectively. Tumor necrosis factor-α has the propensity to prevent pre-adipocyte differentiation as well as promote apoptosis of mature adipocytes (234, 235). These observations could help further studies on inflammation and show that there is a link between these cells and inflammation.

Effect of reactive oxygen species on adipogenesis

There have been a number of studies demonstrating the effect of ROS on adipogenesis. Carrière and colleagues carried out one such study. They tested the implication of endogenous ROS, produced by the mitochondria, in adipogenic differentiation of ASCs. The researchers demonstrated that intracellular ROS inhibited adipogenesis (236). An earlier study also by Carrière and colleagues demonstrated that an increase in mitochondrial ROS (increasing intracellular H_2O_2) inhibited the growth of preadipocytes. The addition of free radical scavengers negated the generation of ROS and thus the effect of ROS, producing the opposite result (237). Adipocytes under oxidative stress had decreased C/EBPα gene expression and decreased binding of C/EBPα-containing dimers resulting in inhibition of adipocyte differentiation (238). Mitochondrial ROS controlled the expression of the adipogenic repressor, CCAAT/enhancer-binding protein homologous protein-10/growth arrest, and DNA damage-inducible protein 153 (CHOP-10/GADD153), and thus inhibited adipocyte differentiation of 3T3-F442A preadipocytes (239).

On a contradictory note, there have been studies that report that ROS generation induces adipogenesis. Human MSCs were treated with D-galactose and galactose oxidase to continuously generate exogenous H_2O_2, subsequently producing an increase in intracellular H_2O_2 even in the presence of mitochondrial-targeted antioxidant MitoCP. The increase in intracellular ROS resulted in the induction of adipogenesis-related genes and lipid droplet accumulation. Thus, the researchers hypothesized that ROS generation promotes adipogenesis (240). Oxidative stress was mimicked by a lentiviral overexpression of Nox4 and exogenous H_2O_2, and both of these exploitations resulted in enhanced adipogenesis (241). Another research group demonstrated using RNA interference that the knock-down of

Nox4 in MSCs inhibited ROS generation and adipocyte differentiation. They discovered that generated ROS mediates differentiation via a cAMP response element-binding protein (CREB) in MSCs. The MSCs were treated with the antioxidant N-acetyl-L-cysteine (NAC), which blocked the transcriptional activation of CREB, a transcription factor involved in adipocyte differentiation. The NAC also inhibited the expression of the adipocyte markers C/EBPα, C/EBPβ, and PPARγ (242). Similarly, Shröder and colleagues demonstrated that by blocking Nox4 expression, using siRNA, it inhibited insulin-induced adipogenic differentiation of 3T3-L1 cells (243).

Hydrogen peroxide mimics the effect of insulin by increasing lipid synthesis from glucose in adipocytes (244). Lee and colleagues reported that when 3T3-L1 cells were treated with H_2O_2, adipogenic differentiation was enhanced. They also noted that ROS was generated during adipogenesis (245). In 2014 it was demonstrated that the knock-down of MnSOD in 3T3-L1 preadipocytes impaired adipogenesis (246). An increase in NO was observed in rat preadipocytes in the initial days of adipogenic differentiation, leading to the conclusion that NO promotes adipogenic differentiation (247). Adipocyte differentiation needs to be further elucidated and the opposing results may in fact be due to inconsistent or differing amounts of ROS and other factors being compared.

Effect of hypoxia and artificial hypoxia on adipogenesis

Oxygen concentrations influence cell fates and are important regulators of differentiation. The consensus appears to be that hypoxia is correlated with an attenuation of adipogenesis. In response to hypoxia, dimerization of HIF-1α and HIF-1β forms HIF-1, which leads to the repression of PPARγ2 and decreases the expression of C/EBPβ. Low levels of O_2 activate HIF-1α–HIF-1β heterodimers, which upregulate *Dec1* gene expression. The DEC1 protein represses PPARγ transcription, which in turn inhibits the differentiation of preadipocytes into adipocytes (248). Kim *et al*. similarly suggested that inhibition of adipogenic differentiation is due to PPARγ repression (249). Lin *et al*. observed that preadipocytes induced to differentiate under hypoxic conditions maintained their precursory phenotype. Following this, they found that MSCs subjected to the same conditions also maintained their phenotype (250). The DNA-binding capability of C/EBPβ was demonstrated by Park *et al*. to be inhibited by hypoxia (251).

A study performed by Fink and colleagues found that under hypoxic conditions, an immortalized MSC cell line formed cytoplasmic lipids and displayed an adipocyte-like phenotype. Upon gene expression analysis however, there was no adipocyte-specific gene expression observed, and they thus concluded that adipogenic differentiation did not take place (252). On the other-hand Valorani *et al*. discovered that pre-conditioning ASCs under hypoxic conditions and then returning them to normoxia improved their adipogenic potential (253). The activation of the HIF transcription factor results in an increase in the expression of genes whose products are considered stemness markers such as OCT4 (254). This supports the concept that hypoxia promotes the proliferation of stem cells and maintains the stem cell phenotype. This may be useful when culturing the large numbers of cells needed for transplantation. Rosovo and colleagues observed that preculturing MSCs under hypoxic conditions prior to transplantation improved their tissue regenerative potential (255).

The effect that artificial hypoxia has on the adipogenic and regenerative potential of stromal cells will need to be elucidated, as very few studies have been performed in this area. The pharmacological inhibition of PHD activity by DMOG during the early stages of adipogenic differentiation of 3T3-L1 preadipocytes abrogated the formation of adipocytes (256). Treatment of C3H10T1/2 cells with DMOG attenuated rosiglitazone-induced adipocyte differentiation. This was accompanied by the reduced expression of fatty acid binding protein 4 (FABP4; also known as aP2) and PPARγ (257). Lastly, a study utilizing MC3T3-E1 pre-osteoblasts found that adipogenic gene expression was increased while osteoblastic genes were suppressed following treatment with DMOG (258).

Concluding remark

There are a number of factors that are hampering the realization of ASC therapeutic potential including indecisive nomenclature, complex niches, inconsistent differentiation results, and the lack of adequate surface markers. This dissertation focuses on the *in vitro* effect of ROS and artificial hypoxia on the adipogenic differentiation capability of ASCs in the hope of being able to contribute to the understanding of how adipogenesis is influenced during inflammation or settings requiring stem cell therapy.

References

1. Hwang WS, Ryu YJ, Park JH, Park ES, Lee EG, Koo JM, et al. Evidence of a pluripotent human embryonic stem cell line derived from a cloned blastocyst. Science. 2004;303(5664):1669-74.
2. Hwang WS, Roh SI, Lee BC, Kang SK, Kwon DK, Kim S, et al. Patient-specific embryonic stem cells derived from human SCNT blastocysts. Science. 2005;308(5729):1777-83.
3. Obokata H, Sasai Y, Niwa H, Kadota M, Andrabi M, Takata N, et al. Retraction: Bidirectional developmental potential in reprogrammed cells with acquired pluripotency. Nature. 2014;511(7507):112.
4. Weissman IL. Translating stem and progenitor cell biology to the clinic: barriers and opportunities. Science. 2000;287(5457):1442-6.
5. Martin GR. Isolation of a pluripotent cell line from early mouse embryos cultured in medium conditioned by teratocarcinoma stem cells. Proceedings of the National Academy of Sciences of the United States of America. 1981;78(12):7634-8.
6. Roobrouck VD, Ulloa-Montoya F, Verfaillie CM. Self-renewal and differentiation capacity of young and aged stem cells. Experimental cell research. 2008;314(9):1937-44.
7. Morrison SJ, Kimble J. Asymmetric and symmetric stem-cell divisions in development and cancer. Nature. 2006;441(7097):1068-74.
8. Ivanova NB, Dimos JT, Schaniel C, Hackney JA, Moore KA, Lemischka IR. A stem cell molecular signature. Science. 2002;298(5593):601-4.
9. Ramalho-Santos M, Yoon S, Matsuzaki Y, Mulligan RC, Melton DA. "Stemness": transcriptional profiling of embryonic and adult stem cells. Science. 2002;298(5593):597-600.
10. Fortunel NO, Otu HH, Ng HH, Chen J, Mu X, Chevassut T, et al. Comment on " 'Stemness': transcriptional profiling of embryonic and adult stem cells" and "a stem cell molecular signature". Science. 2003;302(5644):393; author reply
11. Evans MJ, Kaufman MH. Establishment in culture of pluripotential cells from mouse embryos. Nature. 1981;292(5819):154-6.
12. Takahashi K, Yamanaka S. Induction of pluripotent stem cells from mouse embryonic and adult fibroblast cultures by defined factors. Cell. 2006;126(4):663-76.
13. Bar-Nur O, Russ HA, Efrat S, Benvenisty N. Epigenetic memory and preferential lineage-specific differentiation in induced pluripotent stem cells derived from human pancreatic islet beta cells. Cell stem cell. 2011;9(1):17-23.
14. Kim K, Doi A, Wen B, Ng K, Zhao R, Cahan P, et al. Epigenetic memory in induced pluripotent stem cells. Nature. 2010;467(7313):285-90.
15. Okita K, Ichisaka T, Yamanaka S. Generation of germline-competent induced pluripotent stem cells. Nature. 2007;448(7151):313-7.
16. Tachibana M, Amato P, Sparman M, Gutierrez NM, Tippner-Hedges R, Ma H, et al. Human Embryonic Stem Cells Derived by Somatic Cell Nuclear Transfer. Cell. 2013.

17. Park IH, Zhao R, West JA, Yabuuchi A, Huo H, Ince TA, et al. Reprogramming of human somatic cells to pluripotency with defined factors. Nature. 2008;451(7175):141-6.
18. Wong DJ, Liu H, Ridky TW, Cassarino D, Segal E, Chang HY. Module map of stem cell genes guides creation of epithelial cancer stem cells. Cell stem cell. 2008;2(4):333-44.
19. Miura K, Okada Y, Aoi T, Okada A, Takahashi K, Okita K, et al. Variation in the safety of induced pluripotent stem cell lines. Nature biotechnology. 2009;27(8):743-5.
20. Altman J. Are new neurons formed in the brains of adult mammals? Science. 1962;135(3509):1127-8.
21. Kaplan MS, Hinds JW. Neurogenesis in the adult rat: electron microscopic analysis of light radioautographs. Science. 1977;197(4308):1092-4.
22. Li A, Simmons PJ, Kaur P. Identification and isolation of candidate human keratinocyte stem cells based on cell surface phenotype. Proceedings of the National Academy of Sciences of the United States of America. 1998;95(7):3902-7.
23. Zulewski H, Abraham EJ, Gerlach MJ, Daniel PB, Moritz W, Muller B, et al. Multipotential nestin-positive stem cells isolated from adult pancreatic islets differentiate ex vivo into pancreatic endocrine, exocrine, and hepatic phenotypes. Diabetes. 2001;50(3):521-33.
24. Spangrude GJ, Heimfeld S, Weissman IL. Purification and characterization of mouse hematopoietic stem cells. Science. 1988;241(4861):58-62.
25. Micklem HS, and Loutit, J. F. Tissue Grafting and Radiation New York: Academic Press Inc.; 1966.
26. Friedenstein AJ, Piatetzky S, II, Petrakova KV. Osteogenesis in transplants of bone marrow cells. Journal of embryology and experimental morphology. 1966;16(3):381-90.
27. Brinster RL, Zimmermann JW. Spermatogenesis following male germ-cell transplantation. Proceedings of the National Academy of Sciences of the United States of America. 1994;91(24):11298-302.
28. Fu YS, Cheng YC, Lin MY, Cheng H, Chu PM, Chou SC, et al. Conversion of human umbilical cord mesenchymal stem cells in Wharton's jelly to dopaminergic neurons in vitro: potential therapeutic application for Parkinsonism. Stem Cells. 2006;24(1):115-24.
29. Ferrari G, Cusella-De Angelis G, Coletta M, Paolucci E, Stornaiuolo A, Cossu G, et al. Muscle regeneration by bone marrow-derived myogenic progenitors. Science. 1998;279(5356):1528-30.
30. Park BS, Jang KA, Sung JH, Park JS, Kwon YH, Kim KJ, et al. Adipose-derived stem cells and their secretory factors as a promising therapy for skin aging. Dermatologic surgery: official publication for American Society for Dermatologic Surgery [et al]. 2008;34(10):1323-6.
31. Dominici M, Le Blanc K, Mueller I, Slaper-Cortenbach I, Marini F, Krause D, et al. Minimal criteria for defining multipotent mesenchymal stromal cells. The International Society for Cellular Therapy position statement. Cytotherapy. 2006;8(4):315-7.

32. Caplan AI. Mesenchymal stem cells. Journal of orthopaedic research: official publication of the Orthopaedic Research Society. 1991;9(5):641-50.
33. Zuk PA, Zhu M, Mizuno H, Huang J, Futrell JW, Katz AJ, et al. Multilineage cells from human adipose tissue: implications for cell-based therapies. Tissue engineering. 2001;7(2):211-28.
34. Amos PJ, Shang H, Bailey AM, Taylor A, Katz AJ, Peirce SM. IFATS collection: The role of human adipose-derived stromal cells in inflammatory microvascular remodeling and evidence of a perivascular phenotype. Stem Cells. 2008;26(10):2682-90.
35. Bourin P, Bunnell BA, Casteilla L, Dominici M, Katz AJ, March KL, et al. Stromal cells from the adipose tissue-derived stromal vascular fraction and culture expanded adipose tissue-derived stromal/stem cells: a joint statement of the International Federation for Adipose Therapeutics and Science (IFATS) and the International Society for Cellular Therapy (ISCT). Cytotherapy. 2013;15(6):641-8.
36. De Ugarte DA, Morizono K, Elbarbary A, Alfonso Z, Zuk PA, Zhu M, et al. Comparison of multi-lineage cells from human adipose tissue and bone marrow. Cells, tissues, organs. 2003;174(3):101-9.
37. Kern S, Eichler H, Stoeve J, Kluter H, Bieback K. Comparative analysis of mesenchymal stem cells from bone marrow, umbilical cord blood, or adipose tissue. Stem Cells. 2006;24(5):1294-301.
38. Fraser JK, Wulur I, Alfonso Z, Hedrick MH. Fat tissue: an underappreciated source of stem cells for biotechnology. Trends in biotechnology. 2006;24(4):150-4.
39. Gonzalez-Rey E, Gonzalez MA, Varela N, O'Valle F, Hernandez-Cortes P, Rico L, et al. Human adipose-derived mesenchymal stem cells reduce inflammatory and T cell responses and induce regulatory T cells in vitro in rheumatoid arthritis. Annals of the rheumatic diseases. 2010;69(1):241-8.
40. Pachon-Pena G, Yu G, Tucker A, Wu X, Vendrell J, Bunnell BA, et al. Stromal stem cells from adipose tissue and bone marrow of age-matched female donors display distinct immunophenotypic profiles. Journal of cellular physiology. 2011;226(3):843-51.
41. Van RL, Bayliss CE, Roncari DA. Cytological and enzymological characterization of adult human adipocyte precursors in culture. The Journal of clinical investigation. 1976;58(3):699-704.
42. Aust L, Devlin B, Foster SJ, Halvorsen YD, Hicok K, du Laney T, et al. Yield of human adipose-derived adult stem cells from liposuction aspirates. Cytotherapy. 2004;6(1):7-14.
43. Kaplan FS, Hahn GV, Zasloff MA. Heterotopic Ossification: Two Rare Forms and What They Can Teach Us. The Journal of the American Academy of Orthopaedic Surgeons. 1994;2(5):288-96.
44. Spalding KL, Arner E, Westermark PO, Bernard S, Buchholz BA, Bergmann O, et al. Dynamics of fat cell turnover in humans. Nature. 2008;453(7196):783-7.
45. Fournier PF, Otteni FM. Lipodissection in body sculpturing: the dry procedure. Plastic and reconstructive surgery. 1983;72(5):598-609.

46. Tholpady SS, Llull R, Ogle RC, Rubin JP, Futrell JW, Katz AJ. Adipose tissue: stem cells and beyond. Clin Plast Surg. 2006;33(1):55-62, vi.
47. Nguyen A, Pasyk KA, Bouvier TN, Hassett CA, Argenta LC. Comparative study of survival of autologous adipose tissue taken and transplanted by different techniques. Plastic and reconstructive surgery. 1990;85(3):378-86; discussion 87-9.
48. Pu LL, Coleman SR, Cui X, Ferguson RE, Jr., Vasconez HC. Autologous fat grafts harvested and refined by the Coleman technique: a comparative study. Plastic and reconstructive surgery. 2008;122(3):932-7.
49. Oedayrajsingh-Varma MJ, van Ham SM, Knippenberg M, Helder MN, Klein-Nulend J, Schouten TE, et al. Adipose tissue-derived mesenchymal stem cell yield and growth characteristics are affected by the tissue-harvesting procedure. Cytotherapy. 2006;8(2):166-77.
50. Kaufman MR, Bradley JP, Dickinson B, Heller JB, Wasson K, O'Hara C, et al. Autologous fat transfer national consensus survey: trends in techniques for harvest, preparation, and application, and perception of short- and long-term results. Plastic and reconstructive surgery. 2007;119(1):323-31.
51. Rodbell M. Metabolism of isolated fat cells. II. The similar effects of phospholipase C (Clostridium perfringens alpha toxin) and of insulin on glucose and amino acid metabolism. The Journal of biological chemistry. 1966;241(1):130-9.
52. Friedenstein AJ, Chailakhjan RK, Lalykina KS. The development of fibroblast colonies in monolayer cultures of guinea-pig bone marrow and spleen cells. Cell and tissue kinetics. 1970;3(4):393-403.
53. Owen M, Friedenstein AJ. Stromal stem cells: marrow-derived osteogenic precursors. Ciba Foundation symposium. 1988;136:42-60.
54. Castro-Malaspina H, Gay RE, Resnick G, Kapoor N, Meyers P, Chiarieri D, et al. Characterization of human bone marrow fibroblast colony-forming cells (CFU-F) and their progeny. Blood. 1980;56(2):289-301.
55. Digirolamo CM, Stokes D, Colter D, Phinney DG, Class R, Prockop DJ. Propagation and senescence of human marrow stromal cells in culture: a simple colony-forming assay identifies samples with the greatest potential to propagate and differentiate. British journal of haematology. 1999;107(2):275-81.
56. Simmons PJ, Torok-Storb B. CD34 expression by stromal precursors in normal human adult bone marrow. Blood. 1991;78(11):2848-53.
57. Sengenes C, Lolmede K, Zakaroff-Girard A, Busse R, Bouloumie A. Preadipocytes in the human subcutaneous adipose tissue display distinct features from the adult mesenchymal and hematopoietic stem cells. Journal of cellular physiology. 2005;205(1):114-22.
58. Planat-Benard V, Silvestre JS, Cousin B, Andre M, Nibbelink M, Tamarat R, et al. Plasticity of human adipose lineage cells toward endothelial cells: physiological and therapeutic perspectives. Circulation. 2004;109(5):656-63.
59. Miranville A, Heeschen C, Sengenes C, Curat CA, Busse R, Bouloumie A. Improvement of postnatal neovascularization by human adipose tissue-derived stem cells. Circulation. 2004;110(3):349-55.

60. Maumus M, Peyrafitte JA, D'Angelo R, Fournier-Wirth C, Bouloumie A, Casteilla L, et al. Native human adipose stromal cells: localization, morphology and phenotype. Int J Obes (Lond). 2011;35(9):1141-53.
61. Gronthos S, Franklin DM, Leddy HA, Robey PG, Storms RW, Gimble JM. Surface protein characterization of human adipose tissue-derived stromal cells. Journal of cellular physiology. 2001;189(1):54-63.
62. De Ugarte DA, Alfonso Z, Zuk PA, Elbarbary A, Zhu M, Ashjian P, et al. Differential expression of stem cell mobilization-associated molecules on multi-lineage cells from adipose tissue and bone marrow. Immunology letters. 2003;89(2-3):267-70.
63. Ishii M, Koike C, Igarashi A, Yamanaka K, Pan H, Higashi Y, et al. Molecular markers distinguish bone marrow mesenchymal stem cells from fibroblasts. Biochemical and biophysical research communications. 2005;332(1):297-303.
64. Zuk PA, Zhu M, Ashjian P, De Ugarte DA, Huang JI, Mizuno H, et al. Human adipose tissue is a source of multipotent stem cells. Molecular biology of the cell. 2002;13(12):4279-95.
65. Gimble J, Guilak F. Adipose-derived adult stem cells: isolation, characterization, and differentiation potential. Cytotherapy. 2003;5(5):362-9.
66. Prockop DJ. Marrow stromal cells as stem cells for nonhematopoietic tissues. Science. 1997;276(5309):71-4.
67. Pittenger MF, Mackay AM, Beck SC, Jaiswal RK, Douglas R, Mosca JD, et al. Multilineage potential of adult human mesenchymal stem cells. Science. 1999;284(5411):143-7.
68. Maniatopoulos C, Sodek J, Melcher AH. Bone formation in vitro by stromal cells obtained from bone marrow of young adult rats. Cell and tissue research. 1988;254(2):317-30.
69. Johnstone B, Hering TM, Caplan AI, Goldberg VM, Yoo JU. In vitro chondrogenesis of bone marrow-derived mesenchymal progenitor cells. Experimental cell research. 1998;238(1):265-72.
70. Hauner H, Schmid P, Pfeiffer EF. Glucocorticoids and insulin promote the differentiation of human adipocyte precursor cells into fat cells. The Journal of clinical endocrinology and metabolism. 1987;64(4):832-5.
71. Wakitani S, Saito T, Caplan AI. Myogenic cells derived from rat bone marrow mesenchymal stem cells exposed to 5-azacytidine. Muscle & nerve. 1995;18(12):1417-26.
72. Caplan AI, Bruder SP. Mesenchymal stem cells: building blocks for molecular medicine in the 21st century. Trends in molecular medicine. 2001;7(6):259-64.
73. Dragoo JL, Samimi B, Zhu M, Hame SL, Thomas BJ, Lieberman JR, et al. Tissue-engineered cartilage and bone using stem cells from human infrapatellar fat pads. The Journal of bone and joint surgery British volume. 2003;85(5):740-7.
74. Erickson GR, Gimble JM, Franklin DM, Rice HE, Awad H, Guilak F. Chondrogenic potential of adipose tissue-derived stromal cells in vitro and in vivo. Biochemical and biophysical research communications. 2002;290(2):763-9.

75. Mizuno H, Zuk PA, Zhu M, Lorenz HP, Benhaim P, Hedrick MH. Myogenic differentiation by human processed lipoaspirate cells. Plastic and reconstructive surgery. 2002;109(1):199-209; discussion 10-1.
76. Benayahu D, Kletter Y, Zipori D, Wientroub S. Bone marrow-derived stromal cell line expressing osteoblastic phenotype in vitro and osteogenic capacity in vivo. Journal of cellular physiology. 1989;140(1):1-7.
77. Zannettino AC, Paton S, Arthur A, Khor F, Itescu S, Gimble JM, et al. Multipotential human adipose-derived stromal stem cells exhibit a perivascular phenotype in vitro and in vivo. Journal of cellular physiology. 2008;214(2):413-21.
78. Safford KM, Hicok KC, Safford SD, Halvorsen YD, Wilkison WO, Gimble JM, et al. Neurogenic differentiation of murine and human adipose-derived stromal cells. Biochemical and biophysical research communications. 2002;294(2):371-9.
79. Jiang Y, Jahagirdar BN, Reinhardt RL, Schwartz RE, Keene CD, Ortiz-Gonzalez XR, et al. Pluripotency of mesenchymal stem cells derived from adult marrow. Nature. 2002;418(6893):41-9.
80. Dezawa M, Kanno H, Hoshino M, Cho H, Matsumoto N, Itokazu Y, et al. Specific induction of neuronal cells from bone marrow stromal cells and application for autologous transplantation. The Journal of clinical investigation. 2004;113(12):1701-10.
81. Petersen BE, Bowen WC, Patrene KD, Mars WM, Sullivan AK, Murase N, et al. Bone marrow as a potential source of hepatic oval cells. Science. 1999;284(5417):1168-70.
82. Schwartz RE, Reyes M, Koodie L, Jiang Y, Blackstad M, Lund T, et al. Multipotent adult progenitor cells from bone marrow differentiate into functional hepatocyte-like cells. The Journal of clinical investigation. 2002;109(10):1291-302.
83. Ashjian PH, Elbarbary AS, Edmonds B, DeUgarte D, Zhu M, Zuk PA, et al. In vitro differentiation of human processed lipoaspirate cells into early neural progenitors. Plastic and reconstructive surgery. 2003;111(6):1922-31.
84. Planat-Benard V, Menard C, Andre M, Puceat M, Perez A, Garcia-Verdugo JM, et al. Spontaneous cardiomyocyte differentiation from adipose tissue stroma cells. Circulation research. 2004;94(2):223-9.
85. Choi KS, Shin JS, Lee JJ, Kim YS, Kim SB, Kim CW. In vitro trans-differentiation of rat mesenchymal cells into insulin-producing cells by rat pancreatic extract. Biochemical and biophysical research communications. 2005;330(4):1299-305.
86. Chen HT, Lee MJ, Chen CH, Chuang SC, Chang LF, Ho ML, et al. Proliferation and differentiation potential of human adipose-derived mesenchymal stem cells isolated from elderly patients with osteoporotic fractures. Journal of cellular and molecular medicine. 2012;16(3):582-93.
87. Choi YS, Vincent LG, Lee AR, Dobke MK, Engler AJ. Mechanical derivation of functional myotubes from adipose-derived stem cells. Biomaterials. 2012;33(8):2482-91.
88. Im GI, Shin YW, Lee KB. Do adipose tissue-derived mesenchymal stem cells have the same osteogenic and chondrogenic potential as bone marrow-derived cells? Osteoarthritis and cartilage/OARS, Osteoarthritis Research Society. 2005;13(10):845-53.

89. Katz AJ, Tholpady A, Tholpady SS, Shang H, Ogle RC. Cell surface and transcriptional characterization of human adipose-derived adherent stromal (hADAS) cells. Stem Cells. 2005;23(3):412-23.
90. Prusa AR, Marton E, Rosner M, Bernaschek G, Hengstschlager M. Oct-4-expressing cells in human amniotic fluid: a new source for stem cell research? Hum Reprod. 2003;18(7):1489-93.
91. Bossolasco P, Montemurro T, Cova L, Zangrossi S, Calzarossa C, Buiatiotis S, et al. Molecular and phenotypic characterization of human amniotic fluid cells and their differentiation potential. Cell research. 2006;16(4):329-36.
92. Gotherstrom C, West A, Liden J, Uzunel M, Lahesmaa R, Le Blanc K. Difference in gene expression between human fetal liver and adult bone marrow mesenchymal stem cells. Haematologica. 2005;90(8):1017-26.
93. Lee CC, Ye F, Tarantal AF. Comparison of growth and differentiation of fetal and adult rhesus monkey mesenchymal stem cells. Stem cells and development. 2006;15(2):209-20.
94. Di Nicola M, Carlo-Stella C, Magni M, Milanesi M, Longoni PD, Matteucci P, et al. Human bone marrow stromal cells suppress T-lymphocyte proliferation induced by cellular or nonspecific mitogenic stimuli. Blood. 2002;99(10):3838-43.
95. Tse WT, Pendleton JD, Beyer WM, Egalka MC, Guinan EC. Suppression of allogeneic T-cell proliferation by human marrow stromal cells: implications in transplantation. Transplantation. 2003;75(3):389-97.
96. McIntosh K, Zvonic S, Garrett S, Mitchell JB, Floyd ZE, Hammill L, et al. The immunogenicity of human adipose-derived cells: temporal changes in vitro. Stem Cells. 2006;24(5):1246-53.
97. Niemeyer P, Kornacker M, Mehlhorn A, Seckinger A, Vohrer J, Schmal H, et al. Comparison of immunological properties of bone marrow stromal cells and adipose tissue-derived stem cells before and after osteogenic differentiation in vitro. Tissue engineering. 2007;13(1):111-21.
98. Krampera M, Glennie S, Dyson J, Scott D, Laylor R, Simpson E, et al. Bone marrow mesenchymal stem cells inhibit the response of naive and memory antigen-specific T cells to their cognate peptide. Blood. 2003;101(9):3722-9.
99. Le Blanc K, Tammik C, Rosendahl K, Zetterberg E, Ringden O. HLA expression and immunologic properties of differentiated and undifferentiated mesenchymal stem cells. Experimental hematology. 2003;31(10):890-6.
100. Rider DA, Dombrowski C, Sawyer AA, Ng GH, Leong D, Hutmacher DW, et al. Autocrine fibroblast growth factor 2 increases the multipotentiality of human adipose-derived mesenchymal stem cells. Stem Cells. 2008;26(6):1598-608.
101. Cui L, Yin S, Liu W, Li N, Zhang W, Cao Y. Expanded adipose-derived stem cells suppress mixed lymphocyte reaction by secretion of prostaglandin E2. Tissue engineering. 2007;13(6):1185-95.
102. Meisel R, Zibert A, Laryea M, Gobel U, Daubener W, Dilloo D. Human bone marrow stromal cells inhibit allogeneic T-cell responses by indoleamine 2,3-dioxygenase-mediated tryptophan degradation. Blood. 2004;103(12):4619-21.

103. Rasmusson I, Ringden O, Sundberg B, Le Blanc K. Mesenchymal stem cells inhibit the formation of cytotoxic T lymphocytes, but not activated cytotoxic T lymphocytes or natural killer cells. Transplantation. 2003;76(8):1208-13.
104. Horwitz EM, Prockop DJ, Fitzpatrick LA, Koo WW, Gordon PL, Neel M, et al. Transplantability and therapeutic effects of bone marrow-derived mesenchymal cells in children with osteogenesis imperfecta. Nature medicine. 1999;5(3):309-13.
105. Koc ON, Day J, Nieder M, Gerson SL, Lazarus HM, Krivit W. Allogeneic mesenchymal stem cell infusion for treatment of metachromatic leukodystrophy (MLD) and Hurler syndrome (MPS-IH). Bone marrow transplantation. 2002;30(4):215-22.
106. Le Blanc K, Rasmusson I, Sundberg B, Gotherstrom C, Hassan M, Uzunel M, et al. Treatment of severe acute graft-versus-host disease with third party haploidentical mesenchymal stem cells. Lancet. 2004;363(9419):1439-41.
107. Karp JM, Leng Teo GS. Mesenchymal stem cell homing: the devil is in the details. Cell stem cell. 2009;4(3):206-16.
108. Yoder MC. Introduction: spatial origin of murine hematopoietic stem cells. Blood. 2001;98(1):3-5.
109. Massberg S, Schaerli P, Knezevic-Maramica I, Kollnberger M, Tubo N, Moseman EA, et al. Immunosurveillance by hematopoietic progenitor cells trafficking through blood, lymph, and peripheral tissues. Cell. 2007;131(5):994-1008.
110. Kucia M, Zhang YP, Reca R, Wysoczynski M, Machalinski B, Majka M, et al. Cells enriched in markers of neural tissue-committed stem cells reside in the bone marrow and are mobilized into the peripheral blood following stroke. Leukemia: official journal of the Leukemia Society of America, Leukemia Research Fund, UK. 2006;20(1):18-28.
111. Mobius-Winkler S, Hilberg T, Menzel K, Golla E, Burman A, Schuler G, et al. Time-dependent mobilization of circulating progenitor cells during strenuous exercise in healthy individuals. J Appl Physiol. 2009;107(6):1943-50.
112. Sugiyama T, Kohara H, Noda M, Nagasawa T. Maintenance of the hematopoietic stem cell pool by CXCL12-CXCR4 chemokine signaling in bone marrow stromal cell niches. Immunity. 2006;25(6):977-88.
113. Wynn RF, Hart CA, Corradi-Perini C, O'Neill L, Evans CA, Wraith JE, et al. A small proportion of mesenchymal stem cells strongly expresses functionally active CXCR4 receptor capable of promoting migration to bone marrow. Blood. 2004;104(9):2643-5.
114. Ji JF, He BP, Dheen ST, Tay SS. Interactions of chemokines and chemokine receptors mediate the migration of mesenchymal stem cells to the impaired site in the brain after hypoglossal nerve injury. Stem Cells. 2004;22(3):415-27.
115. Togel F, Hu Z, Weiss K, Isaac J, Lange C, Westenfelder C. Administered mesenchymal stem cells protect against ischemic acute renal failure through differentiation-independent mechanisms. American journal of physiology Renal physiology. 2005;289(1):F31-42.
116. Gnecchi M, He H, Liang OD, Melo LG, Morello F, Mu H, et al. Paracrine action accounts for marked protection of ischemic heart by Akt-modified mesenchymal stem cells. Nature medicine. 2005;11(4):367-8.

117. Haynesworth SE, Baber MA, Caplan AI. Cytokine expression by human marrow-derived mesenchymal progenitor cells in vitro: effects of dexamethasone and IL-1 alpha. Journal of cellular physiology. 1996;166(3):585-92.
118. Tang YL, Zhao Q, Zhang YC, Cheng L, Liu M, Shi J, et al. Autologous mesenchymal stem cell transplantation induce VEGF and neovascularization in ischemic myocardium. Regulatory peptides. 2004;117(1):3-10.
119. Rehman J, Traktuev D, Li J, Merfeld-Clauss S, Temm-Grove CJ, Bovenkerk JE, et al. Secretion of angiogenic and antiapoptotic factors by human adipose stromal cells. Circulation. 2004;109(10):1292-8.
120. Kinnaird T, Stabile E, Burnett MS, Shou M, Lee CW, Barr S, et al. Local delivery of marrow-derived stromal cells augments collateral perfusion through paracrine mechanisms. Circulation. 2004;109(12):1543-9.
121. Zhu W, Chen J, Cong X, Hu S, Chen X. Hypoxia and serum deprivation-induced apoptosis in mesenchymal stem cells. Stem Cells. 2006;24(2):416-25.
122. Matzinger P. Tolerance, danger, and the extended family. Annual review of immunology. 1994;12:991-1045.
123. Stewart CR, Stuart LM, Wilkinson K, van Gils JM, Deng J, Halle A, et al. CD36 ligands promote sterile inflammation through assembly of a Toll-like receptor 4 and 6 heterodimer. Nature immunology. 2010;11(2):155-61.
124. Kawai T, Akira S. The role of pattern-recognition receptors in innate immunity: update on Toll-like receptors. Nature immunology. 2010;11(5):373-84.
125. Liotta F, Angeli R, Cosmi L, Fili L, Manuelli C, Frosali F, et al. Toll-like receptors 3 and 4 are expressed by human bone marrow-derived mesenchymal stem cells and can inhibit their T-cell modulatory activity by impairing Notch signaling. Stem Cells. 2008;26(1):279-89.
126. Hwa Cho H, Bae YC, Jung JS. Role of toll-like receptors on human adipose-derived stromal cells. Stem Cells. 2006;24(12):2744-52.
127. Akira S, Takeda K. Toll-like receptor signalling. Nature reviews Immunology. 2004;4(7):499-511.
128. Morgan MJ, Liu ZG. Crosstalk of reactive oxygen species and NF-kappaB signaling. Cell research. 2011;21(1):103-15.
129. Liu SP, Ding DC, Wang HJ, Su CY, Lin SZ, Li H, et al. Nonsenescent Hsp27-upregulated MSCs implantation promotes neuroplasticity in stroke model. Cell transplantation. 2010;19(10):1261-79.
130. Choi H, Lee RH, Bazhanov N, Oh JY, Prockop DJ. Anti-inflammatory protein TSG-6 secreted by activated MSCs attenuates zymosan-induced mouse peritonitis by decreasing TLR2/NF-kappaB signaling in resident macrophages. Blood. 2011;118(2):330-8.
131. Prockop DJ, Oh JY. Mesenchymal stem/stromal cells (MSCs): role as guardians of inflammation. Molecular therapy: the journal of the American Society of Gene Therapy. 2012;20(1):14-20.
132. Banas A, Teratani T, Yamamoto Y, Tokuhara M, Takeshita F, Osaki M, et al. IFATS collection: in vivo therapeutic potential of human adipose tissue mesenchymal stem

cells after transplantation into mice with liver injury. Stem Cells. 2008;26(10):2705-12.

133. Spees JL, Olson SD, Whitney MJ, Prockop DJ. Mitochondrial transfer between cells can rescue aerobic respiration. Proceedings of the National Academy of Sciences of the United States of America. 2006;103(5):1283-8.
134. Wang X, Gerdes HH. Transfer of mitochondria via tunneling nanotubes rescues apoptotic PC12 cells. Cell Death Differ. 2015;22(7):1181-91.
135. Rustom A, Saffrich R, Markovic I, Walther P, Gerdes HH. Nanotubular highways for intercellular organelle transport. Science. 2004;303(5660):1007-10.
136. Marzo L, Gousset K, Zurzolo C. Multifaceted roles of tunneling nanotubes in intercellular communication. Front Physiol. 2012;3:72.
137. Cselenyak A, Pankotai E, Horvath EM, Kiss L, Lacza Z. Mesenchymal stem cells rescue cardiomyoblasts from cell death in an in vitro ischemia model via direct cell-to-cell connections. BMC cell biology. 2010;11:29.
138. Wang Y, Huang L, Abdelrahim M, Cai Q, Truong A, Bick R, et al. Stanniocalcin-1 suppresses superoxide generation in macrophages through induction of mitochondrial UCP2. Journal of leukocyte biology. 2009;86(4):981-8.
139. Mates JM, Perez-Gomez C, Nunez de Castro I. Antioxidant enzymes and human diseases. Clinical biochemistry. 1999;32(8):595-603.
140. Mates JM. Effects of antioxidant enzymes in the molecular control of reactive oxygen species toxicology. Toxicology. 2000;153(1-3):83-104.
141. Takeda M, Shirato I, Kobayashi M, Endou H. Hydrogen peroxide induces necrosis, apoptosis, oncosis and apoptotic oncosis of mouse terminal proximal straight tubule cells. Nephron. 1999;81(2):234-8.
142. Saito Y, Nishio K, Ogawa Y, Kimata J, Kinumi T, Yoshida Y, et al. Turning point in apoptosis/necrosis induced by hydrogen peroxide. Free radical research. 2006;40(6):619-30.
143. Rhee SG, Bae YS, Lee SR, Kwon J. Hydrogen peroxide: a key messenger that modulates protein phosphorylation through cysteine oxidation. Science's STKE: signal transduction knowledge environment. 2000;2000(53):pe1.
144. Ohba M, Shibanuma M, Kuroki T, Nose K. Production of hydrogen peroxide by transforming growth factor-beta 1 and its involvement in induction of egr-1 in mouse osteoblastic cells. The Journal of cell biology. 1994;126(4):1079-88.
145. Lo YY, Wong JM, Cruz TF. Reactive oxygen species mediate cytokine activation of c-Jun NH2-terminal kinases. The Journal of biological chemistry. 1996;271(26):15703-7.
146. Cadenas E, Boveris A, Ragan CI, Stoppani AO. Production of superoxide radicals and hydrogen peroxide by NADH-ubiquinone reductase and ubiquinol-cytochrome c reductase from beef-heart mitochondria. Archives of biochemistry and biophysics. 1977;180(2):248-57.
147. Liu Y, Fiskum G, Schubert D. Generation of reactive oxygen species by the mitochondrial electron transport chain. Journal of neurochemistry. 2002;80(5):780-7.
148. Loschen G, Azzi A, Richter C, Flohe L. Superoxide radicals as precursors of mitochondrial hydrogen peroxide. FEBS letters. 1974;42(1):68-72.

149. Brand MD. The sites and topology of mitochondrial superoxide production. Experimental gerontology. 2010;45(7-8):466-72.
150. Turrens JF, Alexandre A, Lehninger AL. Ubisemiquinone is the electron donor for superoxide formation by complex III of heart mitochondria. Archives of biochemistry and biophysics. 1985;237(2):408-14.
151. Trenam CW, Blake DR, Morris CJ. Skin inflammation: reactive oxygen species and the role of iron. The Journal of investigative dermatology. 1992;99(6):675-82.
152. Mates JM, Sanchez-Jimenez FM. Role of reactive oxygen species in apoptosis: implications for cancer therapy. The international journal of biochemistry & cell biology. 2000;32(2):157-70.
153. Segal AW, Jones OT. Novel cytochrome b system in phagocytic vacuoles of human granulocytes. Nature. 1978;276(5687):515-7.
154. Piccoli C, Ria R, Scrima R, Cela O, D'Aprile A, Boffoli D, et al. Characterization of mitochondrial and extra-mitochondrial oxygen consuming reactions in human hematopoietic stem cells. Novel evidence of the occurrence of NAD(P)H oxidase activity. The Journal of biological chemistry. 2005;280(28):26467-76.
155. Park SG, Kim JH, Xia Y, Sung JH. Generation of reactive oxygen species in adipose-derived stem cells: friend or foe? Expert opinion on therapeutic targets. 2011;15(11):1297-306.
156. Kim JH, Park SH, Park SG, Choi JS, Xia Y, Sung JH. The pivotal role of reactive oxygen species generation in the hypoxia-induced stimulation of adipose-derived stem cells. Stem cells and development. 2011;20(10):1753-61.
157. Ushio-Fukai M, Urao N. Novel role of NADPH oxidase in angiogenesis and stem/progenitor cell function. Antioxidants & redox signaling. 2009;11(10):2517-33.
158. Battino M, Ferri E, Gorini A, Villa RF, Rodriguez Huertas JF, Fiorella P, et al. Natural distribution and occurrence of coenzyme Q homologues. Membrane biochemistry. 1990;9(3):179-90.
159. Cornell BA, Keniry MA, Post A, Robertson RN, Weir LE, Westerman PW. Location and activity of ubiquinone 10 and ubiquinone analogues in model and biological membranes. Biochemistry. 1987;26(24):7702-7.
160. Turunen M, Wehlin L, Sjoberg M, Lundahl J, Dallner G, Brismar K, et al. beta2-Integrin and lipid modifications indicate a non-antioxidant mechanism for the anti-atherogenic effect of dietary coenzyme Q10. Biochemical and biophysical research communications. 2002;296(2):255-60.
161. Dallner G, Sindelar PJ. Regulation of ubiquinone metabolism. Free radical biology & medicine. 2000;29(3-4):285-94.
162. Ernster L, Dallner G. Biochemical, physiological and medical aspects of ubiquinone function. Biochimica et biophysica acta. 1995;1271(1):195-204.
163. Villalba JM, Navas P. Plasma membrane redox system in the control of stress-induced apoptosis. Antioxidants & redox signaling. 2000;2(2):213-30.
164. Witort EJ, Pattarino J, Papucci L, Schiavone N, Donnini M, Lapucci A, et al. Autologous lipofilling: coenzyme Q10 can rescue adipocytes from stress-induced apoptotic death. Plastic and reconstructive surgery. 2007;119(4):1191-9.

165. Abe J, Berk BC. Reactive oxygen species as mediators of signal transduction in cardiovascular disease. Trends in cardiovascular medicine. 1998;8(2):59-64.
166. Wojcicki J, Rozewicka L, Barcew-Wiszniewska B, Samochowiec L, Juzwiak S, Kadlubowska D, et al. Effect of selenium and vitamin E on the development of experimental atherosclerosis in rabbits. Atherosclerosis. 1991;87(1):9-16.
167. Rosen DR, Siddique T, Patterson D, Figlewicz DA, Sapp P, Hentati A, et al. Mutations in Cu/Zn superoxide dismutase gene are associated with familial amyotrophic lateral sclerosis. Nature. 1993;362(6415):59-62.
168. Sano M, Ernesto C, Thomas RG, Klauber MR, Schafer K, Grundman M, et al. A controlled trial of selegiline, alpha-tocopherol, or both as treatment for Alzheimer's disease. The Alzheimer's Disease Cooperative Study. The New England journal of medicine. 1997;336(17):1216-22.
169. Parker WD, Jr., Boyson SJ, Parks JK. Abnormalities of the electron transport chain in idiopathic Parkinson's disease. Annals of neurology. 1989;26(6):719-23.
170. Sun AY, Chen YM. Oxidative stress and neurodegenerative disorders. Journal of biomedical science. 1998;5(6):401-14.
171. Harman D. Aging: a theory based on free radical and radiation chemistry. Journal of gerontology. 1956;11(3):298-300.
172. Guyton KZ, Kensler TW. Oxidative mechanisms in carcinogenesis. British medical bulletin. 1993;49(3):523-44.
173. Sauer H, Wartenberg M, Hescheler J. Reactive oxygen species as intracellular messengers during cell growth and differentiation. Cellular physiology and biochemistry: international journal of experimental cellular physiology, biochemistry, and pharmacology. 2001;11(4):173-86.
174. Valle-Prieto A, Conget PA. Human mesenchymal stem cells efficiently manage oxidative stress. Stem cells and development. 2010;19(12):1885-93.
175. Lee JY, Qu-Petersen Z, Cao B, Kimura S, Jankowski R, Cummins J, et al. Clonal isolation of muscle-derived cells capable of enhancing muscle regeneration and bone healing. The Journal of cell biology. 2000;150(5):1085-100.
176. Scadden DT. The stem-cell niche as an entity of action. Nature. 2006;441(7097):1075-9.
177. Schofield R. The relationship between the spleen colony-forming cell and the haemopoietic stem cell. Blood cells. 1978;4(1-2):7-25.
178. Discher DE, Mooney DJ, Zandstra PW. Growth factors, matrices, and forces combine and control stem cells. Science. 2009;324(5935):1673-7.
179. Lennon DP, Edmison JM, Caplan AI. Cultivation of rat marrow-derived mesenchymal stem cells in reduced oxygen tension: effects on in vitro and in vivo osteochondrogenesis. Journal of cellular physiology. 2001;187(3):345-55.
180. Kanichai M, Ferguson D, Prendergast PJ, Campbell VA. Hypoxia promotes chondrogenesis in rat mesenchymal stem cells: a role for AKT and hypoxia-inducible factor (HIF)-1alpha. Journal of cellular physiology. 2008;216(3):708-15.
181. Ishikawa Y, Ito T. Kinetics of hemopoietic stem cells in a hypoxic culture. European journal of haematology. 1988;40(2):126-9.

182. Chow DC, Wenning LA, Miller WM, Papoutsakis ET. Modeling pO(2) distributions in the bone marrow hematopoietic compartment. II. Modified Kroghian models. Biophysical journal. 2001;81(2):685-96.
183. Harrison JS, Rameshwar P, Chang V, Bandari P. Oxygen saturation in the bone marrow of healthy volunteers. Blood. 2002;99(1):394.
184. Pasarica M, Sereda OR, Redman LM, Albarado DC, Hymel DT, Roan LE, et al. Reduced adipose tissue oxygenation in human obesity: evidence for rarefaction, macrophage chemotaxis, and inflammation without an angiogenic response. Diabetes. 2009;58(3):718-25.
185. Rodesch F, Simon P, Donner C, Jauniaux E. Oxygen measurements in endometrial and trophoblastic tissues during early pregnancy. Obstetrics and gynecology. 1992;80(2):283-5.
186. Gu YZ, Hogenesch JB, Bradfield CA. The PAS superfamily: sensors of environmental and developmental signals. Annual review of pharmacology and toxicology. 2000;40:519-61.
187. Tian H, McKnight SL, Russell DW. Endothelial PAS domain protein 1 (EPAS1), a transcription factor selectively expressed in endothelial cells. Genes & development. 1997;11(1):72-82.
188. Wiesener MS, Jurgensen JS, Rosenberger C, Scholze CK, Horstrup JH, Warnecke C, et al. Widespread hypoxia-inducible expression of HIF-2alpha in distinct cell populations of different organs. FASEB journal: official publication of the Federation of American Societies for Experimental Biology. 2003;17(2):271-3.
189. Gu YZ, Moran SM, Hogenesch JB, Wartman L, Bradfield CA. Molecular characterization and chromosomal localization of a third alpha-class hypoxia inducible factor subunit, HIF3alpha. Gene expression. 1998;7(3):205-13.
190. Iyer NV, Kotch LE, Agani F, Leung SW, Laughner E, Wenger RH, et al. Cellular and developmental control of O2 homeostasis by hypoxia-inducible factor 1 alpha. Genes & development. 1998;12(2):149-62.
191. Kaelin WG, Jr., Ratcliffe PJ. Oxygen sensing by metazoans: the central role of the HIF hydroxylase pathway. Molecular cell. 2008;30(4):393-402.
192. Maxwell PH, Wiesener MS, Chang GW, Clifford SC, Vaux EC, Cockman ME, et al. The tumour suppressor protein VHL targets hypoxia-inducible factors for oxygen-dependent proteolysis. Nature. 1999;399(6733):271-5.
193. Lando D, Peet DJ, Gorman JJ, Whelan DA, Whitelaw ML, Bruick RK. FIH-1 is an asparaginyl hydroxylase enzyme that regulates the transcriptional activity of hypoxia-inducible factor. Genes & development. 2002;16(12):1466-71.
194. Gu J, Milligan J, Huang LE. Molecular mechanism of hypoxia-inducible factor 1alpha - p300 interaction. A leucine-rich interface regulated by a single cysteine. The Journal of biological chemistry. 2001;276(5):3550-4.
195. Elvidge GP, Glenny L, Appelhoff RJ, Ratcliffe PJ, Ragoussis J, Gleadle JM. Concordant regulation of gene expression by hypoxia and 2-oxoglutarate-dependent dioxygenase inhibition: the role of HIF-1alpha, HIF-2alpha, and other pathways. The Journal of biological chemistry. 2006;281(22):15215-26.

196. Nathan C. Immunology: Oxygen and the inflammatory cell. Nature. 2003;422(6933):675-6.
197. Cramer T, Yamanishi Y, Clausen BE, Forster I, Pawlinski R, Mackman N, et al. HIF-1alpha is essential for myeloid cell-mediated inflammation. Cell. 2003;112(5):645-57.
198. Hartmann G, Tschop M, Fischer R, Bidlingmaier C, Riepl R, Tschop K, et al. High altitude increases circulating interleukin-6, interleukin-1 receptor antagonist and C-reactive protein. Cytokine. 2000;12(3):246-52.
199. Karhausen J, Furuta GT, Tomaszewski JE, Johnson RS, Colgan SP, Haase VH. Epithelial hypoxia-inducible factor-1 is protective in murine experimental colitis. The Journal of clinical investigation. 2004;114(8):1098-106.
200. Chen LW, Egan L, Li ZW, Greten FR, Kagnoff MF, Karin M. The two faces of IKK and NF-kappaB inhibition: prevention of systemic inflammation but increased local injury following intestinal ischemia-reperfusion. Nature medicine. 2003;9(5):575-81.
201. Bruder SP, Jaiswal N, Haynesworth SE. Growth kinetics, self-renewal, and the osteogenic potential of purified human mesenchymal stem cells during extensive subcultivation and following cryopreservation. Journal of cellular biochemistry. 1997;64(2):278-94.
202. Grayson WL, Zhao F, Bunnell B, Ma T. Hypoxia enhances proliferation and tissue formation of human mesenchymal stem cells. Biochemical and biophysical research communications. 2007;358(3):948-53.
203. Hung SP, Ho JH, Shih YR, Lo T, Lee OK. Hypoxia promotes proliferation and osteogenic differentiation potentials of human mesenchymal stem cells. Journal of orthopaedic research: official publication of the Orthopaedic Research Society. 2012;30(2):260-6.
204. Grayson WL, Zhao F, Izadpanah R, Bunnell B, Ma T. Effects of hypoxia on human mesenchymal stem cell expansion and plasticity in 3D constructs. Journal of cellular physiology. 2006;207(2):331-9.
205. Tamama K, Kawasaki H, Kerpedjieva SS, Guan J, Ganju RK, Sen CK. Differential roles of hypoxia inducible factor subunits in multipotential stromal cells under hypoxic condition. Journal of cellular biochemistry. 2011;112(3):804-17.
206. Fehrer C, Brunauer R, Laschober G, Unterluggauer H, Reitinger S, Kloss F, et al. Reduced oxygen tension attenuates differentiation capacity of human mesenchymal stem cells and prolongs their lifespan. Aging cell. 2007;6(6):745-57.
207. Hubbi ME, Kshitiz, Gilkes DM, Rey S, Wong CC, Luo W, et al. A nontranscriptional role for HIF-1alpha as a direct inhibitor of DNA replication. Sci Signal. 2013;6(262):ra10.
208. Forristal CE, Winkler IG, Nowlan B, Barbier V, Walkinshaw G, Levesque JP. Pharmacologic stabilization of HIF-1alpha increases hematopoietic stem cell quiescence in vivo and accelerates blood recovery after severe irradiation. Blood. 2013;121(5):759-69.
209. Hu X, Yu SP, Fraser JL, Lu Z, Ogle ME, Wang JA, et al. Transplantation of hypoxia-preconditioned mesenchymal stem cells improves infarcted heart function via enhanced survival of implanted cells and angiogenesis. The Journal of thoracic and cardiovascular surgery. 2008;135(4):799-808.

210. Danforth E, Jr. Failure of adipocyte differentiation causes type II diabetes mellitus? Nature genetics. 2000;26(1):13.
211. Yang X, Jansson PA, Nagaev I, Jack MM, Carvalho E, Sunnerhagen KS, et al. Evidence of impaired adipogenesis in insulin resistance. Biochemical and biophysical research communications. 2004;317(4):1045-51.
212. Christodoulides C, Lagathu C, Sethi JK, Vidal-Puig A. Adipogenesis and WNT signalling. Trends in endocrinology and metabolism: TEM. 2009;20(1):16-24.
213. Rosen ED, MacDougald OA. Adipocyte differentiation from the inside out. Nature reviews Molecular cell biology. 2006;7(12):885-96.
214. Gregoire FM, Smas CM, Sul HS. Understanding adipocyte differentiation. Physiological reviews. 1998;78(3):783-809.
215. Samuelsson L, Stromberg K, Vikman K, Bjursell G, Enerback S. The CCAAT/enhancer binding protein and its role in adipocyte differentiation: evidence for direct involvement in terminal adipocyte development. The EMBO journal. 1991;10(12):3787-93.
216. Wu Z, Bucher NL, Farmer SR. Induction of peroxisome proliferator-activated receptor gamma during the conversion of 3T3 fibroblasts into adipocytes is mediated by C/EBPbeta, C/EBPdelta, and glucocorticoids. Molecular and cellular biology. 1996;16(8):4128-36.
217. Farmer SR. Transcriptional control of adipocyte formation. Cell metabolism. 2006;4(4):263-73.
218. Student AK, Hsu RY, Lane MD. Induction of fatty acid synthetase synthesis in differentiating 3T3-L1 preadipocytes. The Journal of biological chemistry. 1980;255(10):4745-50.
219. Green H, Kehinde O. An established preadipose cell line and its differentiation in culture. II. Factors affecting the adipose conversion. Cell. 1975;5(1):19-27.
220. Lillie RDA, L. L. . Supersaturated solutions of fat stains in dilute isopropanol for demonstration of acute fatty degeneration not shown by Herxheimer's technique. Arch Pathol. 1943.
221. Greenspan P, Mayer EP, Fowler SD. Nile red: a selective fluorescent stain for intracellular lipid droplets. The Journal of cell biology. 1985;100(3):965-73.
222. Fowler SD, Greenspan P. Application of Nile red, a fluorescent hydrophobic probe, for the detection of neutral lipid deposits in tissue sections: comparison with oil red O. The journal of histochemistry and cytochemistry: official journal of the Histochemistry Society. 1985;33(8):833-6.
223. Greenspan P, Fowler SD. Spectrofluorometric studies of the lipid probe, nile red. Journal of lipid research. 1985;26(7):781-9.
224. Cousin B, Munoz O, Andre M, Fontanilles AM, Dani C, Cousin JL, et al. A role for preadipocytes as macrophage-like cells. FASEB journal: official publication of the Federation of American Societies for Experimental Biology. 1999;13(2):305-12.
225. Zhang Y, Proenca R, Maffei M, Barone M, Leopold L, Friedman JM. Positional cloning of the mouse obese gene and its human homologue. Nature. 1994;372(6505):425-32.

226. Trayhurn P, Beattie JH. Physiological role of adipose tissue: white adipose tissue as an endocrine and secretory organ. The Proceedings of the Nutrition Society. 2001;60(3):329-39.
227. Lau DC, Dhillon B, Yan H, Szmitko PE, Verma S. Adipokines: molecular links between obesity and atheroslcerosis. American journal of physiology Heart and circulatory physiology. 2005;288(5):H2031-41.
228. Nedergaard J, Bengtsson T, Cannon B. Unexpected evidence for active brown adipose tissue in adult humans. American journal of physiology Endocrinology and metabolism. 2007;293(2):E444-52.
229. Koppen A, Kalkhoven E. Brown vs white adipocytes: the PPARgamma coregulator story. FEBS letters. 2010;584(15):3250-9.
230. Cousin B, Casteilla L, Dani C, Muzzin P, Revelli JP, Penicaud L. Adipose tissues from various anatomical sites are characterized by different patterns of gene expression and regulation. The Biochemical journal. 1993;292 (Pt 3):873-6.
231. Vidal H. Gene expression in visceral and subcutaneous adipose tissues. Annals of medicine. 2001;33(8):547-55.
232. Linder K, Arner P, Flores-Morales A, Tollet-Egnell P, Norstedt G. Differentially expressed genes in visceral or subcutaneous adipose tissue of obese men and women. Journal of lipid research. 2004;45(1):148-54.
233. Starr ME, Evers BM, Saito H. Age-associated increase in cytokine production during systemic inflammation: adipose tissue as a major source of IL-6. The journals of gerontology Series A, Biological sciences and medical sciences. 2009;64(7):723-30.
234. Hotamisligil GS, Arner P, Caro JF, Atkinson RL, Spiegelman BM. Increased adipose tissue expression of tumor necrosis factor-alpha in human obesity and insulin resistance. The Journal of clinical investigation. 1995;95(5):2409-15.
235. Hotamisligil GS, Shargill NS, Spiegelman BM. Adipose expression of tumor necrosis factor-alpha: direct role in obesity-linked insulin resistance. Science. 1993;259(5091):87-91.
236. Carriere A, Ebrahimian TG, Dehez S, Auge N, Joffre C, Andre M, et al. Preconditioning by mitochondrial reactive oxygen species improves the proangiogenic potential of adipose-derived cells-based therapy. Arteriosclerosis, thrombosis, and vascular biology. 2009;29(7):1093-9.
237. Carriere A, Fernandez Y, Rigoulet M, Penicaud L, Casteilla L. Inhibition of preadipocyte proliferation by mitochondrial reactive oxygen species. FEBS letters. 2003;550(1-3):163-7.
238. Pessler-Cohen D, Pekala PH, Kovsan J, Bloch-Damti A, Rudich A, Bashan N. GLUT4 repression in response to oxidative stress is associated with reciprocal alterations in C/EBP alpha and delta isoforms in 3T3-L1 adipocytes. Archives of physiology and biochemistry. 2006;112(1):3-12.
239. Carriere A, Carmona MC, Fernandez Y, Rigoulet M, Wenger RH, Penicaud L, et al. Mitochondrial reactive oxygen species control the transcription factor CHOP-10/GADD153 and adipocyte differentiation: a mechanism for hypoxia-dependent effect. The Journal of biological chemistry. 2004;279(39):40462-9.

240. Tormos KV, Anso E, Hamanaka RB, Eisenbart J, Joseph J, Kalyanaraman B, et al. Mitochondrial complex III ROS regulate adipocyte differentiation. Cell metabolism. 2011;14(4):537-44.
241. Higuchi M, Dusting GJ, Peshavariya H, Jiang F, Hsiao ST, Chan EC, et al. Differentiation of human adipose-derived stem cells into fat involves reactive oxygen species and Forkhead box O1 mediated upregulation of antioxidant enzymes. Stem cells and development. 2013;22(6):878-88.
242. Kanda Y, Hinata T, Kang SW, Watanabe Y. Reactive oxygen species mediate adipocyte differentiation in mesenchymal stem cells. Life sciences. 2011;89(7-8):250-8.
243. Schroder K, Wandzioch K, Helmcke I, Brandes RP. Nox4 acts as a switch between differentiation and proliferation in preadipocytes. Arteriosclerosis, thrombosis, and vascular biology. 2009;29(2):239-45.
244. May JM, de Haen C. The insulin-like effect of hydrogen peroxide on pathways of lipid synthesis in rat adipocytes. The Journal of biological chemistry. 1979;254(18):9017-21.
245. Lee H, Lee YJ, Choi H, Ko EH, Kim JW. Reactive oxygen species facilitate adipocyte differentiation by accelerating mitotic clonal expansion. The Journal of biological chemistry. 2009;284(16):10601-9.
246. Krautbauer S, Eisinger K, Hader Y, Neumeier M, Buechler C. Manganese superoxide dismutase knock-down in 3T3-L1 preadipocytes impairs subsequent adipogenesis. Molecular and cellular biochemistry. 2014;393(1-2):69-76.
247. Yan H, Aziz E, Shillabeer G, Wong A, Shanghavi D, Kermouni A, et al. Nitric oxide promotes differentiation of rat white preadipocytes in culture. Journal of lipid research. 2002;43(12):2123-9.
248. Yun Z, Maecker HL, Johnson RS, Giaccia AJ. Inhibition of PPAR gamma 2 gene expression by the HIF-1-regulated gene DEC1/Stra13: a mechanism for regulation of adipogenesis by hypoxia. Developmental cell. 2002;2(3):331-41.
249. Kim KH, Song MJ, Chung J, Park H, Kim JB. Hypoxia inhibits adipocyte differentiation in a HDAC-independent manner. Biochemical and biophysical research communications. 2005;333(4):1178-84.
250. Lin Q, Lee YJ, Yun Z. Differentiation arrest by hypoxia. The Journal of biological chemistry. 2006;281(41):30678-83.
251. Park YK, Park H. Prevention of CCAAT/enhancer-binding protein beta DNA binding by hypoxia during adipogenesis. The Journal of biological chemistry. 2010;285(5):3289-99.
252. Fink T, Abildtrup L, Fogd K, Abdallah BM, Kassem M, Ebbesen P, et al. Induction of adipocyte-like phenotype in human mesenchymal stem cells by hypoxia. Stem Cells. 2004;22(7):1346-55.
253. Valorani MG, Montelatici E, Germani A, Biddle A, D'Alessandro D, Strollo R, et al. Pre-culturing human adipose tissue mesenchymal stem cells under hypoxia increases their adipogenic and osteogenic differentiation potentials. Cell proliferation. 2012;45(3):225-38.

254. Covello KL, Kehler J, Yu H, Gordan JD, Arsham AM, Hu CJ, et al. HIF-2alpha regulates Oct-4: effects of hypoxia on stem cell function, embryonic development, and tumor growth. Genes & development. 2006;20(5):557-70.
255. Rosova I, Dao M, Capoccia B, Link D, Nolta JA. Hypoxic preconditioning results in increased motility and improved therapeutic potential of human mesenchymal stem cells. Stem Cells. 2008;26(8):2173-82.
256. Floyd ZE, Kilroy G, Wu X, Gimble JM. Effects of prolyl hydroxylase inhibitors on adipogenesis and hypoxia inducible factor 1 alpha levels under normoxic conditions. Journal of cellular biochemistry. 2007;101(6):1545-57.
257. Kim J, Kwak HJ, Cha JY, Jeong YS, Rhee SD, Cheon HG. The role of prolyl hydroxylase domain protein (PHD) during rosiglitazone-induced adipocyte differentiation. The Journal of biological chemistry. 2014;289(5):2755-64.
258. Irwin R, LaPres JJ, Kinser S, McCabe LR. Prolyl-hydroxylase inhibition and HIF activation in osteoblasts promotes an adipocytic phenotype. Journal of cellular biochemistry. 2007;100(3):762-72.

> Imagination is more important than knowledge. Knowledge is limited. Imagination encircles the world.
>
> - Albert Einstein

Chapter 2

Research questions

The questions that were addressed in this dissertation were:

1. How can we measure ROS in MSC cultures?
2. Does modulation of ROS via the addition of a pro- or anti-oxidant to primary cultures affect differentiation of MSCs into adipocytes?
3. Does artificial hypoxia affect the adipogenic differentiation potential of MSCs?

Aim

The proposed project aims to assess the effects that hydrogen peroxide (H_2O_2) and the antioxidants, Trolox and CoQ10, have on the differentiation of MSCs into adipocytes under normoxic conditions as well as the effect of artificial hypoxia on the differentiation of MSCs into adipocytes.

Hypothesis

Reactive oxygen species will enhance adipogenesis and artificial hypoxia will diminish the adipogenic potential of MSCs *in vitro*.

Objectives

a. To determine the concentrations of ROS, antioxidants, and DMOG to be used to test for their effects on long term MSC cultures and cultures induced to differentiate into adipocytes.
b. To measure the levels of ROS using MitoSOX™ Red mitochondrial superoxide indicator.
c. To assess MSC phenotypic markers using flow cytometry.
d. To measure cell viability via the MTT and SRB assays.
e. To assess for adipogenic differentiation under the different conditions and to characterize this differentiation quantitatively using Nile Red and qualitatively using Oil Red O staining.
f. To assess for osteogenic differentiation qualitatively using Alizarin Red stain.

g. To assess for chondrogenic differentiation qualitatively using the micromass pellet culture technique, and histological assessment using Toluidine Blue O stain.

In science one tries to tell people, in such a way as to be understood by everyone, something that no one ever knew before. But in poetry, it's the exact opposite.

- Paul Dirac

Chapter 3

Characterization of isolated human adipose-derived mesenchymal stromal/stem cells: Phenotypic analysis and tri-lineage differentiation

Introduction

There has been a paradigm shift in the tissue engineering and regenerative medicine field. The idea that a disease or damaged organ could be treated with stem cells has heightened interest in this field. The exponential increase in stem cell research in the last two decades has raised the hope of patients. This is globally attributed to the promise that stem cell-based therapies will cure them of their disease. Unfortunately there are clinics exploiting the hopes of these vulnerable patients and enticing them with the offer of effective stem cell treatments without a substantial scientific foundation. This has jeopardized the progression of honest translational stem cell research. The tissue engineering and regenerative potential of embryonic stem cells (ESCs), nuclear transfer (NT)-ESCs, and induced pluripotent stem (iPS) cells has, understandably, lead to much excitement. Limitations to their practical use include ethical concerns and legal regulations.

Mesenchymal stromal cells (MSCs) contain a sub-population of adult stem cells that display promising potential in the field of cell-based therapy and regenerative medicine. Adult stem cells are multipotent cells that have the ability to differentiate into a limited number of cell types characteristic of the embryonic germ layer of origin (1). Mesenchymal stromal cells are a heterogeneous group of cells, first discovered in 1867 that have become a fundamental point of focus in stem cell research. Adult stem cells have tremendous potential to be applied in a large number of unrelated disorders. Studies on MSCs range from their isolation, characterization, differentiation potential and their *in vivo* competencies. Mesenchymal stromal cells were investigated for clinical safety as early as 1995 and have since been studied in numerous clinical trials. It is the plasticity to generate cells of different lineages and the paracrine effects of adult stem cells that are being exploited. The need for Good

Manufacturing Practice (GMP) and pre-clinical data is tantamount to success in this research area.

The definition of a stem cell is that it has the ability to self-renew and the capacity to undergo differentiation. The ideal stem cell should be found in abundant quantities, harvested by a minimally invasive route, and should have the ability to differentiate along multiple cell lineages in a reproducible manner. From a clinical aspect, additionally, a stem cell should be safe to transplant into either an autologous or allogeneic host and can be manufactured in accordance with current GMP guidelines (2). Bone marrow was the original and main source of multipotent adult stem cells to be investigated (1). Literature states that a draw-back of using bone marrow-derived MSCs for therapeutic purposes is that their differentiation capabilities decline with age and thus perhaps the therapeutic potential decreases as well (3, 4). A second source of adult stem cells is adipose tissue which is advantageous because larger quantities can be obtained with relative ease when compared to bone marrow (5). Alternative sources of stem cells known as neonatal stem cells are from umbilical cord blood (6) and the Wharton's jelly of the umbilical cord (7). These mesenchymal-like cells are obtained via a less invasive manner and pose no risk to the baby or mother. The numbers of cells obtained, however, are fewer, but it is said that these neonatal stem cells are rapidly self-renewing and can be expanded over a longer period of time than MSCs from bone marrow (6, 8).

The International Society for Cellular Therapy (ISCT) states that the proper term for mesenchymal stem cell is "multipotent mesenchymal stromal cell". Despite this term gaining popular use, the International Federation for Adipose Therapeutics and Science (IFATS) and the ISCT released a joint statement in 2013 defining that stromal cells obtained from the stromal vascular fraction (SVF) of adipose tissue should be termed adipose-derived stromal cells (ASCs) (9). Due to the ease of isolation and adequate numbers obtained, ASCs have become a popular alternative choice of adult stem cell to study. The intrinsic properties of these cells make them attractive candidates for clinical and regenerative applications. Adipose-derived stromal cells display an immune-privilege nature and therefore, have the potential to evade immune recognition and rejection by the host's immune system (10, 11). In addition, ASCs have the ability to differentiate into tissues of mesodermal origin. It is well established that ASCs can differentiate into adipose, bone, cartilage, and muscle cells upon *in vitro* induction (12). It has also been shown that once these cells have been transplanted,

they can repair damaged tissues at the site of injury by differentiating into the damaged tissue type (13). An exciting development was the discovery that ASCs can also transdifferentiate into non-mesodermal lineages (14).

A more recent mechanism discovered to be associated with ASCs' function is the ability to secrete growth factors and other molecules that can initiate repair in distant tissues by providing a regenerative microenvironment within an injured or inflamed tissue. This is referred to as the paracrine activity of ASCs and has been successfully demonstrated in several studies (15). Following systemic delivery, these cells purportedly respond to chemical signaling molecules, which are elevated in settings of inflammation. Moving up the concentration gradient, created by a number of cytokines in settings of inflammation or injury, MSCs are able to home to the site of injury where they can mediate repair locally following distant systemic delivery (16, 17). ASCs, however, have been discovered to lack some cell surface markers involved in homing. Mesenchymal stromal cells isolated from the bone marrow are CD106 (vascular cell adhesion molecule 1; VCAM-1) positive, but ASCs are CD106 negative. Vascular cell adhesion molecule 1 plays a role in hematopoietic stem cell (HSC) and progenitor cell homing (18). Stromal cell-derived factor-1 (SDF-1) is an important molecule involved in homing. However, Muehlberg and colleagues demonstrated in an *in vivo* study that SDF-1 was secreted by ASCs and promoted the invasion as well as metastasis of breast cancer (19). There have been mixed reports about the effects of ASCs on tumours. This is one area of research that will need to be investigated further for the safe clinical translation of these cells.

The minimal criteria to define ASCs (Figure 3.1) are that they adhere to plastic under standard culture conditions, undergo fibroblastoid colony forming unit (CFU-F) formation and differentiate into osteoblasts, chondrocytes and adipocytes. Further characterization of ASCs is by their expression of cell surface markers and the lack of others (9, 20, 21). Unfortunately there is no cell-surface marker specific for ASCs. Heterogeneous ASC populations can be distinguished from other cell populations due to their lack of hematopoietic characteristic markers and the expression of other common phenotypic markers (20). The expression of markers may vary between tissues. According to the literature, cluster of differentiation (CD) 13, CD29, CD44, CD73, CD90, CD105 (>80% in ASCs) can be considered primary stable positive markers. The primary negative markers can be considered as CD31, CD45, CD235a (<2%). An unstable marker that can be present at

variable levels is CD34 (22). Three commonly characterized surface markers expressed on ASCs appear to be CD73, CD90, and CD105.

Adipose tissue is an abundant and accessible source of stem cells. There are many preclinical studies assuring the safety and efficacy of ASCs and various clinical trials that have revealed the regenerative capability of ASCs. We are in possession of a great deal of knowledge concerning the isolation, characterization, and culture of ASCs. However, standardization of GMP practices, a greater understanding of the mechanisms of differentiation, and an appreciation of the interactions among ASCs, growth factors, and tissues for engineering and regeneration are needed to cross this threshold into clinical therapy. With these concepts in mind, this chapter aimed to characterize these cells and the succeeding chapters present a more in-depth understanding of ASC adipogenic differentiation in terms of disease, inflammation and niche environment.

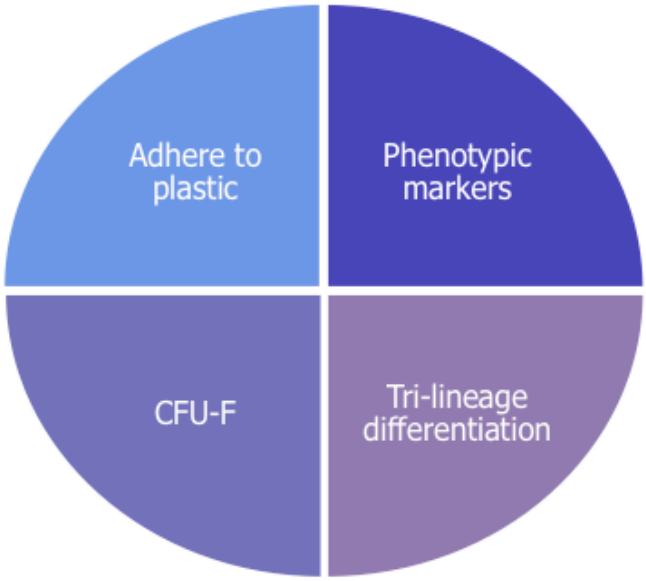

Figure 3.1. Minimal criteria defining adipose-derived stromal cells. The International Federation for Adipose Therapeutics and Science (IFATS) and the International Society for Cellular Therapy (ISCT) released a joint statement of criteria to be met for cells to be considered ASCs. 1) adherence to plastic under standard culture conditions; 2) phenotype positive (>95%) for common MSC surface markers CD73, CD90 and CD105 with the complementary CD44 recommended, and phenotype negative (<2%) for CD45 and CD31. 3) *In vitro* differentiation into the osteogenic, adipogenic, and chondrogenic lineages. The CFU-F assay is recommended. Adherence to these criteria by scientists would help to standardize the protocols used in obtaining the ASCs.

Materials and methods

Consent and confidentiality

Written approval for the following studies was obtained from the Research Ethics Committee of the Faculty of Health Sciences at the University of Pretoria (protocol no: 422-2013) and amendments to the current blanket ethics that was previously obtained in 2010 were approved (protocol no: 218-2010). Prof. Piet Coetzee (Head of Plastic Surgery, Steve Biko Academic Hospital), Dr. Danie Hoffman (private practice in Pretoria), and Dr. Sterna Franzsen (private practice in Pretoria) acquired discarded lipoaspirates from human donors following written informed consent. No personal information, except donor's gender and age, was collected from the participants and lipoaspirate samples were coded to ensure patient anonymity. The nomenclature used is the first letter of the tissue of origin, next the date of surgery (day; month; year), and the participant on that day, for example, A270311/01 (Figure 3.2).

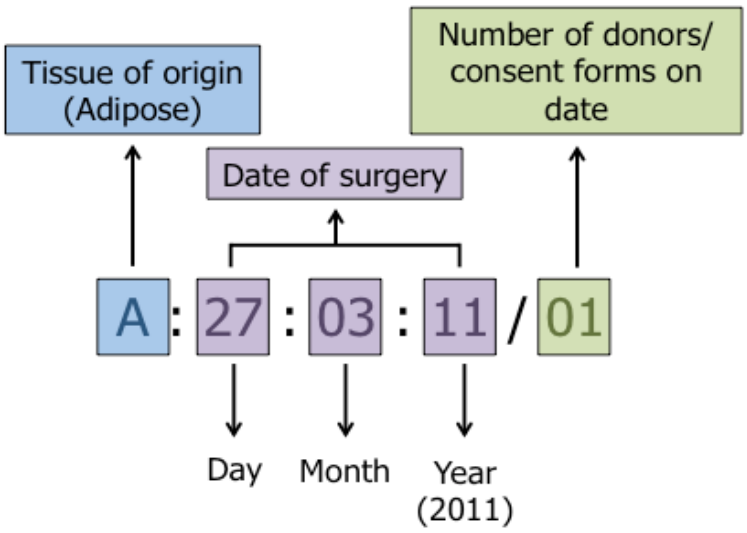

Figure 3.2. Nomenclature used to code donor samples. Nomenclature indicates the tissue of origin, the date of acquisition and the number of donors.

Isolation of the stromal vascular fraction of adipose tissue

Subcutaneous abdominal adipose tissue from 10 female participants of the ages between 20 and 50 years was selected for the entire study. There were five lipoaspirates from which primary cells were previously isolated and cryopreserved and five lipoaspirates from which primary cells were freshly isolated. Liposuction was obtained using a modified Coleman method with dry needle aspiration using a 3 mm blunt-tipped cannula (23). The collected raw lipoaspirates were transferred into 50 ml Corning® CentriStar™ Centrifuge Tubes (Corning Incorporated, New York, USA) with the addition of sterile phosphate buffered saline (PBS) and centrifuged for 3 minutes at 1 152 *g*. The top oil layer of low density that was produced following centrifugation was aspirated. Centrifugation and aspiration of the oil layer were repeated twice more. The second layer consisting of the adipose tissue was transferred into sterile tissue culture dishes (Nunc, Thermo Fisher Scientific, Roskilde, Denmark) and digested with filtered 0.1% (w/v) Collagenase A Type I (Sigma-Aldrich, St Louis, Missouri, USA) prepared in PBS containing 2% (v/v) of the combined antibiotics, Penicillin-Streptomycin mix (Pen/Strep; Sigma-Aldrich). The samples were incubated for 45 minutes at 37°C and 5% CO_2. Dispersion of the collagenase throughout the samples by pipetting using a disposable serological pipette (ALP, Chorges, France) enhanced the dissociation of the adipose tissue. Thus frequent agitation, approximately every 15 minutes, during the incubation period promoted the digestion of the tissue and released the cellular fraction. The digested samples were transferred into new sterile 50 ml CentriStar™ Centrifuge Tubes and centrifuged for 5 minutes at 512 *g*. The centrifuged samples were shaken vigorously and the pellets disrupted to allow the cells to re-disperse. Centrifugation was repeated once more for 5 minutes at 512 *g*. The upper-most layer consisting of adipose tissue and collagenase was removed from each pellet. Any remaining collagenase was neutralized by the addition of Minimum Essential Medium-alpha (α-MEM; Gibco®, Invitrogen Corporation, Carlsbad, California, USA) containing 10% (v/v) fetal bovine serum (FBS; Biochrom AG, Berlin, Germany) and 2% (v/v) Pen/Strep (Gibco®) to every pellet. The FBS is the component that neutralizes the collagenase.

The resuspended pellets in complete α-MEM were transferred to 15 ml CentriStar™ Centrifuge Tubes, followed by washing of the suspensions with PBS. The samples were pipetted up and down several times to disrupt any cell aggregates. The samples were then centrifuged for 5 minutes at 184 *g*. The supernatant of each sample was aspirated carefully

to ensure that the stromal vascular fraction (SVF) cells were not disrupted. The remaining pelleted SVF was resuspended in VersaLyse Lysing Solution® (Beckman Coulter, Krefeld, Germany), which lyses red blood cells, for 10 minutes at room temperature. Once again PBS was added and the samples were centrifuged for 5 minutes at 184 *g*. This was followed by a final wash with PBS containing 2% (v/v) Pen/Strep. The suspension was centrifuged for 5 minutes at 184 *g* and the supernatant removed. The remaining cell pellet was resuspended in a maximum of 2 ml of complete growth medium (α-MEM supplemented with 10%, v/v FBS, and 2%, v/v Pen/Strep). The cell suspension was filtered through a 70 μm Falcon® cell strainer (Becton, Dickinson and Company (BD), Franklin Lakes, New Jersey, USA). The cell strainer was washed with an additional 1 ml of complete growth medium to ensure that all the cells were obtained. The collected cells were counted using flow cytometry and plated in a tissue culture flask (Summarized in Figure 3.3).

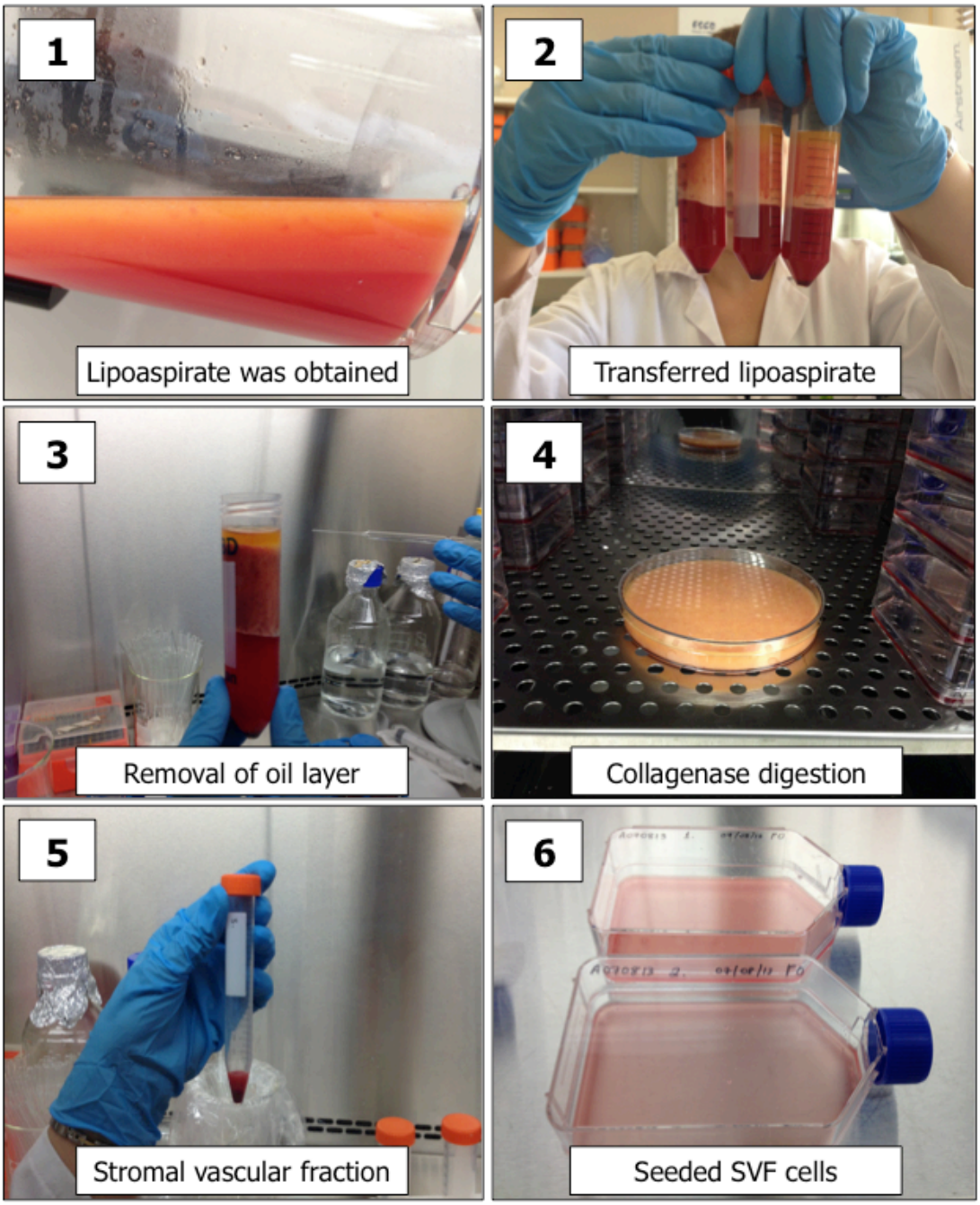

Figure 3.3. Sequential processing of lipoaspirate and isolation of the stromal vascular fraction cells. The principal steps of enzymatic processing of the lipoaspirate. (**1**) Lipoaspirate; (**2**) Lipoaspirate transferred to conical tubes; **(3)** Removal of oil layer; (**4**) Collagenase digestion; (**5**) Acquisition of the stromal vascular fraction (SVF); and (**6**) Seeding of the heterogenous adipose-derived stromal cell (ASC) population into tissue culture flasks.

Expansion and maintenance of human adipose-derived stromal cells in cell culture

Large numbers of ASCs were required for all of the experiments in this study and large numbers of ASCs can be generated by expansion of the cells in tissue culture flasks. The isolated cells were allowed to attach optimally to the plastic surface of the flask for 24 to 96 hours. Following attachment, any contaminating red blood cells, dead cells and cell debris were removed and the conditioned growth medium was replaced with complete growth medium. The isolated cells were cultured for another two days and then the conditioned medium was replenished. The adherent cell cultures were maintained in an incubator at 37°C with a humidified atmosphere containing 5% CO_2. The changing and replenishment of media were carried out every second day until the cells reached ± 80% confluence. These primary cells were defined as "passage 0" (P0). The adherent cells were detached from the flask's plastic surface using Trypsin-EDTA (0.25%, w/v) (Gibco®) and counted using Flow-Count™ Fluorospheres (Beckman Coulter) on a Gallios™ flow cytometer (Beckman Coulter). Following flow cytometric phenotypic confirmation the plastic-adherent cells were now considered ASCs. The ASCs were re-plated at a density of 5 x 10^3 cells/cm^2 in 80 cm^2 Nunclon™ Sphera™ Flasks for expansion (Nunc).

Aliquots of 1 million Trypsin-EDTA-detached primary ASCs that were transferred to cryovials (Greiner Bio-One, Frickenhausen, Germany) were cryopreserved in growth medium supplemented with 10% (v/v) FBS and 10% (v/v) Dimethyl sulfoxide, $(CH_3)_2SO$, (DMSO; Sigma-Aldrich) and placed in a Mr Frosty™ freezing container (Nalgene®, Thermo Fisher Scientific) to slowly freeze in a -80°C freezer for 24 hours. This freezing container reduces the temperature by 1°C per minute (linearized cooling rate), which is optimal for freezing the cells. Dimethyl sulfoxide is a cryoprotectant, which partially solubilizes the cell membrane and interrupts ice lattices, leading to the formation of fewer crystals. The formation of crystals is detrimental because they may puncture the cell membrane leading to cell death. The cryovials were transferred to liquid nitrogen at -196°C after the 24 hours for further storage and subsequent experimentation. Rapid thawing was implemented, when the need for the ASCs arose, as DMSO is toxic to cells at room temperature. The thawed ASCs were transferred into complete growth medium within a sterile 15 ml Centrifuge Tube and centrifuged at 184 *g* for 5 minutes. The DMSO/complete growth medium mix was aspirated and the cell pellet was resuspended in complete growth medium for plating.

Sample preparation for the PROCLEIX ULTRIO Plus® assay

Apart from excess bodily fat or obesity all participants to our knowledge were healthy and isolated ASCs were tested for HIV-1, hepatitis B and C to ensure that only non-infected cells were used for experimentation. The South African National Blood Services (SANBS) in 2011 implemented the Procleix ULTRIO Plus® assay (Novartis Diagnostics, Emeryville, California, USA), to test for HIV-1, hepatitis B and C positivity in human plasma and serum specimens. The Procleix ULTRIO Plus® assay is a nucleic acid amplification test (NAT) that has been validated for the simultaneous detection of HIV-1, hepatitis B and hepatitis C. Validation of the Procleix ULTRIO Plus® assay for HIV-1 positivity in ASC cultures was determined previously by spiking samples with serum containing HIV-1 of a known viral load (van Vollenstee *et al*. submitted).

Conditioned medium and cellular extract were both prepared for the Ultrio plus assay. Conditioned medium was removed from the flasks during cellular expansion, four days following the changing of medium, and transferred into a 15 ml Centrifuge Tube. The conditioned medium contained serum, cellular cytokines released from the cells, cellular waste products and cellular debris. The cellular debris had the potential to block the Procleix TIGRIS instrument that SANBS uses, thus the conditioned medium was sonicated to break up the debris. The conditioned medium was sonicated on high for five seconds with a two second rest and repeated twice more giving a total of three bursts. Following this process the samples were incubated on ice to prevent protein denaturation caused by the heat generated by the sonication process.

The Procleix ULTRIO Plus® assay requires one to two million cells. Adipose derived-stromal cultures at 80% confluence were detached using Trypsin-EDTA and centrifuged at 184 *g* for five minutes. The supernatant was removed, the cells were resuspended in complete growth medium and 100 µl of the cell suspension was counted using the Flow-Count™ Fluorospheres. Between one and two million cells were then resuspended in 5 ml of PBS in a 15 ml conical tube. The cellular extract underwent the same sonication process as the conditioned medium. Both the cellular extract and the conditioned medium of each sample were labeled and stored at -20°C. The samples were transported to the SANBS laboratory on dry ice.

Multi-colour flow-cytometric analysis of immunophenotype

Multi-colour flow cytometry was employed for the immunophenotypic analysis. Adherent cell phenotypes were assessed at each passage. Confluent cultures were trypsinized and centrifuged for 5 minutes at 184 *g*. The supernatant was aspirated and the pellet resuspended in PBS. The cell suspension was incubated with Phycoerythrin-Cyanin 7-conjugated CD34 (CD34-PC7) and Krome orange-conjugated CD45 (CD45-KO) antibodies (Both Beckman Coulter), which are directed against cell-surface molecules, present on human HSCs and thus act as negative expression markers. Adipose-derived stromal cells should be <2% positive for surface markers CD34 and CD45. The cell suspension was also incubated with fluorescein isothiocyanate-conjugated CD73 (CD73-FITC; eBioscience, San Diego, California, USA), Phycoerythrin-Cyanin 5.1-conjugated CD90 (CD90-PC5; Beckman Coulter), and phycoerythrin-conjugated CD105 (CD105-PE; Beckman Coulter) antibodies directed against cell-surface molecules present on stromal cells. The panel of 5 antibodies (Table 3.1) was incubated for 10 to 15 minutes in the dark at room temperature. The ASCs-antibody mixture was subsequently washed with PBS once to remove any unbound antibodies that may cause background fluorescence. The ASC-antibody mixture was then resuspended in PBS. Cells that were not stained with antibodies represented a negative control allowing for the detection of any autofluorescence from the cells. Data was obtained by flow cytometric analysis (Gallios™). The unstained cell events were measured within the first decade of single-parameter plots. A minimum of 5 000 events per flow cytometric sample was collected and dead cells, cellular aggregates and debris were excluded from the analysis. The list mode data (LMD) generated was analyzed using Kaluza® Analysis Software 1.2 (Beckman Coulter). In order to keep the settings uniform during the experiments, the flow cytometer was checked before each experiment with Flow-Check™ Fluorospheres (Beckman Coulter) and the voltage was maintained.

Table 3.1. The antibody panel and the corresponding fluorescent channels that were used in this study.

Antibody panel	Fluorochromes				
	FL1	FL2	FL4	FL5	FL10
	CD73-FITC	CD105-PE	CD90-PC5	CD34-PC7	CD45-KO

Monoclonal mouse anti-human antibodies were available for use.

Viability

The cells were harvested by trypsinization and the viability analyzed by staining with propidium iodide (PI; Sigma-Aldrich). Percentages of viable and non-viable cells were detected using flow cytometry and detector FL3. A PI working solution of 50 μg/ml was prepared in PBS. Propidium iodide is membrane impermeant and thus was excluded from viable cells. Non-viable cells stained positive for PI because of a loss in cell membrane integrity.

Fibroblastoid colony-forming unit assay

Plastic-adhering cells were serially diluted and seeded onto 100 x 20 mm CELLSTAR® tissue culture dishes (Greiner Bio-One) in triplicate at a final density of 100 cells per dish, which is an average cell density of 1.72 cells/cm^2 (number of cells/growth area). Clonal growth was carried out for 13 days of culture. The colonies were washed twice with PBS and fixed with 4% (v/v) formaldehyde for 60 minutes. After fixation, colonies were washed twice again with PBS and stained with Toluidine Blue O stain (Sigma-Aldrich) and enumerated. The colony sizes consisted of three categories: 0-25 cells, 25-50 cells or >50 cells.

In vitro tri-lineage differentiation analyses

Adipose-derived stromal cells were seeded into 6-well plates at a density of 5 x 10^3 cells/cm^2. The cells were grown to confluence under standard growth medium conditions and then induced to differentiate. In a preliminary study various seeding densities were used. A seeding density of 5 000 cells/cm^2 was determined to be optimal. Adipogenic and osteogenic differentiation were induced by the replacement of complete αMEM with specific induction medium in the differentiation wells and complete DMEM containing 10% (v/v) FBS and 2% (v/v) Pen/Strep in the control wells. Micromass pellets were maintained for chondrogenic differentiation.

Adipogenic induction

At confluence, in triplicate, the standard growth medium was replaced with adipogenic induction medium consisting of DMEM culture medium supplemented with 1 μM Dexamethasone (Sigma-Aldrich), 500 μM 3-iosbutyl-methylxanthine (Sigma-Aldrich), 200 μM Indomethacin (Sigma-Aldrich), 1.72 μM (10 μg/ml) human Insulin (Gibco®), 10% (v/v) FBS and 2% (v/v) Pen/Strep (1). Insulin increases lipogenic activity (24). Indomethacin

accelerates adipogenesis by increasing CCAAT/enhancer-binding protein (C/EBP)-β and peroxisome proliferator-activated receptor (PPAR)-γ gene expression (25, 26). Respective experimental control medium (used for non-differentiated cells) consisted of DMEM supplemented with 10% (v/v) FBS and 2% (v/v) Pen/Strep. Medium was replaced on the 1st and 5th days of the induction week and the cells were replenished with medium on the 3rd day of the induction week.

Following 21 days of induction, the non-induced and induced cells were fixed for 60 minutes using a 4% (v/v) formaldehyde solution. The fixed cells were stored in PBS until staining took place. An Oil Red O stock solution consisting of 10 mM (0.5%, w/v) of Oil Red O in absolute isopropanol (C_3H_7OH) was prepared. The stock solution was stirred overnight and filtered through two layers of Whatman® filter paper (Grade 1:11 μm, 500 mm diameter). An Oil Red O working solution was prepared from the stock solution. The fixed cells were washed with 60% (v/v) isopropanol prior to staining. Staining the cells with a 0.3% (v/v) Oil Red O working solution for 40 minutes at room temperature qualitatively assessed lipid droplet accumulation in the cells. The Oil Red O stain was removed and the cells were washed extensively with double distilled water (ddH_2O). Cells were then counter-stained with 0.01% (w/v) Toluidine Blue O (0.01%, w/v Na_2CO_3) for 5 minutes. Any remaining stain was removed by washing the cells three times with ddH_2O. Images were acquired using an Axiovert 200 fluorescence microscope (Zeiss, Jena, Germany).

Osteogenic induction

At confluence, on the day of induction, the conditioned medium was replaced with osteogenic induction medium or control complete DMEM. Complete DMEM was supplemented with 10 mM B-glycerophosphate disodium salt hydrate, 50 μM 2-Phospho-L-ascorbic acid trisodium salt (Both from Sigma-Aldrich), 1 μM Dexamethasone, 10% (v/v) FBS and 2% (v/v) Pen/Strep. Medium was replaced on the 1st and 5th days of culture and the cells were replenished with medium on the 3rd day of culture. Alizarin Red S (Sigma-Aldrich) was used as an indicator of osteogenic differentiation as Alizarin Red S stains calcium-rich deposits, known as mineralization, in culture. Cultures were fixed using 4% (v/v) formaldehyde and washed twice with ddH_2O. Prior to Alizarin Red S staining the cultures were washed with PBS (pH4.2) for 5 minutes. The cells were stained with a 2% (w/v, 58.44 mM) Alizarin Red S solution at a pH 4.2 for 20 minutes. Following staining any remaining

stain was removed and the cells were extensively washed with ddH_2O. Images were acquired using a fluorescence microscope.

Chondrogenic induction

Approximately 200 000 cells were aliquoted into 15 ml Centrifuge Tubes for chondrogenic micromass pellet formation (27, 28). The ASCs were initially centrifuged at 184 *g* for 5 minutes and then resuspended in 1 ml of chondrogenic medium containing DMEM supplemented with 0.91 mM (100 μg/ml) Pyruvic acid sodium salt (Merck, Darmstadt, Germany), 0.35 mM (40 μg/ml) L-Proline (Merck), 0.16 mM (50 μg/ml) 2-Phospho-L-ascorbic acid trisodium salt, 1 μM Dexamethasone, 1% (v/v) BD Biosciences ITS™ premix (BD), and 0.39 μM (10 ng/mL) Transforming growth factor (TGF)-β_3 (Invitrogen). The ASCs were centrifuged for a second time at 400 *g* for 10 minutes to form pellets and these pellets were maintained in culture in the Centrifuge Tubes for 21 days, with the medium replaced on the 1st and 5th days of culture and the cells were replenished with medium on the 3rd day of culture.

Following 21 days of chondrogenic induction the micromass pellets were fixed in 4% (v/v) formaldehyde. The micromass pellets were sequentially dehydrated in 30%, 50%, 70% and 90% ethanol (EtOH) for 15 minutes at each step. Following the 90% EtOH dehydration step, the micromass pellets were dehydrated with absolute EtOH for 15 minutes. This final step was repeated twice more. The absolute EtOH was removed and the micromass pellets were infiltrated with 50% (v/v) LR White Resin and the other 50% (v/v) absolute EtOH and incubated for 1 hour. The micromass pellets were infiltrated with 100% LR White Resin and incubated in the fridge overnight. The micromass pellets embedded in resin were transferred to gelatinous capsules and the resin was polymerized by thermal curing for 24 hours. Sections of 1 μm in thickness from each micromass pellet were obtained using an ultramicrotome (Reichert Ultracut E, Vienna, Austria) and a glass blade. Slides of the sections were created and stained with 1% (w/v) Toluidine Blue O, and cover slips (22 x 22 mm) were mounted and fixed using Entellan® (Merck). Images were acquired using a fluorescence microscope and an AxioCamMR5 (Zeiss).

Statistical analysis

Kaluza statistics files were exported into Microsoft® Excel® for Mac 2011 Version 14.4.4 (140807) for further analysis. Other statistics were performed using Prism 6 for Mac 2013 (GraphPad Software) Version 6.0d. Data are represented as mean ± standard deviation (SD). The D'Agostino-Pearson omnibus K2 normality test was utilized to quantify how much a data set deviated from a Gaussian distribution. If the data followed a Gaussian distribution, statistical differences were calculated using One–way analysis of variance (One-way ANOVA) followed by a Tukey multiple comparisons test. If the data did not follow a Gaussian distribution then a non-parametric statistical method was followed. The Kruskal-Wallis test was utilized followed by the multiple comparisons test, the Dunn's post test. The multiple comparison tests indicate the significance level of a comparison. Differences were considered significant at $P<0.05$.

Results

The ASCs from abdominal adipose tissue were characterized according to the common criteria for defining MSCs (20) and the guidelines proposed to define ASCs (9), both published in Cytotherapy; 1) adherence to tissue culture plastic, 2) >90% viability, 3) expression and lack of expression of specific surface markers, 4) ability to form colonies, and 5) multipotent differentiation potential.

Isolation and expansion of adipose-derived stromal cells

Upon plating the SVF cells were observed to take approximately 24 hours to adhere to the plastic surface of the tissue culture flasks. Initially, contaminating cells of the hematopoietic lineage were detected in the flasks but were rapidly lost from the cultures due to the inability to adhere to the plastic surface (except macrophages and monocytes which are known to adhere) (29). The adherent cells during days 2 to 5 of primary culture, were observed as sparsely distributed individual cells. Individual cells varied in size from elongated and spindle-shaped to flat round cells. The spindle-shaped cells grew rapidly, and the cells that were more round grew slower. It was also noted by phase contrast microscopy, that the highly proliferative cells' nuclei contained refractive bodies as the cells lifted slightly to divide. Long cell protrusions or processes between cells were also noted.

The cells maintained plastic adherence throughout the passages. The adherent ASC population reached 80-90% subconfluence based on visual inspection within 7.80 ± 0.84 days for A180313, 9.20 ± 2.86 days for A220313, and 8.00 ± 1.41 days for A070813; from P0 to P5. The length of time that it took to reach 80-90% confluence at each passage was not significantly different between donor samples. The morphology was also maintained although later passages had increased numbers of the flat round cells. Figure 3.4 depicts the morphologies of the observed adherent cells. If the cells were left to become over-confluent the cultures formed storiform patterns in wavelike bundles. Decreased proliferation rate was also noted in subsequent cultures if the cultures were trypsin detached closer to confluence or when over-confluent.

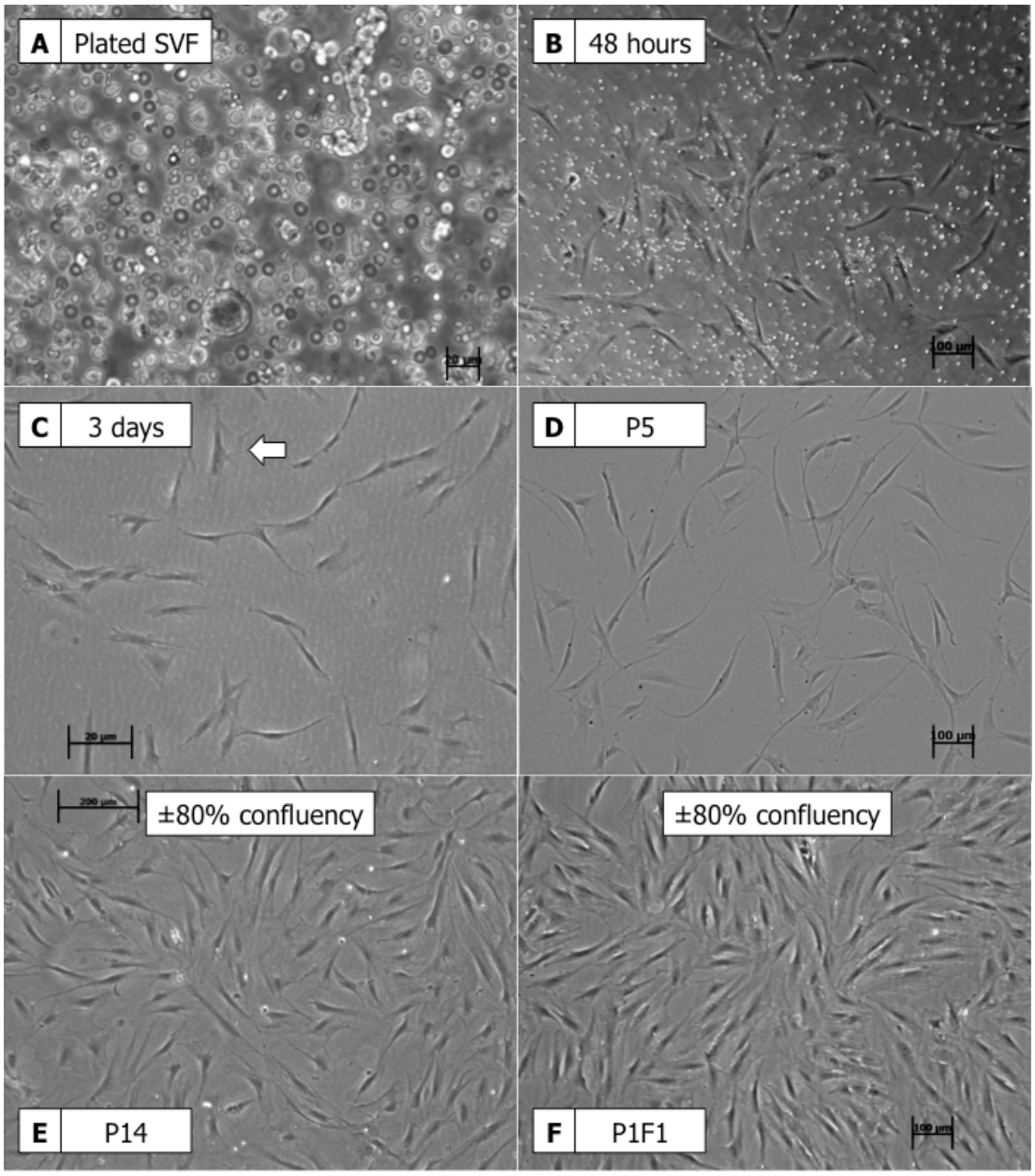

Figure 3.4. Morphology of ASCs from subcutaneous adipose tissue cultured *in vitro*. (**A**) The heterogenous nature of the plated isolated SVF with contaminating cells of the blood lineage (A270813, P0, 20x objective, scale bar 20 μm). (**B**) The adherent ASC population before removal of cell debris and contaminating non-adherent cells (A270813, P0, 5x objective, scale bar 100 μm). (**C**) Cells cultured for 3 days after initial plating displayed the typical adherent morphology consisting of spindle-shaped cells; however, cells with a flat more rounded morphology were also observed as indicated by the arrow (A270813, P0, 5x objective, scale bar 20 μm). (**D**) Another example of the spindle-shaped morphology that was observed (A070813, P5, 5x objective, scale bar 20 μm). The

adherent cells were cultured up to ±80% confluency in a T80 flask (**E**, A180313, P14, 5x objective, scale bar 200 μm; and **F**, A180313, P1F1, 5x objective, scale bar 100 μm).

Screening of adipose-derived stromal cell samples for HIV-1, hepatitis B and hepatitis C

The donor samples were all screened for HIV-1 Ribonucleic acid (RNA), hepatitis B RNA and hepatitis C RNA on the Procleix TIGRIS instrument using the Procleix ULTRIO Plus® assay. Both the cellular extract and the conditioned medium of all the samples used in this study tested negative for HIV-1, hepatitis B, and hepatitis C. When a sample demonstrates an analyte signal/analyte cutoff (S/CO) ratio of ≥1, it is considered to be reactive for the target RNA (Table 3.2). The table indicates the samples received during this study that were tested. Samples that were previously collected and tested, but used during the study, were not included in the table. All of the adipose-derived stromal cell samples that were used were non-reactive.

Table 3.2. Outcome of PROCLEIX ULTRIO Plus® Assay.

Cell sample	Analyte S/CO	
	Cellular extract	Conditioned medium
A180313	0.05	0.06
A220313	0.1	0.12
A160413	0.06	0.15
A070813	0.1	0.06
A270813	0.1	0.06

Adipose-derived stromal cells exhibit a mesenchymal stromal cell-like phenotype

Adipose-derived stromal cell populations isolated on the basis of adherence to tissue culture plastic were evaluated according to their immunophenotypic profile using mouse anti-human

monoclonal antibodies and flow cytometry. The cells were analyzed for the lack of expression of CD45, and CD34 and for the positive expression of CD73 (also known as ecto-5'-nucleotidase), CD90 (also called Thy-1), and CD105 (Endoglin). The immunophenotype protocol was set-up by selecting for the required parameters. A two-parameter linear forward-scatter (FS; y-axis) versus logarithmic side-scatter (SS; x-axis) plot was created and for the analysis of the cell's immunophenotype; all of the possible fluorochrome-combinations for the two-parameter and single-parameter histogram plots were created. Two-parameter plots are representative of four different populations displayed over quadrants. The lower left quadrant represents the cell population that is negative for both fluorochromes. The lower right quadrant represents the cell population that is positive for the fluorochrome on the x-axis and negative for the fluorochrome on the y-axis. The upper right quadrant represents the cell population that is positive for both fluorochromes. The upper left quadrant represents the population that is negative for the fluorochrome on the x-axis and positive for the fluorochrome on the y-axis. A single-parameter plot represents the frequency distribution of the number of events per channel.

The voltages on the flow cytometer were adjusted to ensure that the unstained cells (autofluorescence) would be visible within the first decade of the single-parameter histogram plots. The voltages were maintained throughout the analysis for consistency. The dead cells, cellular aggregates and debris were excluded on the FS versus SS plot by gating only the viable cells of interest (Unstained cells in Figure 3.5**A**). Sequential gating was applied and all other plots were gated on this region of interest. Due to the multi-colorimetric nature of this analysis, fluorochrome/colour compensation for spectral overlap was necessary. This spectral overlap colloquially known as "spillover" is the result of the fluorochrome being measurable in more than just one detector. Colour compensating corrects this spillover so that information is gathered from a single fluorochrome in a single detector.

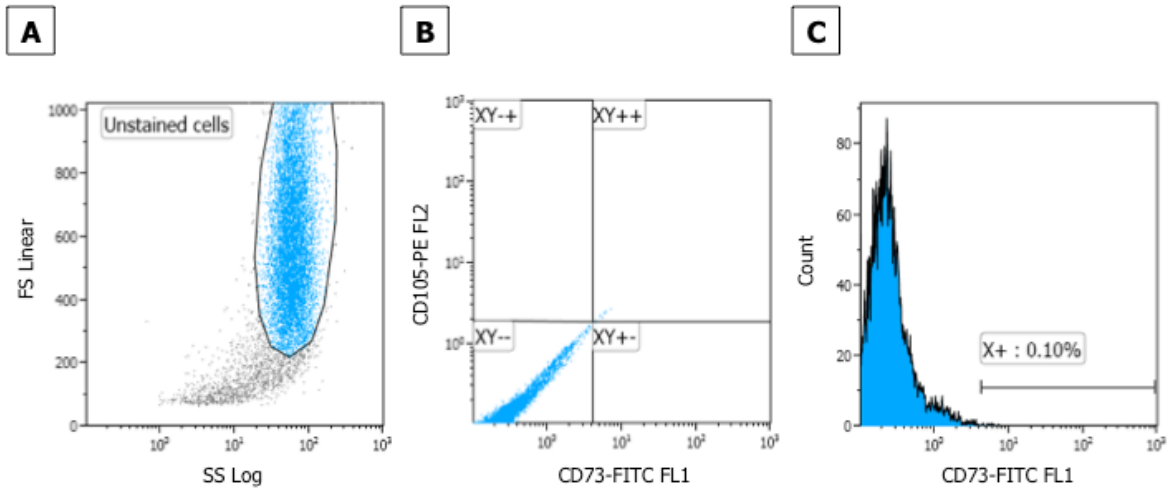

Figure 3.5. Gating principle. The figures represent an unstained flow cytometric A070813 cell sample at P0. All of the plots were gated on the [Unstained cells] region of interest on the FS versus SS dot plot (**A**). The voltages were set to indicate a negative reading within the XY-- quadrant (lower left quadrant) of the two-parameter plot and in the first decade of the single-parameter histogram plot (**B**). The unstained cells are highly autofluorescent as indicated by the fluorescence signal in the second decade of the single-parameter histogram plot in the FL1 detector channel (**C**).

Unstained cell suspensions were used to set gates which were maintained for the stained cell suspensions. Any cell population appearing to the right of the unstained cell population (in the second and greater decades of the four decades) of the single-parameter histogram plots was viewed as positively stained. The unstained cells appear to have a high level of autofluorescence as indicated by the distribution over two of the four decades. This was further investigated by looking at the autofluorescence emitted by another adult stem cell population. The fluorescence emitted by an unstained HSC population from mobilized peripheral blood was compared to an unstained ASC population. The fluorescence that was detected in the FL1 detector channel indicated that the ASC population was a highly autofluorescent cell population. The fluorescence of the unstained HSC population was set to appear in the first decade of FL1 single-parameter plot. The ASCs were then run through the exact same protocol. The fluorescence, detected in the FL1 detector channel, increased as was conveyed by the distribution in the greater decades with the ASCs (Figure 3.6**B**). Similar autofluorescence was observed in all 10 FL detector channels. The voltages were set to compensate correctly for this autofluorescence and thus the high intrinsic fluorescence of the ASCs did not affect any fluorescence results. The autofluorescence could be faintly detected using fluorescence microscopy and an emission of 488 nm, which is equivalent to the

emission detected in FL1 on the flow cytometer. The autofluorescence is mainly detected around the nuclei and unknown cellular bodies.

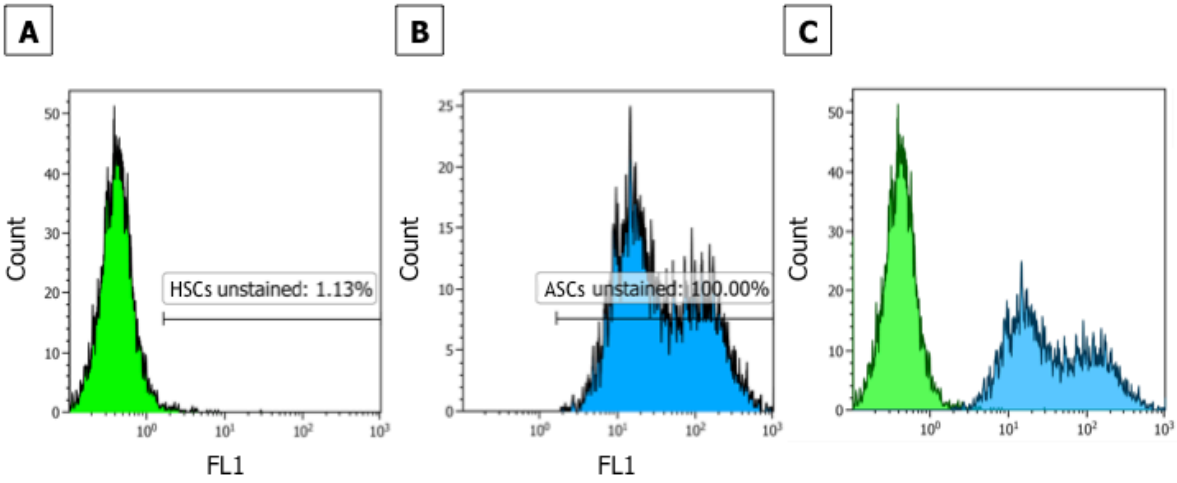

Figure 3.6. Autofluorescence. Single-parameter histogram plots of FL1 fluorescence detection were created for unstained HSCs (**A**) and unstained ASCs (**B**). The first two plots were gated on the cells of interest, excluding dead cells and cell debris, on the FS versus SS dot plot. An overlay histogram plot was created from the single-parameter histogram plots (**C**). The unstained ASCs appear to have a high level of autofluorescence as indicated by the distribution over the higher decades compared to the HSCs in the first decade. The voltages were set to compensate correctly for the ASC autofluorescence.

To be considered ASCs, positive staining was defined as ≥95% of the population expressing CD105, CD73 and CD90. The cells must also display ≤2% expression of CD45 and CD34. Creating overlay histograms for each cell surface marker indicates the differences between the unstained cells and the stained cells. The more surface markers situated on a cell surface, the more epitopes available for antibody binding. The result is more fluorescence being emitted from a particular cell and subsequently, an increase in fluorescence on the histogram plot, which is demonstrated by a shift to the right of the plot. A representative example of the histogram plots of an unstained A220313 P1 cell population (3.7**A**) and a CD90-stained A220313 P1 cell population (3.7**B**) is demonstrated in Figure 3.7. An overlay plot (3.7**C**) was created from these two histogram plots to easily distinguish between the unstained and stained cell populations (Figure 3.7). The CD90-stained cell population was positive for this surface marker, as indicated by the distinct shift to the right compared to the unstained histogram plot. The immunophenotypic profile was assessed for three individual

cultures, consecutively from Passage 0 to Passage 4. A representative overlay plot matrix of all the surface markers and passages of culture A180313 is presented in Figure 3.8. The considered ASC-specific immunophenotype consisting of the surface markers CD73, CD90, CD105, CD34, and CD45 was evaluated for every individual culture over the four passages.

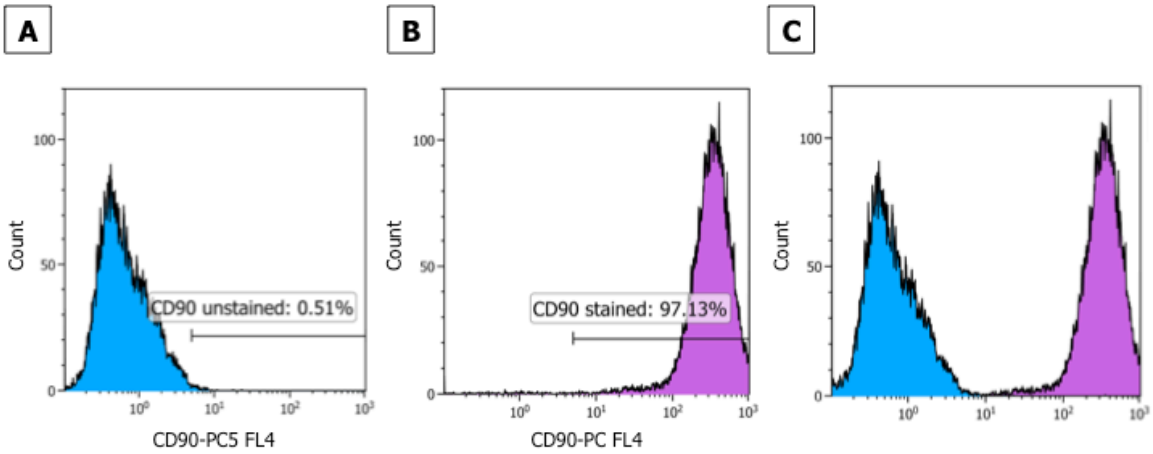

Figure 3.7. Overlay plot of FL4 fluorescence detection. The overlay histogram plot indicates the differences between the unstained and stained cell populations. Unstained (**A**) and stained (**B**) single-parameter histogram plots of CD90-PC5 fluorescence were used to create the overlay histogram plot (**C**). The x-axis of the histograms refers to fluorescence intensity (4 decades logscale), while the y-axis refers to linear cell number (count). This flow cytometric analysis is of sample A220313 at P1 and shows positive expression for CD90.

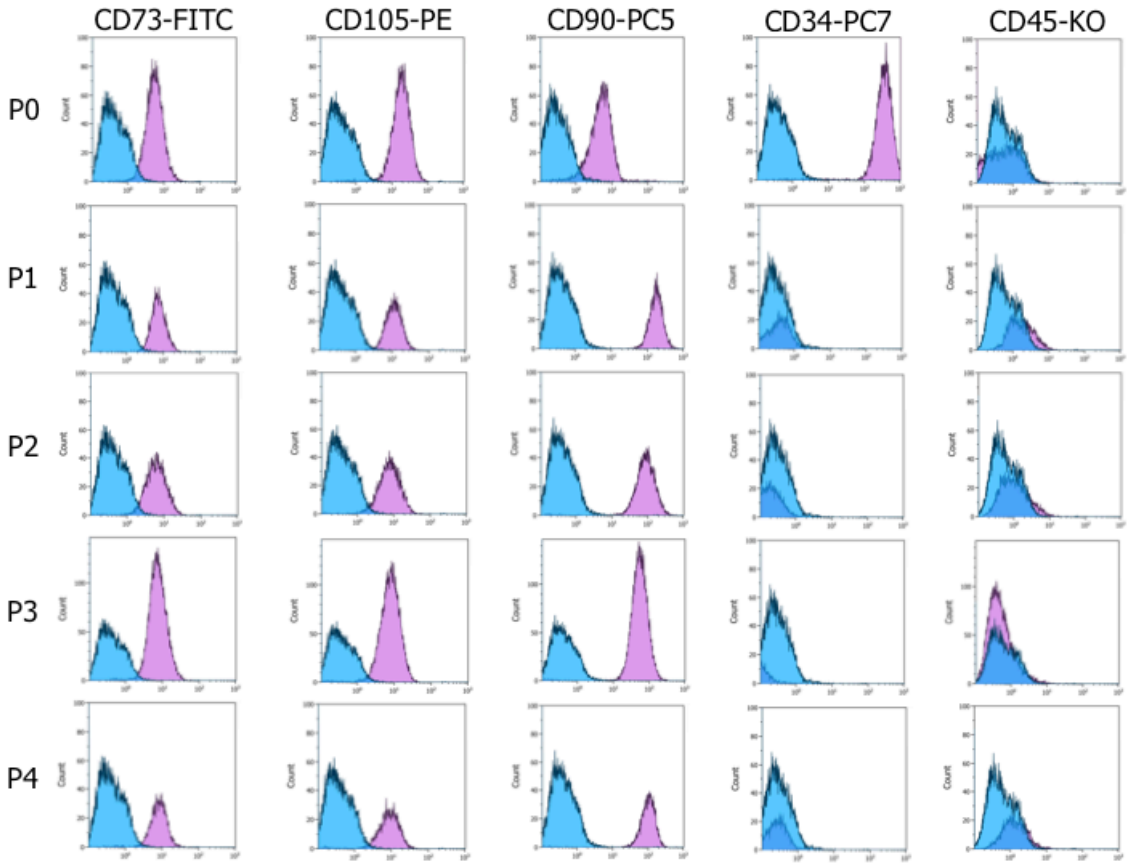

Figure 3.8. Immunophenotypic characterization of the adherent cells. Overlay plots for selected surface markers were generated for culture A180313 from passages 0 to 4 showing positive expression for markers, CD73, CD105, CD90 and the lack of CD34 and CD45 expression. The surface marker expression for CD34 was positive at P0.

The cells at P0 contained a subset that were positive for the HSC-associated marker, CD34 and the leukocyte common antigen, CD45. Approximately 34% of the P0 cells were positive for CD34. This expression remained high through P1 with more than 15% positive for CD34. Expression of CD34 declined from P2 as shown in Table 3.3. A mean of 4.21% of the P0 cells expressed the CD45 marker. The CD45 levels remained comparable in the P0 cell population through to P2 and decreased, but not significantly, in P3 and subsequent passages. The individual expression levels of CD73, CD90 and CD105 at P0 met the required >95%. The percentage of cells staining positive for each of these markers remained high throughout the passages. The required marker expression appeared to stabilize around P3. The ASCs displayed the following mean (± SD) percentage positive cells (n = 3 donors) at P3 for the indicated surface antigens: CD73, 97.89 ± 0.65%; CD90, 99.29 ± 0.58%; CD105, 98.67 ±

0.95%; CD34, 0.91 ± 1.56%; and CD45, 1.65 ± 1.77%. The earlier passages varied more in surface marker expression than later passages. The A220313 donor culture had a particularly strong CD45 expression at P0 compared to the other cultures, thus increasing the SD. Variable surface marker expression was observed to some degree for each marker between the different donor cultures.

Table 3.3. Phenotypic characterization of human adipose-derived stromal cells at specific passages.

Antibody	P0	P1	P2	P3	P4	P10
CD73-FITC	96.01 ± 2.32%	98.06 ± 0.91%	96.77 ± 1.49%	97.89 ± 0.65%	98.33 ± 0.83%	97.52 ± 2.59%
CD90-PC5	98.18 ± 1.68%	98.61 ± 1.28%	99.16 ± 0.64%	99.29 ± 0.58%	98.99 ± 1.13%	97.83 ± 2.14%
CD105-PE	98.23 ± 1.75%	98.60 ± 1.05%	98.53 ± 0.77%	98.67 ± 0.95%	98.66 ± 1.02%	97.42 ± 1.02%
CD34-PC7	34.24 ± 48.00%	15.77 ± 23.36%	0.60 ± 1.00%	0.91 ± 1.56%	1.94 ± 3.14%	0.15 ± 0.21%
CD45-KO	4.21 ± 4.00%	5.20 ± 4.53%	4.23 ± 4.16%	1.65 ± 1.77%	1.22 ± 1.38%	0.58 ± 0.71%

Data are presented as mean ± SD. Data represents n = 3. * $P<0.05$ relative to P0 by Kruskal-Wallis test. No significant differences.

The majority of the literature assesses individual marker expression. Tree plots, such as the one shown in Figure 3.9, were generated from the stained cells to indicate all fluorochrome expression combinations that exist within the cell population of interest. The % Gated data from all the tree plots were used to generate graphs of the conventional fluorochrome combination and other sub-populations. Figure 3.10 reiterates that the typical CD73+CD90+CD105+CD34-CD45- surface marker profile was detected in all ASC cultures from P3 and was maintained through progressive passages. The variability in expression of this profile in earlier passages (P0 and P1), as observed by the large SDs, was elucidated by the increase in mainly CD34 (3.10**B**) and partially CD45 (3.10**C**) positive populations of cells; however, the remainder of the passages were not affected by this variability.

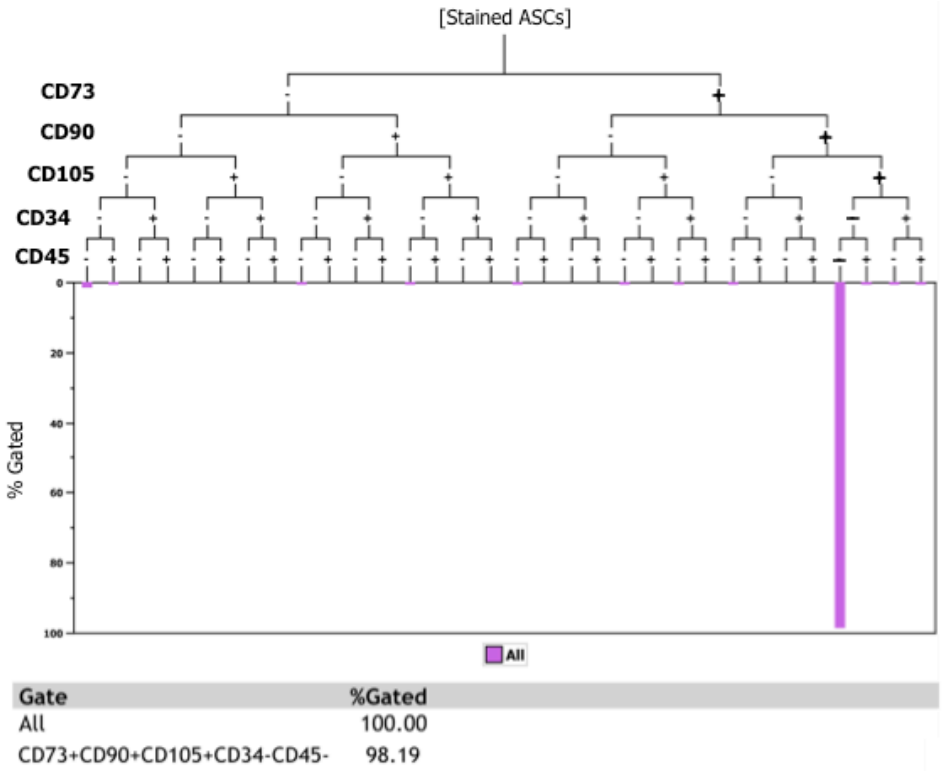

Gate	%Gated
All	100.00
CD73+CD90+CD105+CD34-CD45-	98.19

Figure 3.9. Tree plot generated to determine surface marker profile of the ASC population. Flow cytometric analysis of sample A180313 at P3 showing an overall ASC phenotype. 98.19% of the cells expressed the ASC CD73+CD90+CD105+CD34-CD45- phenotype.

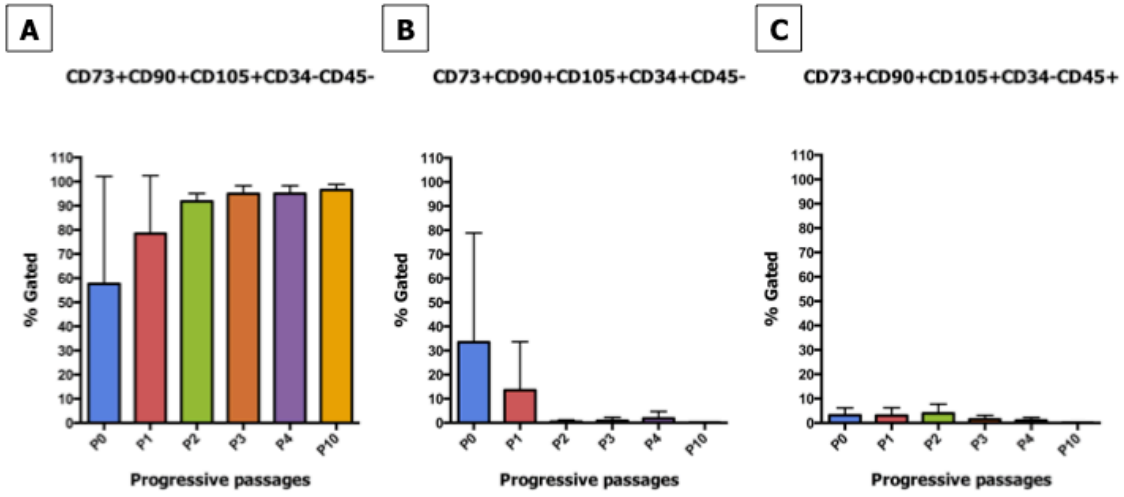

Figure 3.10. Graph of flow cytometric data generated from tree plots determining the combined phenotypic profile of the ASC population. Flow cytometric analysis of cultures A180313, A220313 and A070813 gave an overall ASC phenotype. The cell population expressed the

ASC CD73+CD90+CD105+CD34-CD45- phenotype from P3 (**A**). The variability in expression of this profile in earlier passages (P0 and P1) of (**A**) was elucidated by the increase in mainly CD34 (**B**) and partially CD45 (**C**) positive populations of cells. Data represents n = 3; error bars represent SD. No significant differences.

Both fresh and thawed previously cryopreserved cells were used in this study. There were no significant differences observed in the expression of surface markers for fresh ASCs and thawed ASCs derived from various passages. The passage number was used to denote fresh ASCs; for example P1 as demonstrated on the x-axis in Figure 3.11. Thawed cryopreserved ASCs were distinguished from fresh ASCs by the passage number and how many times the cells had been frozen/thawed. An example is P1F1 which demonstrates that the culture is at passage 1 and has been thawed once.

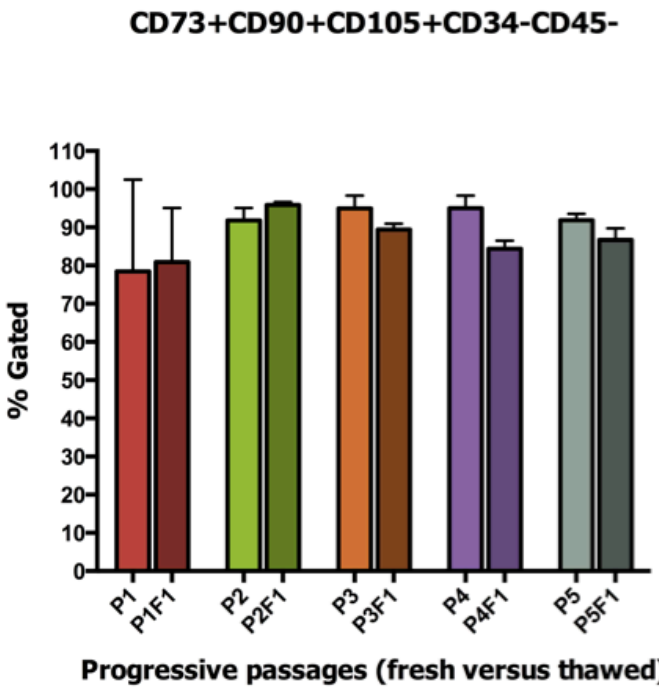

Figure 3.11. Phenotypic comparison of fresh versus thawed ASCs. There were no significant differences in surface marker expression between fresh and thawed ASCs. Data represents n = 3; error bars represent SD.

Viability of adipose-derived stromal cell samples

To investigate the viability of the ASCs while maintained in culture, uptake of the cell viability stain, PI, was monitored. Propidium iodide is only permeable to cells with compromised membrane integrity; thus non-viable cells can be distinguished from viable cells by the fluorescence of PI which binds to DNA in the nucleus. A two-parameter linear FS (y-axis) versus logarithmic SS (x-axis) plot was created and the dead cells, cellular aggregates and debris were excluded on this plot by gating only the region of intact cells (3.12**A** and **C** of Figure 3.12). Propidium iodide signals were detected using the FL3 detector of the flow cytometer and thus for the analysis of viability a second two-parameter SS (y-axis) versus FL3 (x-axis) plot was created. Non-viable cells were discernible from viable cells on the basis of their fluorescence in FL3, and due to their loss in cell membrane integrity there was an increase in fluorescence to the right of the plot.

This second two-parameter plot was gated on the "Intact cells" region (3.12**B** and **D**). A high concentration of hydrogen peroxide (H_2O_2; 100 μM) is not conducive to cell viability and the non-viable and viable regions were set using this condition (3.12**B**). These viable and non-viable regions were maintained throughout the analysis. The viable cells were recognized by a shift in distribution to the left of the non-viable cells and thus a decrease in FL3 fluorescence on the plot (3.12**D**). The >90% cell viability criteria was met at each passage over 5 passages (Table 3.4). An average of 93.67 ± 1.65% of the intact cells were viable over 5 passages.

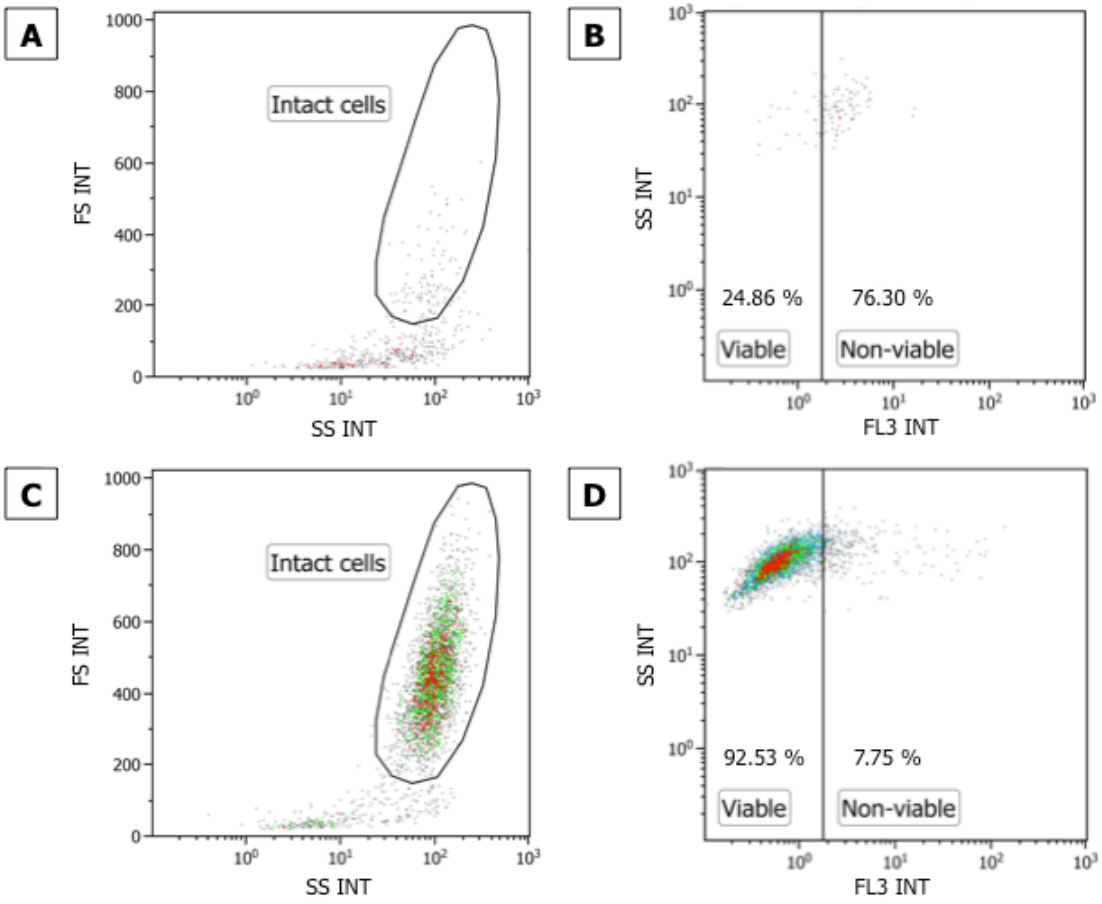

Figure 3.12. Viability of ASCs as determined by flow cytometry measuring PI uptake. A representation of the gating strategy used to assess cell viability. Only intact cells were analyzed. A culture (A180313) treated with 100 μM of H_2O_2 resulted in the majority of the cells in (**A**) not being viable. Thus a region was drawn, capturing the non-viable cells (**B**). Intact cells from the culture (A180313) without treatment (**C**) were monitored for any shift to the left of this region as in (**D**). The cells situated on the left of the region in (**D**) indicated the percentage of intact cells that were viable.

Table 3.4. Viability of adipose-derived stromal cells over progressive passages.

	P1	P2	P3	P4	P5
Viable cells	94.30 ± 2.39%	90.78 ± 4.12%	94.04 ± 0.47%	94.24 ± 3.03%	94.98 ± 2.67%

Data are presented as mean ± SD. Data represents n = 2 cultures. No significant differences. Abbreviation: SD, standard deviation; P, passage.

Colony-Forming Unit (CFU) assays

Adult stem cells are defined by a number of functional capabilities, one of these being the ability to form colonies from single cells. The isolated, plastic-adherent ASCs were plated in triplicate at a cell concentration of 1.72 cells/cm^2. This low density consisting of just 100 cells per tissue culture dish allowed each cell to result in a clone separate from other clones. At 13 days, the tissue culture dishes were washed with PBS and stained with Toluidine Blue O to reveal the colonies. The heterogeneous nature of the ASC population was apparent upon inspection of individual colonies. There was a broad range of colony sizes, indicative of varied cell growth rates. Even individual cells within each colony varied in morphology, with numerous cells being spindle in shape; however, larger flat cells were also present. Some colonies were visible to the naked eye; however the majority of colonies could not be seen in the photograph (Figure 3.13). All cultures were able to form colonies and had a great proliferative ability as seen by the large number of colonies containing greater than 50 cells. Great intra-culture and inter-culture variability was observed.

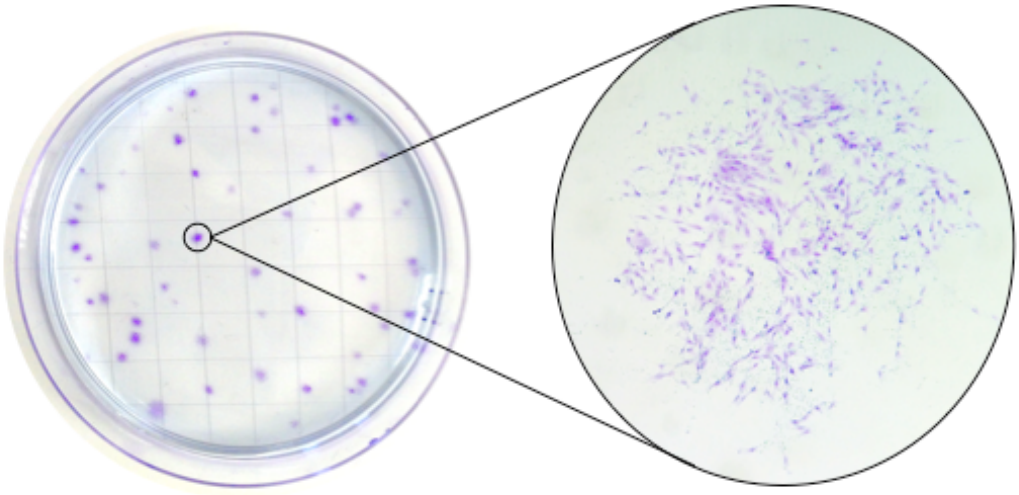

Figure 3.13. Colony-Forming Unit (CFU) assays of ASCs. Photograph of the Toluidine Blue O stained colonies obtained using a CFU-F assay. This is a colony containing greater than 50 cells.

To elucidate the variation that exists from donor to donor, the colony forming potential of the individual donor cultures was plotted in a bar graph for comparison (Figure 3.14). Cells were sparsely distributed and it is assumed that one cell led to the formation of a single colony. The numbers of CFUs from donors, A180313 and A270813, differed significantly from the A220313 donor. The number of colonies formed consisting of >50 cells from the 100

seeded cells for A180313 P4F1 was 33.33 ± 9.81. The number of colonies formed consisting of >50 cells from the 100 seeded cells for A220313 P4F1 was 56.67 ± 0.58, and the number of colonies formed consisting of >50 cells from the 100 seeded cells for A270813 P4F1 was 28.33 ± 4.04. Thus, 1 cell of every 3.00 cells plated formed a colony from donor A180313, 1 cell of every 1.76 cells plated formed a colony from donor A220313. Finally, 1 cell of every 3.53 cells plated formed a colony from donor A270813.

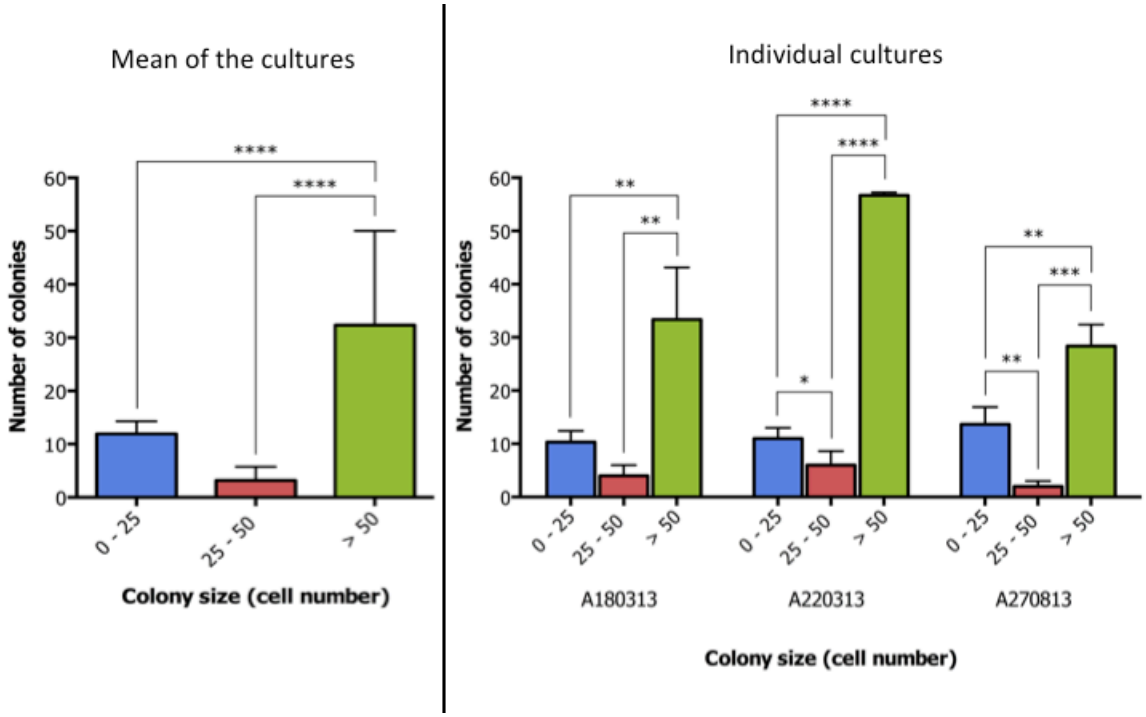

Figure 3.14. Colony-Forming Unit (CFU) assays of ASCs. The size distribution of colonies obtained following 13 days of culture after seeding 100 cells per dish. Values are from approximately 55.11 ± 15.65 colonies per plate from three donors (A180313, A220313, and A270813 at P4F1) carried out in triplicate. Values are colony sizes consisting of 0-25 cells, 25-50 cells or ≥50 cells. The results show that the cells were able to form colonies and have a high proliferative potential. Great intra-culture and inter-culture variability was observed.

Multi-differentiation potential of adipose-derived stromal cells *in vitro*

The tri-lineage differentiation potential of the ASCs into adipocytes, osteoblasts and chondrocytes was assessed. To evaluate the multipotentiality of the ASCs, cells from three donors (A180313, A220313 and A070813) at passage 3 to 5 were induced to differentiate

using lineage specific cocktails. All three of these cultures demonstrated the ability to differentiate into the adipogenic, osteogenic and chondrogenic lineages.

Adipogenic differentiation

The culture-expanded ASCs were used at the fifth passage, at confluence, for adipogenic differentiation. Under the appropriate adipogenic induction conditions, the ASCs exhibited adipose differentiation *in vitro*, changing their fibroblastic spindle shape to rounded cells with multiple intracytoplasmic lipid droplets. The conventional histologic Oil Red O lipid-based detection method was employed to detect lipid droplets. Lipid droplets consist of a neutral lipid (triacylglycerols and sterol esters) core surrounded by a phospholipid monolayer with embedded proteins (30). Oil Red O is used to detect triacylgycerols and sterol esters and stains these neutral lipids red/orange in colour. Following up to three weeks of differentiation, the non-induced and induced cultures were fixed and stained with Oil Red O and counter-stained with Toluidine Blue O. Figure 3.15**A** and **B** shows Oil Red O-stained non-induced and induced cultures, respectively. No lipid droplets were observed in the non-induced cultures and thus Oil Red O staining was absent. Figure 3.15**C** and **D** shows Oil Red O-stained and Toluidine Blue O counter-stained non-induced and induced cultures, respectively. Oil Red O positive lipid droplets were observed in the adipogenic induced cultures. Toluidine Blue O stains DNA and RNA rich tissues and is commonly used in histological studies to highlight cell features and thus in this case was used for clearer observation of the cells.

During the first week of exposure to the adipogenic induction medium, a small proportion of cells acquired lipid droplets (3.16**B**). The initial acquisition of lipid droplets occurred at one pole of the cell. This was then followed by an increase in the number of lipid droplets. As the number of lipid droplets increased, an extensive coalescing of these small lipid droplets took place, spreading around the nucleus. There was a vast array of different cells which varied in size and shape. They ranged from the starting spindle-shape with some not containing lipid droplets, to those containing few lipid droplets. Through the second week (3.16**D**), the numbers of lipid droplets increased and they continued to aggregate into clusters. The spindle shape became progressively modified to a bigger more spherical shape. At three weeks (3.16**F**), the observed trend towards larger and numerous droplets continued. The masses of accumulated lipid droplets within the cytoplasm often displaced the nucleus to the

periphery of the cells. In some cases the nucleus also acquired a crescent shape. In the adipogenic induced cultures of this study no large unilocular lipid droplets indicative of a mature adipocyte were observed. The lipid droplets detected throughout the induction period varied in size, volume and number.

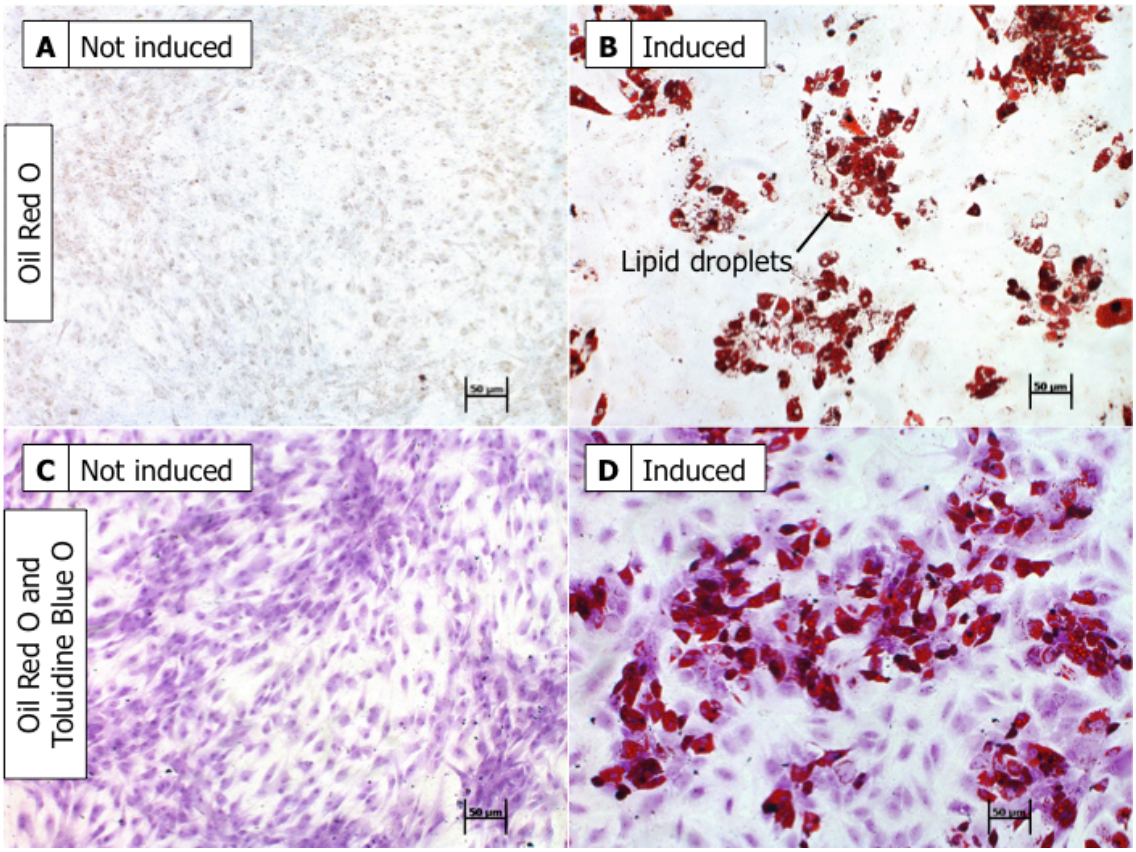

Figure 3.15. Adipogenic-differentiation capacity of ASCs. Light microscopy photographs of ASCs not induced (left) and induced with adipogenic medium (right) for 14 days. Confluent ASCs upon adipogenic-induction were exposed to adipogenic differentiation cocktail. The non-induced (**A**) and induced cultures (**B**) were both stained with only Oil Red O. Induced adipogenic cultures stained positive for Oil Red O staining as indicated by the red lipid droplets. Note that the differentiated cells occur in clusters. The non-induced cultures lacked positive staining with Oil Red O. The non-induced (**C**) and induced cultures (**D**) were both stained with Oil Red O and counter-stained with Toluidine Blue O for better visualization. Original magnification: 10x, scale bars: 50 μm.

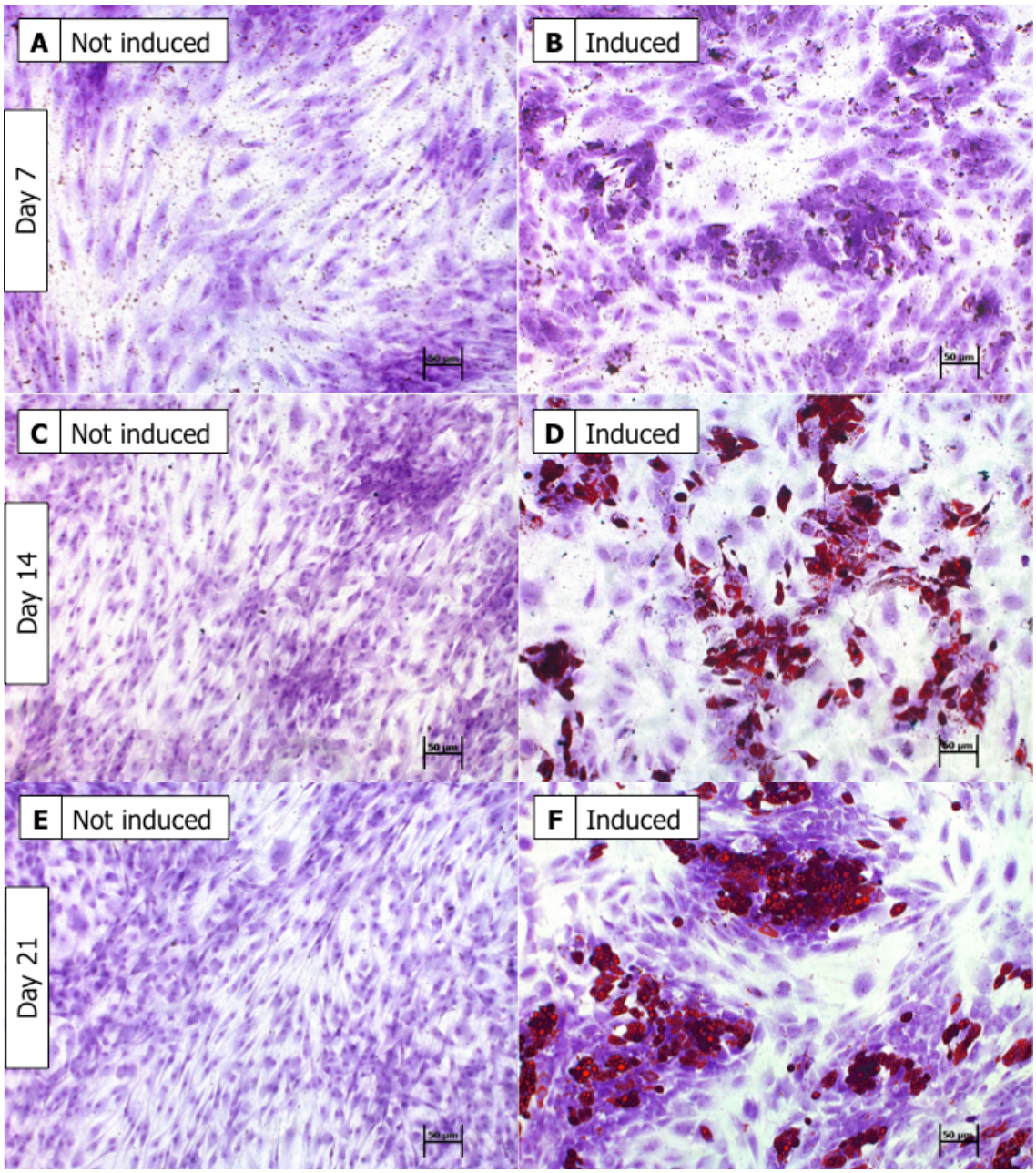

Figure 3.16. *In vitro* lipid droplet accumulation over three weeks of adipogenic induction. Light microscopy photographs of hASCs not induced and induced with adipogenic medium. Confluent ASCs were exposed to control DMEM or to an adipogenic differentiation cocktail for 7 (**B**), 14 (**D**), and 21 (**F**) days. The cells in all of the figures are from donor A220313 at P5. Non-induced (left) and induced (right) cultures were both stained with Oil Red O and counter-stained with Toluidine Blue O. Induced adipogenic cultures stained positive for Oil Red O staining as indicated by the red lipid droplets. The non-induced cultures (**A**, **C**, **E**) lacked positive staining with Oil Red O. Original magnification: 10x, scale bars: 50 μm.

Osteogenic differentiation

Adipose-derived stromal cells were induced over 21 days in osteogenic induction medium following the third passage and gradually produced Alizarin Red S-stained mineral which appeared initially as dense nucleation points (3.17**B**, **D**, **F**) compared to cells cultured in control DMEM (3.17**A**, **C**, **E**). Matrix deposition was detected by staining both the osteogenic-induced cells and control cells with 2% (w/v) Alizarin Red S. The non-induced cultures lacked deposition of calcium in the extracellular matrix. Variable extracellular matrix deposition was observed between the three cultures.

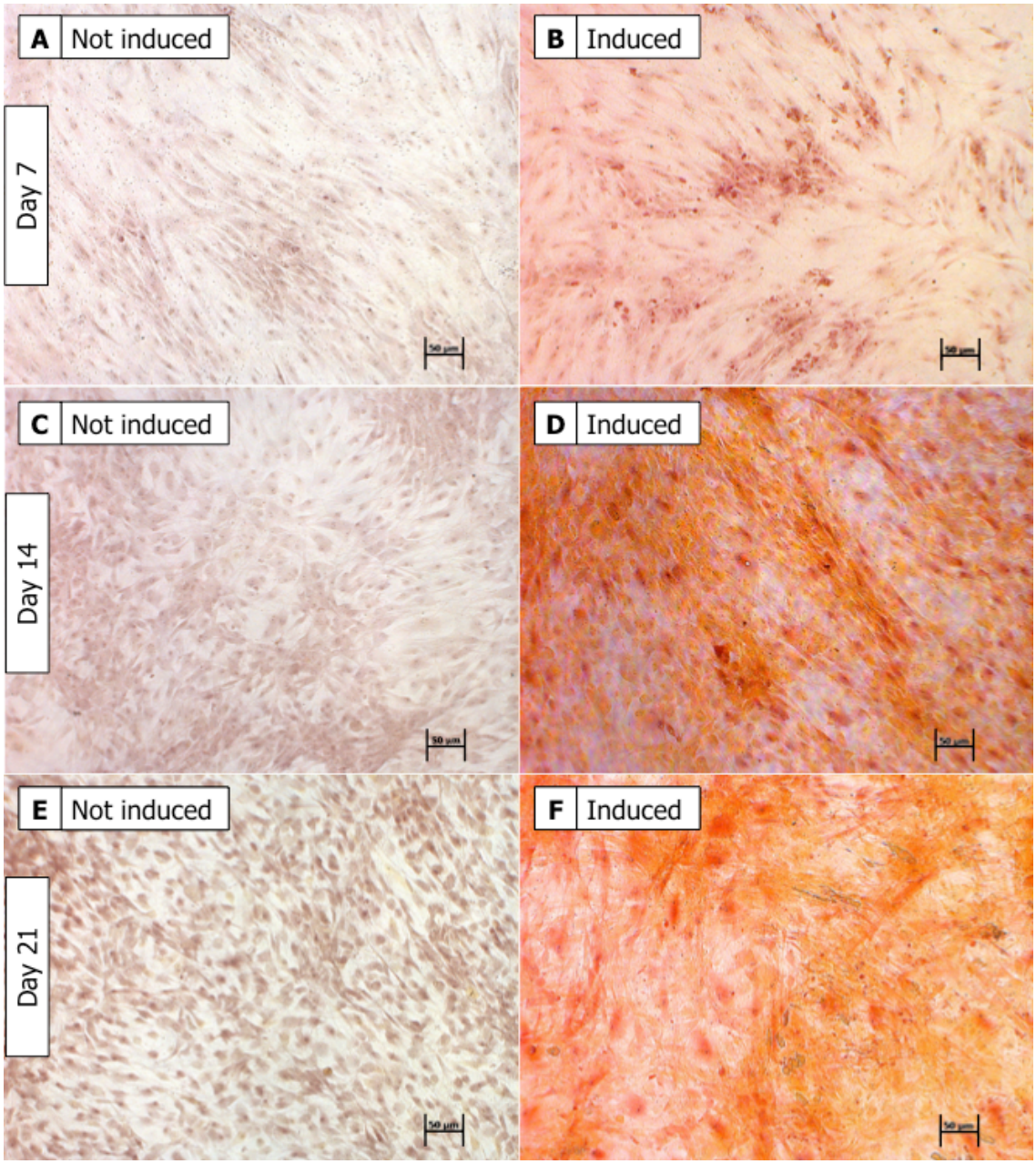

Figure 3.17. *In vitro* matrix deposition analysis over three weeks of osteogenic induction. Light microscopy photographs of hASCs not induced and induced with osteogenic medium. Confluent ASCs were exposed to control DMEM or to osteogenic induction medium for 7 (**B**), 14 (**D**), and 21 (**F**) days. The cells in all of the figures are from donor A220313 at P3. Non-induced and induced cultures were both stained with Alizarin Red S at each time point. The ASCs exhibited osteoblastic potential following osteogenic induction as shown by the positive staining with Alizarin Red S. This indicates the formation of the mineralized extracellular matrix. The non-induced cultures lacked deposition of the extracellular matrix. Original magnification: 10x; scale bars: 50 μm.

Chondrogenic differentiation

The multipotential property of ASCs was further assessed under chondrogenic inductive conditions *in vitro*. The cultures demonstrated chondrogenic differentiation capacity over 21 days of induction. Following 21 days of chondrogenic differentiation, the micromass pellet cultures were fixed, dehydrated, and embedded in resin. Sections of the pellets were stained with Toluidine Blue O. The chondrogenic medium-induced pellets appeared to consist of two zones compared to the control pellets. The control pellets were smaller in diameter (3.18**A** and **C**) than the chondrogenic-induced pellets when observed microscopically at the same magnification and similar micromass pellet section. The stained surface zone, which is the outer region of the pellet, appeared to consist of more densely-packed spindle-shaped cells. An inner zone consisted of interspersed polygonal cells. The non-induced micromass pellets lacked these two separate zones. At a higher magnification of 140x the different zones were clearer (Figure 3.19).

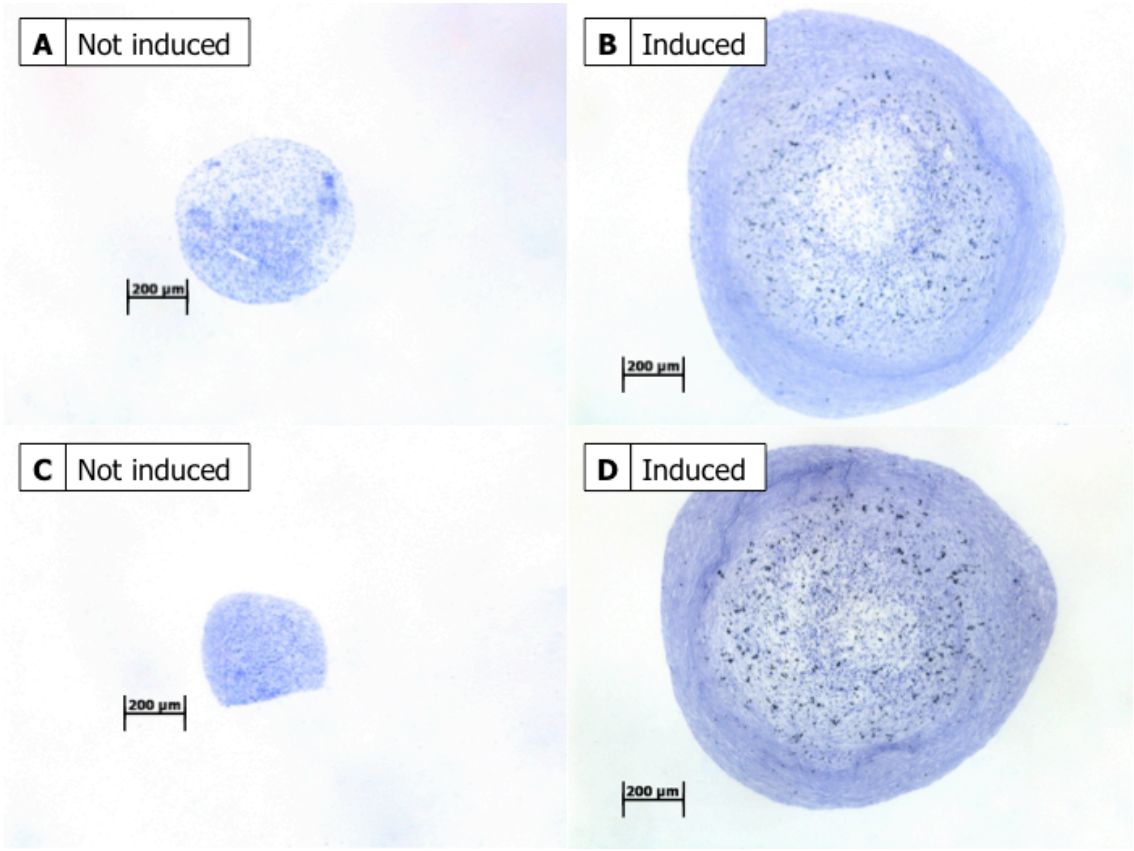

Figure 3.18. Histologic examination of micromass pellets following three weeks of chondrogenic induction. Light microscopy photographs of sections of ASC micromass pellets

cultured under control DMEM or chondrogenic induction medium. The micromass pellet culture was histologically examined using 1% (w/v) Toluidine Blue O at day 21 of induction. Row 1 (**A** and **B**) is from donor A180313 at passage 4. Row 2 (**C** and **D**) is from donor A220313 at passage 4. The induced micromass pellets had two visible zones. The non-induced micromass pellets were smaller in diameter compared to the induced micromass pellets, although variable diameters were observed overall. Original magnification: 74x; scale bars: 200 μm.

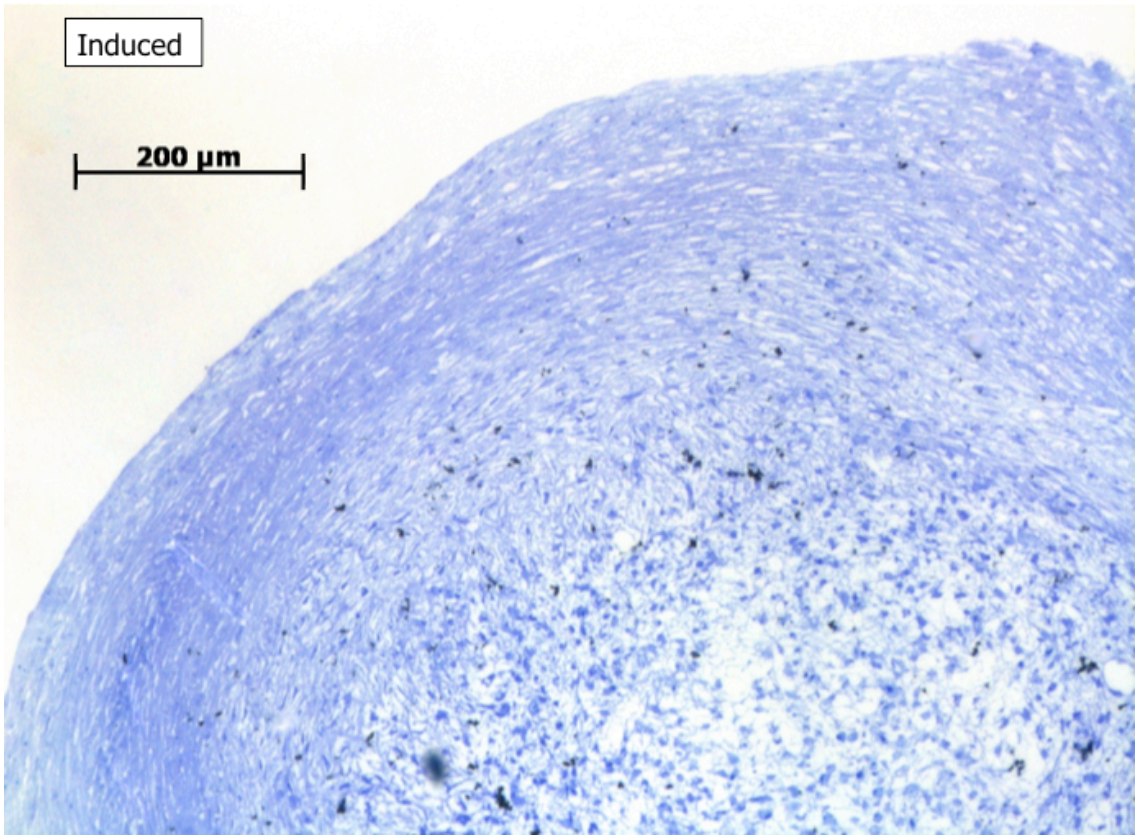

Figure 3.19. Higher magnification of a micromass pellet following three weeks of chondrogenic induction. The induced micromass pellet zones at 140x. The surface zone consisted of more densely-packed spindle-shaped cells. An inner zone consisted of interspersed polygonal cells. Scale bar: 200 μm.

Discussion

Isolation of adipose-derived stromal cells

Phenotypically, the cells were defined by adherence to a plastic surface, spindle-shaped morphology, a panel of surface markers, the ability to form CFU-F, and their capacity to give rise to adipocytes, chondrocytes, and osteoblasts. The use of adipose tissue as a source is advantageous due to the high yield of stem cells obtained (31). All donor lipoaspirates provided viable cells. The adherent cells varied in size from elongated and spindle-shaped to flat round cells. The spindle-shaped cells grew rapidly, and the cells that were more round grew slower. Mets and Verdonk also observed two different cell types in adherent MSC populations (32). It was also noted by phase contrast microscopy, that the highly proliferative cells' nuclei became brightly fluorescent as the cells lifted slightly to divide. Long cell protrusions or processes between cells were also noted. These cell processes form cellular junctions and were also observed by Wuchter and colleagues in MSCs but the role they play is still being elucidated (33). The cells maintained plastic adherence throughout the passages. The morphology was also maintained although later passages had increased numbers of the flat round cells. If the cells were left to become over-confluent the cultures formed storiform patterns in wavelike bundles. Decreased proliferation rate was also noted in subsequent cultures if the cultures were trypsin detached closer to confluence or when over-confluent. Krinner and colleagues attribute this property to contact inhibition (34).

Many research groups, including our own, are intent on using ASCs for therapeutic purposes in the not-too-distant future. Protocols for the acquisition of lipoaspirate, isolation of the SVF, and *in vitro* expansion of ASCs have been extremely heterogeneous. Protocols in the MSC and ASC research industry are not standardized and the current characterization criteria for ASCs are inaccurate. Good manufacturing practices and quality control need to be of very high standards and utmost priority when dealing with human therapeutic products. In addition to standardizing protocols all use of xenogeneic products needs to be eliminated. Using xenogeneic products results in the transfer of foreign proteins that could cause an immune response or infection in the recipient (35). Standard growth medium is usually supplemented with FBS. This is not only of bovine origin and thus xenogeneic but, Bieback and colleagues, discovered through whole genome gene expression analysis, that FBS induces altered gene expression compared to the human counterparts (36). Primary cells

and thawed stocks have both been used to expand the cells for therapeutic purposes. Frozen stocks were made from the different donor samples at different passages for subsequent experiments in this study. Literature states that cryopreservation does not alter the characteristic properties of MSCs and ASCs but an effect on the molecular level cannot be excluded (37, 38). Dimethyl sulfoxide, the cryopreservation agent, has been deemed safe for use with stem cells; however, serious side effects, including fatal cardiovascular problems, have been reported for patients receiving transplants of thawed cells (39, 40). The way forward for ASC research would be to standardize ASC preparations and eliminate all xenogeneic products from culture. Using primary cells would be ideal, but the numbers required for therapy necessitates expansion of the ASCs and often their cryopreservation for future use. Although these are all factors that can be standardized, donor variability cannot be standardized. The ASC populations have each been isolated from genetically different individuals and differences in results due to this heterogeneity need to be taken into account.

Screening of adipose-derived stromal cell samples for HIV-1, hepatitis B and hepatitis C

Human immunodeficiency virus (HIV) can be subdivided into two main groups, HIV type 1 (HIV-1) and type 2 (HIV-2). Around 90% of HIV/AIDS cases are derived from HIV-1 infection which is considered the most common strain and most pathogenic. HIV-1 is divided into groups with group M (Major group) being the predominant group (41). Group M is also made up of subtypes, with subtype C being the dominant type in Southern Africa (42). All of the samples used in this study tested negative for HIV-1, hepatitis B, and hepatitis C.

Adipose-derived stromal cells exhibit a mesenchymal stem cell-like phenotype

The second criterion for defining adipose-derived stromal cell populations following demonstration of their ability to adhere to tissue culture plastic is their immunophenotype profile which was determined using five-colour flow cytometry at each passage during the first 4 passages and thereafter once an experiment was seeded. A lack of expression (≤2%) of CD45 (hematopoietic marker/surface antigen), and CD34 (hematopoietic progenitor marker) was necessary in order to be able to define these cells as ASCs. The combination of these two markers represents the peripheral blood stem/progenitor cell compartment. The

cells were assessed for expression of CD73 (also known as ecto-5'-nucleotidase) and CD90 (a membrane glycoprotein, also called Thy-1), which are used as stem cell markers, and CD105 (Endoglin) is a proliferation-associated protein that is generally considered an important marker for ASCs (9, 43). An expression of ≥95% is required in order to be able to define these cells as ASCs. The more of these surface markers situated on a cell surface, the more epitopes available for antibody binding. The result is more fluorescence being emitted from a particular cell and subsequently, an increase in fluorescence on the single-parameter histogram plot, which is demonstrated by a shift to the right of the plot.

Positive staining was estabilished by comparison to unstained samples. Cellular autofluorescence is commonly found when utilising flow cytometry. Autofluorescence can interfere with the detection of low level fluorescence. The ASCs had a high level of autofluorescence but this was accounted-for throughout the experiments by shifting the unstained sample's fluorescence to within the first decade of the single-parameter histogram plots. Overlay plots for all the selected surface markers were generated. The number of cells acquired for unstained samples compared to stained samples were different and this was because all acquisitions were stopped after a fixed time period and not following a fixed number of events. This resulted in differences in the heights of the histograms observed. The percentage of cells staining positive for CD73, CD90, and CD105 surface markers was above the recommended >95%. All three markers were consistently expressed on the vast majority of the cells following culture with CD90 being present at higher levels than the other markers following P0.

A great variability of CD34 expression was observed between donors during early passages (P0 and P1). The CD34 expression levels remained above 2% and then declined to below 2% from P2 and successive passages. It has been proposed that CD34 expression depends on culture conditions and disappears upon expansion in culture (44, 45). This concept was also observed as early as 2001 by Gronthos and colleagues with gene and protein expression confirmation. They proposed that CD34-positivity may be due to the proliferative stage of the cells or donor heterogeneity (46). De Ugarte and colleagues observed low positive expression of CD34 on ASCs but not on MSCs. Thus it is hypothesized that the decrease of CD34 expression seen in this study is due to its expression in adipose-tissue resident stromal cells, possibily of hematopoietic origin, and loss with subsequent culturing. The variability in CD34 expression observed throughout the initial passages between donors could be due to

donor heterogeneity. Studies have also mentioned variability in expression of CD45. Deschaseaux and colleagues found expression of CD45 in freshly isolated cells from the bone marrow and no expression in cultured MSCs (47). It was suggested by Bourin *et al*. 2013 that the SVF was positive for CD45 expression but ASCs have low or undetectable levels of CD45. However, the authors did not expand on the reason for this loss in CD45 expression. In the study described herein CD45 expression was seen in a subset of cells in the earlier passages (P0-P2) but was lost in later passages. The $CD45^+$ cells could be contaminating macrophages and dendritic cells that are also initially plastic adherent. McIntosh and colleagues also observed this disappearance in expression of CD45 (11). An important consideration is whether trypsinization affects cell surface marker expression. Trypsinization, although a standardized technique, has in fact been shown to affect cell surface markers (48, 49). This technique was used consistently throughout all experiments, thus the effects would be constant throughout.

Literature mainly looks at the expression of individual markers and not the combined ASC CD73+CD90+CD105+CD34-CD45- phenotype obtained from the tree plots. Individual expression for positive surface markers CD73, CD90 and CD105 was greater than 95%, but when the panel of markers was combined in one tube, less than 95% positive expression was observed at certain passages. This was due to the variable expression of CD34 and CD45 influencing the immunophenotype. In summary, overall ASCs expressed the classical MSC CD73+CD90+CD105+CD34-CD45- phenotype proposed by Dominici *et al*. 2006 (20).

Viability of adipose-derived stromal samples

Percentages of viable and non-viable cells were analyzed on a Gallios flow cytometer. The results demonstrated that >90% cell viability was maintained over 5 passages of culture upon assaying PI uptake. This fulfills the requirements to characterize ASCs as described by Bourin and colleagues. Kerr and colleagues proposed the name "apoptosis" for programmed cell death in 1972 (50). They described that apoptosis can be classified by morphological changes. These changes are nuclear and cytoplasmic condensation, followed by the breaking-up of the cell into a number of membrane bound compartments. Thus the cells undergo shrinkage and would have decreased FS. Each viability experiment underwent initial FS versus SS analysis. This decrease in FS was observed with the intact cells that were treated with 100 μM H_2O_2. Disruption of the cell membrane and loss of DNA has been

utilized in flow cytometric methods for the detection of cell viability. Popular viability assays use Annexin V, which detects the membrane exposure of phosphatidylserine, or use PI, which intercalates between the nucleotide bases of DNA, evaluating any loss in DNA. Zamai and colleagues state that various treatments that are used to detach adherent cells, such as trypsin, interfere with the binding of Annexin V to membrane phosphatidylserine, perhaps affecting the measurement of apoptosis. They mention that the binding of PI to the DNA or RNA structures is stable enough to withstand trypsinization (51). Living cells are PI negative, and non-viable cells are PI positive. Zamai and colleagues classify non-viable cells further into PI dim apoptotic cells and PI bright necrotic cells.

Fibroblastoid colony-forming unit (CFU-F) assay

A stem cell is any cell with a high capacity for self-renewal (52) and differentiation capacity. Terminally differentiated cells are replaced following cell death through the proliferation of progenitor or stem cells. The CFU-F assay is used to define the number of progenitor cells (9). Bourin and colleagues characterize adult stromal cells by a number of properties with one of these being the ability to form colonies from single cells. The assay that was used is a modification of the one applied to MSCs (53). The cell concentrations were optimized and the isolated, plastic-adherent ASCs were plated in triplicate with 100 cells per dish (average cell density 1.72 cells/cm^2). At 13 days, the tissue culture dishes were washed with PBS and stained with Toluidine Blue O for enumeration of the colonies. According to Bourin and colleagues, a group of >50 cells can be considered a colony (9). The frequency of ASCs able to form colonies should be greater than 5%. This was demonstrated with all donor cultures.

The heterogeneous nature of the ASC population, in size and cell morphology, was apparent upon inspection of individual colonies. There was a large variation in colony sizes, indicative of varied cell growth rates, observed between plates from the same donor and different donors. The individual cells within each colony varied in morphology, with numerous cells being spindle in shape; however, a few larger flat cells also existed. The two types of cell morphology were also noted during expansion of the cultures. There was a trend in colony size distribution towards having >50 cells per colony with all donors. This indicated that the ASCs have self-renewal potential. Donor A220313, in particular, appeared to have a greater replicative potential. Suga and colleagues indicated in their 2009 study that CD34+ ASCs were more proliferative and had a greater ability to form colonies (54). The expression of

CD34 of donor A220313 (P4F1) was examined to see if the differences in colony-forming potential of A220313 (P4F1) could be due to variation in CD34 expression. This was not the case and donor A220313 did not have increased CD34 expression compared to the other donors.

The intra-culture variability observed may be due to the heterogeneous nature of the individual ASC population. An example could be that out of the 100 cells initially plated in one of the tissue culture dishes from A220313, there were cells with a more proliferative potential seeded and thus larger colonies were obtained in this tissue culture dish. However, perhaps, in another dish, cells with less replicative potential were seeded and thus smaller colonies were obtained for this dish from the same donor culture. A schematic representation of this scenario is presented in Figure 3.20. The inter-culture variability is likely to be due to the genetic variability that inherently exists between donors. The heterogeneous nature of individual cultures as well as donor-to-donor variation is a common observation. Phinney *et al.* noticed this exact variation within and among different donor populations of MSCs (Phinney et al., 1999).

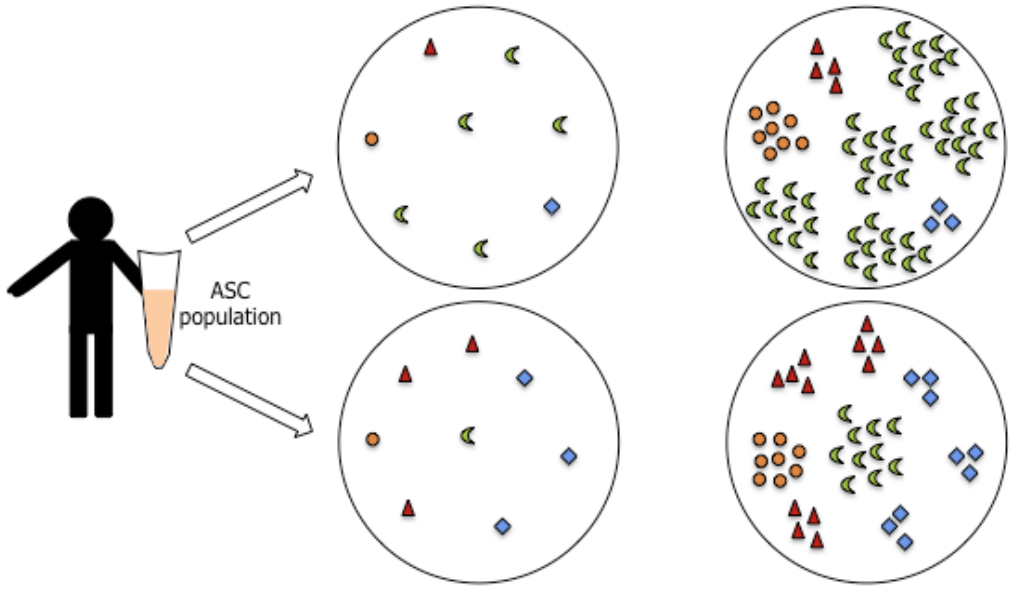

Figure 3.20. A schematic representation of heterogeneity within an individual ASC population. In one scenario many cells with a greater replicative potential (such as the green moon shape) may be seeded in a tissue culture dish leading to numerous larger colonies (top pair). In the second scenario, cells with less replicative potential (such as the red triangles and blue diamonds) may be seeded leading to the growth of smaller-sized colonies (bottom pair).

Multi-differentiation potential of adipose-derived stromal cells *in vitro*

Many previous studies have demonstrated that *in vitro* expanded ASCs have the potential to differentiate into multiple cell types (5, 12, 55, 56). It is in fact one of the criteria for defining ASCs; thus the tri-lineage potential of the ASCs into adipocytes, osteoblasts and chondrocytes was assessed. To assess the multipotentiality of the ASCs, cells from three donors (A180313, A220313 and A070813) at passage 3 to 5 were induced to differentiate using lineage specific cocktails. All three of these cultures demonstrated the ability to differentiate down the adipogenic, osteogenic and chondrogenic lineages.

Adipogenic differentiation

The culture-expanded ASCs were used following the third passage, at confluence, for adipogenic differentiation. Adipose differentiation relies on pre-adipocyte growth arrest. This growth arrest is said to occur upon cell-cell contact at confluence (57, 58). Under the appropriate adipogenic induction conditions, the ASCs exhibited adipose differentiation *in vitro*, changing their fibroblastic spindle shape to rounded cells with multiple intracytoplasmic lipid droplets. The conventional histological Oil Red O lipid-based detection method was employed to detect the lipid droplets. Lipid droplets consist of a neutral lipid (triacylglycerols and sterol esters) core surrounded by a phospholipid monolayer with embedded proteins (30). Oil Red O is used to detect triacylgycerols and sterol esters and stains these neutral lipids red/orange in colour. At 7, 14 and 21 days of differentiation, the non-induced and induced cultures were fixed and stained with Oil Red O and counter-stained with Toluidine Blue O. Lack of Oil red O staining was observed in the non-induced cultures. Oil Red O positive lipid droplets were observed in the adipogenic induced cultures. The lipid droplets detected throughout the induction period varied in size, volume and number.

During the first week of exposure to the adipogenic induction medium, a proportion of the cells acquired lipid droplets. Initially there was a vast array of different cells which varied in size and shape. They ranged from the starting spindle-shape with some not containing lipid droplets, to those containing few lipid droplets. The initial acquisition of lipid droplets occurred at one pole of the cell. This was then followed by an increase in the number of lipid droplets around the nucleus of the cell. As the number of lipid droplets increased, an extensive coalescing of these small lipid droplets took place. Through the second week, the numbers of lipid droplets increased and they continued to aggregate into clusters. The

spindle shape became progressively modified to a bigger more spherical shape. At three weeks, the observed trend towards larger droplets continued. The masses of accumulated lipid droplets within the cytoplasm displaced the nucleus to the periphery in some cases. The accumulation of lipid droplets is a noticeable criterion for describing the progression of adipogenesis (59).

A typical mature white adipocyte is said to contain one large lipid droplet of approximately 100 μm, in diameter (60). In the adipogenic induced cultures of this study no large unilocular lipid droplets indicative of a mature adipocyte were observed. These cells are, however, rather fragile and are prone to bursting resulting in the leakage of lipid droplets into the medium. Many of the cells also lift off the plastic surface possibly due to increased buoyancy. It is possible that mature adipocytes would form but were lost before reaching this stage of differentiation. Another possible reason for not observing a single large lipid droplet could be that these cells did not differentiate into white adipocytes but differentiated into beige adipocytes. Beige adipocytes are classified by multilocular lipid droplet morphology and they can be found interspersed within subcutaneous white adipose tissue (61). One theory is that beige and white adipocytes develop from a common mesenchymal predecessor and another theory is that white adipocytes can undergo transdifferentiation into beige adipocytes under the influence of many different factors (62). On the other hand Seale and colleagues demonstrated that brown adipocytes have a different origin (63). To confirm whether the ASCs differentiated into beige adipocytes, expression of uncoupling protein-1 (UCP1), Cidea, and PPARγ, coactivator 1 (Pgc1)-α, could be assessed. During basal states beige adipocytes have similar gene expression patterns to white adipocytes (64).

It was observed that some of the cultures stained with Oil Red O had irregular uptake of the stain with a few of the differentiated cells. This could be due to the cells being at different stages of adipogenesis. The Oil Red O staining protocol was previously optimized to diminish background staining and prevent crystallization of the Oil Red O because these are common occurrences. The more intracytoplasmic lipid droplets contained within a cell, the more the clarity of the lipid droplets was affected. The addition of Toluidine Blue O confounded the decrease in clarity. The use of Nile red staining of the lipid droplets as an alternative stain would be more reliable and would lead to more punctate staining of the lipid droplets. Image acquisition and analysis is not representative of the entire cell population and can be subjective. Aldridge and colleagues compared four different methods for determining adipose

differentiation of a heterogenous MSC population. They proposed that the use of Nile red in conjunction with flow cytometry was useful for determining *in vitro* adipogenic differentiation (65). The use of Nile red staining and flow cytometry for confirmation of adipogenesis are used in further chapters. Terminal adipogenic differentiation as stated previously is marked by a change in morphology and the accumulation of intracytoplasmic lipid droplets. This adipocyte phenotype is initiated by the expression of C/EBPδ and C/EBPβ, in early differentiation which leads to the synergistic activation of both the PPARγ and C/EBPα genes (66, 67). In addition to the qualitative Oil Red O method, expression of these genes and other additional genes would allow us to quantify adipogenesis and confirm that adipogenesis and not just lipogenesis has occurred. A panel of real-time (q)PCR primers as well as Nile red and flow cytometry will be included for a more robust assessment of adipogenesis in future studies.

Osteogenic differentiation

Bone formation is a complex process. There are two pathways essential for bone formation. During endochondral ossification, MSCs differentiate into chondrocytes, which are replaced by osteoblasts further down the differentiation pathway. Intramembranous ossification is the second process of bone formation that occurs in a few discrete areas of the skull and clavicle. In this case MSCs develop directly into osteoblasts and there is no cartilage formation involved in the process (68). The basic principle behind bone formation is that it involves the initial proliferation of MSCs, the migration of these MSCs to the site of bone formation, their subsequent differentiation into osteoblasts, extracellular matrix maturation and finally mineralization (69, 70). Mature osteoblasts are cuboidal cells that secrete type I collagen and non-collagenous proteins that make up a bone extracellular matrix. Osteoblasts, and the bone matrix proteins (BMPs) they produce, are thought to facilitate calcium and phosphate ion accumulation and the regulation of the mineralization process. Osteoblasts can become compacted into the calcified matrix and differentiate further into osteocytes during new bone formation. Osteocytes are the most abundantly found cells in the bone and are stellate in shape. Osteoclasts, another cell type unique to bone which are derived through a different process, are multinucleated cells that are involved in bone resorption and remodelling.

In vitro, the ASCs can be induced to form the extracellular matrix in culture by treatment with an osteogenic inducing medium. This osteogenic medium contains a source of phosphate, ascorbic acid, and dexamethasone. Extracellular matrix vesicles that bud and are released from the surface of osteoblasts initiate bone mineralization. These vesicles contain calcium binding molecules and sodium-dependent phosphate ion transporters that allow the ingress and accumulation of calcium and phosphate ions within the vesicles. The calcium and phosphate ions are utilized for the formation of hydroxyapatite ($Ca_{10}(PO_4)_6(OH_2)_2$), the main inorganic component of bone. Mineralization is initiated with the release of the preformed hydroxyapatite crystals (71, 72). Alizarin Red S staining demonstrated calcium-rich deposits in the extracellular matrix produced by the cells in culture. In aqueous solution Alizarin Red S and calcium ions precipitate to form brick-red deposits (73). Following induction in the presence of osteogenic induction medium, the cell monolayers were stained brick-red and the staining was visible to the naked eye. Variability in osteogenic differentiation was observed across the three donor cultures but all cultures underwent osteogenic differentiation.

Morphologic examination is not adequate in the analysis of osteogenic differentiation. The extracellular matrix formed a red stained layer above the cells that made it difficult to focus with the microscope on the underlying cells. Apart from the difficulty in identifying the changes in cell shape from spindle to cuboid beneath the matrix in areas of the culture, this method of identification is not quantitative. Assaying alkaline phosphatase enzyme activity has been implemented more frequently to quantify osteogenic differentiation. However, alkaline phosphatase is not specific to just osteoblasts. Osteocytes, preosteoblasts, osteosarcoma cells, and chondrocytes express it as well as other cell types, although to a lesser extent. Isoenzymes of alkaline phosphatase have been discovered in the liver, intestine and placenta (74, 75). A more reliable quantitative method would be to detect the expression of alkaline phosphatase along with the expression of other genes known to be involved in osteogenic differentiation. The panel of genes would consist of alkaline phosphatase, type I collagen, bone sialoprotein, osteopontin, osteonectin, and osteocalcin. Type I collagen is the most abundantly found component in the bone extracellular matrix and is associated with the formation of the extracellular matrix (76). Bone sialoprotein has the ability to nucleate (initial crystallization step) hydroxyapatite and is thus believed to initiate mineralization (77). Osteopontin may control mineralization by inhibiting hydroxyapatite deposition (78). Osteonectin is produced by osteoblasts and contains two

high affinity calcium ion binding sites and may mediate hydroxyapatite nucleation and deposition (79). Osteocalcin is also produced by osteoblasts and is required to stimulate bone mineral maturation (80) and may be involved in osteoclast differentiation (81). Extensive research has been carried out to investigate each step of osteogenic differentiation including molecular characterisation of the osteogenic pathway and should be utilised for future studies on osteogenic differentiation determination.

Chondrogenic differentiation

Cartilage is an avascular connective tissue composed of chondrocytes that secrete an extracellular matrix comprising collagen, proteoglycans and noncollagenous proteins (82, 83). There are three main but distinct types of cartilage: hyaline cartilage, fibrocartilage, and elastic cartilage. Hyaline cartilage is the most common form of cartilage that is found in the ribcage, nose, larynx and trachea. Articular cartilage is a subtype of hyaline cartilage that covers the articular surfaces of bones and joints. Hyaline cartilage is a precursor of bone. It is the main constituent of the fetal skeleton. During embryogenesis, MSCs differentiate into chondrocytes and secrete an extracellular matrix. As the fetus grows and develops, the chondrocytes located near to what will become bone (central zone) convert into hypertrophic chondrocytes which secrete proteins important for the calcification of the extracellular matrix. The hypertrophic chondrocytes are eventually replaced by osteoclasts and then osteoblasts during ossification. Hyaline cartilage is made up of chondrocytes that are embedded in chambers called lacunae within the matrix. Chondrocytes are found sparingly in all of the cartilage types (83). Type II collagen accounts for approximately 90% of the collagen in the extracellular matrix. Fibrocartilage is found in menisci, intervertebral discs, tendons, ligaments, and the temporomandibular joint (84). It has chondrocytes situated in lacunae that secrete an extracellular matrix comprised of dense collagen fibres, mainly consisting of type I collagen, although this can vary according to location, because fibrocartilage is a transitional tissue between hyaline cartilage and tendon or ligament (85). Elastic cartilage is found in the external ear, epiglottis and larynx. In elastic cartilage, the chondrocytes are also situated in an extracellular matrix; however, a mesh of elastic fibers (elastin) permeates the extracellular matrix in addition to collagen (86).

In vivo cartilage has no or very low regenerative ability and the fact that cartilage is comprised of just one cell type has made it a popular target for tissue engineering. Research

has demonstrated that dedifferentiated chondrocytes expanded as a two-dimensional monolayer culture (87, 88) and MSCs grown as monolayer cultures struggle to undergo cartilage differentiation (89). These studies demonstrate the importance of cell-cell and cell-extracellular matrix interactions and the need for a three-dimensional structure, similar to the *in vivo* environment. Geiger reviews the importance of the three-dimensionality of the matrix and the formation of cellular adhesions in culture systems (90). To promote chondrogenic differentiation of MSCs in culture, Johnstone used the micromass pellet culture system in 1998 (27). The cells are placed in a tube and centrifuged to form a cell aggregate. This aggregate is then treated with chondrogenic induction medium that lacks serum and contains amongst other components TGF-β_3. Our research group has previously done extensive literature searches on the composition of all of the induction media. Serum is a very important factor for cell culturing; however, the use of serum-free media and the addition of ITS^{TM} premix supplement has been optimized to enhance chondrogenic differentiation. Transforming growth factor-β_3 is an essential inducer of chondrogenesis and was thus included in the chondrogenic induction medium. Indrawattana and colleagues demonstrated via qPCR that induction medium containing TGF-β_3 alone significantly increased the expression of genes Sry-type high mobility group box 9 (sox 9), aggrecan, and type I and type II collagen (91). Sry-type high mobility group box 9 is a transcription factor that is critical for chondrogenic differentiation and regulates the expression of aggrecan and type II collagen (92, 93).

Following 21 days of chondrogenic induction, the micromass pellet cultures were stained with Toluidine Blue O. The chondrogenic medium induced pellets appeared to consist of two zones compared to the control pellets. The control pellets were also all smaller than the chondrogenic-induced pellets. The stained surface layer appeared to consist of more spindle-shaped cells. An inner zone consisted of polygonal cells. At a magnification of 140x the different cell shapes were clearer. Some of the pellet sections appeared to have a disrupted outer layer. It is unknown whether this could be due to the dehydration process or polymerization of the resin or a genuine artifact of the cartilage pellet. Ichinose and colleagues also made this observation. Magne and colleagues discuss that articular cartilage consists of three layers; a surface or superficial zone, mid zone, and deeper zone (94). Ichinose and colleagues also observed three layers at 14 days of induction, but at a later time-point, of 21 days, only two layers were detected. To confirm the chondrogenic phenotype further immunohistochemistry with antibodies against type I, II, X collagen and

aggregan should be carried out in future. Type II collagen is a basic cartilage-specific marker and type X collagen is a marker for chondrocyte hypertrophy (95). Type I collagen expression should be negligible as this is a marker for fibrocartilage (96). Literature states that at 21 days of induction type I collagen and proteoglycan were detected only in the superficial zone of the pellet. Type II collagen and aggregan were detected in the mid zone and in the deeper zone of the pellet. Type X collagen was detected in the deep zone of the pellet (94, 97). The cultures in this study were able to undergo pellet formation but Toluidine Blue O staining was not sufficient to delineate the different zones within the pellet and no chondrogenic-specific markers were included. Chondrogenic differentiation should be assessed via histology, immunohistochemistry, and quantitative analysis of the expression of the chondrogenic-specific genes using qPCR.

Conclusion

The results from this chapter underscore the importance of a thorough initial characterization of the cells. In order to answer the objectives of the entire study it had to be determined if the isolated cells were indeed ASCs. The cell populations described herein presented characteristics that enabled their classification as ASCs. The isolated cells, both fresh and thawed cryopreserved cells, derived from human lipoaspirate (adipose tissue), were examined on the basis of adherence characteristics, immunophenotype, viability, colony-forming ability, and differentiation potential. It must be noted that ASCs are isolated from individuals with different genetic backgrounds. Donor variability needs to be taken into account. The heterogeneity of the ASC populations renders comparison of results difficult. A further challenge, eloquently put by Potten and Loeffler, was that stem cells are defined in terms of their functional capabilities. These capabilities "can only be assessed by testing the abilities of the cells, which itself may alter their characteristics during the assay procedure" (98). The stromal cells isolated from fat are complex and their functions are not well defined; however, with more worldwide collaborations, as seen with the IFATS and ISCT provisional statement, this will inevitably improve. The findings presented here cannot be directly extrapolated to an *in vivo* environment, but describe a multipotent stromal cell population within adult human lipoaspirate. Thus, the primary goal of this chapter was satisfied, characterizing ASCs according to the criteria described by Bourin *et al.*, 2013 (9).

References

1. Pittenger MF, Mackay AM, Beck SC, Jaiswal RK, Douglas R, Mosca JD, et al. Multilineage potential of adult human mesenchymal stem cells. Science. 1999;284(5411):143-7.
2. Gimble JM. Adipose tissue-derived therapeutics. Expert opinion on biological therapy. 2003;3(5):705-13.
3. Nishida S, Endo N, Yamagiwa H, Tanizawa T, Takahashi HE. Number of osteoprogenitor cells in human bone marrow markedly decreases after skeletal maturation. Journal of bone and mineral metabolism. 1999;17(3):171-7.
4. Stenderup K, Justesen J, Clausen C, Kassem M. Aging is associated with decreased maximal life span and accelerated senescence of bone marrow stromal cells. Bone. 2003;33(6):919-26.
5. Zuk PA, Zhu M, Ashjian P, De Ugarte DA, Huang JI, Mizuno H, et al. Human adipose tissue is a source of multipotent stem cells. Molecular biology of the cell. 2002;13(12):4279-95.
6. Lee OK, Kuo TK, Chen WM, Lee KD, Hsieh SL, Chen TH. Isolation of multipotent mesenchymal stem cells from umbilical cord blood. Blood. 2004;103(5):1669-75.
7. Wang HS, Hung SC, Peng ST, Huang CC, Wei HM, Guo YJ, et al. Mesenchymal stem cells in the Wharton's jelly of the human umbilical cord. Stem Cells. 2004;22(7):1330-7.
8. Erices A, Conget P, Minguell JJ. Mesenchymal progenitor cells in human umbilical cord blood. British journal of haematology. 2000;109(1):235-42.
9. Bourin P, Bunnell BA, Casteilla L, Dominici M, Katz AJ, March KL, et al. Stromal cells from the adipose tissue-derived stromal vascular fraction and culture expanded adipose tissue-derived stromal/stem cells: a joint statement of the International Federation for Adipose Therapeutics and Science (IFATS) and the International Society for Cellular Therapy (ISCT). Cytotherapy. 2013;15(6):641-8.
10. Yanez R, Lamana ML, Garcia-Castro J, Colmenero I, Ramirez M, Bueren JA. Adipose tissue-derived mesenchymal stem cells have in vivo immunosuppressive properties applicable for the control of the graft-versus-host disease. Stem Cells. 2006;24(11):2582-91.
11. McIntosh K, Zvonic S, Garrett S, Mitchell JB, Floyd ZE, Hammill L, et al. The immunogenicity of human adipose-derived cells: temporal changes in vitro. Stem Cells. 2006;24(5):1246-53.
12. Zuk PA, Zhu M, Mizuno H, Huang J, Futrell JW, Katz AJ, et al. Multilineage cells from human adipose tissue: implications for cell-based therapies. Tissue engineering. 2001;7(2):211-28.
13. Yoon E, Dhar S, Chun DE, Gharibjanian NA, Evans GR. In vivo osteogenic potential of human adipose-derived stem cells/poly lactide-co-glycolic acid constructs for bone regeneration in a rat critical-sized calvarial defect model. Tissue engineering. 2007;13(3):619-27.

14. Kang SK, Putnam LA, Ylostalo J, Popescu IR, Dufour J, Belousov A, et al. Neurogenesis of Rhesus adipose stromal cells. Journal of cell science. 2004;117(Pt 18):4289-99.
15. Nakagami H, Maeda K, Morishita R, Iguchi S, Nishikawa T, Takami Y, et al. Novel autologous cell therapy in ischemic limb disease through growth factor secretion by cultured adipose tissue-derived stromal cells. Arteriosclerosis, thrombosis, and vascular biology. 2005;25(12):2542-7.
16. Chapel A, Bertho JM, Bensidhoum M, Fouillard L, Young RG, Frick J, et al. Mesenchymal stem cells home to injured tissues when co-infused with hematopoietic cells to treat a radiation-induced multi-organ failure syndrome. J Gene Med. 2003;5(12):1028-38.
17. Spring H, Schuler T, Arnold B, Hammerling GJ, Ganss R. Chemokines direct endothelial progenitors into tumor neovessels. Proceedings of the National Academy of Sciences of the United States of America. 2005;102(50):18111-6.
18. De Ugarte DA, Alfonso Z, Zuk PA, Elbarbary A, Zhu M, Ashjian P, et al. Differential expression of stem cell mobilization-associated molecules on multi-lineage cells from adipose tissue and bone marrow. Immunology letters. 2003;89(2-3):267-70.
19. Muehlberg FL, Song YH, Krohn A, Pinilla SP, Droll LH, Leng X, et al. Tissue-resident stem cells promote breast cancer growth and metastasis. Carcinogenesis. 2009;30(4):589-97.
20. Dominici M, Le Blanc K, Mueller I, Slaper-Cortenbach I, Marini F, Krause D, et al. Minimal criteria for defining multipotent mesenchymal stromal cells. The International Society for Cellular Therapy position statement. Cytotherapy. 2006;8(4):315-7.
21. Friedenstein AJ, Gorskaja JF, Kulagina NN. Fibroblast precursors in normal and irradiated mouse hematopoietic organs. Experimental hematology. 1976;4(5):267-74.
22. Lin CS, Ning H, Lin G, Lue TF. Is CD34 truly a negative marker for mesenchymal stromal cells? Cytotherapy. 2012;14(10):1159-63.
23. Pu LL, Coleman SR, Cui X, Ferguson RE, Jr., Vasconez HC. Autologous fat grafts harvested and refined by the Coleman technique: a comparative study. Plastic and reconstructive surgery. 2008;122(3):932-7.
24. Ullah M, Stich S, Haupl T, Eucker J, Sittinger M, Ringe J. Reverse differentiation as a gene filtering tool in genome expression profiling of adipogenesis for fat marker gene selection and their analysis. PloS one. 2013;8(7):e69754.
25. Williams IH, Polakis SE. Differentiation of 3T3-L1 fibroblasts to adipocytes. The effect of indomethacin, prostaglandin E1 and cyclic AMP on the process of differentiation. Biochemical and biophysical research communications. 1977;77(1):175-86.
26. Styner M, Sen B, Xie Z, Case N, Rubin J. Indomethacin promotes adipogenesis of mesenchymal stem cells through a cyclooxygenase independent mechanism. Journal of cellular biochemistry. 2010;111(4):1042-50.
27. Johnstone B, Hering TM, Caplan AI, Goldberg VM, Yoo JU. In vitro chondrogenesis of bone marrow-derived mesenchymal progenitor cells. Experimental cell research. 1998;238(1):265-72.

28. Barry F, Boynton RE, Liu B, Murphy JM. Chondrogenic differentiation of mesenchymal stem cells from bone marrow: differentiation-dependent gene expression of matrix components. Experimental cell research. 2001;268(2):189-200.
29. Koller CA, King GW, Hurtubise PE, Sagone AL, LoBuglio AF. Characterization of glass adherent human mononuclear cells. J Immunol. 1973;111(5):1610-2.
30. Bartz R, Zehmer JK, Zhu M, Chen Y, Serrero G, Zhao Y, et al. Dynamic activity of lipid droplets: protein phosphorylation and GTP-mediated protein translocation. Journal of proteome research. 2007;6(8):3256-65.
31. Kern S, Eichler H, Stoeve J, Kluter H, Bieback K. Comparative analysis of mesenchymal stem cells from bone marrow, umbilical cord blood, or adipose tissue. Stem Cells. 2006;24(5):1294-301.
32. Mets T, Verdonk G. In vitro aging of human bone marrow derived stromal cells. Mechanisms of ageing and development. 1981;16(1):81-9.
33. Wuchter P, Boda-Heggemann J, Straub BK, Grund C, Kuhn C, Krause U, et al. Processus and recessus adhaerentes: giant adherens cell junction systems connect and attract human mesenchymal stem cells. Cell and tissue research. 2007;328(3):499-514.
34. Krinner A, Hoffmann M, Loeffler M, Drasdo D, Galle J. Individual fates of mesenchymal stem cells in vitro. BMC systems biology. 2010;4:73.
35. Spees JL, Gregory CA, Singh H, Tucker HA, Peister A, Lynch PJ, et al. Internalized antigens must be removed to prepare hypoimmunogenic mesenchymal stem cells for cell and gene therapy. Molecular therapy : the journal of the American Society of Gene Therapy. 2004;9(5):747-56.
36. Bieback K, Ha VA, Hecker A, Grassl M, Kinzebach S, Solz H, et al. Altered gene expression in human adipose stem cells cultured with fetal bovine serum compared to human supplements. Tissue engineering Part A. 2010;16(11):3467-84.
37. Bruder SP, Jaiswal N, Haynesworth SE. Growth kinetics, self-renewal, and the osteogenic potential of purified human mesenchymal stem cells during extensive subcultivation and following cryopreservation. Journal of cellular biochemistry. 1997;64(2):278-94.
38. Pu LL, Cui X, Fink BF, Gao D, Vasconez HC. Adipose aspirates as a source for human processed lipoaspirate cells after optimal cryopreservation. Plastic and reconstructive surgery. 2006;117(6):1845-50.
39. Davis JM, Rowley SD, Braine HG, Piantadosi S, Santos GW. Clinical toxicity of cryopreserved bone marrow graft infusion. Blood. 1990;75(3):781-6.
40. Keung YK, Lau S, Elkayam U, Chen SC, Douer D. Cardiac arrhythmia after infusion of cryopreserved stem cells. Bone marrow transplantation. 1994;14(3):363-7.
41. Sharp PM, Bailes E, Robertson DL, Gao F, Hahn BH. Origins and evolution of AIDS viruses. The Biological bulletin. 1999;196(3):338-42.
42. Fenyo EM, Esbjornsson J, Medstrand P, Jansson M. Human immunodeficiency virus type 1 biological variation and coreceptor use: from concept to clinical significance. Journal of internal medicine. 2011;270(6):520-31.
43. Barry FP, Boynton RE, Haynesworth S, Murphy JM, Zaia J. The monoclonal antibody SH-2, raised against human mesenchymal stem cells, recognizes an epitope on

endoglin (CD105). Biochemical and biophysical research communications. 1999;265(1):134-9.

44. Mitchell JB, McIntosh K, Zvonic S, Garrett S, Floyd ZE, Kloster A, et al. Immunophenotype of human adipose-derived cells: temporal changes in stromal-associated and stem cell-associated markers. Stem Cells. 2006;24(2):376-85.
45. Maumus M, Peyrafitte JA, D'Angelo R, Fournier-Wirth C, Bouloumie A, Casteilla L, *et al*. Native human adipose stromal cells: localization, morphology and phenotype. Int J Obes (Lond). 2011;35(9):1141-53.
46. Gronthos S, Franklin DM, Leddy HA, Robey PG, Storms RW, Gimble JM. Surface protein characterization of human adipose tissue-derived stromal cells. Journal of cellular physiology. 2001;189(1):54-63.
47. Deschaseaux F, Gindraux F, Saadi R, Obert L, Chalmers D, Herve P. Direct selection of human bone marrow mesenchymal stem cells using an anti-CD49a antibody reveals their CD45med,low phenotype. British journal of haematology. 2003;122(3):506-17.
48. Biddle A, Gammon L, Fazil B, Mackenzie IC. CD44 staining of cancer stem-like cells is influenced by down-regulation of CD44 variant isoforms and up-regulation of the standard CD44 isoform in the population of cells that have undergone epithelial-to-mesenchymal transition. PloS one. 2013;8(2):e57314.
49. Tabatabaei M, Mosaffa N, Nikoo S, Bozorgmehr M, Ghods R, Kazemnejad S, et al. Isolation and partial characterization of human amniotic epithelial cells: the effect of trypsin. Avicenna J Med Biotechnol. 2014;6(1):10-20.
50. Kerr JF, Wyllie AH, Currie AR. Apoptosis: a basic biological phenomenon with wide-ranging implications in tissue kinetics. British journal of cancer. 1972;26(4):239-57.
51. Zamai L, Canonico B, Luchetti F, Ferri P, Melloni E, Guidotti L, et al. Supravital exposure to propidium iodide identifies apoptosis on adherent cells. Cytometry. 2001;44(1):57-64.
52. Lajtha LG. Stem cell concepts. Differentiation; research in biological diversity. 1979;14(1-2):23-34.
53. Castro-Malaspina H, Gay RE, Resnick G, Kapoor N, Meyers P, Chiarieri D, et al. Characterization of human bone marrow fibroblast colony-forming cells (CFU-F) and their progeny. Blood. 1980;56(2):289-301.
54. Suga H, Matsumoto D, Eto H, Inoue K, Aoi N, Kato H, et al. Functional implications of CD34 expression in human adipose-derived stem/progenitor cells. Stem cells and development. 2009;18(8):1201-10.
55. Gimble J, Guilak F. Adipose-derived adult stem cells: isolation, characterization, and differentiation potential. Cytotherapy. 2003;5(5):362-9.
56. Digirolamo CM, Stokes D, Colter D, Phinney DG, Class R, Prockop DJ. Propagation and senescence of human marrow stromal cells in culture: a simple colony-forming assay identifies samples with the greatest potential to propagate and differentiate. British journal of haematology. 1999;107(2):275-81.
57. Pairault J, Green H. A study of the adipose conversion of suspended 3T3 cells by using glycerophosphate dehydrogenase as differentiation marker. Proceedings of the National Academy of Sciences of the United States of America. 1979;76(10):5138-42.

58. Lefterova MI, Lazar MA. New developments in adipogenesis. Trends in endocrinology and metabolism: TEM. 2009;20(3):107-14.
59. Napolitano L. The Differentiation of White Adipose Cells. An Electron Microscope Study. The Journal of cell biology. 1963;18:663-79.
60. Murphy DJ, Vance J. Mechanisms of lipid-body formation. Trends in biochemical sciences. 1999;24(3):109-15.
61. Harms M, Seale P. Brown and beige fat: development, function and therapeutic potential. Nature medicine. 2013;19(10):1252-63.
62. Rosen ED, Spiegelman BM. What we talk about when we talk about fat. Cell. 2014;156(1-2):20-44.
63. Seale P, Bjork B, Yang W, Kajimura S, Chin S, Kuang S, et al. PRDM16 controls a brown fat/skeletal muscle switch. Nature. 2008;454(7207):961-7.
64. Park A, Kim WK, Bae KH. Distinction of white, beige and brown adipocytes derived from mesenchymal stem cells. World J Stem Cells. 2014;6(1):33-42.
65. Aldridge A, Kouroupis D, Churchman S, English A, Ingham E, Jones E. Assay validation for the assessment of adipogenesis of multipotential stromal cells--a direct comparison of four different methods. Cytotherapy. 2013;15(1):89-101.
66. Yeh WC, Cao Z, Classon M, McKnight SL. Cascade regulation of terminal adipocyte differentiation by three members of the C/EBP family of leucine zipper proteins. Genes & development. 1995;9(2):168-81.
67. Cao Z, Umek RM, McKnight SL. Regulated expression of three C/EBP isoforms during adipose conversion of 3T3-L1 cells. Genes & development. 1991;5(9):1538-52.
68. Karsenty G, Wagner EF. Reaching a genetic and molecular understanding of skeletal development. Developmental cell. 2002;2(4):389-406.
69. Stein GS, Lian JB, Owen TA. Relationship of cell growth to the regulation of tissue-specific gene expression during osteoblast differentiation. FASEB journal : official publication of the Federation of American Societies for Experimental Biology. 1990;4(13):3111-23.
70. Siggelkow H, Rebenstorff K, Kurre W, Niedhart C, Engel I, Schulz H, et al. Development of the osteoblast phenotype in primary human osteoblasts in culture: comparison with rat calvarial cells in osteoblast differentiation. Journal of cellular biochemistry. 1999;75(1):22-35.
71. Anderson HC. Molecular biology of matrix vesicles. Clinical orthopaedics and related research. 1995(314):266-80.
72. Anderson HC. Matrix vesicles and calcification. Current rheumatology reports. 2003;5(3):222-6.
73. Lievremont M, Potus J, Guillou B. Use of alizarin red S for histochemical staining of Ca^{2+} in the mouse; some parameters of the chemical reaction in vitro. Acta anatomica. 1982;114(3):268-80.
74. McKenna MJ, Hamilton TA, Sussman HH. Comparison of human alkaline phosphatase isoenzymes. Structural evidence for three protein classes. The Biochemical journal. 1979;181(1):67-73.
75. Fishman WH. Perspectives on alkaline phosphatase isoenzymes. The American journal of medicine. 1974;56(5):617-50.

76. Owen TA, Aronow M, Shalhoub V, Barone LM, Wilming L, Tassinari MS, et al. Progressive development of the rat osteoblast phenotype in vitro: reciprocal relationships in expression of genes associated with osteoblast proliferation and differentiation during formation of the bone extracellular matrix. Journal of cellular physiology. 1990;143(3):420-30.
77. Hunter GK, Goldberg HA. Nucleation of hydroxyapatite by bone sialoprotein. Proceedings of the National Academy of Sciences of the United States of America. 1993;90(18):8562-5.
78. Boskey AL, Maresca M, Ullrich W, Doty SB, Butler WT, Prince CW. Osteopontin-hydroxyapatite interactions in vitro: inhibition of hydroxyapatite formation and growth in a gelatin-gel. Bone and mineral. 1993;22(2):147-59.
79. Termine JD, Kleinman HK, Whitson SW, Conn KM, McGarvey ML, Martin GR. Osteonectin, a bone-specific protein linking mineral to collagen. Cell. 1981;26(1 Pt 1):99-105.
80. Boskey AL, Gadaleta S, Gundberg C, Doty SB, Ducy P, Karsenty G. Fourier transform infrared microspectroscopic analysis of bones of osteocalcin-deficient mice provides insight into the function of osteocalcin. Bone. 1998;23(3):187-96.
81. Liggett WH, Jr., Lian JB, Greenberger JS, Glowacki J. Osteocalcin promotes differentiation of osteoclast progenitors from murine long-term bone marrow cultures. Journal of cellular biochemistry. 1994;55(2):190-9.
82. Buckwalter JA, Mankin HJ. Articular cartilage: tissue design and chondrocyte-matrix interactions. Instructional course lectures. 1998;47:477-86.
83. Dijkgraaf LC, de Bont LG, Boering G, Liem RS. Normal cartilage structure, biochemistry, and metabolism: a review of the literature. Journal of oral and maxillofacial surgery : official journal of the American Association of Oral and Maxillofacial Surgeons. 1995;53(8):924-9.
84. Benjamin M, Ralphs JR. Biology of fibrocartilage cells. International review of cytology. 2004;233:1-45.
85. Eyre DR, Wu JJ. Collagen of fibrocartilage: a distinctive molecular phenotype in bovine meniscus. FEBS letters. 1983;158(2):265-70.
86. Sheldon H, Robinson RA. Studies on cartilage: electron microscope observations on normal rabbit ear cartilage. The Journal of biophysical and biochemical cytology. 1958;4(4):401-6.
87. Lefebvre V, Garofalo S, Zhou G, Metsaranta M, Vuorio E, De Crombrugghe B. Characterization of primary cultures of chondrocytes from type II collagen/beta-galactosidase transgenic mice. Matrix biology: journal of the International Society for Matrix Biology. 1994;14(4):329-35.
88. Benya PD, Shaffer JD. Dedifferentiated chondrocytes reexpress the differentiated collagen phenotype when cultured in agarose gels. Cell. 1982;30(1):215-24.
89. Worster AA, Brower-Toland BD, Fortier LA, Bent SJ, Williams J, Nixon AJ. Chondrocytic differentiation of mesenchymal stem cells sequentially exposed to transforming growth factor-beta1 in monolayer and insulin-like growth factor-I in a three-dimensional matrix. Journal of orthopaedic research: official publication of the Orthopaedic Research Society. 2001;19(4):738-49.

90. Geiger B. Cell biology. Encounters in space. Science. 2001;294(5547):1661-3.
91. Indrawattana N, Chen G, Tadokoro M, Shann LH, Ohgushi H, Tateishi T, et al. Growth factor combination for chondrogenic induction from human mesenchymal stem cell. Biochemical and biophysical research communications. 2004;320(3):914-9.
92. Akiyama H, Chaboissier MC, Martin JF, Schedl A, de Crombrugghe B. The transcription factor Sox9 has essential roles in successive steps of the chondrocyte differentiation pathway and is required for expression of Sox5 and Sox6. Genes & development. 2002;16(21):2813-28.
93. Furumatsu T, Tsuda M, Taniguchi N, Tajima Y, Asahara H. Smad3 induces chondrogenesis through the activation of SOX9 via CREB-binding protein/p300 recruitment. The Journal of biological chemistry. 2005;280(9):8343-50.
94. Magne D, Vinatier C, Julien M, Weiss P, Guicheux J. Mesenchymal stem cell therapy to rebuild cartilage. Trends in molecular medicine. 2005;11(11):519-26.
95. Hirsch MS, Cook SC, Killiany R, Hartford Svoboda KK. Increased cell diameter precedes chondrocyte terminal differentiation, whereas cell-matrix attachment complex proteins appear constant. The Anatomical record. 1996;244(3):284-96.
96. Eyre DR. The collagens of articular cartilage. Seminars in arthritis and rheumatism. 1991;21(3 Suppl 2):2-11.
97. Ichinose S, Tagami M, Muneta T, Sekiya I. Morphological examination during in vitro cartilage formation by human mesenchymal stem cells. Cell and tissue research. 2005;322(2):217-26.
98. Potten CS, Loeffler M. Stem cells: attributes, cycles, spirals, pitfalls and uncertainties. Lessons for and from the crypt. Development. 1990;110(4):1001-20.

> The great thing about science is that you can get it wrong over and over again because what you're after - call it truth or understanding - waits patiently for you. Ultimately, you'll find the answer because it doesn't change.
>
> - Dudley Herschbach

Chapter 4

The effect of induced oxidative stress and antioxidant supplementation on the adipogenic differentiation potential of adipose-derived mesenchymal stromal/stem cells

Introduction

The prevalence of obesity is increasing in both developing and developed countries. South Africa is ranked the third most obese country after the United States of America and Great Britain. One of the associated risk factors for obesity is dyslipidemia (abnormal amounts of lipids), adipose tissue hyperplasia (cell number proliferation and/or differentiation) and hypertrophy (cell size increase due to lipid droplet accumulation) (1, 2). Preadipocyte cell lines, particularly the 3T3- and Ob17 murine preadipocyte cell lines, have been valuable tools for the study of adipocyte differentiation *in vitro* and the mechanisms behind obesity (3, 4). The disadvantage of using cell lines is that they are aneuploidic (3, 4). Furthermore, murine cell lines may not reflect the same repertoire of gene expression that occurs during human adipogenesis. A human primary cell model would therefore provide better insights into adipose differentiation and metabolism, thus increasing our understanding of obesity and diabetes. Human adipose-derived stromal cells (ASCs) are capable of differentiating down the adipocyte lineage providing a useful human primary stromal cell model of adipogenesis. An added advantage is that human ASCs are capable of differentiating not only down the adipocyte lineage but also chondrocyte, osteoblast, myoblast and neuronal lineages providing further utility in tissue engineering and regeneration (5-10).

In order to understand the role of adipose tissue in obesity it will be necessary to understand the process of adipogenesis in its entirety. There is a deficit in our understanding of the intermediate adipocyte sub-populations that exist. Our understanding of adipogenesis is that it is a two-step process. The first step is the determination step, which consists of the commitment of the stem cells of mesodermal origin [mesenchymal stromal/stem cells (MSCs) or in all probability ASCs] to preadipocytes. These precursor cells possess no defining morphological features or specific gene expression markers (11). The second differentiation

step is the onset of terminal differentiation into functional mature adipocytes with the accumulation of cytoplasmic lipid droplets (12). Lipid droplets appear in the cytoplasm near the periphery of preadipocytes. The lipid droplets aggregate and enlarge through fusion. The enlarged lipid droplets migrate more centrally in the preadipocytes and a mature adipocyte is classified as containing a large unilocular lipid droplet. Lipid droplets are constitutively formed in adipocytes. However, non-adipocytes may contain small mobile lipid droplets (13).

The long-standing hypothesis was that lipid droplets are formed within the leaflets of the endoplasmic reticulum bilayer, eventually budding off as a mobile droplet into the cytosol. There is new evidence that suggests this is not the case and that lipid droplet formation occurs adjacent to the endoplasmic reticulum bilayer in cup-shaped regions (14). The core of the lipid droplet is occupied by hydrophobic neutral lipids, such as diacyglycerols, triacylglycerol, cholesteryl esters, retinyl esters in various ratios dependent on the cell type (15). The lipid droplet surface is an amphipathic phospholipid monolayer containing one or more of the perilipin–adipophilin-TIP47 (PAT) family of proteins and cholesterol. Adipophilin, one of the PAT family proteins found in clusters in the cytoplasm of the endoplasmic reticulum, adjacent to the forming lipid droplet, appears to function in transferring lipids from the endoplasmic reticulum to the droplet surface (14). Newly synthesized lipid droplets accumulate new lipids from both local and distal locations and acquire phospholipids, an array of enzymes, and recruit additional proteins (15, 16). This suggests a role not just in lipid storage but also as organelles functioning in cell signaling, lipid metabolism, membrane trafficking and storage, and degradation of proteins (17-19). Adipocytes can expand and shrink according to their lipid loading. Upon fusion of the lipid droplets, the surface-to-volume ratio decreases, which then should cause a surplus in amphipathic phospholipids. Boström and colleagues found that lipid droplets could grow after they had been assembled but that this increase in size is independent of triglyceride biosynthesis (20).

A popular histochemical stain, Oil red O, has been used to detect neutral lipids within adipocytes and qualitatively define adipose differentiation. This qualitative detection method cannot be used to distinguish between preadipocyte sub-populations. Researchers have previously extracted the Oil red O dye in an attempt to quantify adipogenesis (21). The use of monoclonal antibodies and cell sorting to define the intermediate adipogenic sub-populations has also been inadequate to date. Nile red (9-diethylamino-5H-benzo[α]phenoxazine-5-one) is a lipophilic stain that is relatively photostable and will not

fluoresce in polar solvents. However, in a lipid-rich environment it will fluoresce strongly. Nile red has been used in fluorescence microscopy and in flow cytometry. If Nile red is dissolved in neutral lipids, it will emit yellow-gold fluorescence (emission wavelength > 528 nm) and if Nile red is dissolved in amphipathic lipids which have a polar and non-polar end, such as the phospholipids, it will emit deep red fluorescence (emission wavelength > 590 nm) (Figure 4.1). The ability to shift its emission spectrum allows one to differentiate between different lipids. The lipid composition of lipid droplets can therefore be determined using the ability of Nile red to distinguish between neutral and amphipathic lipids (22). The progression in size from many small lipid droplets to one unilocular lipid droplet can be monitored during adipocyte maturation using Nile red. During the maturation of preadipocytes, the larger number of amphipathic lipids that are obtained as the lipid droplets merge and increase in size is correlated with an increase in deep red fluorescence. If one couples the Nile red measurement with DAPI (4′,6-diamidino-2-phenylindole dihydrochloride), a fluorescent stain that binds to nuclei, the actual number of cells with a specific lipid content ratio can be determined.

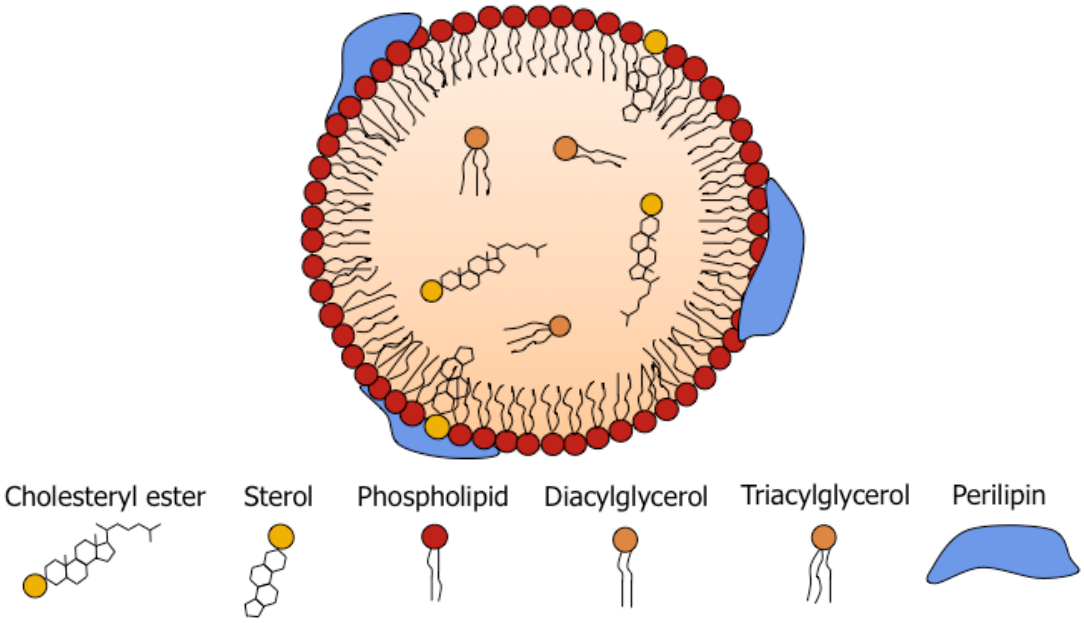

Figure 4.1. Schematic of the composition of a lipid droplet and how it relates to fluorescent staining with Nile red. Hydrophobic neutral lipids, such as diacyglycerols, triacylglycerol, and cholesteryl esters in various ratios, occupy the core of the lipid droplet. The lipid droplet surface is an amphipathic phospholipid monolayer containing one or more of the perilipin–adipophilin-TIP47 (PAT) family of proteins and cholesterol. This schematic indicates the unique ability of Nile red to distinguish between neutral (yellow/orange in colour) and amphipathic lipids (red in colour) and which parts of

the lipid droplet would emit yellow-gold and deep-red fluorescence after Nile red staining. Adapted from (23).

It has now been established that lipid droplets are involved in inflammatory processes. It was found that the production of reactive oxygen species (ROS), particularly hydrogen peroxide (H_2O_2), and lipid peroxidation is increased in white adipose tissue (WAT), but is not increased in muscle and liver tissue of obese mice. This is accompanied by expression of the transcription factor Spi-1 (spleen focus-forming virus proviral integration 1) which upregulates the transcription of the nicotinamide adenine dinucleotide phosphate (NADPH) oxidase (Nox) and high expression of the subunits of Nox, hence causing an increase in oxidative stress (Figure 4.2) (24). Inflammation is associated with the generation of ROS and the accumulation of ROS leads to oxidative stress. Thus, there is a close relationship between oxidative stress and inflammation. Oxidative stress is also implicated in the pathogenesis of many diseases including obesity, diabetes, cardiovascular disease, and cancer (25-27). In obesity, fat accumulation is correlated with increased oxidative stress and chronic inflammation. There are multiple underlying mechanisms for this increase in oxidative stress. The accumulation of adipocytes and adipose tissue itself is one such mechanism. Oxidative stress is accompanied by the augmented production of adipocytokines and cytokines by adipocytes and preadipocytes (Figure 4.2) (28). These are bioactive substances from WAT, comprised of, but not limited to, adiponectin, angiotensin II, interleukin-6 (IL-6), leptin, resistin, and tumor necrosis factor (TNF)-α (29, 30).

The majority of these adipocytokines and cytokines are pro-inflammatory (adiponectin is anti-inflammatory) and are potent stimulators of ROS and reactive nitrogen species (RNS) production. Adipose tissue has the capability to secrete angiotensin II. Angiotensin II stimulates Nox. This results in the production of superoxide (O_2^-) and the subsequent generation of H_2O_2 (31). NADPH oxidases, and in particular Nox4, are the major sources of ROS production in adipocytes (32). NADPH oxidase 4 is distinct from the other Nox proteins, as it constitutively produces copious amounts of H_2O_2. It is also situated on intracellular membranes (33). The cytokine, IL-6 is pro-inflammatory (34). Leptin can act directly on macrophage phagocytosis and increase the synthesis of the acute-phase reactant, C-reactive protein (CRP) as well as TNF-α and IL-6 (31, 35). Resistin has pro-inflammatory properties (36). Tumor necrosis factor-α is involved in inflammation, through the activation of nuclear factor $\kappa\beta$ (NF-$\kappa\beta$), and production of ROS, amongst other properties, and influences the

production of IL-6 (34, 37). In contrast, adipose tissue from lean individuals secretes anti-inflammatory adipocytokines such as adiponectin (38).

Another source of oxidative stress associated with adipose tissue is pressure on surrounding cells from the excessive adipose tissue accumulation leading to cellular damage. Cellular damage consequently results in the high production of TNF-α and ROS. This in turn leads to increased lipid peroxidation. Furthermore, calorie overconsumption leads to increased oxygen consumption and increased mitochondrial respiration and thus amplified ROS production (34, 39). Lastly, a pro-inflammatory response often results in the recruitment of phagocytic cells, such as macrophages, which release ROS and other oxidants in a respiratory burst which may damage neighboring cells thereby perpetuating the inflammatory cycle (40).

Recently it was recognized that ROS are widely used as second messengers to propagate stimulatory signals implicated in proliferation, survival mechanisms, and differentiation (41). Literature suggests that ROS play a role in adipogenesis (42). Furukawa and colleagues demonstrated that increased ROS production accompanied 3T3-L1 adipogenesis. They also suggested that Nox is the source of ROS during adipogenesis because a Nox inhibitor attenuated the increase in ROS (24). A second source of ROS that may promote adipogenesis is derived from mitochondrial Complex III (Figure 4.2). Tormos and colleagues found that mitochondrial ROS resulted in the upregulation of adipogenic transcriptional machinery in human MSCs (43). It was therefore hypothesized for this study that the addition of exogenous ROS would enhance the adipogenic differentiation potential of ASCs. Thus the effect of ROS on the adipogenic differentiation potential of ASCs was determined. An added advantage of carrying out a study involving ROS is that the target of ASC therapy is either a wound or an injury with the presence of inflammation, and therefore the generation of ROS.

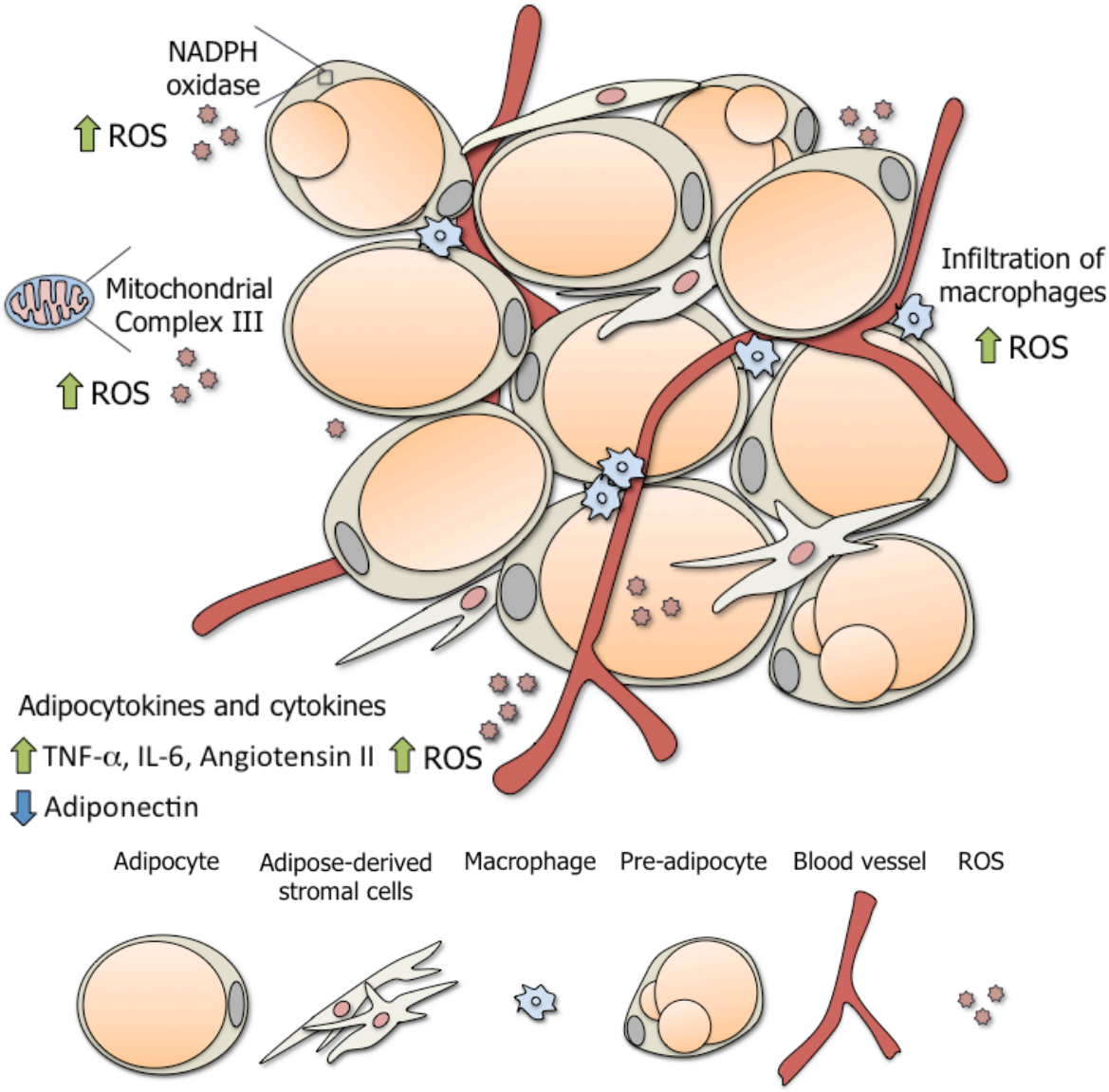

Figure 4.2. Schematic illustrating how ROS production is increased in accumulating adipose tissue and how ROS may contribute to adipogenesis. Oxidative stress is associated with the dysregulated production of adipocytokines and cytokines, which contributes to increased inflammation and ROS. Adipose tissue accumumlation itself can increase oxidative stress. Reactive oxygen species derived from NADPH oxidase (Nox) and mitochondrial Complex III may promote adipogenesis.

Materials and methods

Adipose-derived stromal cell culture and characterization

Lipoaspirates were obtained from consenting human donors following a modified Coleman technique using a syringe and a 3 mm blunt-tipped cannula (44). The isolation of the stromal vascular fraction (SVF) from the adipose tissue was performed as described in Chapter 3. The SVF cells were analyzed for adherence to plastic. Once the cells adhered to the plastic and contaminating erythrocytes, non-adherent cells and cell debris were removed, the cells could be termed ASCs (45). Positivity for cell surface markers (≥95%) CD73, CD90, CD105 and (≤2%) CD34, CD45 under standard culture conditions using flow cytometry (Gallios; Beckman Coulter, Krefeld, Germany) further characterized these cells. The ASCs were also characterized by tri-lineage differentiation into adipocytes, osteoblasts, and chondrocytes *in vitro*. These characteristics are all indicative of ASCs (Chapter 3).

Adipose-derived stromal cells were grown in Minimum Essential Medium-alpha (α-MEM; Gibco®, Invitrogen Corporation, Carlsbad, California, USA) containing 10% (v/v) fetal bovine serum (FBS; Biochrom AG, Berlin, Germany) and 2% (v/v) penicillin and streptomycin (Pen/Strep; Sigma-Aldrich, St. Louis, MO, USA) at 37°C in a humidified air incubator containing 5% CO_2. Adherent ASCs reached 80% subconfluency approximately 7 days after seeding. Adherent cells were detached from the plastic surface of the flask using Trypsin-EDTA (0.25%, w/v) (Gibco®) and counted using Flow-Count™ Fluorospheres (Beckman Coulter) on a 10-colour, 3-laser Gallios flow cytometer. Cells were seeded at 5.0×10^3 cells/cm^2 and complete growth medium was changed on the 1st and 5th days. The cells were fed on the 3rd day. Both freshly cultured and cryopreserved–thawed ASCs were used in the experiments. Mainly early-passage ASCs were used. Late passage ASCs were considered as greater than passage 15 (P15; 15 trypsinizations).

Three different types of cell culture media were used during the study to account for the ROS scavenging ability of pyruvate contained in the media: Dulbecco's minimal Eagle's medium with (+) pyruvate (Cat no. 31966-021), DMEM without (–) pyruvate (Cat no. 41965-039), and α-MEM + pyruvate (Cat no. 32561-029).

Cell viability assays

Two assays were used to determine the effects of the pro-oxidant, hydrogen peroxide (H_2O_2; Merck, Darmstadt, Germany), and the antioxidants, Trolox (Sigma-Aldrich) and CoQ10 (Sigma-Aldrich) on ASC viability *in vitro*. The pro-oxidant and antioxidants were made up in distilled water (dH_2O) and ethanol (EtOH) respectively, immediately prior to use. The two cell viability assay protocols are summarized in Figure 4.3.

MTT assay

Cell viability was analyzed using the 3-(4,5-dimethylthiazol-2-yl)-2,5-diphenyltetrazolium bromide (MTT; Sigma-Aldrich) assay. Stock was made up by dissolving MTT in PBS (pH 7.4) at 5 mg/ml and filtered. Mosmann suggested that filtering removes small amounts of insoluble residue that is present in some batches of MTT (46). At the times indicated below, stock MTT solution (10% of the medium volume) was added to all wells of an assay, and plates were incubated at 37°C for 4 hours. The supernatant was removed from the cells and allowed to dry in the flow cabinet (until visibly dry). The formazan blue crystals were solubilized by the addition of dimethyl sulfoxide (DMSO; Sigma-Aldrich) to all the wells. The plates were shaken on a plate shaker for 20 minutes to ensure that all crystals were dissolved. A 0.1 ml aliquot of each sample was then transferred to 96-well plates, and the absorbance of each well was measured at a wavelength of 570 nm against a reference wavelength of 630 nm using a microplate spectrophotometer (Power Wave X; BioTek Instruments, Winooski, VT, USA). The value that was used, as a measure of cell viability, was that of ASCs incubated in medium with the added conditions with subtraction of the blank (DMSO). The data was then expressed as a percentage of the control measured in the absence of conditions with the blank subtracted (considered 100% viable). As recommended by Mosmann, plates were read within 1 hour of adding the DMSO.

Initially the ASCs were seeded at 5 x 10^3 cells/cm^2 in 96-well plates (Nunc, Thermo Fisher Scientific, Roskilde, Denmark) in standard α-MEM growth medium and allowed to adhere for 24 hours. To establish H_2O_2 concentrations to use in further experiments α-MEM was exchanged for DMEM either + pyruvate or – pyruvate or fresh α-MEM. The media were supplemented with 10% (v/v) FBS and 2% (v/v) Pen/Strep. Following 24, 48, 72, 96 and 120 hours of exposure to a range of different H_2O_2 concentrations (0, 0.2, 0.4, 0.8, 1.56,

3.125, 6.25, 12.5, 25, 50, 100, 200 μM), viability was assessed using the MTT assay. Larger 12-well plates (Nunclon Delta; Nunc) were used for further experiments.

SRB assay

Cell viability was also analyzed using the Sulforhodamine B (SRB) colourimetric assay following the protocol proposed by Vichai and Kirtikara (47). The ASC cultures were fixed with cold 10% (w/v) trichloroacetic acid (TCA) and incubated at 4°C for 1 hour. Following incubation the cells were washed gently with water four times and left to dry. The ASC cultures were stained for 30 minutes with 0,057% (w/v) SRB dye dissolved in 1% acetic acid. Unbound dye was removed by four washes with 1% (v/v) acetic acid, and left to dry. Protein-bound dye was solubilized with 10 mM unbuffered Tris base (pH 10.5) [tris (hydroxymethyl)aminomethane] and shaking on a plate shaker for 5 minutes. The protein-bound dye was extracted for determination of optical density (OD) at 510 nm using a spectrophotometer. The OD is directly proportional to the cell number. The Tris blank was also subtracted from the OD values. The data was expressed as a percentage of the control.

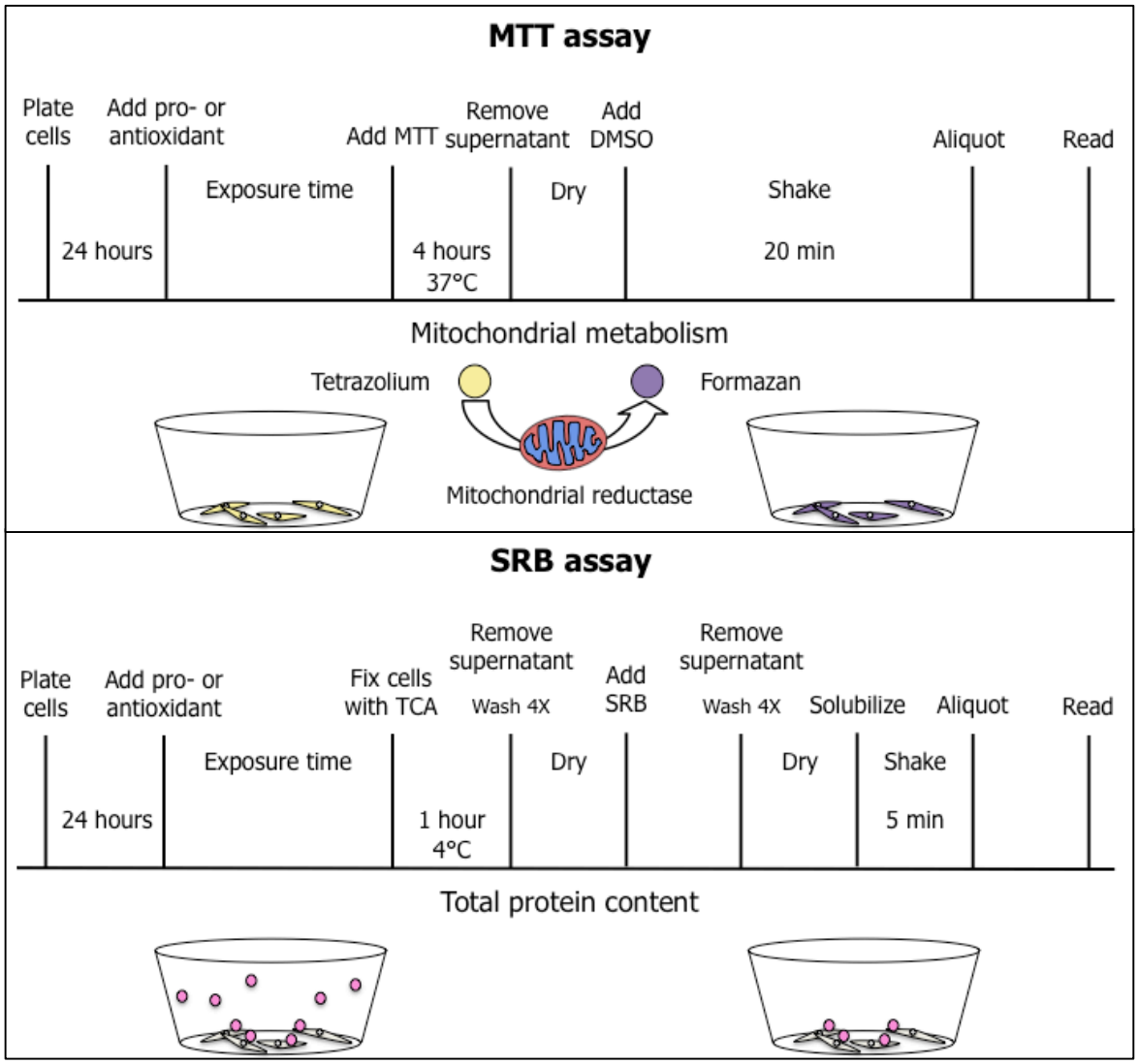

Figure 4.3. Protocol comparison of the MTT and SRB cell viability assays. The MTT assay is featured in the top half of the figure and the SRB assay in the bottom half of the figure. Cell seeding densities, cellular growth conditions, pro-oxidant and anti-oxidant concentrations, as well as exposure times were kept constant for both assays.

Fluorescent detection of intracellular ROS levels

MitoSOX™ red mitochondrial O_2^- indicator (Molecular Probes, Invitrogen, Eugene, Oregon, USA), a derivative of hydroethidine (HE), was used to detect intracellular O_2^-. Early-passage (P4, 5 and 9) thawed-cryopreserved ASC cultures from three different adipose tissue isolations were seeded in 6-well plates at 5 x 10^3 cells/cm^2 and grown to 80% confluency. In triplicate, cells were then supplemented with DMEM + pyruvate or – pyruvate for 24 hours. Positive control conditions consisting of tert-Butyl hydroperoxide (tBHP; provided by Professor van der Westhuizen at North-West University) and H_2O_2 were used. A negative control was provided by the O_2^- dismutase (SOD) mimetic (Manganese(III)tetrakis(4-benzoic acid)porphyrin chloride, MnTBAP; Calbiochem, San Diego, California). Following the 24 hours incubation period the ASCs were washed with PBS twice to remove any traces of FBS and phenol red, which can quench the fluorescence generated by MitoSOX™ red. A 5 mM stock of MitoSOX™ red was made in DMSO. A preliminary experiment determined that the appropriate concentration of MitoSOX™ red to add to the ASCs was 5 μM and an incubation period of 10 minutes. The cells were incubated at 37°C in the dark with a 5 μM working solution of the MitoSOX™ red probe for the 10 minutes. After incubation, the cells were washed twice with PBS to eliminate excess staining solution. The cells were trypsinized and the intracellular ROS was detected by flow cytometry using the Gallios flow cytometer in FL1 by 525/40 nm band pass (BP) filter. Data analysis was carried out using Kaluza analysis software (Beckman Coulter). Cell debris, non-viable cells and aggregated cells were excluded by gating only viable cells.

In vitro adipocyte differentiation

ASCs were seeded at a density of 5 x 10^3 cells/cm^2 in 6-well plates and cultured using standard growth medium (α-MEM). At confluence, in triplicate, the standard growth medium was replaced with adipogenic induction medium consisting of DMEM culture medium + or – pyruvate supplemented with 1 μM dexamethasone (Sigma-Aldrich), 0.5 mM 3-iosbutyl-methylxanthine (Sigma-Aldrich), 200 μM indomethacin (Sigma-Aldrich), 10 μg/ml human insulin (Sigma-Aldrich), 10% (v/v) FBS and 2% (v/v) Pen/Strep (48). Insulin and indomethacin increase the rate of expression of lipogenic activity (49). Respective experimental control media (used for non-differentiated cells) consisted of DMEM supplemented with 10% (v/v) FBS and 2% (v/v) Pen/Strep + or – pyruvate. Media were replaced on the 1st and 5th days of culture and the cells were replenished with media on the

3rd day of culture. Cryopreserved–thawed ASCs were used for the adipogenic differentiation experiments. The effect of oxidative stress and antioxidant supplementation on adipocyte differentiation was determined at 14 and 21 days after adipogenic differentiation was induced.

Fluorescence microscopy

Staining with Nile red (lipid stain) and DAPI (nuclear stain), both purchased from Molecular Probes, Invitrogen, were used to confirm adipocyte differentiation. Both non-induced and adipogenic-induced ASCs were cultured in 6-well plates as previously described. Growth medium and adipogenic induction medium was removed and the wells were rinsed with PBS to remove non-adherent cells and any fluorescence quenching phenol red and FBS. Phosphate buffered saline was added to the wells of both non-induced as well as induced cultures. The cultures were simultaneously stained with 5 μg/ml (final concentration) DAPI and 1 μg/ml (final concentration) Nile red and incubated for 10 minutes at 37°C. Fluorescence was viewed using an AxioVert A1 inverted microscope (Carl Zeiss, Gottigen, Germany). Images were obtained using the AxioCam Cm1 camera (Carl Zeiss) using 10x, 20x and 40x objective lens magnifications. Images were captured initially in single channels and subsequently overlaid using Axiovision software (Version 4.8.2). Single channel images were captured using Filter Set 09 for green fluorescence (Excitation BP 450-490 nm; Emission long pass (LP) 515 nm; Carl Zeiss) to visualize the lipid droplets and Filter Set 49 for blue DAPI-fluorescent nuclei (Excitation BP 365 nm (G 365); Emission BP 445/50 nm; Carl Zeiss). Nile red also fluoresces in the deep red spectrum. Deep red fluorescence was visualized using Filter set 00 for Texas red (Excitation BP 530-585 nm; Emission LP 615 nm). Image J 1.47v was downloaded from http://imagej.nih.gov/ij and used for all image analysis (50). Images were not enhanced.

Quantification of adipogenesis using flow cytometry

The induced and non-induced cells were trypsinized and washed using the respective DMEM (+ or – pyruvate). The cells were not centrifuged as centrifugation caused the adipocytes to burst. Single cell suspensions were prepared and were simultaneously stained with Nile red (1 μg/ml) and DAPI (5 μg/ml) for 20 minutes at room temperature. Working solutions of DAPI (500 μg/ml) and Nile red (100 μg/ml) were prepared in staining buffer (100 mM Tris, 150 mM NaCl, 1 mM $CaCl_2$, 0.5 mM $MgCl_2$, pH 7.4) and protected from light. The cells were

analyzed on a Gallios flow cytometer. Nile Red was excited with a 488 nm laser and yellow-gold fluorescence was detected in FL2 by 575/30 nm BP filter and deep red fluorescence was detected in FL5 by 755 nm LP filter. The nuclear stain DAPI was excited with a 405 nm laser and fluorescent emissions were detected in FL9 by 450/40 nm BP filter. The data collected from the experiments were analyzed using Kaluza analysis software. The compensation matrix was determined using the dedicated function of the Kaluza software. Any replicate having less than 100 viable cells was excluded.

Statistical analysis

Kaluza statistics files were exported into Microsoft® Excel® for Mac 2011 Version 14.4.4 (140807) for further analysis. Statistics were also performed using GraphPad PRISM 6 Version 6.0d (GraphPad, UK). Data are represented as mean ± standard error of the mean (SEM). The D'Agostino-Pearson omnibus K2 normality test was utilized to quantify how much a data set deviated from a Gaussian distribution. If the data followed a Gaussian distribution, statistical differences were calculated using One–way analysis of variance (One-way ANOVA) followed by a Tukey's multiple comparisons test. If the data did not follow a Gaussian distribution then a non-parametric statistical method was followed. The Kruskal-Wallis test was utilized followed by the multiple comparisons test, the Dunn's post test. The multiple comparison tests indicate the significance level of a comparison. Differences were considered significant at $P \leq 0.05$. All of the data presented are the results of at least two biological replicates performed in at least triplicate.

Results

Selection of the appropriate oxidative stress inducer and antioxidant concentrations

In order to investigate the effect of oxidative stress and antioxidant supplementation on the adipogenic differentiation potential of human ASCs, the appropriate concentrations of the oxidative stress inducer, H_2O_2 (Figure 4.4), and the antioxidant CoQ10 (Figure 4.5), were established.

Tetrazolium salt (MTT) reduction with increasing concentrations of H_2O_2 from 0 to 200 μM was examined every 24 hours over a period of 120 hours. Raw OD values were obtained

after spectrophotometric analysis of the plates. A blank (no cells) OD value was subtracted from each sample OD value obtained.

The percent viability relative to the control for the H_2O_2 concentrations was determined using the following equation:

$$\text{Percentage (\%) of control} = [(\text{MeanOD}_{\text{sample}} - \text{MeanOD}_{\text{blank}})/(\text{MeanOD}_{\text{control}} - \text{MeanOD}_{\text{blank}})] \times 100$$

The standard growth medium that is used in the MRC Extramural Unit for Stem Cell Research and Therapy is α-MEM and is considered the optimal medium for the expansion of MSCs (51, 52) The induction medium used to induce the cells to differentiate into adipocytes consists of DMEM (+ pyruvate) containing adipogenic inducers (5, 53). Exposure of ASCs, grown in α-MEM or DMEM + pyruvate, to the range of H_2O_2 concentrations resulted in less cell death with increasing concentrations of H_2O_2 than expected. Thus, a proportional relationship between increasing concentration and increase in cell death was not obtained, resulting in less than 50% reduction in formazan product for the ASCs grown in α-MEM and DMEM + pyruvate. A half maximal inhibitory concentration (IC_{50}) value with α-MEM and DMEM + pyruvate could not be established. It was determined that the medium had eliminated the H_2O_2. The presence of pyruvate in the medium scavenges the H_2O_2. Dulbecco's minimal Eagle's medium – (minus) pyruvate was therefore added to the comparison. The results confirmed that the amount of H_2O_2 that was added was greatly lessened in medium containing pyruvate (Figure 4.4). Analysis of cell viability with the increasing H_2O_2 concentrations displayed similar trends with regard to each medium on each consecutive day over the 120-hour period.

The data passed the D'Agostino-Pearson omnibus K2 normality test and thus experimental data were analyzed using a One-way ANOVA. Statistical differences were determined by the Tukey's multiple comparisons test. GraphPad PRISM 6 indicates the extent of significance up to $P<0.0001$ (****). For simplification and ease of visibility of the graph the extent of the significance was only indicated if the results had a $P\leq0.05$ (*) relative to the respective control (0 μM H_2O_2). There were no significant differences obtained with increasing H_2O_2 concentrations when the cells were grown in α-MEM and DMEM + pyruvate. Comparative viability data for H_2O_2 demonstrated that toxicity was more pronounced with the higher H_2O_2

concentrations when ASCs were grown in medium – pyruvate. The true effect of H_2O_2 on the ASCs was observed when using DMEM – pyruvate. Due to the attenuating effect of pyruvate on oxidative stress, it was ascertained that the appropriate medium for use in further experiments would be DMEM – pyruvate.

Table 4.1 depicts the H_2O_2 IC_{50} concentration that was obtained at each 24-hour time point over the 120 hour period using DMEM – pyruvate. The IC_{50} decreased with increasing time due to the accumulation of ROS. The strongest effect was seen at 120 hours. It was therefore decided for further experiments that two different concentrations of H_2O_2 would be used; a concentration of 20 μM and a higher concentration of 100 μM H_2O_2 were chosen. An IC_{50} value of 21.91 μM H_2O_2 aided the choice of using 20 μM H_2O_2 for further experiments Literature also aided in the choice of 20 μM (54) and 100 μM H_2O_2 (55) concentrations.

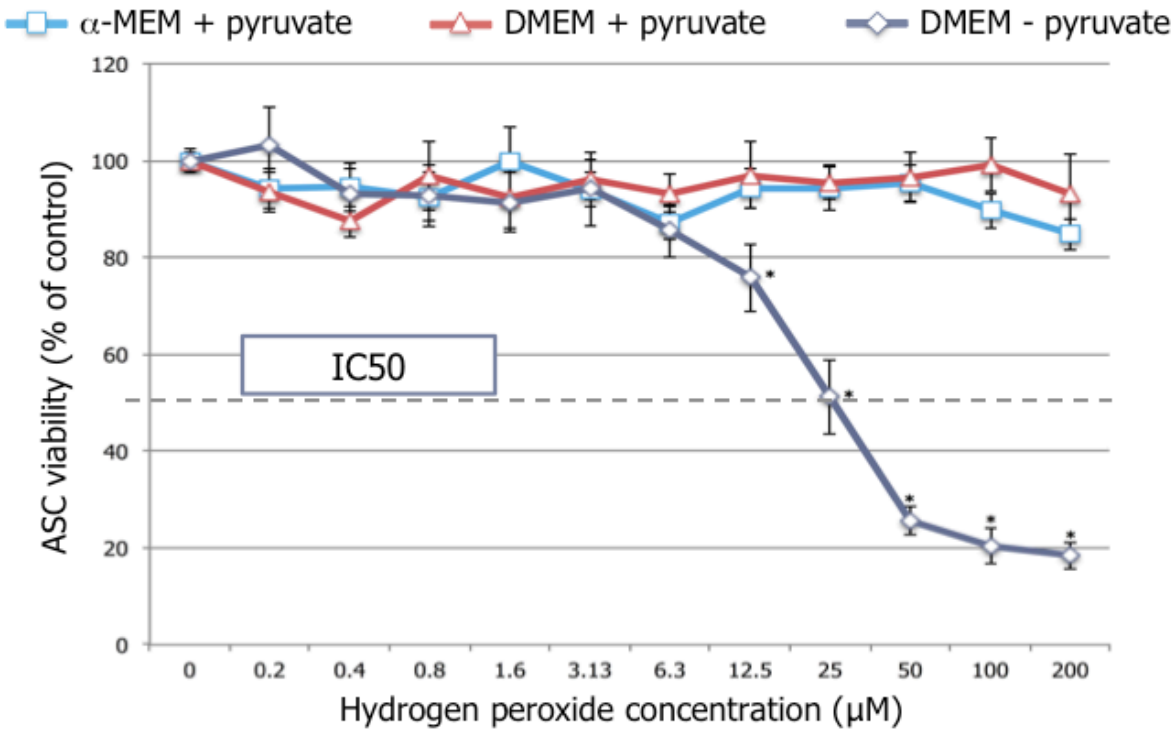

Figure 4.4. The cytoprotective effect of pyruvate against H_2O_2 insult. Cell viability was assessed using the MTT assay after exposure of the ASCs to a range of H_2O_2 concentrations. This graph is indicative of the effect at 96 hours. The pyruvate in α-MEM and DMEM + pyruvate prevented the decrease in cell viability seen with increasing H_2O_2 concentrations. ASCs cultured in DMEM – pyruvate showed a statistically significant increase in susceptibility to H_2O_2 from a concentration of

12.5 μM and upward compared to the control (0 μM H_2O_2). Values are means ± SEM from thawed cryopreserved ASC cultures from four different adipose tissue isolations, each in triplicate. *P<0.05.

Table 4.1. The half-maximal inhibitory (IC_{50}) concentrations of H_2O_2-treated ASCs for each time point.

ASCs grown in DMEM - pyruvate	IC50 (μM)
24 hours	69.48
48 hours	44.12
72 hours	33.44
96 hours	26.51
120 hours	21.91

Cell viability was assessed using the MTT assay. IC_{50} concentrations could not be obtained using media containing pyruvate since pyruvate scavenges H_2O_2. The table depicts the H_2O_2 IC_{50} concentration that was obtained at each 24-hour time point over the 120 hour period using DMEM – pyruvate. The IC_{50} decreased with increasing time due to the accumulation of ROS. The strongest effect was seen at 120 hours. An IC_{50} value of 21.91 μM H_2O_2 aided in the choice of using 20 μM H_2O_2 for further experiments. n = 4.

Antioxidants are said to interfere with the MTT reaction and reduce the tetrazolium used in the MTT assay to formazan without having any effects on viability. The SRB assay was therefore chosen in addition to the MTT assay as a viability assay. ASCs were cultured in the presence of a range of increasing CoQ10 concentrations from 0 to 100 μM. Figure 4.5 represents the assessed viability at 96 hours after treatment with the various CoQ10 concentrations. The highest concentration of CoQ10, which did not elicit a profound effect on viability, was chosen for further experimentation. The literature recommends using a concentration of 10 μM of CoQ10 (56). The antioxidant, Trolox, is commonly used as a control (57), displays strong antioxidant potential (58) and has been greatly studied. An equivalent concentration of 10 μM of Trolox was chosen for further experiments. Alves and colleagues assessed the effect of different Trolox concentrations (0, 50, 100, 200, 300 μM) on MSC proliferation (Supplementary Figure S2) (59). No significant reduction in cell viability was observed with a range between 0 and 50 μM of Trolox. No detrimental effects were observed on MSC viability with all Trolox concentrations that were used.

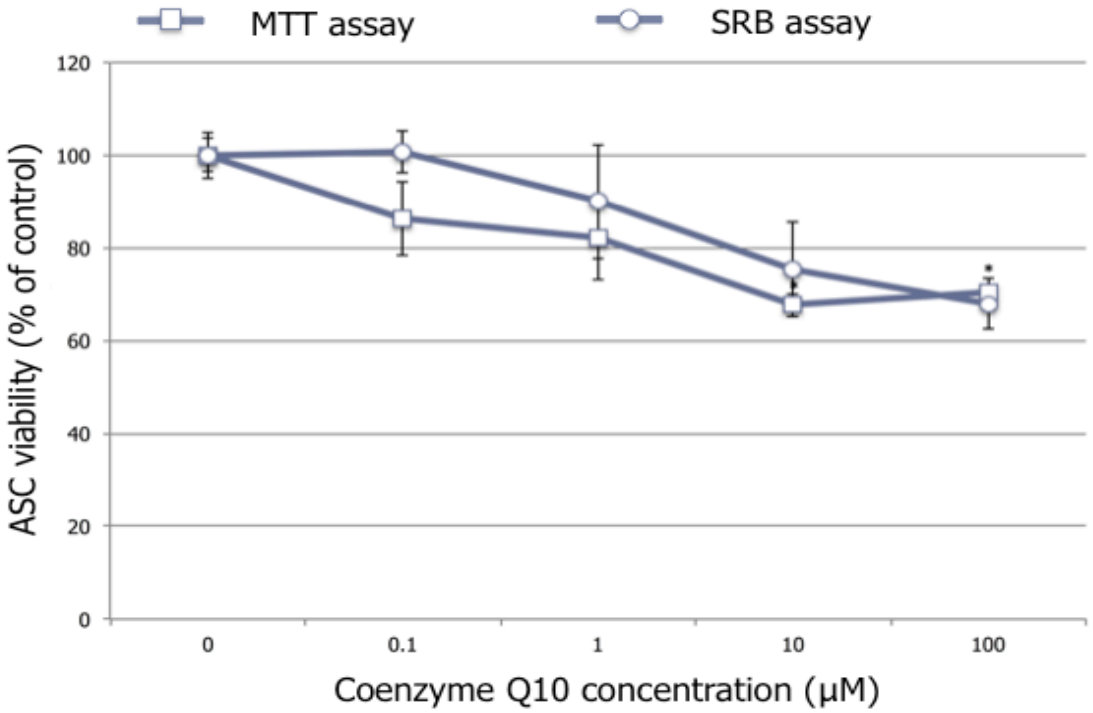

Figure 4.5. The effect of the antioxidant, CoQ10, on the viability of ASCs. Adipose-derived stromal cells were cultured in DMEM – pyruvate and supplemented with an increasing range of CoQ10 concentrations. The viability of the ASCs was assessed after 96 hours using the MTT and SRB assays. Values are means ± SEM from 2 donor samples, four experiments per assay each in triplicate.

The cells were prone to lifting off the plastic surface of the culture dish particularly during the process of the MTT assay. Any wells where this was observed were excluded from analysis so as to not include any potential erroneous data. All three media used in this study are conducive to ASC growth and the SRB assay confirmed this as shown by no significant differences in the means (Figure 4.6).

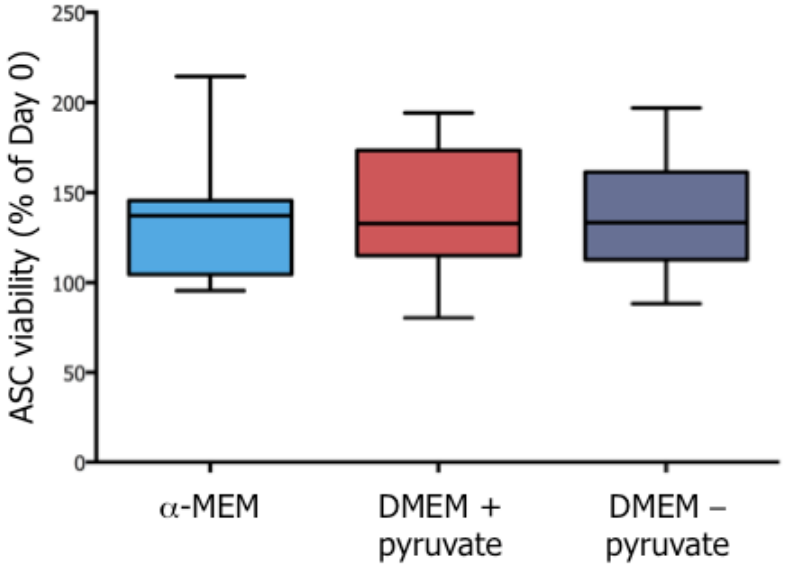

Figure 4.6. The viability of ASCs grown in the three different media. The viability of ASCs cultured in standard growth medium, α-MEM (blue), DMEM + pyruvate (red) and DMEM – pyruvate (purple) relative to Day 0 growth was assessed after 96 hours using the SRB assay. Values are means ± SEM from 2 donor samples each in triplicate.

Effects of co-supplementation of an oxidative stress inducer and antioxidants on ASC viability

Following the previous experiments, we assessed whether the decrease in ASC viability caused by the oxidative damage inducer could be rescued by co-supplementation with the ROS scavengers, Trolox and CoQ10 (Figure 4.7). Treatment of ASCs with the higher 100 μM H_2O_2 concentration caused a 2.4-fold reduction in viability from 138.10% ± 4.11% to 56.92% ± 10.04 using the SRB assay. This was partially rescued by the addition of the antioxidant Trolox, which resulted in an increase in ASC viability to 79.91% ± 4.03% (1.4-fold increase). However, the means were not significantly different. We further investigated whether the effect of H_2O_2 on ASC viability could be reduced by co-supplementation with another antioxidant, CoQ10. The addition of 10 μM CoQ10 to ASCs treated with 100 μM H_2O_2 resulted in an increase in viability from 56.92% ± 10.04% to 70.17% ± 4.80% (1.2-fold increase). The mean value of the H_2O_2-treated ASCs and the mean values of the ROS and antioxidant co-supplemented ASCs were not significantly different. There was thus a small trend towards partially rescuing oxidative damage induced loss of viability; however, the viability was not restored to the original state of the DMEM – pyruvate cultured ASCs. The addition of the antioxidants did not significantly rescue oxidative-induced damage by H_2O_2.

Vehicle controls were added to observe any possible negative effect on viability, but no negative effects were observed.

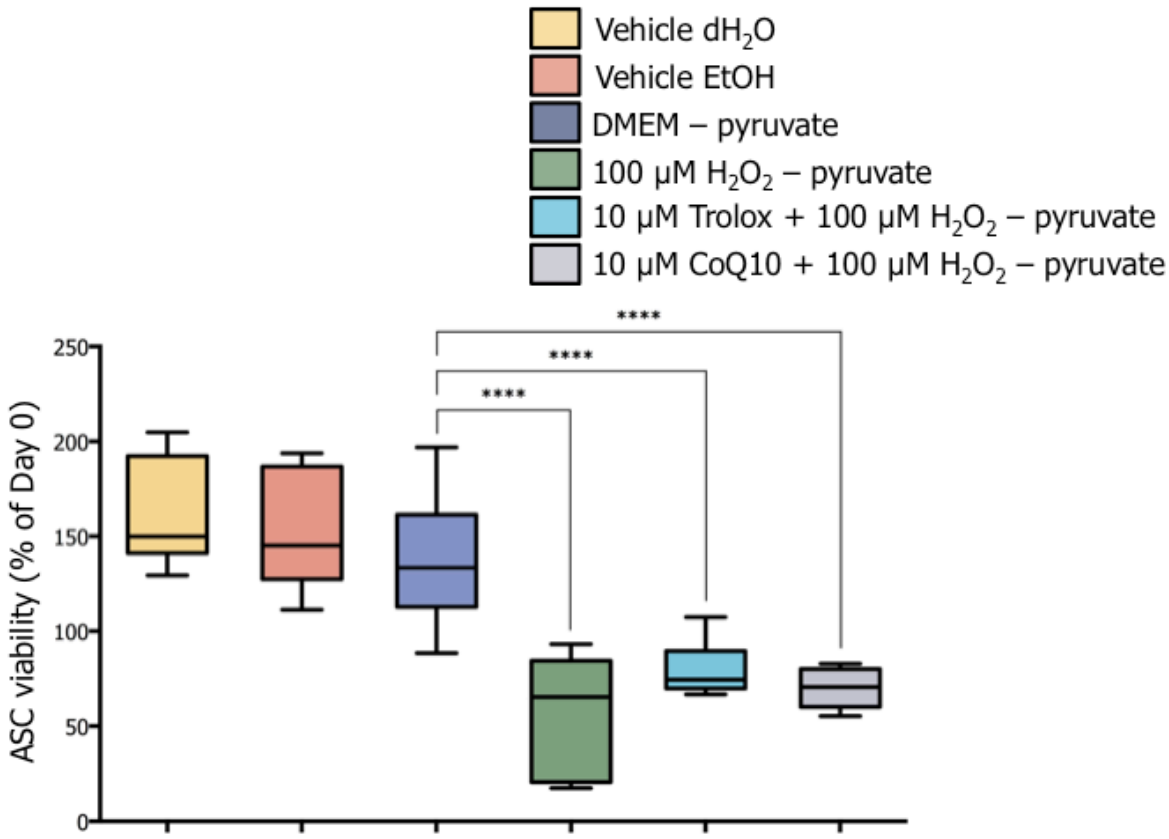

Figure 4.7. The effect of antioxidant supplementation on the ROS-induced reduction in ASC viability. The H_2O_2-treated ASCs were co-supplemented with 10 µM Trolox or 10 µM CoQ10 for 24 hours and the viability was assessed using the SRB assay. Values are means ± SEM from 2 biological replicates each in triplicate using passage, P6, thawed-cryopreserved ASC cultures. ****P<0,0001.

Intracellular ROS levels in adipose tissue-derived stromal cells

The effect of pyruvate on intracellular ROS was assessed using MitoSOX™ red mitochondrial O_2^- indicator. A preliminary experiment revealed that the appropriate concentration of MitoSOX™ red to add to the ASCs was 5 µM (also manufacturer's suggestion) with an incubation period of 10 minutes. Oxidation of MitoSOX™ red emits red fluorescence, which was measured in the FL1 fluorescence detection channel of the flow cytometer. Two-parameter side-scatter (SS; complexity) versus FL1 fluorescence (MitoSOX red) plots were created by gating on viable cells (Figure 4.8). An increase in the intracellular ROS was

detected with the removal of pyruvate and a mean fluorescence intensity (MFI) of 1.15 was obtained. Upon comparison with DMEM + pyruvate, which resulted in an MFI of 0.75, there was a resultant 1.5-fold increase. The addition of a positive control, tBHP, increased intracellular ROS further with a 3-fold increase in mean fluorescence intensity compared to DMEM + pyruvate.

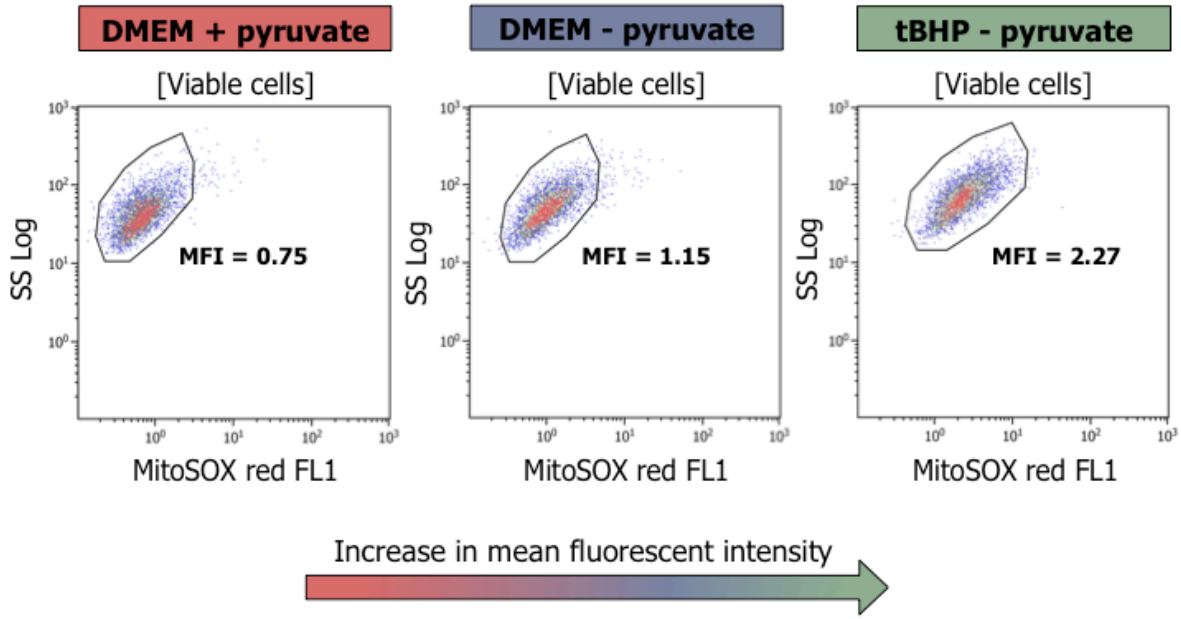

Figure 4.8. Determination of intracellular ROS in ASCs. Intracellular ROS levels were determined using MitoSOX™ red. The plots are the result of MitoSOX™ red stained ASCs grown in either DMEM + pyruvate or DMEM – pyruvate or DMEM – pyruvate treated with the pro-oxidant tBHP. The ASCs grown in DMEM – pyruvate were more FL1 fluorescent than ASCs grown in DMEM + pyruvate, as indicated by the shift in fluorescence signal to the right of the two-parameter plot. The addition of a positive control increased the MFI a further 3-fold relative to cells grown in DMEM + pyruvate.

An overlay plot was created for visual clarity (Figure 4.9). The number of cells and the intensity of the MitoSOX™ red fluorescence are shown on the y-axis and x-axis, respectively. The increase in fluorescence with the removal of pyruvate and a further increase in fluorescence with the addition of the positive control were observed in this plot.

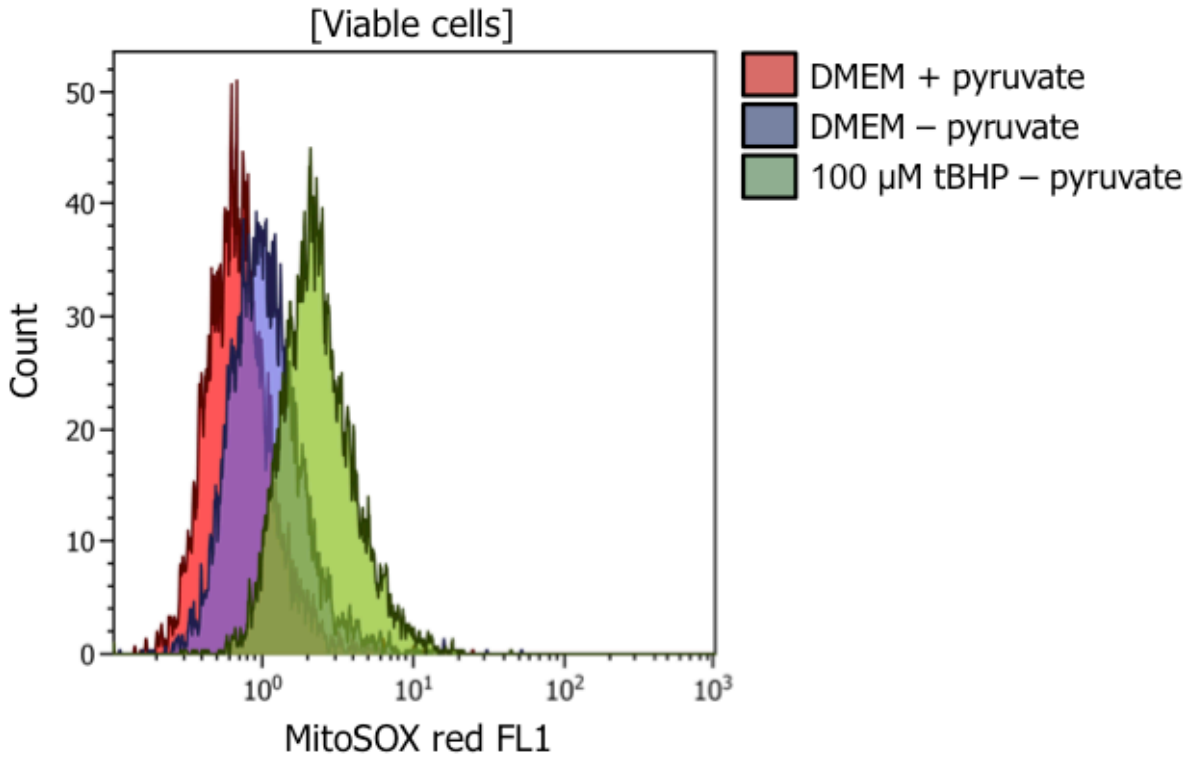

Figure 4.9. Overlay plot of MitoSOX™ red fluorescence under different conditions. The overlay plot displayed an increase in FL1 fluorescence with the removal of pyruvate and a further increase with the addition of the positive control, tBHP.

The resulting graph was produced from the MFIs of three ASC cultures (Figure 4.10). Treatment of ASCs with H_2O_2 (100 µM) in DMEM – pyruvate, the right bar in purple, caused an increase in mean MitoSOX™ red fluorescence from a basal level of 0.96 ± 0.13 (the right bar in grey) to 1.41 ± 0.19. The positive control, tBHP in DMEM – pyruvate, the bar in green, had a significant ± 2.6-fold increase in intracellular ROS to 2.05 ± 0.11. Treating the cells with the SOD mimetic, MnTBAP (100 µM) in DMEM – pyruvate, the right bar in red, inhibited the increase in ROS as evidenced by the decrease in mean MitoSOX™ red fluorescence (0.81 ± 0.22). These results indicate that exogenously added ROS do increase intracellular ROS generated through the mitochondria. The addition of an antioxidant enzyme, MnTBAP, decreases ROS accumulation. The increase in fluorescence can also be attenuated by the elimination of ROS due to the scavenging effect of pyruvate.

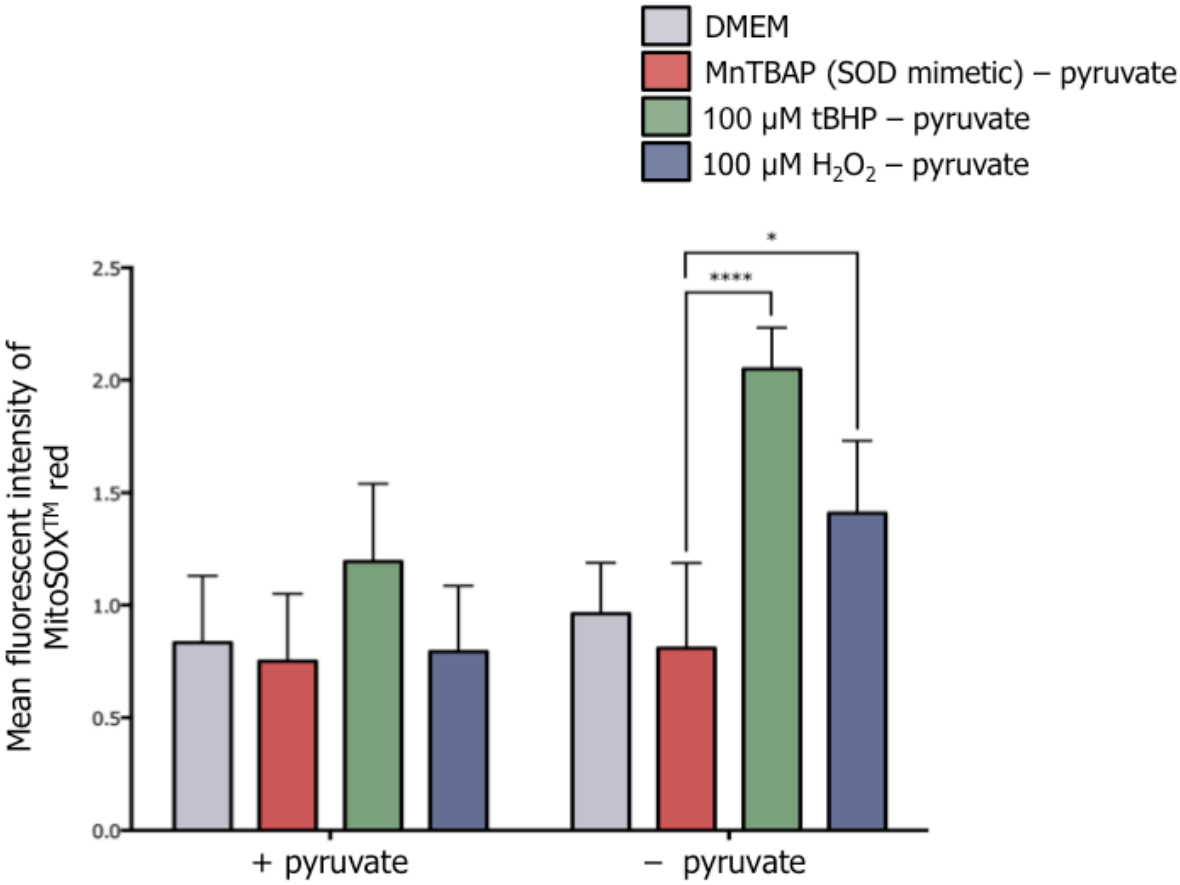

Figure 4.10. Fluorescent detection of intracellular ROS levels. The treatment with exogenous H_2O_2 and a positive control, tBHP, induces intracellular O_2^- generation. The effect is counteracted by the addition of a negative control, MnTBAP, and the scavenging effect of pyruvate. The ASCs were treated with 100 µM of the test conditions at 37°C for 24 hours, and then incubated with 5 µM MitoSOX™ red for 10 minutes. The fluorescence was measured using the FL1 channel of the Gallios flow cytometer and analyzed using Kaluza software. Cell debris and non-viable cells, represented by clear low forward- and side-scatter were gated out of the analysis. The data are shown as means of the FL1 channel fluorescence intensity, and represent mean ± SEM. n = 3; early-passage 4, 5 and 9 thawed-cryopreserved ASC cultures. $^{*}P<0.05$; $^{****}P<0.0001$. See Table 4.2 for all significance values.

Table 4.2. Statistical differences relating to Figure 4.10.

		With pyruvate				Without pyruvate			
		DMEM	100 µM MnTBAP	100 µM tBHP	100 µM H_2O_2	DMEM	100 µM MnTBAP	100 µM tBHP	100 µM H_2O_2
With pyruvate	DMEM		ns	ns	ns	ns	ns	***	ns
	100 µM MnTBAP	ns		ns	ns	ns	ns	****	ns
	100 µM tBHP	ns	ns		ns	ns	ns	*	ns
	100 µM H_2O_2	ns	ns	ns		ns	ns	****	ns
Without pyruvate	DMEM	ns	ns	ns	ns		ns	***	ns
	100 µM MnTBAP	ns	ns	ns	ns	ns		****	*
	100 µM tBHP	***	****	*	****	***	****		ns
	100 µM H_2O_2	ns	ns	ns	ns	ns	*	ns	

The data passed the normality test and the results of the Tukey's multiple comparisons test are represented in the above table. The mean difference is significant at the 0.05 level. *P<0,05, ***P<0,001, ****P<0,0001.

Effect of an oxidative stress inducer and antioxidants on the differentiation potential of ASCs

Having confirmed that exogenously added H_2O_2 affects intracellular ROS, the effect of exogenously added ROS on the adipogenic differentiation potential of ASCs was investigated. In this study, cultured ASCs were subjected to not only adipogenic induction medium but also prolonged treatment with H_2O_2. The ASCs induced to differentiate were supplemented with the adipogenic differentiation-inducing agents, dexamethasone, 3-iosbutyl-methylxanthine, indomethacin and human insulin. Lipid droplets started to accrue within 7 days after induction. The day 14 adipogenic-induced cells, + pyruvate and without exogenous ROS, continued to accumulate lipid droplets within their cytoplasm.

Treatment of adipogenic differentiated ASCs with 1 μg/ml Nile red resulted in intense fluorescent staining of the lipid droplets. Treatment with 5 μg/ml of the fluorescent nuclear stain, DAPI, resulted in nuclear staining. Fluorescence was viewed using an AxioVert A1 inverted microscope. Fluorescence microscopy images were taken of the Nile red and DAPI stained cells. Images were captured as single channel images. The Texas red channel (red) and the green fluorescent protein (GFP; green) channel were used for lipid droplet identification and the DAPI (blue) channel was used for visualization of nuclei. The exposure times were optimized for each individual channel. Figure 4.11 provides an overview of the steps involved in acquiring the images and the resultant merged image. Images were captured using the DAPI channel option (4.11**A**) and the Texas red (4.11**B**) and GFP channel options (4.11**C**). These three images were then overlaid using Axiovision software (4.11**D**).

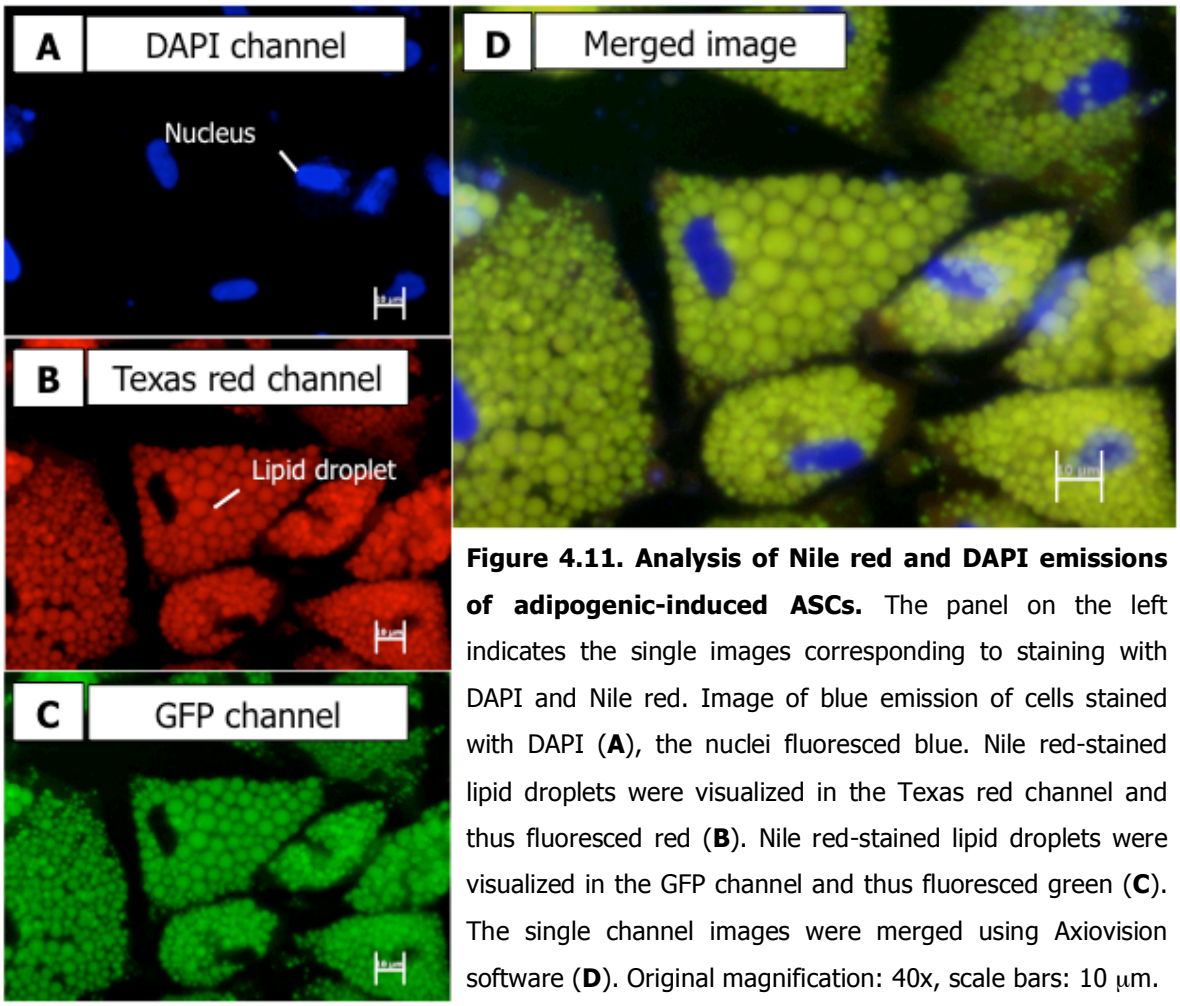

Figure 4.11. Analysis of Nile red and DAPI emissions of adipogenic-induced ASCs. The panel on the left indicates the single images corresponding to staining with DAPI and Nile red. Image of blue emission of cells stained with DAPI (**A**), the nuclei fluoresced blue. Nile red-stained lipid droplets were visualized in the Texas red channel and thus fluoresced red (**B**). Nile red-stained lipid droplets were visualized in the GFP channel and thus fluoresced green (**C**). The single channel images were merged using Axiovision software (**D**). Original magnification: 40x, scale bars: 10 μm.

The photographs presented in Figure. 4.12 reveal the appearance of Nile red and DAPI stained cells, at day 21 after adipogenic induction was commenced. The DAPI and Nile red-stained non-induced cultured ASCs exhibited small discrete lipid bodies distributed throughout the cytoplasm (4.12**A**). Staining the adipogenic-induced ASCs, cultured in standard induction medium containing DMEM + pyruvate and without exogenous ROS, with Nile red confirmed that the cells had the capacity to differentiate down the adipogenic lineage (4.12**B**). The differentiated cells had numerous fluorescent spherical lipid droplets, which varied dramatically in size, situated in the cytosol. The majority of the differentiated cells in the culture had lipid droplets, although in varying numbers per cell. However, no mature adipocytes, having a large unilocular lipid droplet, were observed.

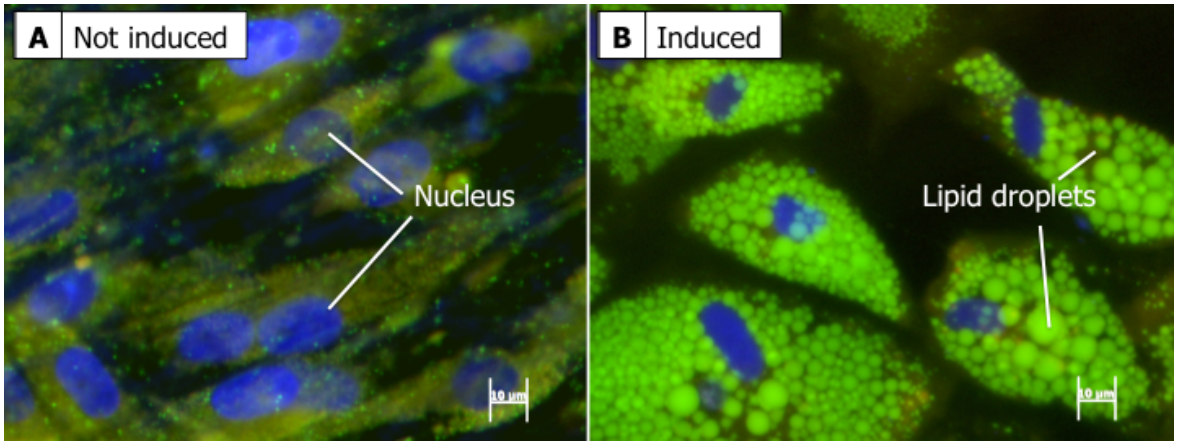

Figure 4.12. Fluorescent images of Nile red and DAPI stained non-induced and induced ASCs. Passage 6 thawed-cryopreserved ASCs that were cultured in standard growth medium and not induced to differentiate into adipocytes did not undergo differentiation at 21 days of growth, but exhibited small discrete lipid bodies distributed throughout the cytoplasm after staining with Nile red (**A**). Cells induced to differentiate into adipocytes exhibited lipid droplets within their cytoplasm at 21 days of induction after staining with Nile red (**B**).

Staining the cells with the lipophilic Nile red and the nuclei stain DAPI clearly indicated the presence of lipid droplets within the adipogenic-induced cells, although, microscopy did not provide any quantitative information regarding the lipid content, lipid accumulation or heterogeneity in adipogenesis among donor samples. Figure 4.13 shows differentiated ASCs grown in adipogenic medium containing DMEM + pyruvate (4.13**A**), DMEM – pyruvate (4.13**B**) and DMEM – pyruvate and the addition of 20 μM H_2O_2 (4.13**C**). Visually, not much of a difference could be observed, although in these photographs there appears to be larger

lipid droplets with the increase in ROS. The need for quantifying the differences between these conditions demonstrates the importance of using flow cytometric measures for this study (see below).

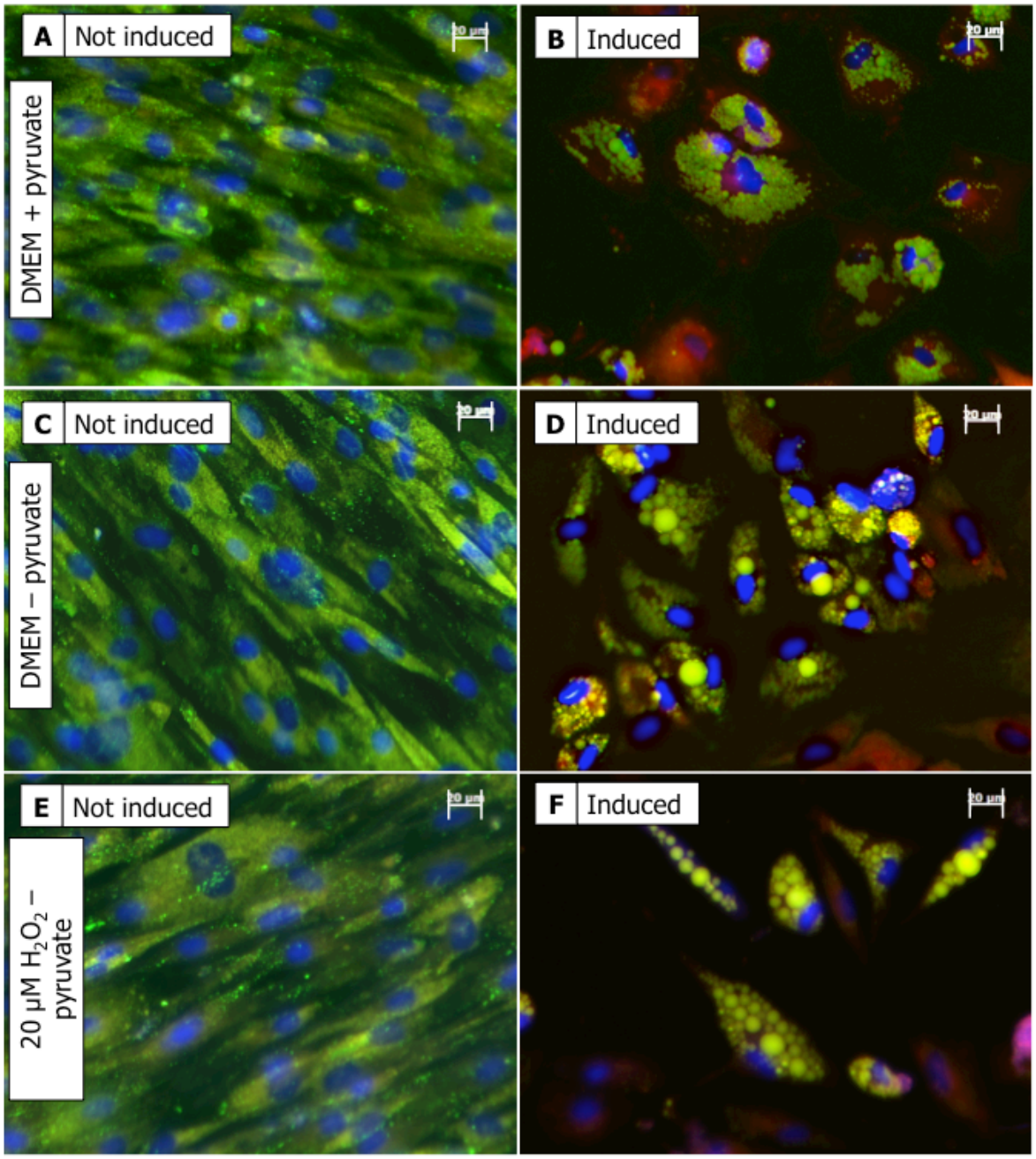

Figure 4.13. Comparison of adipogenic differentiation under different media conditions. The photographs represent differentiated ASCs grown in adipogenic medium containing DMEM + pyruvate (**A**), DMEM – pyruvate (**B**) and DMEM – pyruvate and the addition of 20 µM H_2O_2 (**C**). There

appears to be an increase in lipid droplet size with an increase in ROS. Original magnification: 10x, scale bars: 20 μm.

Flow cytometric analysis of the accumulation of lipid droplets based on Nile red positive staining at day 14 of adipogenic induction

The ASCs, upon confluence, were induced to differentiate into adipocytes using an adipogenic induction cocktail. Following an induction period of 14 days the adipogenic differentiation potential of the ASCs was analysed using flow cytometry. Nile red and DAPI staining were used to quantify the lipid accumulation flow cytometrically. A total run time of 5 minutes was set per condition because using the number of events such as, 10000 events, instead of time, extended the run period between conditions further and there was the concern of affecting cell viability. Acquiring events based on a set time of 5 minutes resulted in an average of 9532 ± 4004 cells being counted for non-induced ASCs, grown in DMEM + pyruvate, and an average of 9023 ± 2386 induced cells grown in DMEM + pyruvate being counted. These cell counts were not significantly different, thus the results were comparable. Following 96 hours, and using the SRB assay, there was no significant difference between the mean ASC viability of the non-induced and adipogenic-induced cells with both DMEM + pyruvate and DMEM – pyruvate containing media (Figure 4.14).

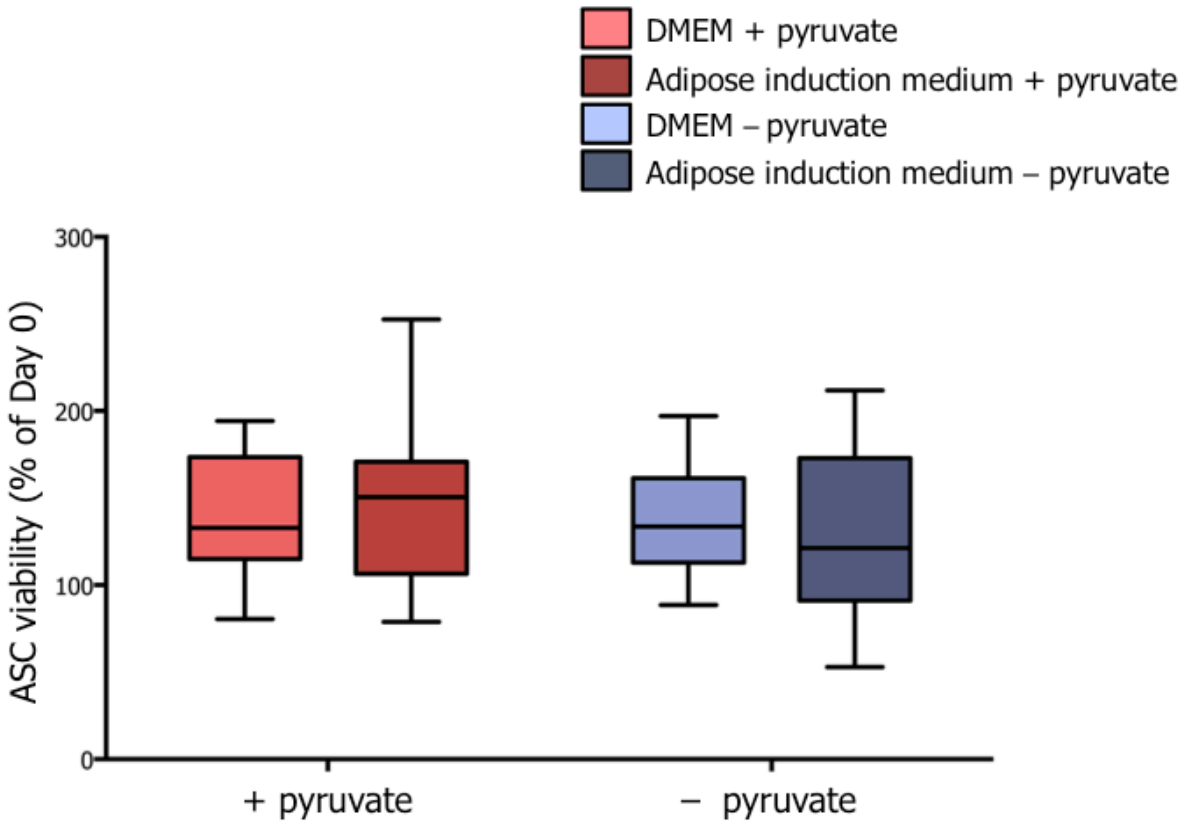

Figure 4.14. The effect of the adipogenic cocktail on ASC viability. The viability of ASCs grown in DMEM + pyruvate medium (light pink), adipogenic medium + pyruvate (pink) and DMEM – pyruvate (light purple), adipogenic medium – pyruvate (purple) was assessed after 96 hours using the SRB assay.

Only viable ASCs were used in the analysis. Viable cells were determined by utilizing DAPI fluorescence, and forward-scatter (FS) and SS properties as visualized in Figure 4.15. Dead cells or cells undergoing necrosis have damaged cell membranes that are more permeable to DAPI, the nucleus stain. Fluorescent emissions of DAPI were detected in FL9, thus if the FL9 fluorescence intensity increased, the cell membranes were compromised and these cells were also counted as non-viable (4.15**A**). Cell debris and non-viable cells were represented by clear low FS and were gated out for analysis (4.15**B**). Nile red content was detected in FL2, and thus, the percentage of cells emitting yellow-gold fluorescence (FL2+) was determined (4.15**C**).

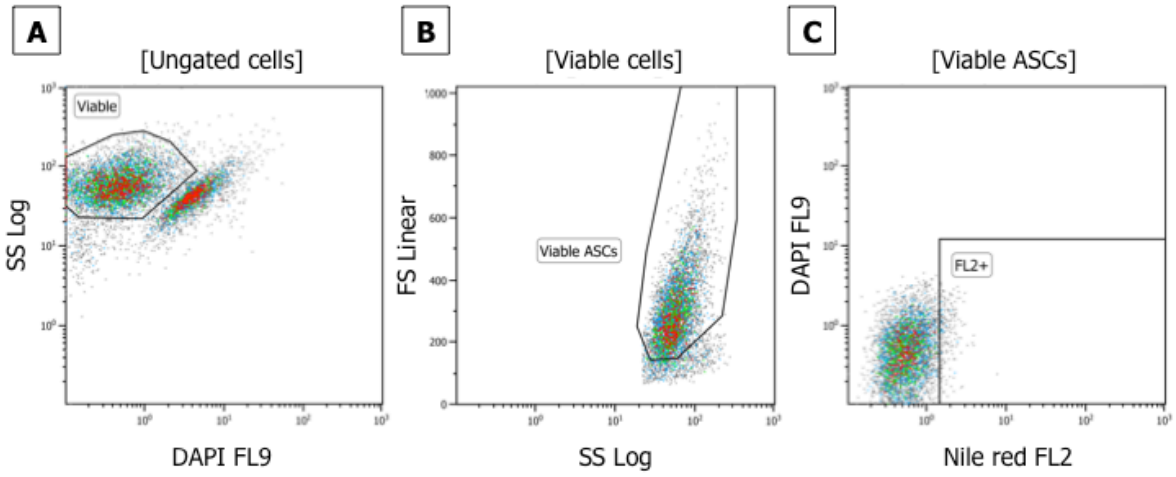

Figure 4.15. Gating strategy for Nile red content detection. A region was drawn around the DAPI and Nile red labeled, non-induced cells, grown in DMEM + pyruvate, which did not have compromised cell membranes. Cells with compromised membranes were brighter in FL9 DAPI fluorescence (**A**). Following this any remaining cellular debris and non-viable cells, represented by low FS and SS, were gated out for analysis (**B**). Nile red content was detected in FL2. The non-induced ASCs did not emit much FL2 yellow-gold fluorescence (**C**).

Regions were set according to the non-induced ASCs, grown in DMEM + pyruvate, for each donor sample, which emitted little yellow-gold fluorescence. These regions were used as gating controls to monitor the increase in yellow-gold fluorescence emitted by the adipogenic-induced ASCs (Figure 4.16; non-induced 4.16**A** and induced 4.16**B**). A shift to the right of the density plot of FL2 fluorescence indicated an increase in lipid content. At day 14 of adipogenesis, quite a large percentage (75.45% ± 13.60%) of the viable cells grown in adipogenic medium + pyruvate appeared not to have differentiated. Heterogeneity existed with respect to the degree of adipogenic differentiation of the ASCs in response to adipogenic induction medium between donor samples as demonstrated in Figure 4.16. For example A220313 was inherently more fluorescent in FL2 and displayed a slightly increased differentiation potential (4.16**D**) compared to A180313 (4.16**B**). This is exhibited in the Figure by the percent of viable cells that emitted yellow-gold fluorescence.

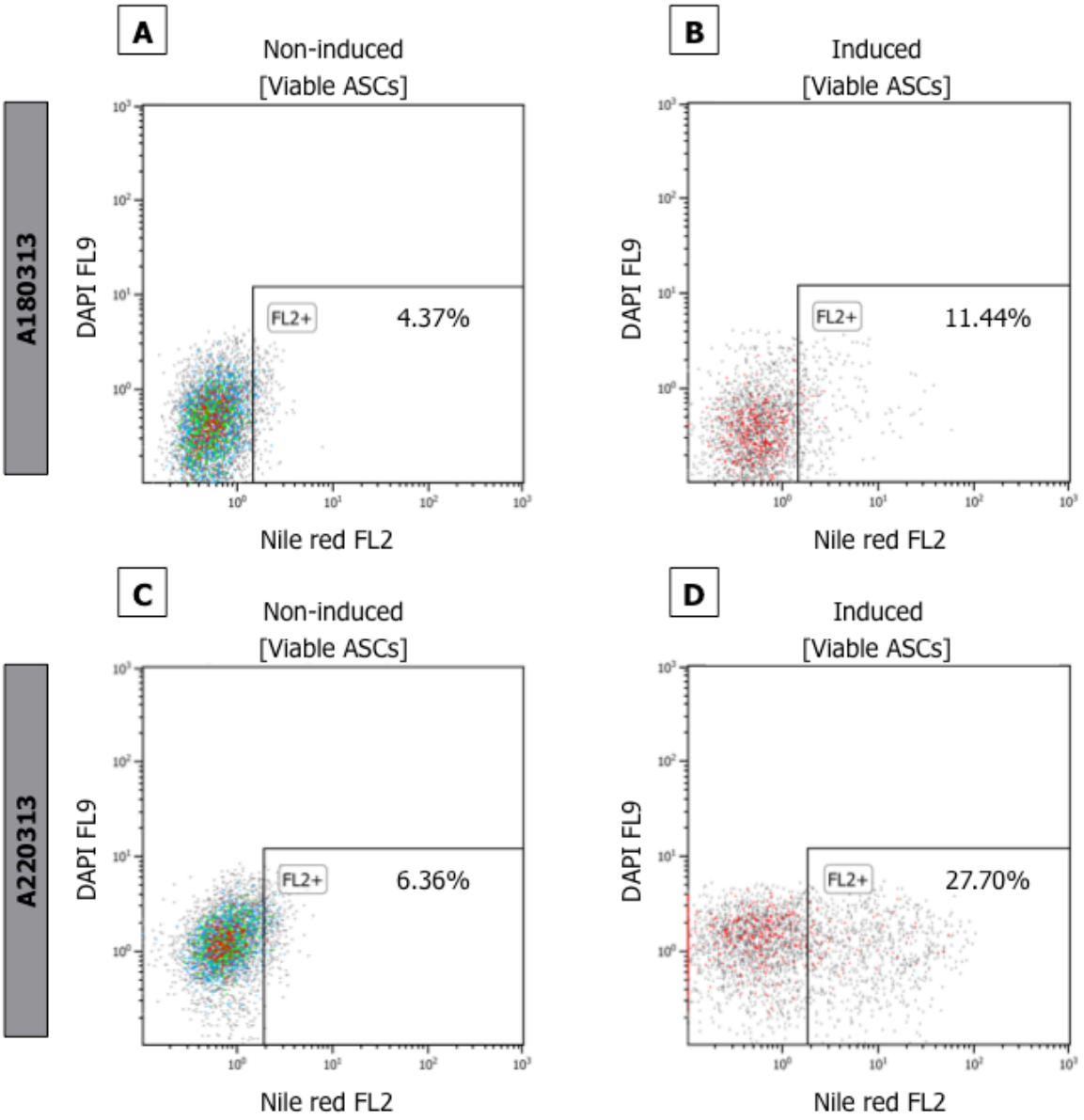

Figure 4.16. Strategy for flow cytometric analysis of adipogenesis. Regions were set according to the yellow-gold fluorescence of the non-induced Nile red stained ASCs (**A**). These regions were used as gating controls to monitor the increase in yellow-gold fluorescence emitted by the Nile red stained adipogenic-induced ASCs (**B**). The rectangular regions indicate the percentage of events/cells that had accumulated lipids after Nile red staining. The differentiation potential varied between donor samples as demonstrated when the percentage of viable cells in the rectangular region of B is compared to the rectangular region in D. These are the results of ASCs grown in DMEM + pyruvate (Non-induced; **A** and **C**) and adipogenic induction medium + pyruvate (Induced; **B** and **D**).

Cells that contained lipid droplets diffracted more light. Increased lipid accumulation within a cell was manifested as increased cellular complexity, which correlated with an increase in SS following flow cytometric analysis. Thus an increase in SS with an increase in lipid accumulation was expected and observed upon addition of adipogenic medium. Four quadrants were used to display increased cellular complexity and increased FL2 fluorescence as shown in Figure 4.17. The A-- quadrant contained cells with a level of intracellular complexity similar to that observed in the control non-induced ASCs, whereas the A++ quadrant contained cells with increased complexity. It was assumed that the cells with the greatest complexity contained higher lipid content, while cells that exhibited lower complexity contained less lipid content. The figure demonstrates that there is a trend in increased complexity with increased FL2 fluorescence.

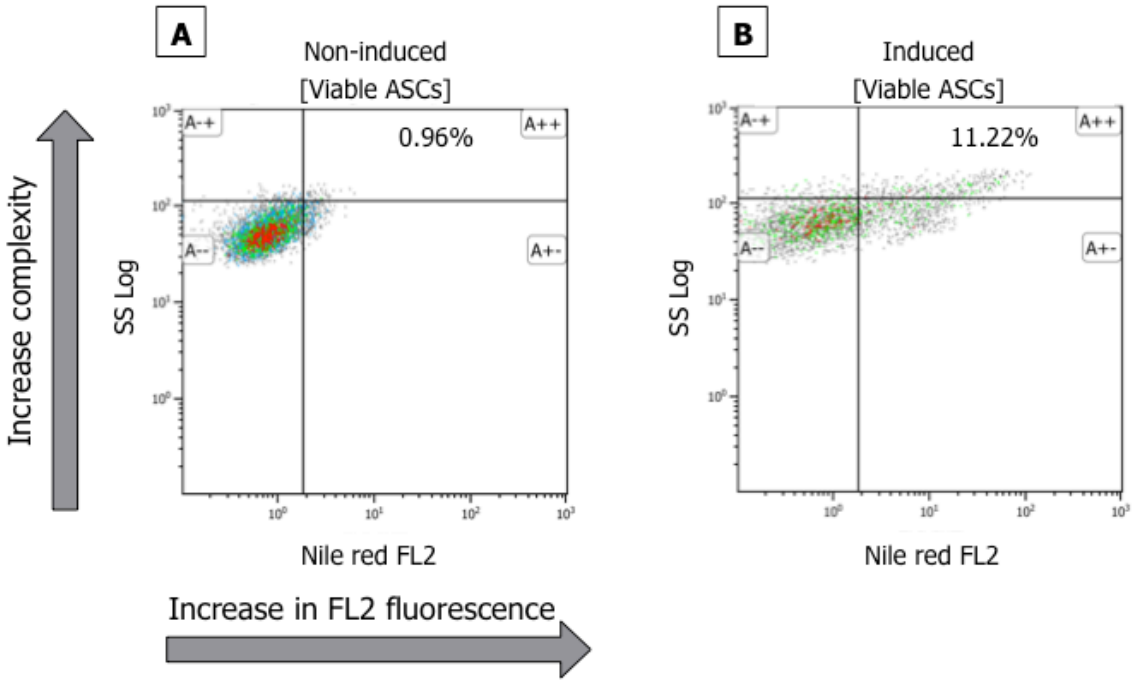

Figure 4.17. Accumulation of lipid droplets based on cell complexity. The x-axis reflected the increase in FL2 fluorescence and y-axis reflected the increase in SS or complexity of the cells. Following standard adipogenic induction, the ASCs became increasingly complex due to an increase in lipid content. This was correlated by an increase in FL2 yellow-gold fluorescence (**B**).

The percentage of non-induced ASCs grown in DMEM + pyruvate that emitted yellow-gold fluorescence (percentage of fluorescence detected in FL2) at day 14 was 5.38% ± 0.80%. This value is expected to be low because the cells were not induced to undergo adipogenic differentiation. The percentage of cells, grown in adipogenic induction medium + pyruvate that emitted yellow-gold fluorescence was 17.24% ± 3.20%, resulting in a ±3-fold increase in neutral lipid containing cells (Figure. 4.18). A popular measure used in literature to illustrate an increase in staining compared to a control is the geometric-mean fluorescence intensity (MFI). The MFI detected in FL2 correlates with the presence of neutral lipids per cell. The mean Nile red (FL2+) fluorescence of the cells in response to DMEM + pyruvate was 1.37 ± 0.03. The MFI detected in FL2 of the cells in response to adipogenic induction medium + pyruvate increased to 2.43 ± 0.33 (Table 4.5(**A**)).

Removing pyruvate from the DMEM resulted in 4.60% ± 1.78% of the non-induced ASCs emitting yellow-gold fluorescence following the staining of the neutral lipids with Nile red at day 14. Exposing the cells to adipogenic induction medium – pyruvate for 14 days resulted in 31.28% ± 3.37% of the cells emitting only yellow-gold fluorescence. This is a ±7-fold increase in adipogenic differentiation (Figure. 4.18). A MFI of 1.41 ± 0.01 was obtained for the non-induced ASCs grown in DMEM – pyruvate for 14 days. The MFI for the cells induced to differentiate with adipogenic induction medium – pyruvate for 14 days increased to 2.58 ± 0.24 (Table 4.5(**B**)). The addition of 20 μM H_2O_2 to the ASCs grown in adipogenic induction medium – pyruvate increased adipogenic differentiation ±2-fold compared to ASCs grown in standard adipogenic medium. This condition also increased adipogenic differentiation ±1-fold compared to ASCs grown in adipogenic medium – pyruvate. The percentage of cells grown in adipogenic induction medium – pyruvate and the addition of 20 μM H_2O_2 that emitted only yellow-gold fluorescence was 35.39% ± 1.99% (Figure. 4.18). The MFI of the adipogenic-induced cells – pyruvate with the addition of 20 μM H_2O_2 was 3.39 ± 0.69 compared to 1.37 ± 0.03 for ASCs grown in DMEM – pyruvate and the addition of 20 μM H_2O_2 (Table 4.5(**C**)).

Trolox attenuated the increase in lipid accumulation seen with the addition of ROS and thus a decrease in adipogenesis was seen. The addition of 10 μM Trolox to the H_2O_2-treated adipogenic-induced ASCs decreased the percentage of adipogenic-induced cells emitting yellow-gold fluorescence from 35.39% ± 1.99% to 21.64% ± 3.13%, resulting in a ±0.6-fold change (Figure. 4.18). There was a non-significant decrease to a MFI of 2.92 ± 0.54 for

the cells induced to differentiate with adipogenic induction medium – pyruvate and the addition of Trolox and H_2O_2 for 14 days compared to the cells induced to differentiate with adipogenic induction medium – pyruvate and the addition of 20 μM H_2O_2 (Table 4.5(**D**)). Coenzyme Q10 also attenuated the increase in lipid accumulation seen with the addition of H_2O_2. The decrease caused by the addition of CoQ10 to H_2O_2 treated adipogenic-induced cells was, however, not significant. The effect of co-supplementation of H_2O_2 with CoQ10 on adipogenic differentiation was not significantly different to the effect of co-supplementation of H_2O_2 with Trolox. The addition of 10 μM CoQ10 to the H_2O_2 treated adipogenic-induced ASCs decreased the percentage of adipogenic-induced ASCs emitting yellow-gold fluorescence from 35.39% ± 1.99% to 25.98% ± 3.75% causing an approximate 0.7-fold change (Figure. 4.18). There was a non-significant decrease in the MFI of the cells induced to differentiate with adipogenic induction medium – pyruvate and the addition of CoQ10 and H_2O_2 for 14 days (2.03 ± 0.31) compared to the MFI of the cells induced to differentiate with adipogenic induction medium – pyruvate and the addition of 20 μM H_2O_2 (Table 4.5(**E**)).

To summarise, there was a significant increase ($P<0.05$) in Nile red positivity with the addition of adipogenic induction medium + pyruvate compared to the non-induced ASCs grown in DMEM + pyruvate (see Table 4.3). There was a significant increase ($P<0.01$) in Nile red positivity with the removal of pyruvate compared to the induced cells cultured in adipogenic induction medium + pyruvate. Nile red positivity increased significantly ($P<0.0001$) with the addition of adipogenic induction medium – pyruvate and with the addition of 20 μM of H_2O_2. Addition of 10 μM of the ROS scavenger, Trolox, to the H_2O_2 treated adipogenic-induced ASCs significantly decreased ($P<0.01$) the percentage of adipogenic-induced ASCs emitting yellow-gold fluorescence. Addition of 10 μM of CoQ10 to the H_2O_2 treated adipogenic-induced ASCs decreased the percentage of adipogenic-induced ASCs emitting yellow-gold fluorescence, but not significantly (Figure. 4.18). The lack of significance with the co-supplementation of H_2O_2-treated ASCs with CoQ10 may be due to the limited number of replicates.

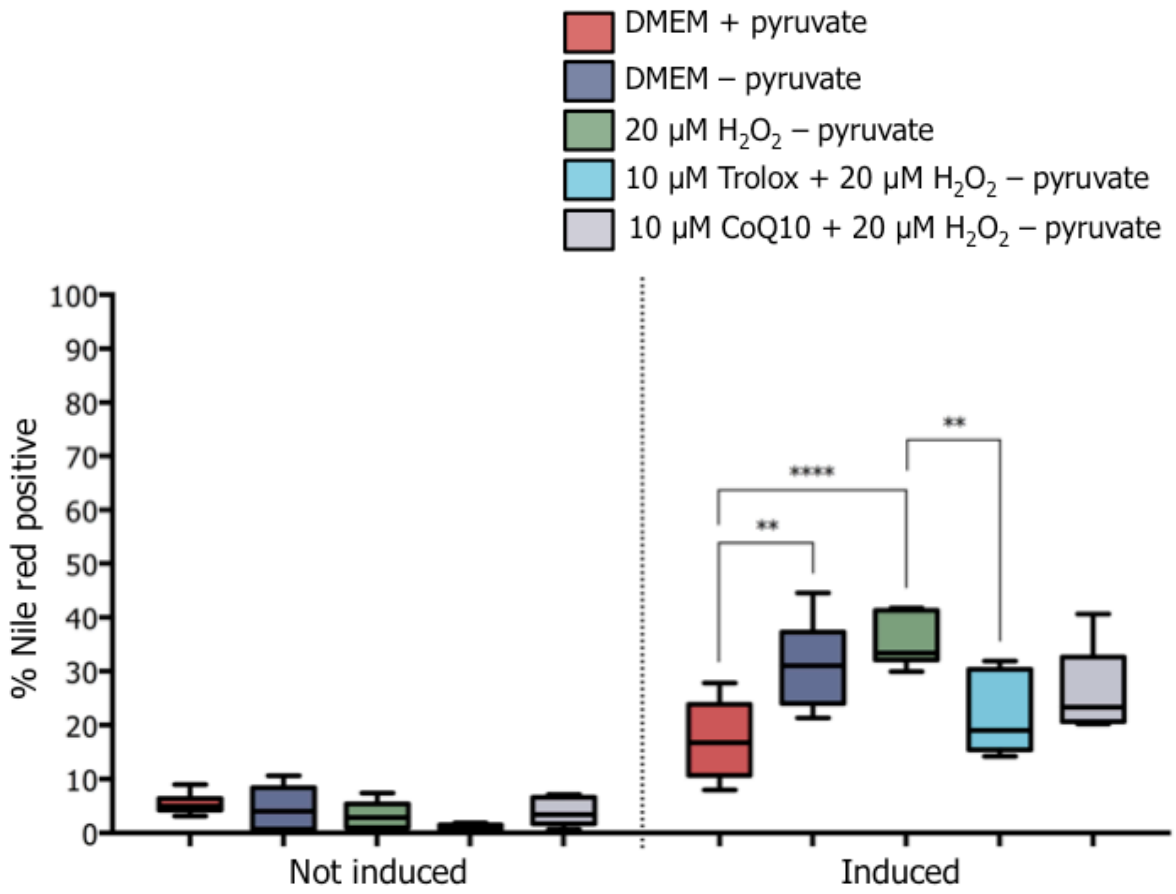

Figure 4.18. Percentage of cells that emit yellow-gold fluorescence after Nile red staining following 14 days of adipogenic induction. This graph indicates the percentage of cells that emit yellow-gold fluorescence after Nile red staining of early-passage, P7, thawed-cryopreserved ASCs at 14 days after adipogenic induction. The box of the box whisker plot extends from the 25th percentile to the 75th percentile. The line situated in the middle of the box represents the median. The lower whisker is the smallest percentage of cells that emitted yellow-gold fluorescence and the upper whisker is the largest percentage of cells that emitted yellow-gold fluorescence. Nile red positivity appeared to increase significantly (P<0.01) without the ROS scavenging effect of pyruvate compared to the induced cells cultured in adipogenic induction medium + pyruvate. Nile red positivity increased significantly (P<0.0001) in adipogenic induction medium – pyruvate and with the addition of 20 μM of H_2O_2. Addition of 10 μM of the ROS scavanger, Trolox, to the H_2O_2 treated adipogenic-induced ASCs significantly P<0.01, decreased the percentage of adipogenic-induced ASCs emitting yellow-gold fluorescence. Addition of 10 μM of CoQ10 to the H_2O_2 treated adipogenic-induced ASCs decreased the percentage of adipogenic-induced ASCs emitting yellow-gold fluorescence, but not significantly. n = 2. $^{**}P$<0.01; $^{****}P$<0.0001. See Table 4.3 for all significance values.

Table 4.3. Statistical differences relating to Figure 4.18.

		Not induced					Induced				
		DMEM + pyruvate	DMEM – pyruvate	20 µM H_2O_2 – pyruvate	10 µM Trolox + 20 µM H_2O_2 – pyruvate	10 µM CoQ10 + 20 µM H_2O_2 – pyruvate	DMEM + pyruvate	DMEM – pyruvate	20 µM H_2O_2 – pyruvate	10 µM Trolox + 20 µM H_2O_2 – pyruvate	10 µM CoQ10 + 20 µM H_2O_2 – pyruvate
Not induced	DMEM + pyruvate		ns	ns	ns	ns	*	****	****	***	****
	DMEM – pyruvate	ns		ns	ns	ns	**	****	****	***	****
	20 µM H_2O_2 – pyruvate	ns	ns		ns	ns	**	****	****	****	****
	10 µM Trolox + 20 µM H_2O_2 – pyruvate	ns	ns	ns		ns	***	****	****	****	****
	10 µM CoQ10 + 20 µM H_2O_2 – pyruvate	ns	ns	ns	ns		**	****	****	****	****
Induced	DMEM + pyruvate	*	**	**	***	**		**	****	ns	ns
	DMEM – pyruvate	****	****	****	****	****	**		ns	ns	ns
	20 µM H_2O_2 – pyruvate	****	****	****	****	****	****	ns		**	ns
	10 µM Trolox + 20 µM H_2O_2 – pyruvate	***	***	****	****	****	ns	ns	**		ns
	10 µM CoQ10 + 20 µM H_2O_2 – pyruvate	****	****	****	****	****	ns	ns	ns	ns	

The data passed the normality test and the results of the Tukey's multiple comparisons test are represented in the above table. The mean difference is significant at the 0.05 level. *P<0,05 **P<0,01, ***P<0,001, ****P<0,0001.

Flow cytometric analysis of the accumulation of lipid droplets based on lipid composition at day 14 of adipogenic induction

The analysis presented here was prompted by the solvatochromatic nature of Nile red. Lipid droplets are made up of a neutral lipid core and an outer amphipathic membrane. Nile red can detect both these types of lipids. The lipophilic dye emits yellow-gold fluorescence when dissolved in neutral lipids, while it fluoresces in the deep red spectrum when dissolved in amphipathic lipids such as the phospholipids of cell membranes. During preadipocyte maturation a larger number of amphipathic lipids are formed upon the merging of the lipid droplets and their increase in size. This causes a correlated increase in deep red fluorescence (FL5 fluorescence). Sub-populations of increasing lipid content were defined according to

their increase in yellow-gold as well as increase in deep-red fluorescence (FL2–/FL5– < FL2+/FL5– < FL2++/FL5+) and are represented in Figure 4.19. The position of the vertical line in 4.19**A** and 4.19**B** is determined by gating the plot on the FL2+ region, set according to the non-induced DMEM + pyruvate control and the position of the horizontal line in 4.19**A** and 4.19**B** is determined by gating the plot on FL5–, also set according to the non-induced DMEM + pyruvate control.

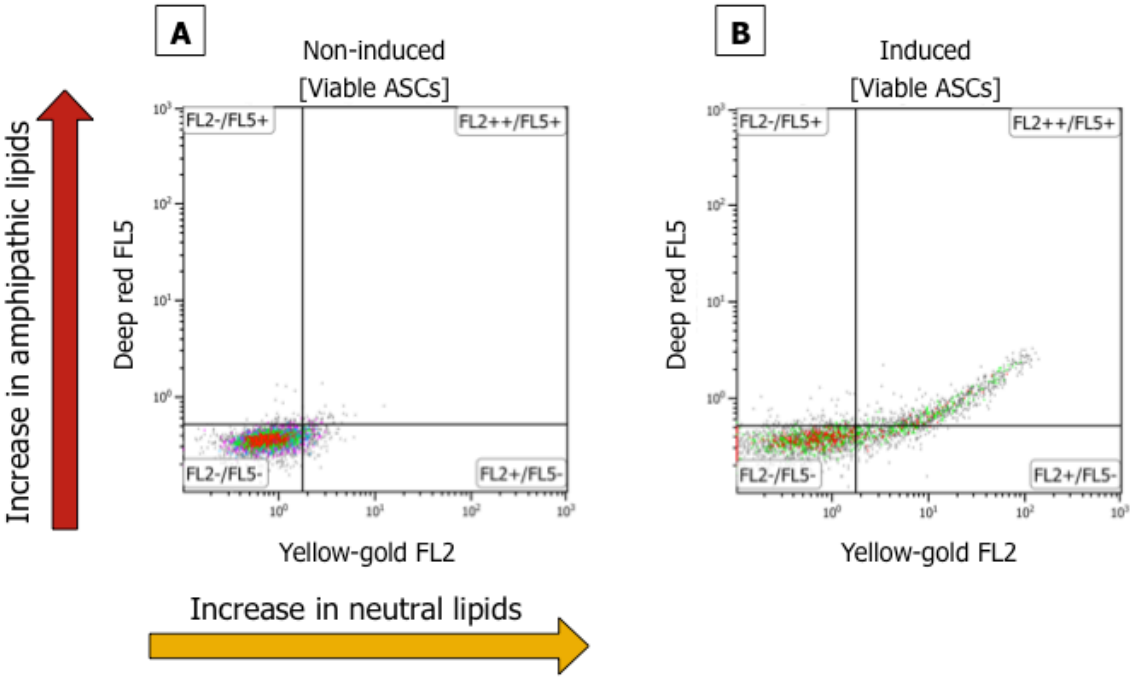

Figure 4.19. Accumulation of lipid droplets based on lipid composition. The x-axis reflected the increase in FL2 yellow-gold fluorescence and y-axis reflected the increase in FL5 deep red fluorescence emitted by cells. The increase in the simultaneous emission of deep red and yellow-gold fluorescence is indicative of the merging of lipid droplets and thus an accumulation of lipid content within the cells. Following standard adipogenic induction, the ASCs were more fluorescent on day 14 post-induction in both FL2 and FL5 (FL2++/FL5+) (**B**).

The following graphs on the left-hand side indicate the percentage of cells per sub-population with increased simultaneous emission of yellow-gold and deep red fluorescence after Nile red staining at 14 days after adipogenic induction. The graphs on the right-hand side indicate the mean Nile red fluorescence intensities per sub-population of increased simultaneous emission of yellow-gold and deep red fluorescence after Nile red staining of the same cells at 14 days after adipogenic induction. Under standard adipogenic conditions + pyruvate there was a significant increase in simultaneous yellow-gold and deep red fluorescence emissions demonstrating an increase in lipid accumulation. The proportion of ASCs, cultured in induction medium + pyruvate that simultaneously emitted yellow-gold and deep-red fluorescence (FL2++/FL5+), indicative of larger lipid droplets, was 9.06% ± 2.46 (Table 4.6(**A**)). The proportion of non-induced ASCs, cultured in DMEM + pyruvate that simultaneously emitted yellow-gold and deep-red fluorescence (FL2++/FL5+) was 0.72% ± 0.19 (Table 4.6(**A**)).

It appeared that with an increase in ROS, either with the removal of pyruvate or the addition of H_2O_2 there was a slight trend towards an increase in the FL2+/FL5– sub-population, which is indicative of lipid droplets of smaller size. Upon removal of pyruvate from the adipogenic induction medium, a greater proportion (14.86% ± 2.22%) of the differentiated cells appeared to be situated in the FL2+/FL5– sub-population than the cells induced with adipogenic medium + pyruvate. The percentage (17.16% ± 2.60%) of cells in the FL2++/FL5+ sub-population was also increased compared to the cells induced with adipogenic medium + pyruvate. An increase in ROS with the addition of 20 μM H_2O_2 also caused an increase in the FL2+/FL5– sub-population with 31.99% ± 1.49% of cells being situated in this sub-population. The trend was continued with the addition of 10 μM Trolox and 10 μM CoQ10 to adipogenic-induced ASCs treated with 20 μM H_2O_2, and the percentages of these sub-populations were decreased. The percentages of cells within the FL2+/FL5– sub-populations were 16.08% ± 0.91% and 26.44% ± 3.62% with the addition of Trolox and CoQ10, respectively (Table 4.6 (**D** and **E**).

It is noticeable and expected that the induced cells (bars on the right of each sub-population), represented in the MFI graphs on the right-hand side of Figure 4.20, demonstrated a higher fluorescence intensity than the non-induced cells (bars on the left of each sub-population), with respect to both yellow-gold and deep red fluorescence. The MFI of ASCs grown in induction medium + pyruvate that simultaneously emitted yellow-gold and

deep-red fluorescence (FL2++/FL5+), was 5.78 ± 1.24. The MFI of the cells in the FL2+/FL2– sub-population was 1.60 ± 0.09. Removal of pyruvate from the adipogenic induction medium resulted in a MFI of 2.58 ± 0.17 for the FL2+/FL2– sub-population. The MFI of the differentiated cells that simultaneously emitted yellow-gold and deep-red fluorescence (FL2++/FL5+) was 6.74 ± 1.02. The addition of 20 μM H_2O_2 caused an increase in the MFI (11.57 ± 1.75) of the FL2++/FL5+ sub-population. The addition of 10 μM Trolox to adipogenic-induced ASCs treated with 20 μM H_2O_2 decreased the MFI of the FL2++/FL5+ sub-population to 1.76 ± 0.15. The addition of 10 μM CoQ10 to adipogenic-induced ASCs treated with 20 μM H_2O_2 decreased the MFI of the FL2++/FL5+ sub-population to 6.31 ± 2.08.

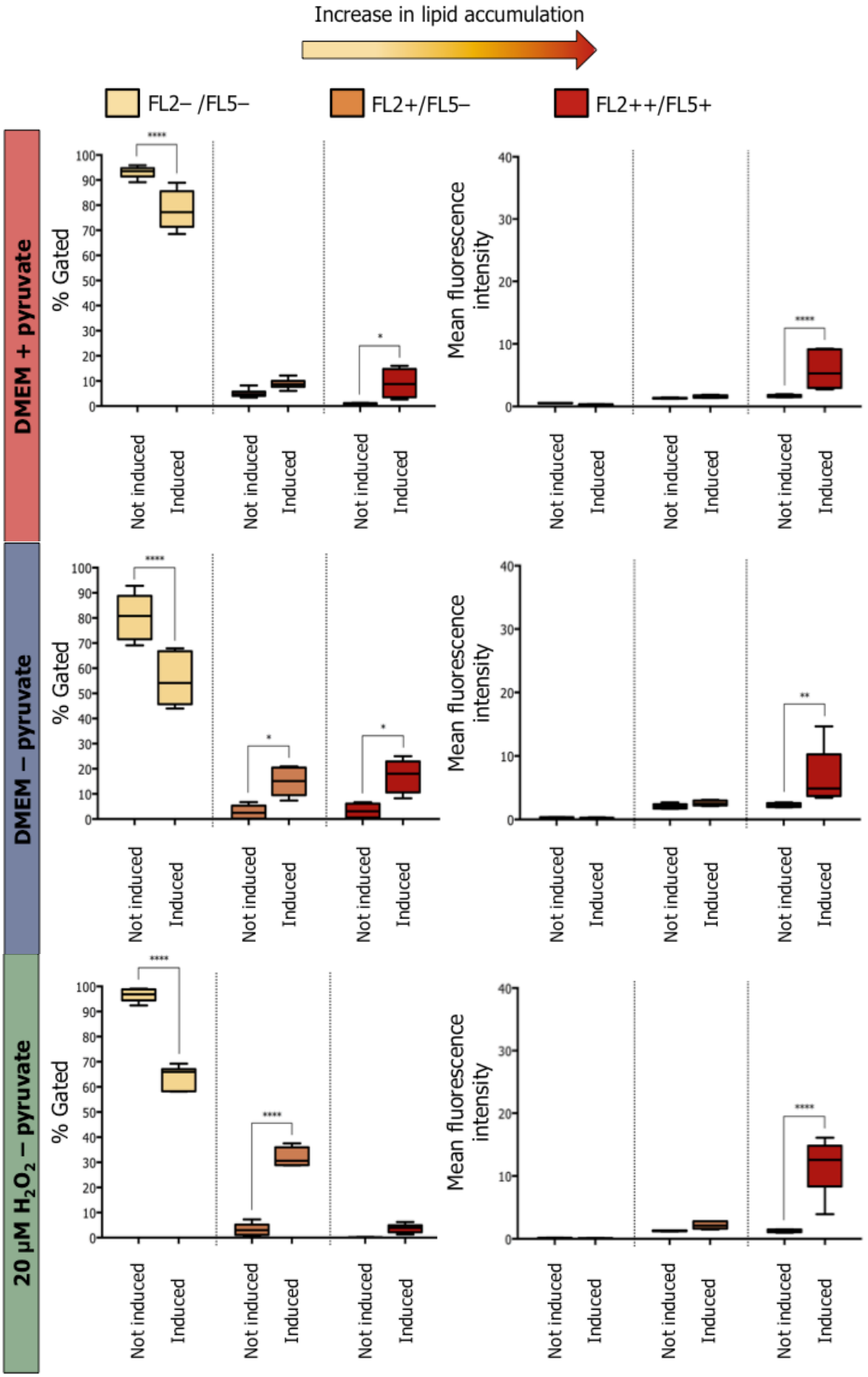

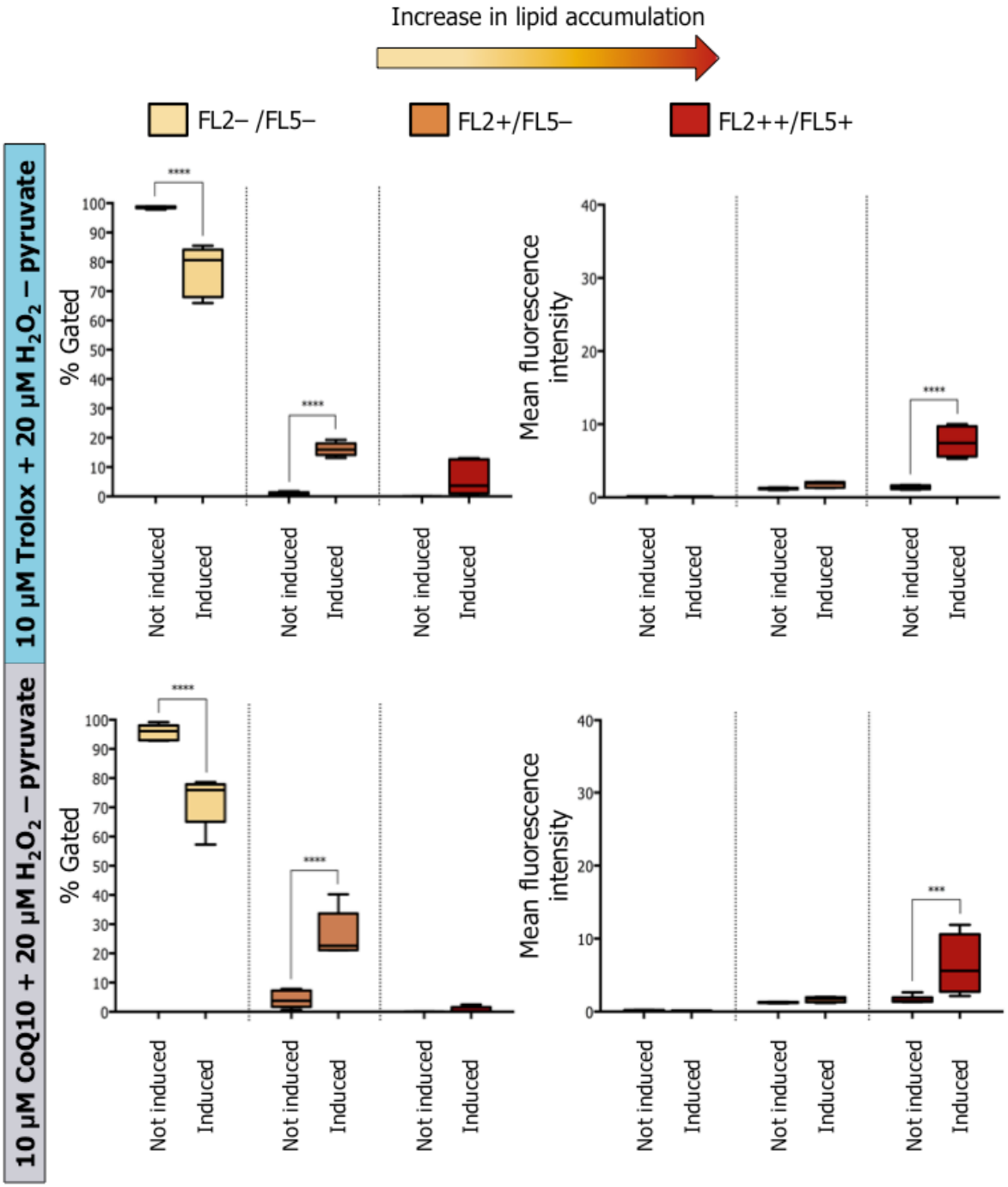

Figure 4.20. Percentages and MFI of cells that emit simultaneous yellow-gold fluorescence and deep-red fluorescence after Nile red staining. The graphs on the left-hand side indicate the percentage of cells per sub-population with increasing simultaneous emission of yellow-gold and deep red fluorescence after Nile red staining of P7 thawed-cryopreserved ASCs at 14 days after adipogenic induction. The graphs on the right-hand side indicate the mean fluorescence per sub-population of increasing simultaneous emission of yellow-gold and deep red fluorescence after Nile red staining of the same cells at 14 days after adipogenic induction. Significant differences are compared between not induced and induced cells of each sub-population. n = 2. *P<0.05; **P<0.01; ***P<0.001; ****P<0.0001.

Flow cytometric analysis of the accumulation of lipid droplets based on Nile red positive staining at day 21 of adipogenic induction

On day 21 of induction, adipogenic differentiation was detected by flow cytometry using Nile red and DAPI. Regions were set using day 14 and these regions were kept for analysis of day 21 of adipogenic differentiation for the same culture (Figure 4.21).

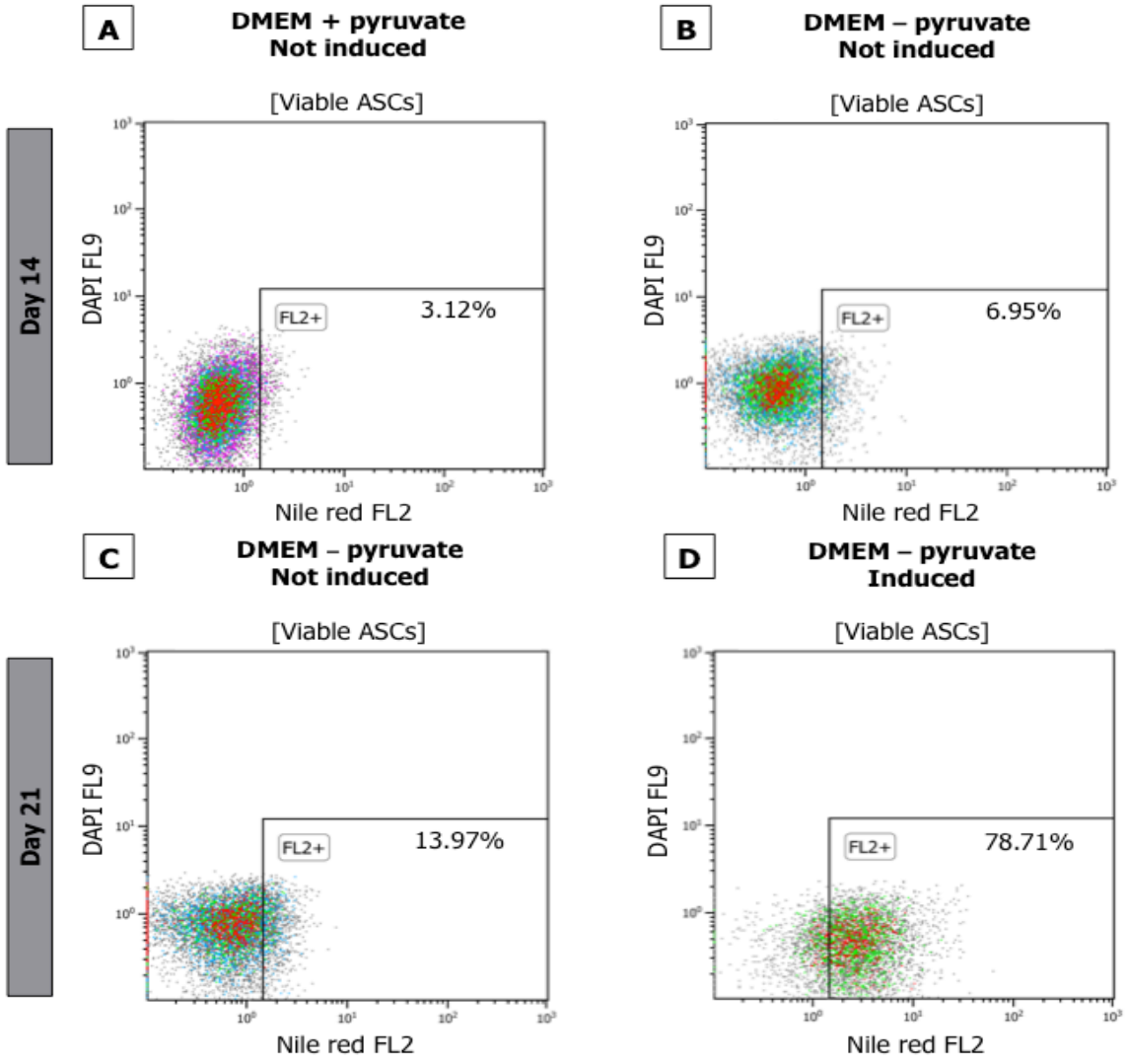

Figure 4.21. Strategy for monitoring adipogenic progression of ASCs at day 21 of induction using flow cytometry and Nile red. Regions were set according to the yellow-gold fluorescence of the non-induced Nile red stained ASCs at 14 days of adipogenic induction. The regions used at 14 days were maintained and used as gating controls for analysis of non-induced and adipogenic-induced ASCs at 21 days of induction. The rectangular regions indicate the percentage of events/cells that had accumulated lipids after Nile red staining. These are the results of ASCs cultured

in DMEM + pyruvate for 14 days (**A**), ASCs cultured in DMEM – pyruvate for 14 days (**B**), ASCs cultured in DMEM – pyruvate for 21 days (**C**), and ASCs cultured in adipogenic induction medium – pyruvate for 21 days (**D**).

All of the cultures induced to differentiate for 21 days underwent adipogenic differentiation. Flow cytometry of Nile red-stained adipogenic-induced cultures confirmed an increase in neutral lipid content and SS following the 21 day-induction period compared to non-induced control cultures. There was a similar trend observed at day 21 to day 14 cells treated under the various pro- and antioxidant conditions, although increased percentages of cells containing lipid were observed. The percentage of cells that emitted yellow-gold fluorescence due to the formation of intracellular lipid droplets increased gradually over the 21 day period when cultured with the standard adipogenic cocktail containing pyruvate. The average overall Nile red content in ASCs under standard adipogenic induction medium + pyruvate on day 21 was ±2-fold higher than on day 14 using the same donor samples. At day 14, 17.24% ± 3.20% of the cells emitted yellow-gold fluorescence. At day 21, the percentage of cells that emitted yellow-gold fluorescence increased to 34.48% ± 6.88%. The MFI, detected in the FL2 channel, of the cells in response to adipogenic induction medium + pyruvate increased to 2.48 ± 0.23 from a MFI of 1.34 ± 0.46 for the ASCs grown in DMEM + pyruvate (Table 4.5(**A**)).

Culturing ASCs in adipogenic induction medium – pyruvate enhanced adipogenic differentiation by ±8-fold compared to ASCs grown in DMEM – pyruvate. Removing pyruvate from the adipogenic induction medium significantly increased the percentage of cells stained positively with Nile red from 34.48% ± 6.88% (standard adipogenic differentiation conditions) to 64.76% ± 4.98% (adipogenic differentiation conditions – pyruvate). The culturing of the ASCs in induction medium – pyruvate for 21 days also caused ± 2-fold increase in FL2+ cells compared to 14 days. The mean Nile red fluorescence of the ASCs grown in DMEM – pyruvate for 21 days was 1.39 ± 0.04 and the mean Nile red fluorescence in response to adipogenic induction medium – pyruvate increased to 3.27 ± 0.22. The addition of 20 μM H_2O_2 to the ASCs grown in adipogenic induction medium – pyruvate markedly enhanced adipogenic differentiation by ±3-fold compared to ASCs grown in standard adipogenic induction medium + pyruvate. At day 14, the MFI of 35.39% ± 1.99% of the cells was 3.39 ± 0.69 (within the gated region FL2+). However, at 21 days, the fluorescence intensity of 85.52% ± 1.21% of the population had increased to greater than 5.

This mean Nile red fluorescence was significantly increased compared to the Nile red MFIs of the cells cultured in adipogenic medium + pyruvate and adipogenic medium – pyruvate. It was also observed that 20 μM H_2O_2 added to non-induced ASCs cultured in DMEM – pyruvate caused substantial lipid accumulation. Analysis showed that 34.09% ± 3.78% of the ASCs cultured in DMEM – pyruvate and 20 μM H_2O_2 had accumulated lipid (Figure. 4.22). However, the observed MFI of these non-induced cells was 1.40 ± 0.02, which was not significantly different from the non-induced cells grown in DMEM + pyruvate (1.34 ± 0.46) and DMEM – pyruvate (1.39 ± 0.04).

Trolox attenuated the increase in lipid accumulation seen with the addition of ROS and thus a decrease in the percentage of Nile red positive cells. The addition of 10 μM Trolox to the H_2O_2 treated adipogenic-induced ASCs decreased the percentage of adipogenic-induced cells emitting yellow-gold fluorescence from 85.52% ± 1.21% to 45.51% ± 10.36%, resulting in a ±0.5-fold change (Figure. 4.22 and Table 4.5(**D**)). There was a significant (P<0.01) decrease in the MFI of the cells induced to differentiate with adipogenic induction medium – pyruvate and H_2O_2 with the addition of Trolox for 21 days compared to the cells induced to differentiate with adipogenic induction medium – pyruvate and the addition of 20 μM H_2O_2 for 21 days. Coenzyme Q10 also attenuated the increase in lipid accumulation seen with the addition of H_2O_2. The addition of CoQ10 to H_2O_2-treated adipogenic-induced cells caused a significant decrease in the percentage of adipogenic-induced ASCs emitting yellow-gold fluorescence from 85.52% ± 1.21% to 30.97% ± 10.49% causing an approximate ±0.4-fold change. There was a significant (P<0.01) decrease in mean Nile red fluorescence of the cells in response to the addition of CoQ10 to the adipogenic induction medium – pyruvate and H_2O_2 for 21 days compared to the cells induced to differentiate with adipogenic induction medium – pyruvate and the addition of H_2O_2.

To summarise, there was a significant (P<0.01) increase in the percentage of Nile red positive cells with the addition of adipogenic induction medium + pyruvate compared to the respective control of non-induced ASCs cultured in DMEM + pyruvate. There was also a significant (P<0.0001) increase in yellow-gold fluorescence with the addition of adipogenic induction medium – pyruvate compared to the non-induced ASCs cultured in DMEM – pyruvate. Nile red positivity also increased significantly (P<0.0001) without the ROS scavenging effect of pyruvate and with the addition of 20 μM of H_2O_2 in the adipogenic

medium compared to the non-induced cells cultured in DMEM – pyruvate with 20 μM of H_2O_2. The addition of pro-oxidant to the adipogenic induction medium – pyruvate significantly (P<0.0001) increased the percentage of cells stained positively with Nile red compared to standard adipogenic differentiation conditions + pyruvate. Adding 20 μM of H_2O_2 to the non-induced ASCs cultured in DMEM – pyruvate caused significant (P<0.01) lipid accumulation within the cells. The addition of 10 μM of the ROS scavengers, Trolox and CoQ10, to the H_2O_2-treated adipogenic-induced ASCs significantly (P<0.001 and P<0.0001 respectively) decreased the percentage of adipogenic-induced ASCs emitting yellow-gold fluorescence (Figure. 4.22).

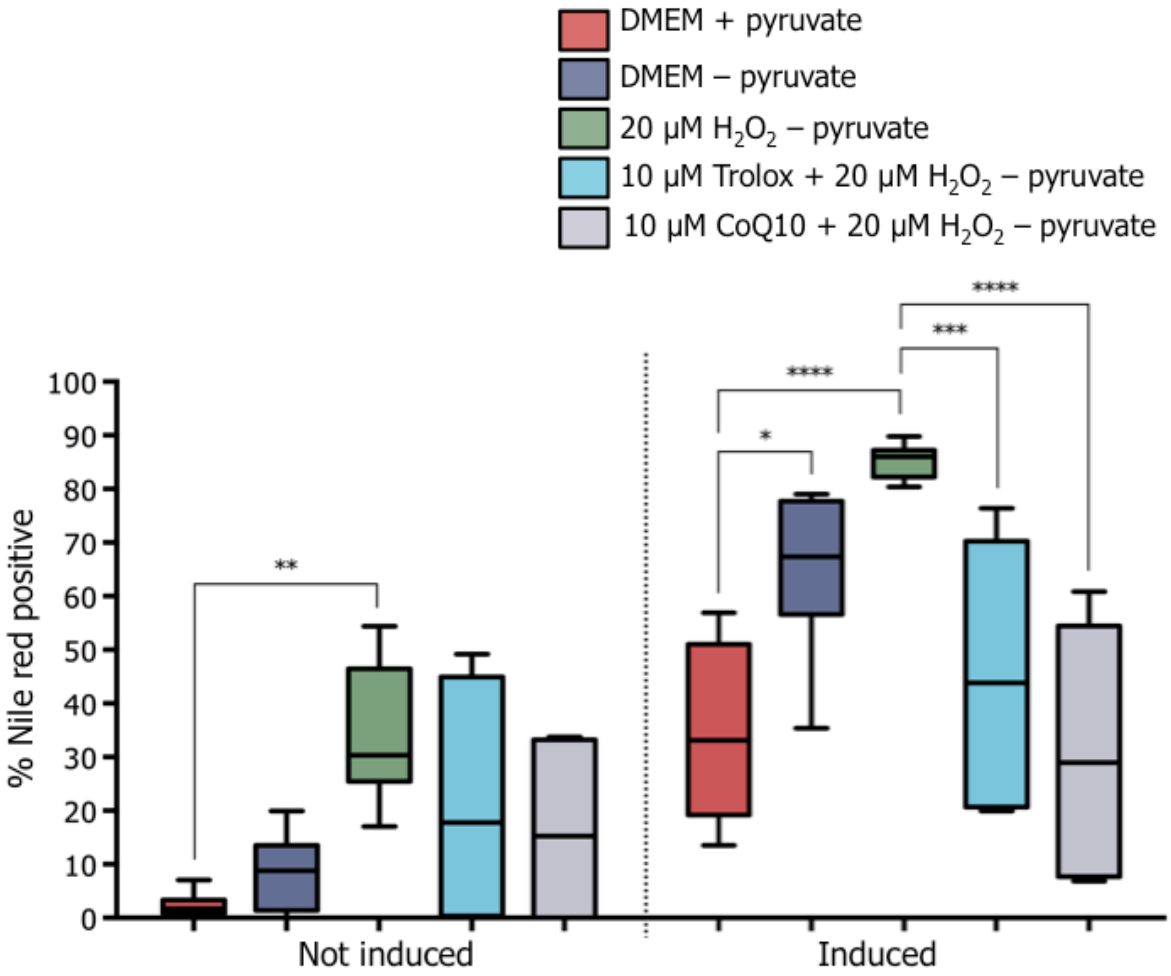

Figure 4.22. Percentage of cells that emit yellow-gold fluorescence after Nile red staining following 21 days of adipogenic induction. This graph indicates the percentage of cells that emit yellow-gold fluorescence after Nile red staining of P8, P9 and P12, thawed-cryopreserved ASCs at 21 days after adipogenic induction. Nile red positivity increased significantly (P<0.0001) without the ROS scavenging effect of pyruvate and with the addition of 20 μM of H_2O_2 in the adipogenic medium

compared to the non-induced cells under the same conditions. The addition of pro-oxidant to the adipogenic induction medium – pyruvate significantly (P<0.0001) increased the percentage of cells stained positively with Nile red compared to standard adipogenic differentiation conditions + pyruvate. Adding 20 μM of H_2O_2 to the non-induced ASCs cultured in DMEM – pyruvate caused significant (P<0.01) lipid accumulation within the cells. The addition of 10 μM of Trolox to the H_2O_2-treated adipogenic-induced ASCs significantly (P<0.001) decreased the percentage of adipogenic-induced ASCs emitting yellow-gold fluorescence. The addition of 10 μM of CoQ10 to the H_2O_2-treated adipogenic-induced ASCs significantly (P<0.0001) decreased the percentage of adipogenic-induced ASCs emitting yellow-gold fluorescence. n = 2. $^{*}P$<0.05; $^{**}P$<0.01; $^{***}P$<0.001; $^{****}P$<0.0001. See Table 4.4 for all significance values.

Table 4.4. Statistical differences relating to Figure 4.22.

		Not induced					Induced				
		DMEM + pyruvate	DMEM – pyruvate	20 μM H_2O_2 – pyruvate	10 μM Trolox + 20 μM H_2O_2 – pyruvate	10 μM CoQ10 + 20 μM H_2O_2 – pyruvate	DMEM + pyruvate	DMEM – pyruvate	20 μM H_2O_2 – pyruvate	10 μM Trolox + 20 μM H_2O_2 – pyruvate	10 μM CoQ10 + 20 μM H_2O_2 – pyruvate
Not induced	DMEM + pyruvate		ns	**	ns	ns	**	****	****	****	*
	DMEM – pyruvate	ns		*	ns	ns	ns	****	****	***	ns
	20 μM H_2O_2 – pyruvate	**	*		ns	ns	ns	**	****	ns	ns
	10 μM Trolox + 20 μM H_2O_2 – pyruvate	ns	ns	ns		ns	ns	****	****	ns	ns
	10 μM CoQ10 + 20 μM H_2O_2 – pyruvate	ns	ns	ns	ns		ns	****	****	ns	ns
Induced	DMEM + pyruvate	**	ns	ns	ns	ns		*	****	ns	ns
	DMEM – pyruvate	****	****	**	****	****	*		ns	ns	**
	20 μM H_2O_2 – pyruvate	****	****	****	****	****	****	ns		***	****
	10 μM Trolox + 20 μM H_2O_2 – pyruvate	****	***	ns	ns	ns	ns	ns	***		ns
	10 μM CoQ10 + 20 μM H_2O_2 – pyruvate	*	ns	ns	ns	ns	ns	**	****	ns	

The data passed the normality test and the results of the Tukey's multiple comparisons test are represented in the above table. The mean difference is significant at the 0.05 level. *P<0,05 **P<0,01, ***P<0,001, ****P<0,0001.

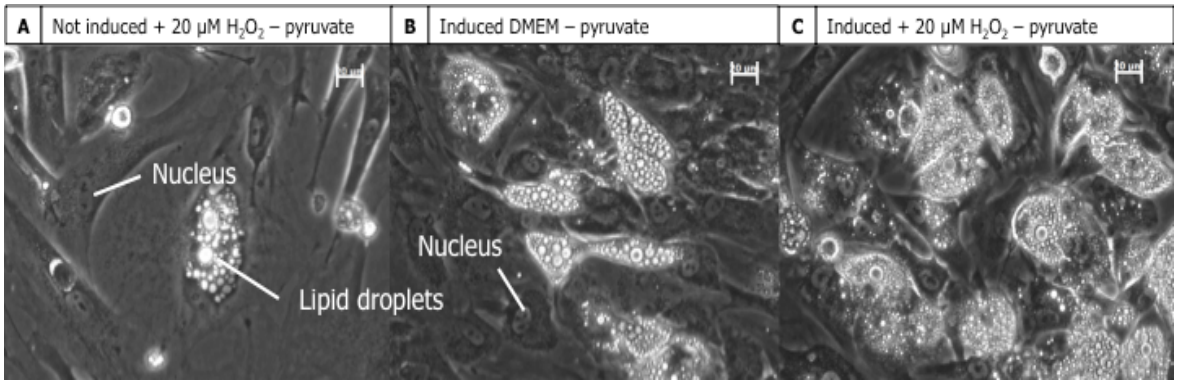

Figure 4.23. Lipid accumulation in non-induced cells with the addition of ROS. The phase contrast microscopy photographs of are of non-induced ASCs cultured in DMEM – pyruvate with the addition of the pro-oxidant H_2O_2 (**A**), induced cells cultured in adipogenic medium – pyruvate (**B**), and induced cells cultured in adipogenic medium – pyruvate with the addition of the pro-oxidant H_2O_2 (**C**). Donor sample: A180313 P7F1. Original magnification: 20x, scale bars: 20 µm.

Flow cytometric analysis of the accumulation of lipid droplets based on lipid composition at day 21 of adipogenic induction

The graphs on the left-hand side below indicate the percentage of cells per sub-population of increasing simultaneous emission of yellow-gold and deep red fluorescence after Nile red staining at 21 days after adipogenic induction. The graphs on the right-hand side indicate the mean Nile red fluorescence intensities per sub-population of increasing simultaneously emission of yellow-gold and deep red fluorescence after Nile red staining of the same cells at 21 days after adipogenic induction. Under standard adipogenic conditions + pyruvate there was a significant increase in simultaneous yellow-gold and deep red fluorescence emissions demonstrating an increase in lipid accumulation. The proportion of ASCs, grown in induction medium + pyruvate that emitted yellow-gold (FL2++/FL5–), and simultaneously emitted yellow-gold and deep-red fluorescence (FL2++/FL5+), were both significantly (P<0.0001) increased compared to the adipogenic-induced FL2–/FL5– sub-population. The percentages of cells in both of the increased lipid sub-populations were similar (non-significant).

The removal of pyruvate also appeared to have differentiated cells situated in both sub-populations, but in increased numbers compared to standard adipogenic conditions + pyruvate. A significantly greater proportion (43.73% ± 9.21%) of the differentiated cells appeared to be situated in the FL2++/FL5+ sub-population (Figure 4.24). An increase in ROS with the addition of 20 µM H_2O_2 also caused a significant increase in the FL2++/FL5+

sub-population with 54.70% ± 10.02% of cells situated in this sub-population. The addition 20 μM H_2O_2 to the non-induced ASCs caused a significant (P<0.0001) increase in both the FL2+/FL5– and FL2++/FL5+ sub-populations compared to the FL2–/FL5– sub-population of the non-induced ASCs. The addition of 10 μM Trolox and 10 μM CoQ10 to the adipogenic-induced ASCs treated with 20 μM H_2O_2 decreased the percentages of cells in the FL2++/FL5+ sub-population substantially compared to the other induced cultures with the various pro- and antioxidant conditions. However, the mean percentage of cells within the FL2+/FL5– sub-population of the adipogenic-induced culture – pyruvate with the addition of 10 μM Trolox was increased to 44.52% ± 9.84%. The mean percentage of cells within the FL2+/FL5– sub-population of the adipogenic-induced culture – pyruvate with the addition of 10 μM CoQ10 was also increased to 29.98% ± 9.98%. These increases were not statistically significant probably due to the large variation in the data and the limited number of replicates.

The induced cells (bars on the right of each sub-population), represented in the MFI graphs on the right-hand side of Figure 4.24, demonstrated a higher fluorescence intensity than the non-induced cells (bars on the left of each sub-population), with respect to both yellow-gold and deep red fluorescence. The MFI of ASCs grown in induction medium + pyruvate that simultaneously emitted yellow-gold and deep-red fluorescence (FL2++/FL5+), was 2.98 ± 0.40. The MFI of the cells in the FL2+/FL2– sub-population was 2.03 ± 0.22. Removal of pyruvate from the adipogenic induction medium resulted in a MFI of 2.29 ± 0.16 for the FL2+/FL2– sub-population. The MFI of the differentiated cells that simultaneously emitted yellow-gold and deep-red fluorescence (FL2++/FL5+) was 4.17 ± 0.41. The addition of 20 μM H_2O_2 caused an ±2-fold increase in the MFI (7.39 ± 1.63) of the FL2++/FL5+ induced sub-population. The addition of 10 μM Trolox to adipogenic-induced ASCs treated with 20 μM H_2O_2 decreased the MFI of the FL2++/FL5+ sub-population to 4.07 ± 0.80. Interestingly, the addition of 10 μM CoQ10 to adipogenic-induced ASCs treated with 20 μM H_2O_2 had a MFI of the FL2++/FL5+ sub-population of 12.46 ± 2.95. This was not statistically significant compared to the MFI of the FL2++/FL5+ sub-population of the adipogenic-induced ASCs treated with 20 μM H_2O_2.

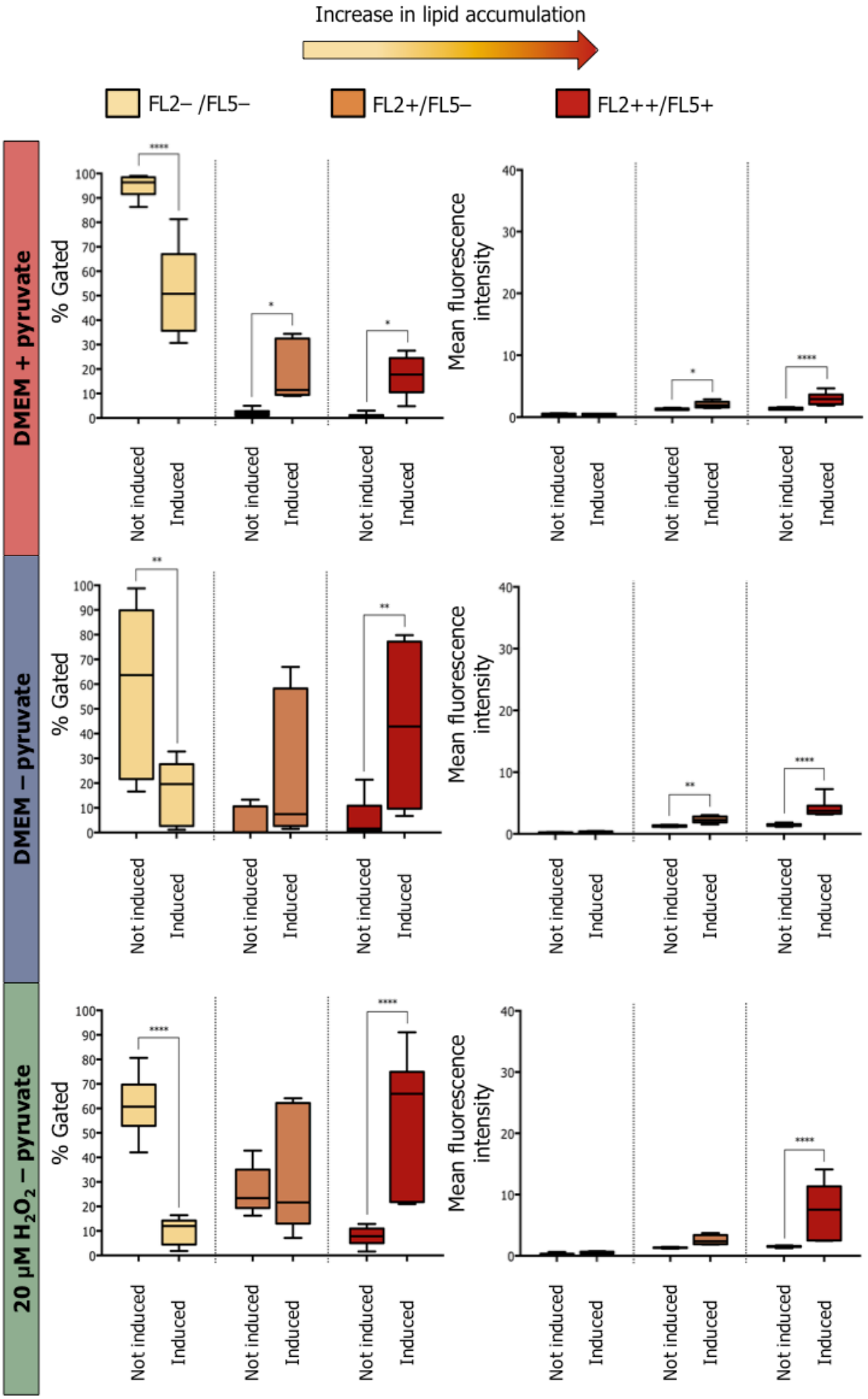

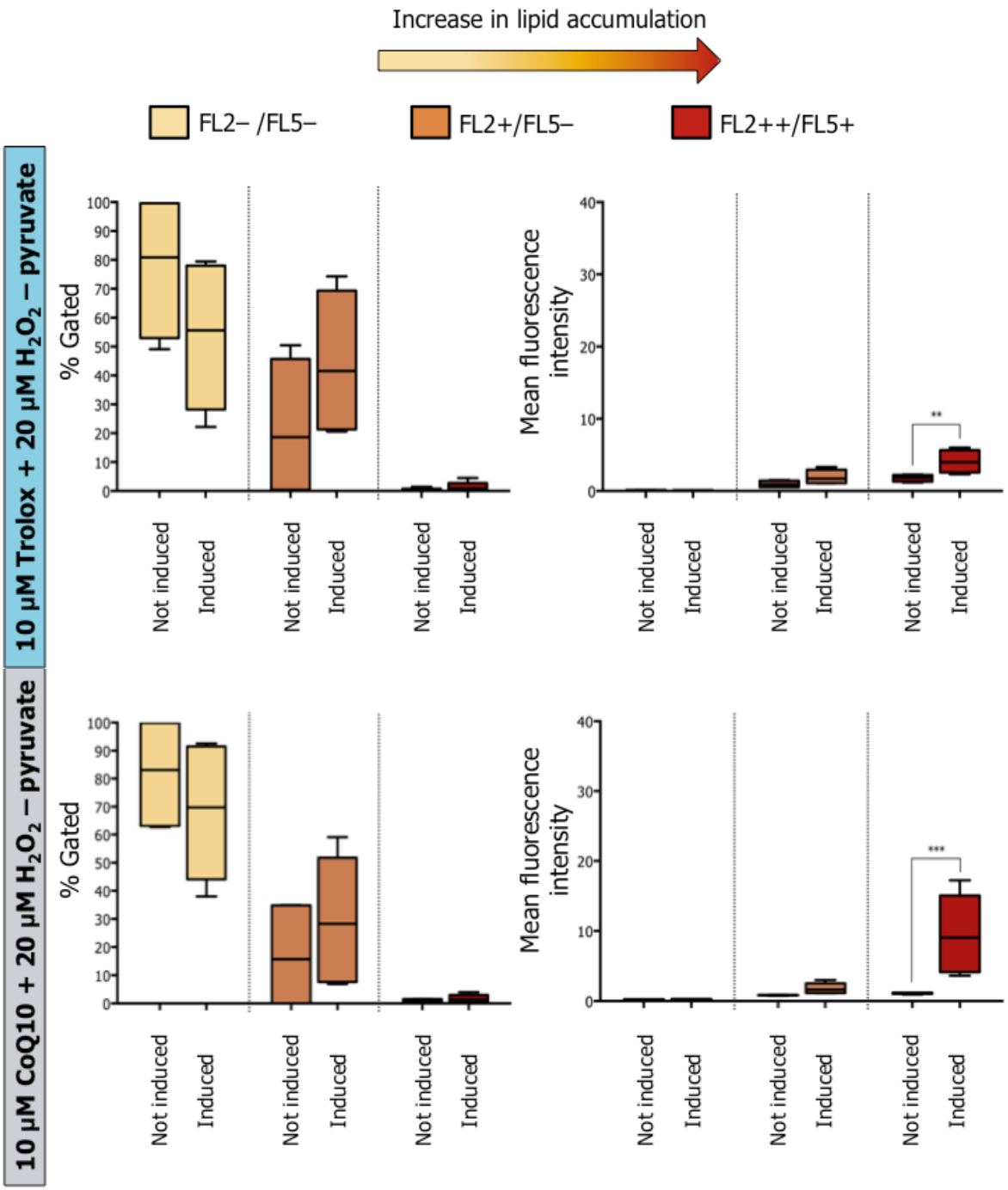

Figure 4.24. Percentages and MFI of cells that emit simultaneous yellow-gold fluorescence and deep-red fluorescence after Nile red staining. The graphs on the left-hand side indicate the percentage of cells per sub-population of increasing simultaneous emission of yellow-gold and deep red fluorescence after Nile red staining of early-passage, P8, P9 and P12, thawed-cryopreserved ASCs at 21 days after adipogenic induction. The graphs on the right-hand side indicate the mean fluorescence per sub-population of increasing simultaneous emission of yellow-gold and deep red fluorescence after Nile red staining of the same cells at 21 days after adipogenic induction. Significant

differences are compared between not induced and induced cells of each sub-population. n = 2. **P*<0.05; ***P*<0.01; ****P*<0.001; *****P*<0.0001.

Tables representing the % Gated cells and MFI of non-induced ASCs and adipogenic differentiated cells that emitted yellow-gold fluorescence after staining with Nile red.

Table 4.5(A). Cells cultured in medium + pyruvate.

	% Nile red positive		MFI	
	Not induced	Induced	Not induced	Induced
Day 14	5.38% ± 0.80%	17.24% ± 3.20%	1.37 ± 0.03	2.43 ± 0.33
Day 21	2.43% ± 0.68%	34.48% ± 6.88%	1.34 ± 0.46	2.48 ± 0.23

Table 4.5(B). Cells cultured in medium – pyruvate.

	% Nile red positive		MFI	
	Not induced	Induced	Not induced	Induced
Day 14	4.60% ± 1.78%	31.28% ± 3.37%	1.41 ± 0.01	2.58 ± 0.24
Day 21	8.06% ± 2.12%	64.76% ± 4.98%	1.39 ± 0.04	3.27 ± 0.22

Table 4.5(C). Cells cultured in medium with the addition of 20 μM H_2O_2 – pyruvate.

	% Nile red positive		MFI	
	Not induced	Induced	Not induced	Induced
Day 14	3.29% ± 1.10%	35.39% ± 1.99%	1.37 ± 0.03	3.39 ± 0.69
Day 21	34.09% ± 3.78%	85.52% ± 1.21%	1.40 ± 0.02	5.72 ± 1.35

Table 4.5(D). Cells cultured in medium with the addition of 20 μM H_2O_2 and 10 μM Trolox – pyruvate.

	% Nile red positive		MFI	
	Not induced	Induced	Not induced	Induced
Day 14	1.00% ± 0.20%	21.64% ± 3.13%	1.35 ± 0.06	2.92 ± 0.54
Day 21	21.49% ± 9.57%	45.51% ± 10.36%	1.65 ± 0.10	2.76 ± 0.25

Table 4.5(E). Cells cultured in medium with the addition of 20 μM H_2O_2 and 10 μM CoQ10 – pyruvate.

	% Nile red positive		MFI	
	Not induced	Induced	Not induced	Induced
Day 14	3.85% ± 1.04%	25.98% ± 3.75%	1.33 ± 0.45	2.03 ± 0.31
Day 21	16.23% ± 7.25%	30.97% ± 10.49%	0.92 ± 0.24	2.50 ± 0.77

Tables representing the % Gated and MFI of non-induced ASCs and adipogenic differentiated cells that simultaneously emitted yellow-gold and deep red fluorescence after staining with Nile red.

Table 4.6(A). Cells cultured in medium + pyruvate.

	% Gated						MFI					
	Not induced			Induced			Not induced			Induced		
	FL2-/ FL5-	FL2+/ FL5-	FL2++/ FL5+	FL2-/ FL5-	FL2+/ FL5-	FL2++/ FL5+	FL2-/ FL5-	FL2+/ FL5-	FL2++/ FL5+	FL2-/ FL5-	FL2+/ FL5-	FL2++/ FL5+
Day 14	93.11% ± 0.96%	5.05% ± 0.67%	0.72% ± 0.19%	78.10% ± 3.27%	8.80% ± 0.80%	9.06% ± 2.46%	0.52 ± 0.02	1.31 ± 0.03	1.69 ± 0.08	0.27 ± 0.04	1.60 ± 0.09	5.78 ± 1.24
Day 21	94.76% ± 1.45%	2.13% ± 0.44%	0.69% ± 0.34%	52.16% ± 7.75%	17.95% ± 4.85%	17.30% ± 3.28%	0.42 ± 0.05	1.28 ± 0.05	1.36 ± 0.07	0.45 ± 0.05	2.03 ± 0.22	2.98 ± 0.40

Table 4.6(B). Cells cultured in medium – pyruvate.

	% Gated						MFI					
	Not induced			Induced			Not induced			Induced		
	FL2-/ FL5-	FL2+/ FL5-	FL2++/ FL5+	FL2-/ FL5-	FL2+/ FL5-	FL2++/ FL5+	FL2-/ FL5-	FL2+/ FL5-	FL2++/ FL5+	FL2-/ FL5-	FL2+/ FL5-	FL2++/ FL5+
Day 14	80.55% ± 3.95%	2.81% ± 1.06%	3.31% ± 1.19%	55.47% ± 4.08%	14.86% ± 2.22%	17.16% ± 2.60%	0.27 ± 0.03	2.09 ± 0.17	2.26 ± 0.13	0.24 ± 0.03	2.58 ± 0.17	6.74 ± 1.78
Day 21	57.91% ± 11.26%	3.53% ± 1.76%	5.41% ± 2.35%	16.30% ± 3.94%	22.65% ± 8.73%	43.73% ± 9.21%	0.20 ± 0.02	1.24 ± 0.05	1.44 ± 0.07	0.28 ± 0.04	2.29 ± 0.16	4.17 ± 0.41

Table 4.6(C). Cells cultured in medium with the addition of 20 μM H_2O_2 – pyruvate.

	% Gated						MFI					
	Not induced			Induced			Not induced			Induced		
	FL2-/ FL5-	FL2+/ FL5-	FL2++/ FL5+	FL2-/ FL5-	FL2+/ FL5-	FL2++/ FL5+	FL2-/ FL5-	FL2+/ FL5-	FL2++/ FL5+	FL2-/ FL5-	FL2+/ FL5-	FL2++/ FL5+
Day 14	96.51% ± 1.09%	3.29% ± 1.04%	0.11% ± 0.04%	63.99% ± 1.90%	31.99% ± 1.49%	3.71% ± 0.70%	0.15 ± 0.02	1.29 ± 0.03	1.32 ± 0.12	0.13 ± 0.01	2.17 ± 0.25	11.57 ± 1.75
Day 21	60.76% ± 3.43%	26.46% ± 2.83%	7.62% ± 1.02%	9.99% ± 1.88%	33.33% ± 8.75%	54.70% ± 10.02%	0.28 ± 0.05	1.32 ± 0.02	1.51 ± 0.04	0.51 ± 0.06	2.58 ± 0.27	7.39 ± 1.63

Table 4.6(D). Cells cultured in medium with the addition of 20 μM H_2O_2 and 10 μM Trolox – pyruvate.

	% Gated						MFI					
	Not induced			Induced			Not induced			Induced		
	FL2-/ FL5-	FL2+/ FL5-	FL2++/ FL5+	FL2-/ FL5-	FL2+/ FL5-	FL2++/ FL5+	FL2-/ FL5-	FL2+/ FL5-	FL2++/ FL5+	FL2-/ FL5-	FL2+/ FL5-	FL2++/ FL5+
Day 14	98.58% ± 0.16%	0.96% ± 0.18%	0.07% ± 0.01%	77.51% ± 3.42%	16.08% ± 0.91%	5.81% ± 2.32%	0.13 ± 0.01	1.21 ± 0.05	1.40 ± 0.14	0.12 ± 0.01	1.76 ± 0.15	7.58 ± 0.86
Day 21	77.40% ± 10.01%	22.05% ± 9.81%	0.42% ± 0.22%	53.44% ± 10.45%	44.52% ± 9.84%	1.49% ± 0.69%	0.13 ± 0.01	0.97 ± 0.20	1.79 ± 0.24	0.11 ± 0.00	1.96 ± 0.38	4.07 ± 0.80

Table 4.6(E). Cells cultured in medium with the addition of 20 μM H_2O_2 and 10 μM CoQ10 – pyruvate.

	% Gated						MFI					
	Not induced			Induced			Not induced			Induced		
	FL2-/ FL5-	FL2+/ FL5-	FL2++/ FL5+	FL2-/ FL5-	FL2+/ FL5-	FL2++/ FL5+	FL2-/ FL5-	FL2+/ FL5-	FL2++/ FL5+	FL2-/ FL5-	FL2+/ FL5-	FL2++/ FL5+
Day 14	95.83% ± 1.07%	4.18% ± 1.18%	0.07% ± 0.01%	72.38% ± 3.89%	26.44% ± 3.62%	0.73% ± 0.46%	0.19 ± 0.01	1.25 ± 0.03	1.67 ± 0.21	0.14 ± 0.01	1.66 ± 0.16	6.31 ± 2.08
Day 21	81.98% ± 8.01%	16.86% ± 7.54%	0.69% ± 0.31%	67.92% ± 10.57%	29.98% ± 9.98%	1.75% ± 0.62%	0.24 ± 0.01	1.31 ± 0.06	1.38 ± 0.13	0.21 ± 0.05	2.71 ± 0.50	12.46 ± 2.95

The relative intensities of Nile Red fluorescence (yellow-gold to deep red spectrum) emitted are expressed as mean percentages and MFIs. All results are expressed as the mean ± SEM. n = 2. All experiments were done in triplicate.

Effect of pre-conditioning with pro-oxidant on the differentiation potential of ASCs

Pre-conditioning stromal cells using chemokines, growth factors, pharmacological agents, or cellular stressors, has been shown to improve cellular adaption to stress, increase cell survival and thus improve transplantation outcomes (60). Pre-conditioning prompts the cells to adapt to an environment they would experience upon transplantation and thus is proposed to enhance their survival. It was hypothesized that exposure of the ASCs to sub-lethal oxidative concentrations of H_2O_2 could alleviate subsequent oxidative stress-induced

apoptosis and select for a sub-population within the cultured ASCs that were more resistant to oxidative damage. The effects of pre-conditioning with 20 μM of H_2O_2 or 100 μM of H_2O_2 for a 24-hour period were assessed on the adipogenic differentiation potential of ASCs.

Flow cytometric analysis of the accumulation of lipid droplets based on Nile red positive staining at day 14 of adipogenic induction

The ASCs were incubated in standard growth medium until confluent and were then pre-treated with medium containing either 20 μM H_2O_2 or 100 μM H_2O_2 for 24 hours. Following the 24-hour incubation period this medium was removed and adipogenic medium – pyruvate was added and cultured for 14 and 21 days. The mean percentage of adipogenic-induced cells cultured for 14 days that had accumulated lipid following pre-conditioning with 20 μM H_2O_2 was 45.27% ± 18.36% compared to conventional adipogenic medium + pyruvate induced cells that had a mean of 17.24% ± 3.20%. At day 14, the MFI of 45.27% ± 18.36% of the cells within the FL2+ region was increased to 7.14 ± 2.48 (Table 4.9(**A**)). This was significantly increased compared to the MFIs for adipogenic medium + pyruvate and adipogenic medium – pyruvate but was not significantly different from the MFI obtained with adipogenic medium – pyruvate treated with 20 μM H_2O_2 at 14 days. Pre-treatment with 20 μM H_2O_2 also had an increased mean percentage of Nile red positive cells compared to adipogenic medium – pyruvate and adipogenic medium – pyruvate treated with 20 μM H_2O_2, however, no statistically significant differences were observed between the 20 μM H_2O_2 pre-treated adipogenic-induced culture and the other adipogenic-induced cultures and this may be due to the large variation observed (Figure 4.25). The heterogeneity between donor samples was particularly evident when the cultures were pretreated with 20 μM H_2O_2 for the 24-hour period. The A220313 culture, as previously mentioned, accumulated more lipid than A180313 (Figure 4.26).

The same heterogeneity between cultures A180313 and A220313 (both at P7F1) was observed when the cultures were pre-conditioned with 100 μM H_2O_2 and induced with adipogenic medium – pyruvate for 14 days. Pre-conditioning with 100 μM H_2O_2 appeared to protect the ASCs from lethal oxidative stress significantly compared to treatment with 100 μM H_2O_2 throughout the induction period of 14 days. Results for adipogenic induction following the 14-day period were obtained. The ASCs that had undergone oxidative pre-conditioning with 100 μM H_2O_2 before being exposed to adipogenic induction medium –

pyruvate for 14 days and had accumulated lipid exhibited a mean percentage of 24.69% ± 11.94% and a MFI of 2.82 ± 0.91. This was an increase mean percentage-wise compared to conventional adipogenic medium + pyruvate, but pre-conditioning with 100 μM H_2O_2 did not significantly increase lipid accumulation compared to conventional adipogenic medium and adipogenic medium – pyruvate (Figure 4.25).

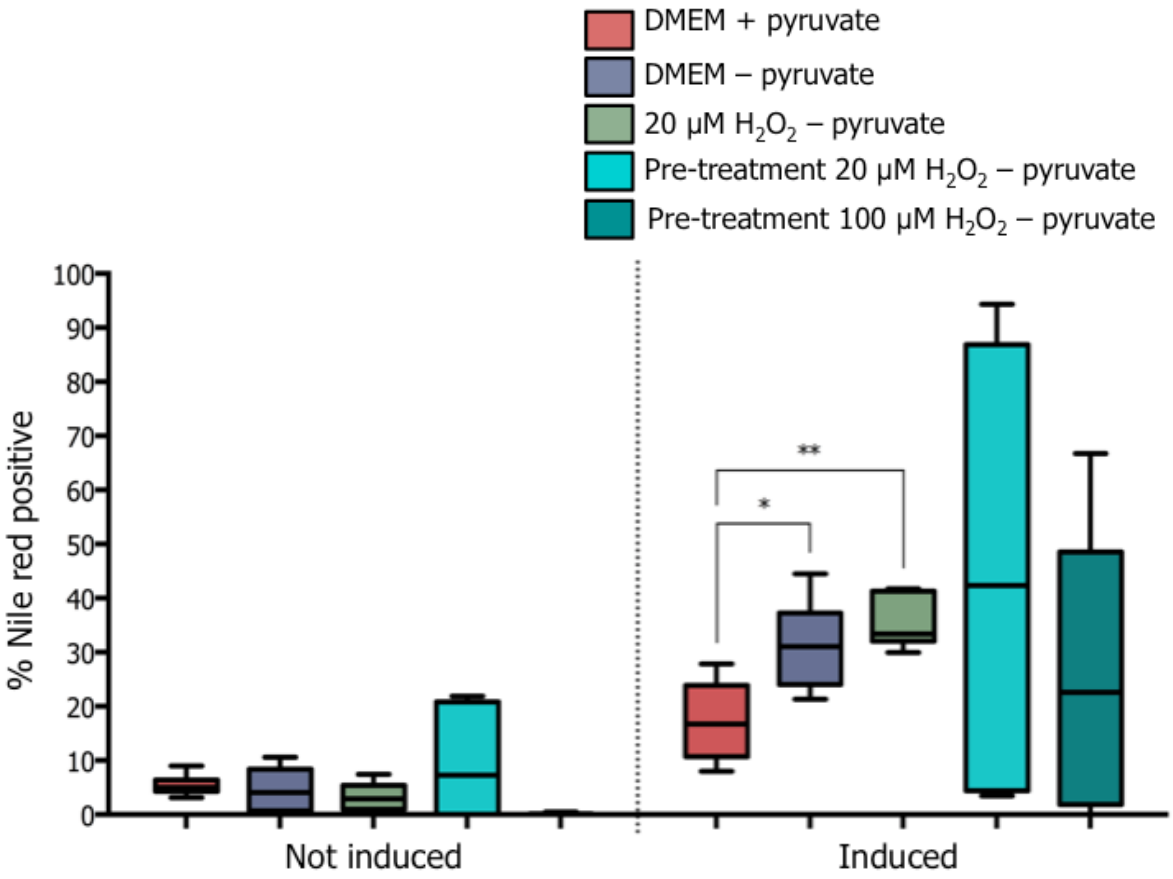

Figure 4.25. Effect of oxidative pre-conditioning on adipogenic differentiation of ASCs. This graph indicates the percentage of cells that emit yellow-gold fluorescence after Nile red staining of P7 thawed-cryopreserved ASCs at 14 days after adipogenic induction under different conditions. There was a non-significant increase in Nile red positivity with pre-conditioning with 20 μM H_2O_2 compared to conventional adipogenic induction medium. Pre-treatment with 100 μM H_2O_2 did not significantly increase lipid accumulation compared to conventional adipogenic induction medium.
n = 2. *P<0.05, **P<0.01

Table 4.7. Statistical differences relating to Figure 4.25.

		Not induced					Induced				
		DMEM + pyruvate	DMEM – pyruvate	20 µM H_2O_2 – pyruvate	Pre-treatment 20 µM H_2O_2 – pyruvate	Pre-treatment 100 µM H_2O_2 – pyruvate	DMEM + pyruvate	DMEM – pyruvate	20 µM H_2O_2 – pyruvate	Pre-treatment 20 µM H_2O_2 – pyruvate	Pre-treatment 100 µM H_2O_2 – pyruvate
Not induced	DMEM + pyruvate		ns	ns	ns	**	*	***	****	ns	ns
	DMEM – pyruvate	ns		ns	ns	ns	**	***	****	ns	ns
	20 µM H_2O_2 – pyruvate	ns	ns		ns	*	**	***	****	ns	ns
	Pre-treatment 20 µM H_2O_2 – pyruvate	ns	ns	ns		ns	ns	**	**	ns	ns
	Pre-treatment 100 µM H_2O_2 – pyruvate	**	ns	*	ns		**	***	****	ns	ns
Induced	DMEM + pyruvate	*	**	**	ns	**		*	**	ns	ns
	DMEM – pyruvate	***	***	***	**	***	*		ns	ns	ns
	20 µM H_2O_2 – pyruvate	****	****	****	**	****	**	ns		ns	ns
	Pre-treatment 20 µM H_2O_2 – pyruvate	ns	ns	ns	ns	ns	ns	ns	ns		ns
	Pre-treatment 100 µM H_2O_2 – pyruvate	ns	ns	ns	ns	ns	ns	ns	ns	ns	

The data passed the normality test and the results of the Tukey's multiple comparisons test are represented in the above table. The mean difference is significant at the 0.05 level. *P<0,05 **P<0,01, ***P<0,001, ****P<0,0001.

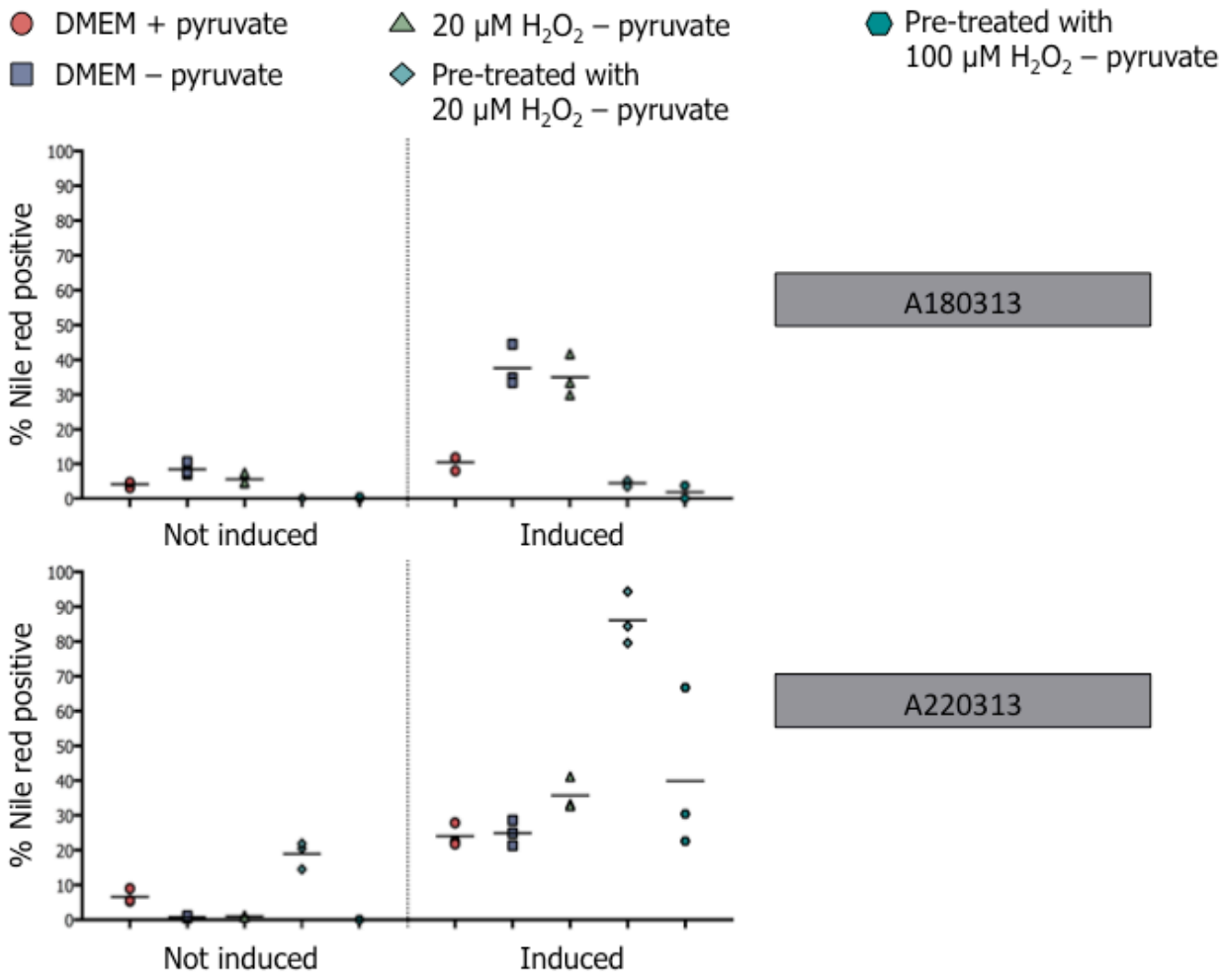

Figure 4.26. Demonstration of inter-culture variation. Pre-conditioning the ASCs with 20 µM H_2O_2 for 24 hours followed by the addition of adipogenic induction medium – pyruvate for 14 days appeared to have opposing effects on A180313 (P7F1) and A220313 (P7F1). The A180313 cells had a mean percentage of Nile red positivity of 4.44% ± 0.50% and the A220313 cells had a mean percentage of Nile red positivity of 86.09% ± 4.35%. This demonstrates that A180313 is either less affected by oxidative pre-conditioning or has a lesser potential to differentiate into adipocytes. The symbols represent technical replicates of the same condition in the same experiment.

Flow cytometric analysis of the accumulation of lipid droplets based on lipid composition at day 14 of adipogenic induction

It appeared that pre-conditioning the ASCs with 20 µM H_2O_2 for 24 hours before induction with adipogenic medium – pyruvate for 14 days increased the simultaneous yellow-gold and deep red fluorescence emissions demonstrating an increase in lipid accumulation. The proportion of ASCs, pre-conditioned with 20 µM H_2O_2 and cultured in induction medium – pyruvate, that emitted yellow-gold (FL2++/FL5–), and simultaneously emitted yellow-gold

and deep-red fluorescence (FL2++/FL5+), were both non-significantly increased compared to the non-induced counterparts. The MFI of the differentiated cells that simultaneously emitted yellow-gold and deep-red fluorescence (FL2++/FL5+) was 12.98 ± 2.41. Pre-conditioning the ASCs with 100 μM H_2O_2 for 24 hours before induction with adipogenic medium – pyruvate for 14 days caused a non-significant increase in the FL2+/FL5– sub-population with 16.68% ± 6.29% of cells situated in this sub-population (Figure 4.27).

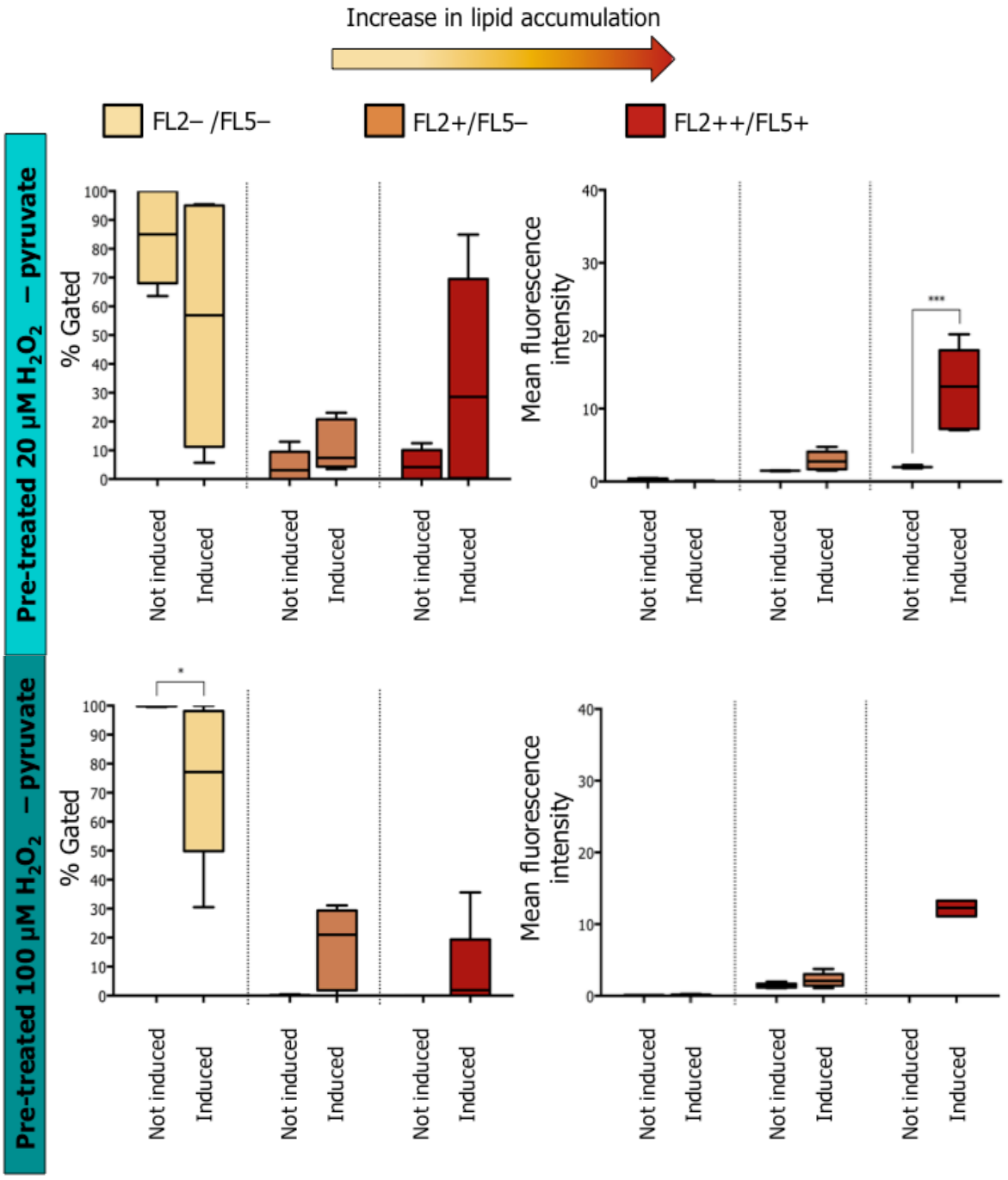

Figure 4.27. Percentages and MFI of cells that emit simultaneous yellow-gold fluorescence and deep-red fluorescence after Nile red staining. The graphs on the left-hand side indicate the percentage of cells per sub-population of increasing simultaneous emission of yellow-gold and deep red fluorescence after Nile red staining of P7, thawed-cryopreserved ASCs that were pre-conditioned with pro-oxidant for 24 hours followed by 14 days of adipogenic induction. The graphs on the right-hand side indicate the mean fluorescence per sub-population of increasing simultaneously emission of yellow-gold and deep red fluorescence after Nile red staining of the same cells at 14 days after

adipogenic induction. Significant differences are compared between Not induced and Induced cells of each sub-population. n = 2. *P<0.05; **P<0.01; ***P<0.001; ****P<0.0001.

Flow cytometric analysis of the accumulation of lipid droplets based on Nile red positive staining at day 21 of adipogenic induction

The effects of H_2O_2 pre-conditioning were assessed on adipogenic differentiation following 21 days of adipogenic induction. The mean percentage of adipogenic-induced cells cultured for 21 days that had accumulated lipid following pre-conditioning with 20 μM H_2O_2 was 3.67% ± 0.96% compared to adipogenic-induced cells treated with 20 μM H_2O_2 that had a mean of 90.29% ± 8.83% positively stained with Nile red. Pre-treatment with 20 μM H_2O_2 significantly inhibited lipid accumulation compared to conventional adipogenic medium, adipogenic medium – pyruvate and adipogenic medium – pyruvate treated with 20 μM H_2O_2.

The cultures were then once again pre-conditioned with 100 μM H_2O_2 for 24 hours and induced with adipogenic medium – pyruvate for 21 days. A percentage of ASCs that had undergone oxidative preconditioning with 100 μM H_2O_2 before being exposed to adipogenic induction medium – pyruvate for 21 days and had accumulated lipid exhibited a mean of 40.65% ± 2.90%. The adipogenic induction of the ASCs pre-conditioned with 100 μM H_2O_2 resulted in a ±2-fold increase in the MFI compared to the ASCs pre-conditioned with 100 μM H_2O_2 and cultured in DMEM – pyruvate. Pre-treatment with 100 μM H_2O_2 increased lipid accumulation to a similar extent as conventional adipogenic medium. The lipid accumulation was, however, significantly lower than adipogenic induction with 20 μM H_2O_2, but significantly higher than the pre-treatment with 20 μM H_2O_2 followed by adipogenic induction (Figure 4.28).

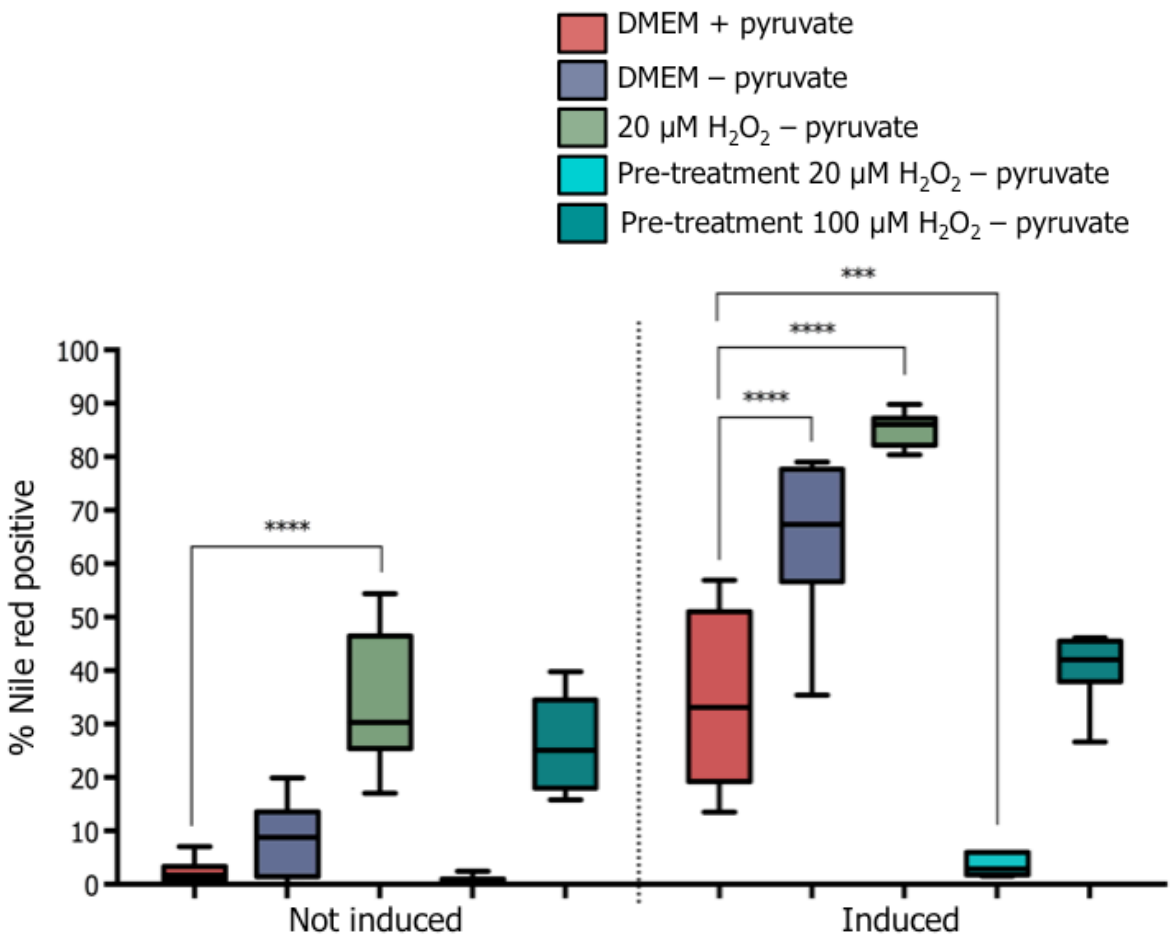

Figure 4.28. Effect of oxidative pre-conditioning on adipogenic differentiation of ASCs. This graph indicates the percentage of cells that emit yellow-gold fluorescence after Nile red staining of P11 and P13 thawed-cryopreserved ASCs at 21 days after adipogenic induction under different conditions. Pre-conditioning with 20 µM H_2O_2 for 21 days is not conducive towards adipogenic differentiation. However, Nile red positivity seems to increase with pre-treatment of 100 µM H_2O_2 and similarly to conventional adipogenic induction medium. n = 2. ***P<0.001, ****P<0.0001

Table 4.8. Statistical differences relating to Figure 4.28.

		Not induced					Induced				
		DMEM + pyruvate	DMEM – pyruvate	20 µM H_2O_2 – pyruvate	Pre-treatment 20 µM H_2O_2 – pyruvate	Pre-treatment 100 µM H_2O_2 – pyruvate	DMEM + pyruvate	DMEM – pyruvate	20 µM H_2O_2 – pyruvate	Pre-treatment 20 µM H_2O_2 – pyruvate	Pre-treatment 100 µM H_2O_2 – pyruvate
Not induced	DMEM + pyruvate		ns	****	ns	***	****	****	****	ns	****
	DMEM – pyruvate	ns		****	ns	*	***	****	****	ns	****
	20 µM H_2O_2 – pyruvate	****	****		****	ns	ns	****	****	****	ns
	Pre-treatment 20 µM H_2O_2 – pyruvate	ns	ns	****		**	****	****	****	ns	****
	Pre-treatment 100 µM H_2O_2 – pyruvate	***	*	ns	**		ns	****	****	*	ns
Induced	DMEM + pyruvate	****	***	ns	****	ns		****	****	***	ns
	DMEM – pyruvate	****	****	****	****	****	****		**	****	***
	20 µM H_2O_2 – pyruvate	****	****	****	****	****	****	**		****	****
	Pre-treatment 20 µM H_2O_2 – pyruvate	ns	ns	****	ns	*	***	****	****		****
	Pre-treatment 100 µM H_2O_2 – pyruvate	****	****	ns	****	ns	ns	***	****	****	

The data passed the normality test and the results of the Tukey's multiple comparisons test are represented in the above table. The mean difference is significant at the 0.05 level. *P<0,05 **P<0,01, ***P<0,001, ****P<0,0001.

Flow cytometric analysis of the accumulation of lipid droplets based on lipid composition at day 21 of adipogenic induction

It appeared that pre-conditioning with 20 µM H_2O_2 for 24 hours before adipogenic induction with medium – pyruvate for 21 days was not conducive towards adipogenic differentiation. Pre-treatment with 100 µM H_2O_2 for 24 hours caused a significant increase in the FL2+/FL5– sub-population with 39.53% ± 2.72% of cells situated in this sub-population. The MFI of this sub-population and the FL2++/FL5+ sub-population was not significantly different to these two sub-populations in the cells induced with conventional adipogenic medium + pyruvate (Figure 4.29).

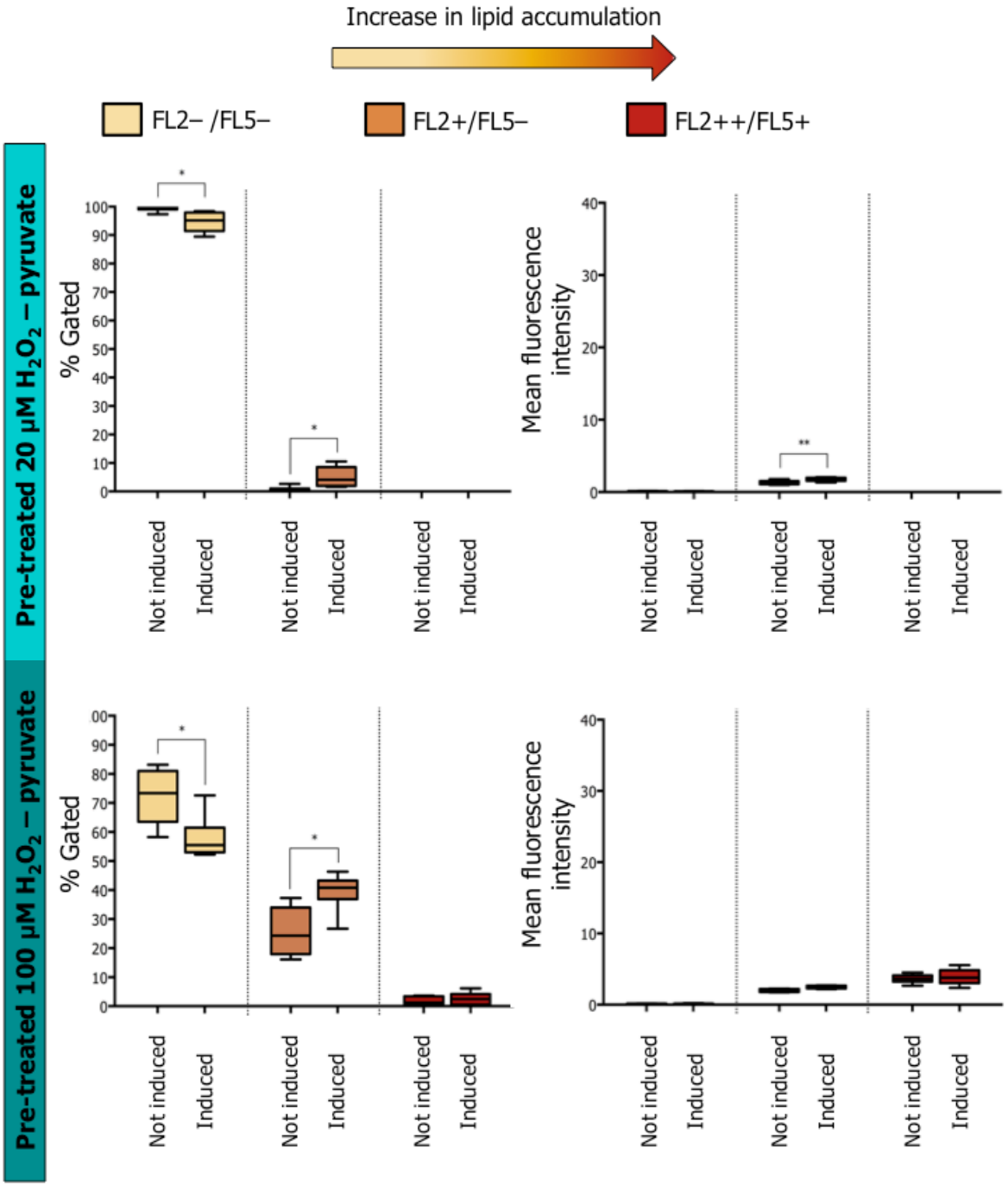

Figure 4.29. Percentages and MFI of cells that emit simultaneous yellow-gold fluorescence and deep-red fluorescence after Nile red staining. The graphs on the left-hand side indicate the percentage of cells per sub-population of increasing simultaneous emission of yellow-gold and deep red fluorescence after Nile red staining of P11 and P13 thawed-cryopreserved ASCs that were pre-conditioned with pro-oxidant for 24 hours followed by 21 days of adipogenic induction. The graphs on the right-hand side indicate the mean fluorescence per sub-population of increasing simultaneously emission of yellow-gold and deep red fluorescence after Nile red staining of the same cells at 21 days

after adipogenic induction. Significant differences are compared between Not induced and Induced cells of each sub-population. n = 2. **P*<0.05; ***P*<0.01

Tables representing the % Gated cells and MFI of non-induced ASCs and adipogenic differentiated cells that emitted yellow-gold fluorescence after staining with Nile red.

Table 4.9(A). Cells pre-treated with 20 μM H_2O_2 and cultured in medium – pyruvate

	% Nile red positive		MFI	
	Not induced	Induced	Not induced	Induced
Day 14	9.48% ± 4.36%	45.27% ± 18.36%	1.68 ± 0.04	7.14 ± 2.48
Day 21	0.52% ± 0.38%	3.67% ± 0.96%	1.38 ± 0.11	2.08 ± 0.28

Table 4.9(B). Cells pre-treated with 100 μM H_2O_2 and cultured in medium – pyruvate

	% Nile red positive		MFI	
	Not induced	Induced	Not induced	Induced
Day 14	0.09% ± 0.07%	24.69% ± 11.94%	1.43 ± 0.15	2.82 ± 0.91
Day 21	26.19% ± 3.98%	40.65% ± 2.90%	2.11 ± 0.10	2.62 ± 0.05

Tables representing the % Gated and MFI of non-induced ASCs and adipogenic differentiated cells that simultaneously emitted yellow-gold and deep red fluorescence after staining with Nile red.

Table 4.10(A). Cells pre-treated with 20 μM H_2O_2 and cultured in medium – pyruvate

	% Gated						MFI					
	Not induced			Induced			Not induced			Induced		
	FL2-/ FL5-	FL2+/ FL5-	FL2++/ FL5+	FL2-/ FL5-	FL2+/ FL5-	FL2++/ FL5+	FL2-/ FL5-	FL2+/ FL5-	FL2++/ FL5+	FL2-/ FL5-	FL2+/ FL5-	FL2++/ FL5+
Day 14	83.86% ± 7.28%	4.60% ± 2.24%	5.03% ± 2.32	53.78% ± 18.46	10.98% ± 3.45%	34.50% ± 15.71%	0.25 ± 0.06	1.48 ± 0.04	2.04 ± 0.14	0.12 ± 0.00	2.90 ± 0.55	12.98 ± 2.41
Day 21	99.39% ± 0.42	0.57% ± 0.43%	0.00% ± 0.00%	94.66% ± 1.46%	5.07% ± 1.50%	0.00% ± 0.00%	0.12 ± 0.01	1.29 ± 0.12	N/A	0.12 ± 0.01	1.75 ± 0.10	N/A

Table 4.10(B). Cells pre-treated with 100 μM H_2O_2 and cultured in medium – pyruvate

	% Gated						MFI					
	Not induced			Induced			Not induced			Induced		
	FL2-/ FL5-	FL2+/ FL5-	FL2++/ FL5+	FL2-/ FL5-	FL2+/ FL5-	FL2++/ FL5+	FL2-/ FL5-	FL2+/ FL5-	FL2++/ FL5+	FL2-/ FL5-	FL2+/ FL5-	FL2++/ FL5+
Day 14	99.89% ± 0.07%	0.09% ± 0.07%	0.00% ± 0.00%	74.59% ± 12.44%	16.68% ± 6.29%	8.12% ± 6.90%	0.11 ± 0.00	1.42 ±0.15	N/A	0.16 ± 0.02	2.20 ± 0.44	12.28 ± 0.64
Day 21	72.28% ± 4.12%	25.58% ± 3.56%	1.83% ± 0.54%	57.79% ± 3.06%	39.53% ± 2.72%	2.57% ± 0.93%	0.14 ± 0.01	1.96 ± 0.09	3.65 ± 0.25	0.14 ± 0.02	2.45 ± 0.08	3.91 ± 0.51

The relative intensities of Nile Red fluorescence (yellow-gold to deep red spectrum) emitted are expressed as mean percentages and MFI. All results are expressed as the mean ± SEM. n = 2. All experiments were done in triplicate.

Discussion

Selection of the appropriate oxidative stress inducer and antioxidant concentrations

The goal was to study adipogenic differentiation under these conditions of oxidative stress. There are numerous ROS and intermediate molecules that are involved in oxidative stress, which interconvert through the help of enzymes, cytokines, metals, and thiols (61-65). The various molecules and ROS involved in the different signaling pathways add to the difficulty in determining which ROS are involved in oxidative stress. Hydrogen peroxide has been implicated in a large proportion of oxidative stress. It can readily diffuse through cell membranes and thus has far-reaching effects, establishing its function as a signaling molecule (66).

Exogenously administered H_2O_2 activates kinase enzymes and inactivates phosphatase enzymes (67). The extracellular signal-regulated kinase (ERK1/2) and p38 mitogen-activated protein kinase (MAPK) pathways, both ERK1/2 and p38 MAPK, as their names suggest, are kinases. The pathways are activated by growth factors and angiotensin II with H_2O_2 as the messenger (68). Adipogenesis is mainly regulated by the transcription factors: CCAAT/enhancer-binding proteins (C/EBPs), specifically C/EBPα, C/EBPβ, and C/EBPδ; and peroxisome proliferator-activated receptor (PPAR)-γ (69). Upon the addition of adipogenic medium, in the early phase of differentiation, there is the induction of C/EBPβ and C/EBPδ. These factors then induce the expression of C/EBPα and PPARγ which together promote the terminal phase of adipogenesis (70, 71).

Studies at the Boston University School of Medicine demonstrated that mitogen/extracellular signal-regulated kinase (MEK)/ERK signaling and C/EBPβ regulate the expression of PPARγ (72). The early proliferative stage, also known as mitotic clonal expansion of adipogenesis is initiated by stimuli such as insulin. Insulin is also known to activate the ERK pathway thus demonstrating a role for the ERK pathway during early adipogenesis (73). Engelman and colleagues demonstrated that treatment of 3T3-L1 fibroblasts with p38 MAPK inhibitors prevented their differentiation into adipocytes (74). It has been demonstrated that H_2O_2 regulates insulin stimulation and plays a role in insulin signal transduction. It was also observed that insulin stimulated H_2O_2 generation through Nox4 (75, 76).

The stimulation of cells by cytokines such as transforming growth factor (TGF)-β1 (77), TNF-α and IL-1 (78) resulted in the production of ROS and once again confirmed the role of ROS, particularly H_2O_2, as signaling messengers. Schreck and colleagues and a few years later Schmidt and colleagues reported that H_2O_2 acted as a messenger and activated nuclear factor κβ (NF-κβ) (79, 80). Berg and colleagues found that NF-κβ subunits were upregulated during adipocyte differentiation (81). The overwhelming evidence implicating H_2O_2 in multiple signaling cascades led to the choice of H_2O_2 as the appropriate ROS for this study.

Upon 100% confluence, preadipocytes enter a growth-arrested state which is important for differentiation (82). Addition of the adipogenic induction cocktail causes the cells to re-enter the cell cycle and undergo mitotic clonal expansion (83, 84). The DNA replication opens up the DNA at reporter and enhancer elements for transcription factors involved in differentiation. The mitotic clonal expansion phase involves C/EBPβ and C/EBPδ. The transcription factors C/EBPα and PPARγ terminate mitotic clonal expansion (85). An expanding amount of literature has focused on the effect of the addition of H_2O_2 concentrations to mammalian cells. Lower concentrations of 10^{-8} M to 10^{-6} M of H_2O_2 stimulated the growth of mammalian cells (86-88). Davies and colleagues found that 3 μM to 15 μM of H_2O_2 also caused this stimulatory mitogenic effect (89). Lee and colleagues observed that growth-arrested 3T3-L1 preadipocytes that were treated with 50 μM or 100 μM of H_2O_2 in conjunction with hormonal stimulation had accelerated cell cycle progression from the S (DNA replication) phase to G_2/M (cell dividing) phase and enhanced adipogenesis (90). However, Weise *et al*. found that 100 μM of H_2O_2 resulted in temporary growth arrest in mammalian fibroblast cells (91). Greater concentrations ranging between 120 to 150 μM of H_2O_2 also caused a temporary growth arrest according to Davies and colleagues. A concentration of 500 μM and greater induced apoptotic cell death (89). Miard and colleagues found that the addition of 20 μM of H_2O_2 to the 3T3-L1 preadipocyte cell line mimicked age-related oxidative stress and increased lipid accumulation (54).

To determine the concentrations of the pro-oxidant and antioxidants to use, cell viability was evaluated. Tetrazolium salt, MTT, reduction with increasing concentrations of H_2O_2 from 0 to 200 μM was examined every 24 hours over a period of 120 hours. MTT reduction has been extensively used for the quantitative assessment of cellular viability. The tetrazolium salt, MTT, is cleaved by mitochondrial succinate-dehydrogenase enzyme (in live mitochondria)

into formazan, which is blue in colour (92). This conversion to the formazan product can thus only take place in live cells and is proportional to the number of live cells. The standard growth medium that is used in the MRC Extramural Unit for Stem Cell Research and Therapy is α-MEM and is considered the optimal medium for the expansion of MSCs (52). The medium base used to induce the ASCs to differentiate into adipocytes is DMEM. DMEM is still nutrient-rich, but has fewer amino acids and vitamins than α-MEM (see Appendix C for comparison). Exposure of ASCs grown in standard complete growth medium, α-MEM, or the basis of the differentiation medium, DMEM, to the H_2O_2 concentrations did not significantly affect ASCs viability and resulted in less cell death than expected for the higher concentrations of H_2O_2. The entire H_2O_2 concentration range gave less than 50% reduction in formazan product for the ASCs grown in α-MEM and DMEM. Thus a half maximal inhibitory concentration (IC_{50}) value could not be established.

Variability in cellular effects with H_2O_2 concentrations and failure to cause cell damage at certain concentrations of H_2O_2 have been observed (93). It was surmised that the loss of H_2O_2 through scavenging by pyruvate might be accountable for these findings. It is known that pyruvate acts as an antioxidant and scavenges H_2O_2 (94, 95). It is formulated into most media, but this is often not taken into account in most of the literature using exogenously added H_2O_2 (96). Pyruvate can be transported into cells and exerts intracellular protection that is not compartmentalized such as in the case of catalase. Hence the choice of medium formulated + or – pyruvate has an influence on the results when assessing the cytotoxicity of oxidants. This leads to many researchers using higher concentrations of H_2O_2. Once DMEM – pyruvate was introduced a decrease in viability that was expected by increasing H_2O_2 concentrations was observed and an IC_{50} value was generated. The results that were obtained confirmed that the amount of H_2O_2 that was added was scavenged in the medium + pyruvate. Growing the cells in medium – pyruvate assessed the true effect of H_2O_2 on the viability ASCs. A concentration of 20 μM of H_2O_2 and a higher concentration of 100 μM of H_2O_2 (Figure 4.4) were chosen for the investigation of the effect of oxidative stress on adipogenic differentiation. The literature and an IC_{50} value of 21.91 μM H_2O_2 over the 120 hours aided in the choice of using 20 μM H_2O_2 for further experiments.

Naturally occurring antioxidant enzymes like SOD, catalase, and glutathione peroxidase (GPx) amongst others remove ROS. Rhee states that the controlled removal of second

messengers is an important feature of signal transduction (66). Trolox is a cell-permeable, water-soluble derivative of α-tocopherol, a member of the vitamin E group. Trolox is advantageous over α-tocopherol in that it can be incorporated into both the hydrophilic and lipophilic compartments of a cell. Lee and colleagues demonstrated that Trolox inhibited H_2O_2-induced activation of the ERK pathway (97). Protein kinase C (PKC) is involved in signal transduction involving cell growth and differentiation. The vitamin E α-tocopherol was found to inhibit PKC. This same vitamin E compound inhibited NF-κβ activity (98, 99). Trolox is commonly used as a standard or positive control and is a potent antioxidant and was thus an easy choice as an antioxidant.

Coenzyme Q, originally known as ubiquinone, is a compound with similar properties to vitamins. In humans the CoQ found in the body contains 10 isoprene units in the side chain, hence it is called CoQ10. Coenzyme Q10 is not considered a vitamin because the body synthesizes it and it is found in all cellular membranes, but it is said to be absorbed similarly to vitamin E (100). Upon a literature search of the effect of Coenzyme Q10 on the adipogenic differentiation of ASCs, no results were found, however if the word "ASC" was changed to "MSC", still no specific adipogenesis-related results were obtained, but results pertaining to viability and apoptosis were obtained (101). The reduced form of CoQ10, known as ubiquinol ($CoQH_2$), is an effective antioxidant (102) and is capable of regenerating tocopherol (103).

In a cell-free system CoQ10 was found to have no antioxidant potential compared to Trolox; however, in a cell culture system CoQ10 did display antioxidant activity (104). There is evidence presented by Carmona *et al*. that Coenzyme Q prevents rosiglitazone-induced adipogenesis in obese mice (105). A concentration of 10 μM CoQ10 rescued adipocytes from stress-induced apoptotic death (106). The essential role of CoQ10 in mitochondrial function and against oxidative stress makes it an important antioxidant, however there is a limitation. It has poor solubility in aqueous media. Bergamini and colleagues observed that treatment with CoQ10 concentrations ranging from 10 nM to 10 μM did not alter cell viability, but more importantly, a concentration of 10 μM was sufficient to significantly increase the amount of cellular CoQ10 (56). The interaction between mitochondria, oxidative stress and the role of CoQ10 in these pathways, as well as the reported changes in antioxidant capacity in WAT

during obesity (107), led to our investigation into the effect of the antioxidant CoQ10 on the adipogenic differentiation potential of ASCs.

Phenolic compounds and antioxidants are said to interfere with the MTT reaction and reduce the tetrazolium used in the MTT assay to formazan without having any direct affects on viability (108). Both Trolox and Coenzyme Q10 are phenolic derivatives and thus the SRB assay was chosen as a cell viability assay. The MTT assay is a widely used viability assay, however, it relies on the cell's ability to metabolize formazan (109). It is also said to have poor linearity with cell number, especially when cell numbers are low, and is influenced by environmental conditions (110). Keepers and colleagues reiterated that the SRB assay provided greater sensitivity and better linearity with regard to cell numbers (111). The OD obtained using the SRB assay is directly proportional to the cell number. Vichai and Kirtikara claimed that the SRB assay was more sensitive than the MTT assay and had a higher reproducibility (47). The adherent monolayer of cells was prone to lifting off the plastic surface of the dish during the process of the MTT assay due to the multiple washing steps. However, the SRB involves a fixation step and less cell loss was observed. The SRB assay appeared to produce more linear results but the general trend for both the MTT and SRB assays was comparable.

The ASC viability results were displayed as percentages of the control. Results were also compared relative to Day 0 of the particular viability experiment. The same trend was observed under the same conditions relative to either the control or Day 0. The different media were observed to have no differing effects on ASC viability. Sotiropoulou and colleagues found that α-MEM was the optimal medium for the isolation, adherence and expansion of MSCs, having the highest final number of MSCs at passage 3. Dulbecco's minimal Eagle's medium + pyruvate was also conducive to MSC expansion (52). All three media including, DMEM – pyruvate, were favourable for ASC growth.

Effects of co-supplementation of oxidative stress inducer and antioxidants on ASC viability

The individual and combined effects of the oxidative inducer and antioxidants were assessed on ASC viability. The vehicle controls, dH_2O and EtOH, had no significant effects on ASC viability. Exposure of ASCs to 100 μM H_2O_2 for 24 hours resulted in a 2.4-fold significant

decrease compared to the DMEM – pyruvate control. Trolox co-supplementation partially, but not significantly, increased cell survival at a concentration of 10 μM. Coenzyme Q10 also partially, but not significantly, increased cell survival at a concentration of 10 μM (Figure 4.7). It must also be taken into account that ROS production and antioxidant turnover occurs continuously in all cells. Thus, the concentration of pro-oxidants and antioxidants will vary with cell density and with time. The actual concentrations may therefore fluctuate at any given time. The cells were all seeded at the same density, but any variation in the data that was generated is likely to reflect the fact that ASCs consist of a heterogeneous population of cells. The individual cells within this population can exhibit variable proliferation capacity and proliferation time, and variable phenotypes, as well as differing consequences regarding exposure to pro-oxidants and antioxidants. Coenzyme Q10 is a participant in the mitochondrial electron transport chain and can act as both an antioxidant and pro-oxidant (112). Coenzyme Q10 could potentially have varying effects on cell viability due to its pro-oxidant ability. Although the antioxidants did not restore cell viability to the same level as the DMEM – pyruvate, they did not decrease cell viability further. Future research should further investigate the mechanism involved.

Intracellular ROS levels in adipose tissue-derived stromal cells

The main ROS produced by the mitochondrial electron transport chain is O_2^- (113). MitoSOX™ red selectively detects O_2^- in the mitochondria of live cells (114). The phosphonium group in MitoSOX™ red is responsible for targeting the MitoSOX™ red to the mitochondria. Upon oxidation, MitoSOX™ red exhibits fluorescence, which was detected via flow cytometry. The antioxidant effects of pyruvate on intracellular mitochondrial ROS were examined by monitoring MitoSOX™ red fluorescence. In addition, to the effects of pyruvate on intracellular ROS, the effects of the pro-oxidants, H_2O_2 and tBHP, and the ROS scavenger, MnTBAP were assessed. It was observed that the level of intracellular ROS increased 1.5-fold after treatment in DMEM – pyruvate with 100 μM H_2O_2, and increased 3-fold after treatment in DMEM – pyruvate with tBHP. This increase in ROS was inhibited by pyruvate. Thus, the ROS scavenging effects of pyruvate were confirmed (96). To date there have been a few studies that have used MitoSOX™ red to detect intracellular ROS within MSCs or ASCs (115-118). Pietilä and colleagues used MitoSOX™ red to detect intracellular O_2^- in human umbilical cord blood- and human bone marrow-derived MSC lines (118).

There are a large number of ROS regulated pathways and ROS targets. Exogenous ROS can influence the production of ROS initiating a self-promoting cycle, either by the production of ROS through Nox or the expression of genes involved in signaling pathways. The outcome of these activated pathways may in turn result in increased ROS. The MAPK pathway is one such pathway that is influenced by ROS (119). This pathway consists of three subfamilies, the ERK, p38 MAPK and c-Jun amino(N)-terminal kinases (JNK) (120). Hydrogen peroxide induced a strong activation of ERKs, JNKs and p38 MAPK in a time- and dose-dependent manner. These MAPKs have overlapping and sometimes contradictory effects on adipogenesis (73). Each successive step of adipogenesis can be modulated by MAPKs. Mitogen activated protein kinases phosphorylate specific serine and threonine residues of target proteins and the pathways consist of a canonical cascade composed of three activated kinases. Mitogen activated protein kinase (MAPK) kinase kinases (MKKK or MAP3K) phosphorylate and induce the activation of specific MAPK kinases (MKK or MAP2K). Mitogen activated protein kinase kinases then phosphorylate MAPKs (120).

Sano and colleagues demonstrated that ROS and angiotensin II induced the activation of MAPK pathways (121). Activation of the p38 MAPK and ERK pathway resulted in the generation of IL-6. Interleukin-6 levels were significantly increased in obese subjects (122). Interleukin-6 is an inflammatory mediator and along with IL-β1 and TNF-α results in increased production of ROS. A decrease in IL-6 was correlated with a decrease in TNF-α and a reduction in weight gain in Zucker rats (123). Engelman *et al*. demonstrated that p38 MAPK was necessary for the differentiation of 3T3-L1 fibroblasts into adipocytes (74). Hirosumi and colleagues showed that the absence of JNK1 resulted in decreased adiposity and JNK was elevated in obese mice (124). Phosphorylation of C/EBPβ by ERK stimulated C/EBPβ-dependent gene expression (125). Mice deficient in ERK1 had decreased adiposity and fewer adipocytes than wild-type mice (126).

Angiotensin II not only activates MAPK pathways but also activates Nox (discussed in the introduction) to generate intracellular ROS (121). NADPH oxidase 4 contributes to the down regulation of pref-1. It is proposed to do this by interfering with pathways controlling pref-1 expression such as the ERK pathway (127). Elevated oxidative stress in accumulated fat is related to obesity-associated metabolic syndrome in humans and mice (24). ROS production by mitochondria can be triggered from ROS generated by the Nox enzyme. The exogenous

addition of H_2O_2 to vascular cells stimulated Nox, resulting in O_2^- production. This O_2^- was converted to H_2O_2. The H_2O_2 that was produced can further stimulate O_2^- production from Nox (128). Hawkins and colleagues demonstrated that the activation of Nox produces extracellular O_2^-. The extracellular O_2^- produced was transported intracellularly through a chloride channel (CIC)-3. This causes a rapid release of Ca^{2+} followed by the mitochondrial production of O_2^- (129).

In addition to answering the first research question of "how can we measure ROS in MSC cultures?" and to elucidate whether augmentation of extracellular oxidative stress may cause enhanced intracellular ROS, the scavenging effect of pyruvate was also confirmed using MitoSOX™ red. This reiterates the importance of noting the presence of pyruvate in cell culture medium when undertaking ROS cellular studies. On this note, however, it must not be forgotten that pyruvate is an important molecule for cell culture. Cells grown without exogenous pyruvate may fail to thrive due to excessive oxidative stress according to O'Donnell-Tormey and colleagues (96). Pyruvate is important in glycolysis where glucose is oxidized to carbon dioxide (CO_2), and reduced nicotinamide adenine dinucleotide (NAD^+), NADH, is produced. The NADH drives oxidative phosphorylation and adenosine triphosphate (ATP) production. Pyruvate is also the starting molecule of the Krebs Cycle. During anaerobic respiration pyruvate is reduced, producing NAD^+. Collectively, these results confirm that pyruvate acts as a scavenger of exogenous ROS and that exogenously added ROS increase intracellular ROS, providing the means for oxidative stress-related signaling responses.

Effect of an oxidative stress inducer and antioxidant on the differentiation potential of ASCs

Having confirmed that H_2O_2 increased intracellular ROS, the effect of exogenously added ROS on the ASC adipogenesis was investigated. This was to answer the second research question and the *raison d'etre* of this study.

The main function of the adipocyte is energy storage, but our understanding of the functions of adipose tissue has expanded and it is now known to act as an endocrine organ (130). The current knowledge of adipocyte differentiation derives largely from studies using preadipocyte cell lines *in vitro*. However, ASCs provide a useful human primary cell model for adipogenesis due to their ability to differentiate down the adipocyte lineage. The intracellular

lipid droplets that form and accumulate during adipogenic differentiation can be detected using the fluorescent dye, Nile red (22). The International Federation for Adipose Therapeutics and Science (IFATS) and the International Society for Cellular Therapy (ISCT) jointly recommend using either Oil red O or Nile red as histological determinants of adipogenic differentiation (45). Popularity in using Nile red, as a lipophilic fluorescence microscopy stain, has increased. Nile red is known as a solvatochromatic dye, meaning that it can change colour due to a change in polarity (131). Specifically its excitation and emission maxima can shift from yellow-gold to deep red depending on the lipid environment, which is related to lipid composition. Upon dissolving in a hydrophobic lipid environment, such as neutral lipid triglycerides, Nile red fluoresces yellow-gold and can be examined at emission wavelengths of > 528 nm. Nile red can also interact with an amphipathic lipid environment, such as phospholipids. The fluorescence of Nile red dissolved in phospholipid-rich regions can be detected in the deep-red spectrum at wavelengths > 590 nm (22). Due to this feature Nile red can be observed through both green (GFP) and red (Texas red) channels of the fluorescent microscope.

At day 21 of adipogenic induction, non-induced and induced ASCs were stained with Nile red and the nucleus-staining dye, DAPI, and were observed using fluorescence microscopy. In particular, the composition of lipid droplets infers an advantage in the use of Nile red in adipogenic differentiation. A lipid droplet is composed of a neutral lipid core surrounded by an amphipathic coat (15). Nile red accumulates in lipid vesicles and does not harm the ASCs. It was observed that following staining of the adipocytes with Nile red there was diffuse staining of the entire cell upon examination of the deep-red fluorescence in the Texas red channel. Observation of the stained cells through the green channel demonstrated bright fluorescence. Images in the green and red channels as well as the images of the nuclei in the blue DAPI channel were overlaid (Figure 4.11). It was observed that the merged images allowed for more discernibility regarding the intracellular lipid droplets.

The DAPI and Nile red-stained non-induced cultured ASCs exhibited a central nucleus, small discrete lipid bodies distributed throughout the cytoplasm, and a fusiform structure. Small cytosolic lipid droplets can occur in the majority of cell types and are often associated with the ER, mitochondria and peroxisomes (15, 132). Lipid droplets can range in diameter from 10 nm to a massive 200 μm (15, 23). Contact inhibition may also lead to lipid biogenesis (133). Fetal bovine serum is rich in lipid content and cells may accumulate lipid droplets

through the uptake of cholesterol provided by lipoproteins within the FBS or serum in the medium (134). Accumulation of lipid droplets was visible in a mouse macrophage-like cell line upon the addition of a DMEM with 10% FBS. An increase in lipid accumulation was also observed when 40% FBS was added compared to 10% FBS (135).

Staining the adipogenic-induced ASCs with Nile red confirmed that the cells had differentiated down the adipogenic lineage. The differentiated cells at 21 days contained numerous fluorescent spherical lipid droplets of varying sizes. The lipid droplets accumulated and increased in size, filling the entire cytoplasm of the cell, as differentiation progressed. In white adipocytes there are usually only a few lipid droplets, of ≥10 μm in diameter observed per cell, with some WAT mature adipocytes attaining a single lipid droplet of 100 μm in diameter (136, 137). There were no images of adipogenic-differentiated ASCs or MSCs containing a large unilocular lipid droplet in the available literature (53, 138). Mature adipocytes containing a large unilocular lipid droplet appeared to be observed only in freshly isolated adipose tissue (139, 140). All of the differentiated cells in the culture contained lipid droplets; however, the adipogenic differentiation of ASCs also failed to result in mature adipocytes that contained large unilocular lipid droplets. This may be due to their loss during culturing. Adipocytes are rather fragile and prone to bursting because the presence of lipid droplets affects the strength and fluidity of the cell membrane. It was thought that the buoyancy of mature adipocytes also influenced the loss of more mature adipocytes during culturing (141). Another reason may be that we are differentiating our cells into beige adipose tissue, which are found within WAT but are formed mainly through *de novo* differentiation (142) and contain multiple lipid droplets (143).

It was difficult to determine the degree of adipogenic differentiation visually concerning differentiated ASCs grown under adipogenic medium conditions containing DMEM + pyruvate, DMEM – pyruvate, and DMEM – pyruvate with the addition of 20 μM H_2O_2. This indicated the need for a more quantitative method for measuring adipogenesis. The aim of this study was to quantitatively analyze the results and the drawback with microscopy in this context is that it is a qualitative technique. Counting the differentiated cells manually is a subjective technique, where a limited number of cells are observed simultaneously, and it is a tedious technique prone to human error. An interesting observation by Dixit and Cyr, and noted by Mukhopadhyay is that exposure of cells to fluorescent probes and fluorescence microscopy could increase ROS generation (114, 144). Lee *et al*. have mooted flow

cytometry as a greater analytical tool to monitor the effects of chemicals on adipogenesis over other lipid detection systems, such as lipid staining and extraction (145). Flow cytometry allows for rapid, quantitative measurements related to cellular morphology. The advantage of using Nile red is that it is a well-established stain that allows for this quantification of adipocytes by flow cytometry following adipogenic differentiation of ASCs.

Flow cytometric analysis of the differentiation potential of ASCs at day 14 of adipogenic induction

In the standard assays for adipogenic differentiation of MSCs/ASCs, the stromal cells are pre-cultured up to confluences ranging from 70% to 100% in complete α-MEM before exposure to adipogenic medium (48, 146-148). The majority of studies, as well as the one described herein, pre-cultured the ASCs until 100% confluence because cell-cell contact upon confluence is said to be associated with withdrawal from the cell cycle and irreversible commitment to adipocyte differentiation requires cell cycle arrest (149, 150). At this point ASCs were exposed to adipogenic medium with the various pro-oxidant and antioxidant conditions and cultured for an additional 14 or 21 days.

All of the cultures induced to differentiate under the different conditions underwent adipogenesis to some extent compared to their non-induced counterparts. However, following adipogenic induction, ASCs responded with varying adipocyte conversion rate and lipid accumulation. Lee and colleagues have mentioned variability in adipocyte differentiation and other research groups have also previously observed variability. Even clonal cells, such as MA-10 tumour cells, show variable lipid droplet size and number (151). This can complicate analyses (6, 145).

At day 14 of adipogenic induction, Nile red and DAPI staining were used to quantify lipid accumulation flow cytometrically. Increase in yellow-gold (FL2) fluorescence, upon lipid staining with Nile red, and lipid droplet composition were employed to demonstrate adipogenic differentiation of the ASCs. Smyth and Wharton used the ability of Nile red to accumulate within lipid droplets (22) and the yellow-gold fluorescence to quantify the accumulation of cytoplasmic triglyceride in individual A31T6 proadipocytes undergoing differentiation into adipocytes (152). Increase in cytoplasmic complexity has also been used to indicate lipid storage within cells (145).

Given the speculative role that the adipose niche plays in adipose tissue formation, it is of no surprise that these cells, when cultured in the right environment such as adipogenic-inducing medium, will develop lipid droplets and express adipogenic-relevant genes. However, little is known about how an environment of ROS or oxidative stress influences adipogenic differentiation of ASCs. It has been shown that oxidative damage accumulates within MSCs during *in vitro* expansion and that antioxidant capacity decreases in aged donors (153, 154). Growing evidence suggests a role of ROS production in adipogenic differentiation. Lee and colleagues reported on ROS production using the murine preadipocyte line, 3T3-L1 cells (90). Kanda and colleagues found a significant decrease in lipid accumulation upon silencing Nox4 in 10T1/2 cells (42). The limitation with many of these studies is that lipid droplet accumulation and thus adipogenic differentiation is analyzed via histological Oil Red O staining which is not a quantitative measure. A second limitation is that the cells are usually only exposed to H_2O_2 for a few hours. Chronic or prolonged inflammation and oxidative stress is associated with obesity and metabolic diseases. In our studies, the cultured ASCs were subjected to prolonged treatment with ROS and antioxidants under adipogenic induction conditions compared to only hours of treatment. Adipogenic differentiation conventionally takes place over an extended period of time of either 14 days (5, 155) or 21 days (156, 157).

If we look at just the yellow-gold fluorescence results, the addition of the standard adipogenic cocktail to the ASCs for 14 days resulted in cells containing lipid droplets. The removal of the antioxidant, pyruvate, or the addition of the pro-oxidant, H_2O_2, over the 14 days of adipogenic induction, resulted in a significant increase in the proportion of differentiated cells associated with a greater neutral lipid content. The trend that more yellow-gold fluorescence was observed without pyruvate and the addition of H_2O_2, demonstrates the role that ROS could play in adipogenesis, and the ROS scavenging effect of pyruvate. To reiterate what was said previously, obesity is said to be associated with disorders that affect mitochondrial metabolism; this favours ROS production and thus the development of oxidative stress (24). Intracellular ROS production, particularly O_2^-, was reported to increase during adipogenesis of OP9 preadipocytes (158). Adipocyte differentiation appeared to be promoted in a more oxidized environment according to Imhoff and colleagues (159). Results presented here, looking at mean yellow-gold fluorescence and the mean percentage of cells stained positive with Nile red, indicated the same trend, thus, provided evidence for an increase in lipid accumulation with an increase in ROS levels. The

addition of 10 μM of the ROS scavengers, Trolox and CoQ10, to the H_2O_2 treated adipogenic-induced ASCs decreased the percentage of adipogenic-induced ASCs emitting yellow-gold fluorescence. It was observed by Lechpammer *et al*. that the addition of the antioxidant, amifostine, reduced the expression of PPARγ to undetectable levels and decreased fat accumulation in both SOD knockout and the wild-type MSCs after adipogenic induction (160).

It was suggested that the ability to collect a wide range of fluorescence emission using Nile red provides a sensitive and general use lipid probe. The composition of a lipid droplet infers an advantage in the use of Nile red staining in adipogenic differentiation. A lipid droplet is composed of a neutral lipid core surrounded by an amphipathic coat (15). During preadipocyte maturation a larger number of amphipathic lipids are formed upon the merging of the lipid droplets and their increase in size. This causes an increase in deep red fluorescence (FL5 fluorescence). Sub-populations of increasing lipid content were defined according to their increase in yellow-gold as well as an increase in deep-red fluorescence (FL2–/FL5– < FL2+/FL5– < FL2++/FL5+). Xia *et al*. demonstrated directly that an accumulation of phospholipids during drug-induced phospholipidosis in leukocytes caused a greater red fluorescence intensity compared to yellow-gold fluorescence following Nile red staining and flow cytometry (161).

There appeared to be a decrease in non-differentiated cells with adipogenic induction medium and the addition of the various pro- and antioxidant conditions as expected. Under standard adipogenic conditions + pyruvate there was a significant increase in simultaneous yellow-gold and deep red fluorescence emissions demonstrating an increase in lipid accumulation. This indicates that the addition of standard adipogenic medium induces the accumulation of both neutral and amphipathic lipids in these cells.

It appeared that with an increase in ROS, either with the removal of pyruvate or the addition of H_2O_2 there was a slight trend towards an increase in the FL2+/FL5– sub-population, which is indicative of lipid droplets of smaller size. The removal of pyruvate also increased the percentage of cells situated in the FL2++/FL5+ sub-population. The variability in the percentage of differentiated cells compared to the MFI of each sub-population could possibly be explained by variability in the cellular hydrolysis of triglycerides and cholesteryl esters and the occurrence of changes in the lipid droplet composition. There are a few possible reasons

as to why we see a decrease in more mature adipocyte populations with the addition of ROS.

High concentrations of H_2O_2 have been shown to inactivate the glycolytic enzyme glyceraldehyde-3-phosphate dehydrogenase in mammalian cells (162). This enzyme is implicated in glycolysis, reducing dihydroxyacetone phosphate to L-glycerol phosphate, providing the glycerol backbone for the synthesis of new triacylglycerols and phospholipids. Dihydroxyacetone phosphate also plays a role in ether-lipid biosynthesis. This mechanism affects both neutral and amphipathic lipids. Another mechanism could be lipid peroxidation, which is the oxidative degradation of lipids.

Lipid peroxidation affects polyunsaturated fatty acids and literature states mainly those that occur in phospholipids. Mature adipocytes have greater amounts of phospholipids and thus fluoresce more in the deep-red spectrum. Thus lipid peroxidation could result in a shift in emission to yellow-gold fluorescence, however lipid peroxidation can affect any unsaturated fatty acids even those found in neutral lipids. However the reasoning here is that the phospholipid monolayer would be attacked first. The relative proportion between cholesterol esters and triglycerides also varies considerably in relation to nutritional and metabolic conditions.

Flow cytometric analysis of the differentiation potential of ASCs at day 21 of adipogenic induction

Adipogenic differentiation was also analysed at 21 days. There was a further increase in lipid content over the 21-day period with standard adipogenic induction medium, demonstrating that the ASCs efficiently differentiated into adipocytes. Once again as was observed with adipogenic differentiation at 14 days, ASCs responded with varying adipocyte conversion pace and lipid accumulation. Investigators usually observes around 50% to 60% adipogenic differentiation (138). Aldridge and colleagues observed between 25% and 100% Oil red O positivity between the adipogenic induction days 14 to 21 (141). Our standard cocktail appears to differentiate from between 10% to 60% of the stromal cells into adipocytes, which demonstrates that adipogenesis does take place, but either genetic variability has a huge influence on our results or the composition of the adipogenic medium could be improved. Possibly our cryopreservation technique could also have an influence on adipogenesis results. Le and Cheng attempted to determine the cause of heterogeneity

during adipogenic differentiation through single-cell profiling. They state that the cell-cell heterogeneity is dependent on insulin signaling cascade responses. They also discuss that increases in adipogenic gene expression do not result in lipid droplet formation (163). Rosen and Spiegelman remark that targeting adipose tissue and adipocyte biology has been thought of as a possible treatment for obesity (164). If the ASCs have variable adipogenic potential, the targeting compounds that potentially reduce or increase adipogenesis may also present variable results.

The implication of ROS in adipocyte differentiation was tested at 21 days of adipogenic induction. A significantly greater increase in adipogenesis was seen when pyruvate was removed from the adipogenic induction medium compared to the standard adipogenic induction medium + pyruvate. There was also a significant accumulation of lipid droplets within the human ASCs exposed to adipogenic medium – pyruvate from 14 days to 21 days. The removal of pyruvate reiterated its position as an antioxidant and thus less ROS was scavenged in its absence. Mitochondria represent the main intracellular source of ROS. The involvement of mitochondria in adipose tissue is of utmost importance. Wilson-Fritch and colleagues found a 20- to 30-fold increase in the concentration of various mitochondrial proteins during adipogenesis (165). McKay *et al*. identified that genes encoding for components of the mitochondrial respiratory chain played a role in lipid storage and that when the mitochondrial respiratory chain was inhibited lipid accumulation was reduced (166).

Indeed, similar to day 14 of adipogenic induction, pharmacological manipulation of intracellular ROS by the addition of exogenous H_2O_2 resulted in a significant increase in lipid accumulation compared to the standard adipogenic induction medium + pyruvate. There was also a significant increase in the accumulation of lipid droplets within the human ASCs exposed to adipogenic medium – pyruvate and treated with H_2O_2 from 14 days to 21 days. Hydrogen peroxide mimics the effect of insulin in stimulating the hexose monophosphate shunt activity, which is required in fatty acid synthesis and cholesterol synthesis (167). Hydrogen peroxide was found to stimulate glucose incorporation into glycogen in adipocytes, and was found to inhibit lipolysis (168, 169). The insulinomimetic effects of H_2O_2 are mediated by insulin receptor phosphorylation and tyrosine kinase activity (170). The activation of C/EBPβ DNA binding was favoured following treatment with H_2O_2 (90). Diallyl disulfide increases the production of intracellular H_2O_2 (171). The increase in H_2O_2 mediated

an increase the expression of genes involved in adipogenesis and lipogenesis, such a PPARγ, FAS (fatty acid synthase), which is involved in fatty acid synthesis, aP2 (adipocyte fatty acid binding protein), which is involved in fatty acid transport, and SREBP-1c (Sterol Regulatory Element-Binding Protein-1c) a transcription factor that regulates genes required for *de novo* lipogenesis. Diallyl disulfide was also found to decrease the expression of Pref-1 (172).

Surprisingly treatment with 20 μM H_2O_2 also resulted in accretion of lipid within the ASCs not induced to undergo adipogenic differentiation for 21 days. The study by Lechpammer *et al*. demonstrated that MSCs, from SOD knockout mice, acquired fat accumulation even though the cells were not induced with adipogenic induction medium (160). A number of studies have implicated oxidative stress in the accumulation of cholesterol and lipogenesis in a variety of cell types (173). Intracellular *de novo* lipogenesis is facilitated through the transcription factor SREBP-1c. The activation of protein kinase B (PKB), also known as Akt, appears to be necessary and adequate for the induction of SREBP-1c in the liver and resulting lipid accumulation (174). Researchers have demonstrated that PKB can be activated by H_2O_2 (175). The expression of the above-mentioned genes involved in adipogenesis and lipogenesis following the oxidative stress conditions of this study would need to be confirmed quantitatively on a molecular level using real-time (q)PCR. It is not known why the MFI for the non-induced ASCs cultured with H_2O_2 was not significantly increased compared to the other non-induced conditions. There was also an increase in the percentage of cells emitting yellow-gold fluorescence when pyruvate was removed over the 21 days compared to 14 days. Aldridge and colleagues found that Nile red fluorescence detection increased over 21 days even in low SS non-induced cells (141). Reporting Nile red results as MFI and the percentage of cells emitting yellow-gold fluorescence are both suitable. Debacq-Chainiaux and colleagues in a study unrelated to adipogenesis, state that MFI is suitable to use in the majority of research, but when a stressor has an effect on only a small number of cells within the cell population, the percentage of positive cells should be used instead (176).

In order to test whether the increase in ROS and increase in adipocyte differentiation of the adipogenic-induced ASCs – pyruvate treated with H_2O_2 could be attenuated following 21 days of culture, the ASCs induced under the same oxidative stress conditions were treated with the ROS scavenger Trolox. The addition of Trolox was able to significantly reduce the adipogenic differentiation induced by H_2O_2 addition to adipogenic induction medium – pyruvate treated ASCs. The addition of 10 μM of the antioxidant CoQ10 to the H_2O_2 treated

adipogenic-induced ASCs significantly decreased the percentage of adipogenic-induced ASCs that emitted yellow-gold fluorescence. The increase in MFI seen with the addition of H_2O_2 to adipogenic-induced ASCs was significantly suppressed with the addition of either Trolox or CoQ10. The increase in lipid accumulation seen with the addition of H_2O_2 to non-induced ASCs was also suppressed with the addition of either Trolox or CoQ10. Lack of statistical significance in the case of the non-induced ASCs treated with Trolox and CoQ10, may be due to the high levels of variance that were observed between the ASC cultures that were investigated. Variation between technical replicates was not substantial but variation between samples was great leading to large ranges for the box whisker plots. The large variation observed upon addition of antioxidants may be due to varying scavenging power. The possibility of changes in the concentration of H_2O_2 and the antioxidants due to the cells own mechanisms over time adds a complicating factor to the interpretation of the data and thus constant seeding density was important, however, once again it should be noted that this is a heterogeneous population of cells.

Previous studies found that by inhibiting the enzyme that catalyzes the attachment of the isoprenoid chain to the quinone ring to form CoQ, the quantity of CoQ was decreased, resulting in an associated increase in adipogenic differentiation (107). Higuchi and colleagues showed that using two different antioxidants, N-acetyl-L-cysteine or EUK-8, a catalytic mimetic of SOD and catalase, not only inhibited adipogenesis but also shrunk the lipid droplets. They suggested that reducing ROS, thus, not only suppressed adipogenic differentiation but also suppressed lipid accumulation within differentiating cells (55). The percentage of adipogenic-induced cells cultured with either CoQ10 or Trolox that simultaneously emitted yellow-gold and deep red fluorescence (FL2++/FL5+ sub-population) at day 21 was dramatically decreased. The shrinkage of lipid droplets and the presence of less amphipathic lipid, thus less deep red fluorescence, could explain the decrease seen in this population compared to the other adipogenic induced conditions. Kanda and colleagues found that N-acetyl-L-cysteine inhibited the induction of C/EBPβ, C/EBPα, and PPARγ in rat MSCs cultured with adipogenic differentiation-inducing agents. Real-time PCR will have to be employed to determine whether a decrease in the expression of these well-known adipocyte genes takes place under culture conditions with the ROS scavengers, Trolox or CoQ10.

The ASCs were also subjected to 100 μM H_2O_2 but the majority of cells did not survive this condition. It was originally suspected that these differentiated cells detached from the

surface of the plate and that the lack of results with 100 μM H_2O_2 could be due to the fact that the more intracellular lipid droplets there are, the more buoyant the cell is, possibly resulting in their loss during the washing steps. Adipocytes are rather fragile and prone to bursting because the presence of lipid droplets affects the strength and fluidity of the cell membrane. Chen and colleagues found no adverse effects with treatment of a H_2O_2 concentration range of between 50 and 300 μM for 2 hours and cell viability relative to untreated controls was unchanged after 24 hours (177). It may however be that 100 μM H_2O_2 was cytotoxic over the 14 and 21 day period and that lipid peroxidation and cellular damage resulted in apoptosis and cell loss. Kanda and colleagues demonstrate that increase in intracellular ROS mediates adipocyte differentiation but treating 10T1/2 cells with 100 μM H_2O_2 did not result in inducing lipid accumulation (42). They suggested that ROS is necessary but not sufficient in 10T1/2 cells. Thus, the effects may be a question of the dosage of the ROS.

Flow cytometry allows for the study of differentiated ASCs from a cell level, and simultaneously utilizing the parameters such as intensity of staining, cell size, granularity, and cell number (141). Nile red is a well established and appropriate dye for use in a study such as ours. An alternative neutral lipid fluorescent dye is BODIPY that has a maximum fluorescence emission range from 510 to 665 nm. The differentiation of ASCs down the adipogenic lineage has been proposed as a useful alternative model to study the process of fat accumulation. Perhaps the next step for improved *in vitro* adipogenesis in our laboratory would be to simulate the *in vivo* microenvironment by using a 3-dimensional scaffold or substrates that mimic the composition and constituency of adipose tissue, such as extracellular matrix cues. Young and colleagues found that culturing ASCs on gels that mimicked the natural stiffness of adipose tissue significantly upregulated adipogenic markers (178).

Effect of pre-conditioning with pro-oxidant on the differentiation potential of ASCs

Stromal cells are currently being tested for their potential use in cell and gene therapy for a number of debilitating diseases and genetic disorders in humans. The increasing number of clinical trials globally and accumulating evidence demonstrates that they are promising candidates in the clinical setting, particularly for cardiovascular disease (179-182). The

intrinsic properties of ASCs could be influenced by the components of the *in vivo* milieu, resulting in low viability and differentiation capacity during tissue repair. Immense progress has been made in optimizing transplantation conditions; however, impediment in survival of the stromal cells upon transplantation is still a concern. Pre-conditioning is proposed to be a promising strategy to promote stromal cell survival in harsh *in vivo* environments (183). Pre-conditioning is synonymous with the ability of cells to survive lethal insults due to activation of survival mechanisms by sub-lethal stimuli. Many researchers believe this is how stem cells within the body cope with changes in the microenvironment.

Multiple studies have endeavored to improve both stromal/stem cell survival and differentiation by pre-conditioning the cells during *in vitro* expansion for better transplantation results. Li and colleagues found that preconditioning MSCs with 20 μM H_2O_2 significantly protected the MSCs against apoptosis that was induced by 500 μM H_2O_2 (184). Pendergrass and colleagues preconditioned progenitor cells with 100 μM H_2O_2 for 2 days and this pre-conditioning restored cardiac function and improved neovascularization of the injured heart following transplantation (185). Thus, it was hypothesized that perhaps we could select for a sub-population within the cultured ASCs that would be more resistant to H_2O_2 and ROS by triggering upregulation of intracellular antioxidant mechanisms. Prompting the cells to adapt to an environment they would experience upon transplantation and possibly enhancing their survival and influencing their differentiation capacity.

Flow cytometric analysis of the differentiation potential of ASCs at day 14 of adipogenic induction

Pre-conditioning the cells with 20 μM H_2O_2 had no significant effect on adipogenic differentiation of the ASCs; however, the mean percentages of cells positive for Nile red fluorescence and MFIs were increased compared to conventional adipogenic induction medium, adipogenic induction medium – pyruvate and culturing the adipogenc-induced cells with 20 μM H_2O_2. The mean percentage of induced cells emitting simultaneous yellow-gold and deep red (FL2++/FL5+) fluorescence also increased with pre-treatment with 20 μM H_2O_2. The heterogeneity of the starting ASC populations for the adipogenic differentiation experiments rendered comparison of results between different cultures difficult. The heterogeneity between donor samples was particularly evident when the cultures were pre-treated with 20 μM of H_2O_2 for the 24-hour period. Pevsner-Fischer *et al*. reviewed the

heterogeneity observed in MSC populations and stated that some cells displayed multipotent differentiation capacity, whereas others were limited in this ability (186). The variability observed in cultures of stromal cells may represent the repertoire of different sub-populations that exist within the population. This was supported by a study that looked at the expression of genes by a single cell-derived colony of MSCs. The transcripts involved in different regulatory networks, such as, mesenchymal cell differentiation markers, wound repair and cell mobility were expressed, as well as, transcripts common to neuronal activities and immunity and defense markers (187). The A180313 culture appeared to be less affected by oxidative pre-conditioning of 20 μM H_2O_2, or antioxidant mechanisms were strongly activated in A180313 upon pre-conditioning with 20 μM H_2O_2, or this culture simply has a lesser potential to differentiate into adipocytes than the A220313 culture.

Data was obtained for adipogenic induction after the 14 day period following pre-conditioning with 100 μM H_2O_2 for 24 hours compared to the lack of results obtained with treatment of 100 μM H_2O_2 for the full 14 days. Pre-conditioning with 100 μM H_2O_2 appeared to protect the ASCs from lethal oxidative stress, significantly, compared to treatment with 100 μM H_2O_2 throughout the induction period of 14 days. It was demonstrated by Yu *et al*. that pre-conditioning with 100 μM H_2O_2 for 90 minutes could noticeably protect cells against apoptosis and later cytotoxicity (188). Boopathy and colleagues also investigated the effect of preconditioning MSCs with 100 μM H_2O_2, but for 7 days, on cardiac differentiation and concluded that oxidative stress may lead to improved adult stem cell-based therapies for cardiac repair and regeneration. Interestingly, the same conditions of 100 μM H_2O_2 for 7 days was not conducive towards adipogenesis. The ASCs that had undergone oxidative preconditioning with 100 μM H_2O_2 before being exposed to adipogenic induction medium – pyruvate for 14 days accumulated around the same amount of lipid as conventional adipogenic medium. Although pre-treatment with 100 μM H_2O_2 significantly increased the survival rate of the ASCs, pre-treatment with 100 μM H_2O_2 did not significantly increase lipid accumulation.

Flow cytometric analysis of the differentiation potential of ASCs at day 21 of adipogenic induction

Pre-conditioning the ASCs with 20 μM H_2O_2 before the addition of adipogenic differentiation medium for 21 days significantly decreased lipid accumulation. It was hypothesized that pre-

conditioning with a pro-oxidant may increase the expression of antioxidants within the ASCs. Calzadilla and colleagues showed that the activities of the antioxidant enzymes SOD and GPx were increased when intracellular ROS levels were increased during differentiation of 3T3-L1 cells (189). Perhaps protective mechanisms were activated with pre-conditioning with 20 μM H_2O_2, protecting the cells from ROS-induced increase in lipid accumulation. Pre-conditioning with 100 μM H_2O_2 followed by the addition of adipogenic differentiation medium for 21 days had the opposite effect and caused lipid accumulation in both the non-induced and induced ASCs. Perhaps the concentration of ROS was efficient enough to trigger the activation of signaling pathways of the adipogenic lineage. Passage numbers will need to be taken into account when trying to explain the differences observed. Increased number of biological replicates and gene expression studies may elucidate the mechanisms taking place due to these effects.

It is clear from this study that the ability of ASCs to adapt to oxidative stress, and the nature of those adaptive strategies, can have a crucial impact on cell fate. It is also clear that the concentration of ROS and culture period play a huge role between cell death and cell fate and the activation of different signaling pathways. The need for larger numbers of donor samples is apparent, but all the *in vitro* work presented above is the starting point in determining the physiological outcome of oxidative stress on adipogenesis *in vivo*.

Conclusion

Obesity and its comorbidities, including type II diabetes, have reached alarming levels both locally and abroad. This has led to an increase into the investigation of the biology of adipose tissue. The development of effective therapeutics for obesity has been hindered by gaps in our understanding of all the molecular mechanisms underlying adipogenesis. A detailed cell model of the process of adipogenesis is needed to identify key molecular targets for therapeutic development. In 1964, Rodbell treated adipose tissue with collagenase and found that the SVF, upon centrifugation, could be released from adipose tissue fragments (190). The turn of the millennium arrived with the characterization of ASCs from the SVF (5). Much remains to be understood about ASCs from a more physiological perspective, but improvement in the understanding of stromal cell biology, and evaluation of WAT expansion and differentiation is underway. Obesity and diabetes are metabolic disorders that are

induced by an increase in body fat, and are associated with oxidative and inflammatory stress. Inflammation is associated with the generation of ROS and the accumulation of ROS leads to oxidative stress. Investigations into adipocyte biology have revealed that adipogenesis is sensitive to redox changes. The interaction between mitochondria, oxidative stress and the role of antioxidants in these pathways, as well as the reported changes in antioxidant capacity in WAT during obesity, led to the aim of this study, namely to investigate the effect of oxidative stress on the adipogenic differentiation potential of ASCs. Exogenously added ROS induce the generation of intracellular ROS. However, whether this phenomenon participates in the adipogenic differentiation of ASCs has remained undecided thus far. To address this issue, the combined effects of pro-oxidants and antioxidants on ASC adipogenic differentiation were examined.

ASCs were induced to differentiate into adipocytes using an adipogenic-inducing cocktail with or without the antioxidant, pyruvate. The adipogenic-induced ASCs were treated with Trolox, CoQ10, H_2O_2 or a combination of both pro-oxidant and antioxidant for 14 and 21 days. Pre-conditioning with the pro-oxidant for 24 hours before the adipogenic induction period of 14 and 21 days was also examined. The effects on adipogenic differentiation were quantitatively assessed using flow cytometry and the emission profiles of Nile Red. It was demonstrated that the addition of exogenous ROS and thus intracellular ROS to adipogenic-induced ASCs enhanced adipose differentiation. It was also observed that H_2O_2 added to non-induced ASCs grown in medium – pyruvate caused substantial lipid accumulation. Scavengers, such as Trolox and CoQ10, attenuated the increase in ROS and thus a decrease in adipogenic differentiation was seen. Pre-conditioning with pro-oxidant could either increase or decrease adipogenic differentiation depending on the concentration of pro-oxidant. The study emphasizes the importance of redox metabolism in adipose tissue biology. Thus, in this context, any compounds which could reduce oxidative stress during adipogenesis are an interesting approach to protect overweight people from this metabolic disease of lifestyle and its comorbidities, mainly insulin resistance and type II diabetes.

Stromal/stem cells are being investigated world-wide for use in cell-based therapies and in a tissue regenerative capacity due to their differentiation capabilities, supposed immunomodulatory effects, and homing ability. Nevertheless, major obstacles to their therapeutic and clinical application, such as low proliferation and survival rates upon transplantation and exposure to *in vivo* oxidative conditions, remain. Park and colleagues

stated: that whether ROS is harmful or beneficial is primarily a question of dosage (191). The results of this study indicate that this statement is true. This study demonstrated that *in vitro* conditioning with ROS mediates adipocyte differentiation. This implicates a self-perpetuating system, which may contribute to the pathogenesis of obesity. Controlled generation of ROS is known to stimulate the proliferation, migration and regenerative potential of ASCs. However, too high concentrations of ROS result in apoptosis and cell death. It should be acknowledged that the improved adipogenic differentiation with oxidative treatment parallels the persisting uncertainties regarding the underlying redox mechanisms in differentiating pathways and the necessity for quantifying adipogenic and lipogenic gene expression by qPCR under these conditions.

The present study has several limitations, which include:

- Fresh and cryopreserved-thawed ASC samples were used and at different passages, due to the limited cell numbers that were obtained at each passage versus the cell numbers required for the different experiments.
- The donors' ages varied and BMI was unknown.
- Fluorescence microscopy photographs were not taken with all the various pro-oxidant and antioxidant conditions.
- More donor samples are required.
- Quantitative gene expression would confirm adipogenic differentiation versus lipogenesis.
- The ASCs in culture may behave differently from the ASCs *in vivo*. Cell culture also imposes a state of oxidative stress on cells.

Contrasting results due to the heterogeneity of the population of ASCs demonstrates the importance of using large donor sample populations. Future studies will incorporate both quantitative gene expression and more donor ASC cultures.

References

1. Rexrode KM, Manson JE, Hennekens CH. Obesity and cardiovascular disease. Current opinion in cardiology. 1996;11(5):490-5.
2. Fei W, Du X, Yang H. Seipin, adipogenesis and lipid droplets. Trends in endocrinology and metabolism: TEM. 2011;22(6):204-10.
3. Negrel R, Grimaldi P, Ailhaud G. Establishment of preadipocyte clonal line from epididymal fat pad of ob/ob mouse that responds to insulin and to lipolytic hormones. Proceedings of the National Academy of Sciences of the United States of America. 1978;75(12):6054-8.
4. Todaro GJ, Green H. Quantitative studies of the growth of mouse embryo cells in culture and their development into established lines. The Journal of cell biology. 1963;17:299-313.
5. Zuk PA, Zhu M, Mizuno H, Huang J, Futrell JW, Katz AJ, et al. Multilineage cells from human adipose tissue: implications for cell-based therapies. Tissue engineering. 2001;7(2):211-28.
6. Sen A, Lea-Currie YR, Sujkowska D, Franklin DM, Wilkison WO, Halvorsen YD, et al. Adipogenic potential of human adipose derived stromal cells from multiple donors is heterogeneous. Journal of cellular biochemistry. 2001;81(2):312-9.
7. Halvorsen YD, Franklin D, Bond AL, Hitt DC, Auchter C, Boskey AL, et al. Extracellular matrix mineralization and osteoblast gene expression by human adipose tissue-derived stromal cells. Tissue engineering. 2001;7(6):729-41.
8. Mizuno H, Zuk PA, Zhu M, Lorenz HP, Benhaim P, Hedrick MH. Myogenic differentiation by human processed lipoaspirate cells. Plastic and reconstructive surgery. 2002;109(1):199-209; discussion 10-1.
9. Erickson GR, Gimble JM, Franklin DM, Rice HE, Awad H, Guilak F. Chondrogenic potential of adipose tissue-derived stromal cells in vitro and in vivo. Biochemical and biophysical research communications. 2002;290(2):763-9.
10. Safford KM, Hicok KC, Safford SD, Halvorsen YD, Wilkison WO, Gimble JM, et al. Neurogenic differentiation of murine and human adipose-derived stromal cells. Biochemical and biophysical research communications. 2002;294(2):371-9.
11. Rosen ED, MacDougald OA. Adipocyte differentiation from the inside out. Nature reviews Molecular cell biology. 2006;7(12):885-96.
12. Gregoire FM, Smas CM, Sul HS. Understanding adipocyte differentiation. Physiological reviews. 1998;78(3):783-809.
13. Murphy S, Martin S, Parton RG. Lipid droplet-organelle interactions; sharing the fats. Biochimica et biophysica acta. 2009;1791(6):441-7.
14. Robenek H, Hofnagel O, Buers I, Robenek MJ, Troyer D, Severs NJ. Adipophilin-enriched domains in the ER membrane are sites of lipid droplet biogenesis. Journal of cell science. 2006;119(Pt 20):4215-24.
15. Murphy DJ. The biogenesis and functions of lipid bodies in animals, plants and microorganisms. Progress in lipid research. 2001;40(5):325-438.

16. Brown DA. Lipid droplets: proteins floating on a pool of fat. Current biology : CB. 2001;11(11):R446-9.
17. Martin S, Parton RG. Lipid droplets: a unified view of a dynamic organelle. Nature reviews Molecular cell biology. 2006;7(5):373-8.
18. Granneman JG, Moore HP. Location, location: protein trafficking and lipolysis in adipocytes. Trends in endocrinology and metabolism: TEM. 2008;19(1):3-9.
19. Fujimoto T, Ohsaki Y, Cheng J, Suzuki M, Shinohara Y. Lipid droplets: a classic organelle with new outfits. Histochemistry and cell biology. 2008;130(2):263-79.
20. Bostrom P, Rutberg M, Ericsson J, Holmdahl P, Andersson L, Frohman MA, et al. Cytosolic lipid droplets increase in size by microtubule-dependent complex formation. Arteriosclerosis, thrombosis, and vascular biology. 2005;25(9):1945-51.
21. Ramirez-Zacarias JL, Castro-Munozledo F, Kuri-Harcuch W. Quantitation of adipose conversion and triglycerides by staining intracytoplasmic lipids with Oil red O. Histochemistry. 1992;97(6):493-7.
22. Greenspan P, Mayer EP, Fowler SD. Nile red: a selective fluorescent stain for intracellular lipid droplets. The Journal of cell biology. 1985;100(3):965-73.
23. Guo Y, Cordes KR, Farese RV, Jr., Walther TC. Lipid droplets at a glance. Journal of cell science. 2009;122(Pt 6):749-52.
24. Furukawa S, Fujita T, Shimabukuro M, Iwaki M, Yamada Y, Nakajima Y, et al. Increased oxidative stress in obesity and its impact on metabolic syndrome. The Journal of clinical investigation. 2004;114(12):1752-61.
25. Griendling KK, FitzGerald GA. Oxidative stress and cardiovascular injury: Part I: basic mechanisms and in vivo monitoring of ROS. Circulation. 2003;108(16):1912-6.
26. Ceriello A, Motz E. Is oxidative stress the pathogenic mechanism underlying insulin resistance, diabetes, and cardiovascular disease? The common soil hypothesis revisited. Arteriosclerosis, thrombosis, and vascular biology. 2004;24(5):816-23.
27. Khandrika L, Kumar B, Koul S, Maroni P, Koul HK. Oxidative stress in prostate cancer. Cancer Lett. 2009;282(2):125-36.
28. Wellen KE, Hotamisligil GS. Inflammation, stress, and diabetes. The Journal of clinical investigation. 2005;115(5):1111-9.
29. Fonseca-Alaniz MH, Takada J, Alonso-Vale MI, Lima FB. Adipose tissue as an endocrine organ: from theory to practice. Jornal de pediatria. 2007;83(5 Suppl):S192-203.
30. Hotamisligil GS, Shargill NS, Spiegelman BM. Adipose expression of tumor necrosis factor-alpha: direct role in obesity-linked insulin resistance. Science. 1993;259(5091):87-91.
31. Tilg H, Moschen AR. Adipocytokines: mediators linking adipose tissue, inflammation and immunity. Nature reviews Immunology. 2006;6(10):772-83.
32. Bedard K, Krause KH. The NOX family of ROS-generating NADPH oxidases: physiology and pathophysiology. Physiological reviews. 2007;87(1):245-313.
33. Martyn KD, Frederick LM, von Loehneysen K, Dinauer MC, Knaus UG. Functional analysis of Nox4 reveals unique characteristics compared to other NADPH oxidases. Cellular signalling. 2006;18(1):69-82.

34. Fernandez-Sanchez A, Madrigal-Santillan E, Bautista M, Esquivel-Soto J, Morales-Gonzalez A, Esquivel-Chirino C, et al. Inflammation, oxidative stress, and obesity. International journal of molecular sciences. 2011;12(5):3117-32.
35. Hukshorn CJ, Lindeman JH, Toet KH, Saris WH, Eilers PH, Westerterp-Plantenga MS, et al. Leptin and the proinflammatory state associated with human obesity. The Journal of clinical endocrinology and metabolism. 2004;89(4):1773-8.
36. Bokarewa M, Nagaev I, Dahlberg L, Smith U, Tarkowski A. Resistin, an adipokine with potent proinflammatory properties. J Immunol. 2005;174(9):5789-95.
37. Chandel NS, Schumacker PT, Arch RH. Reactive oxygen species are downstream products of TRAF-mediated signal transduction. The Journal of biological chemistry. 2001;276(46):42728-36.
38. Ouchi N, Parker JL, Lugus JJ, Walsh K. Adipokines in inflammation and metabolic disease. Nature reviews Immunology. 2011;11(2):85-97.
39. Wallace DC. A mitochondrial paradigm of metabolic and degenerative diseases, aging, and cancer: a dawn for evolutionary medicine. Annu Rev Genet. 2005;39:359-407.
40. Anderson EK, Gutierrez DA, Hasty AH. Adipose tissue recruitment of leukocytes. Current opinion in lipidology. 2010;21(3):172-7.
41. Hamanaka RB, Chandel NS. Mitochondrial reactive oxygen species regulate cellular signaling and dictate biological outcomes. Trends in biochemical sciences. 2010;35(9):505-13.
42. Kanda Y, Hinata T, Kang SW, Watanabe Y. Reactive oxygen species mediate adipocyte differentiation in mesenchymal stem cells. Life sciences. 2011;89(7-8):250-8.
43. Tormos KV, Anso E, Hamanaka RB, Eisenbart J, Joseph J, Kalyanaraman B, et al. Mitochondrial complex III ROS regulate adipocyte differentiation. Cell metabolism. 2011;14(4):537-44.
44. Coleman SR. Structural fat grafting: more than a permanent filler. Plastic and reconstructive surgery. 2006;118(3 Suppl):108S-20S.
45. Bourin P, Bunnell BA, Casteilla L, Dominici M, Katz AJ, March KL, et al. Stromal cells from the adipose tissue-derived stromal vascular fraction and culture expanded adipose tissue-derived stromal/stem cells: a joint statement of the International Federation for Adipose Therapeutics and Science (IFATS) and the International Society for Cellular Therapy (ISCT). Cytotherapy. 2013;15(6):641-8.
46. Mosmann T. Rapid colorimetric assay for cellular growth and survival: application to proliferation and cytotoxicity assays. Journal of immunological methods. 1983;65(1-2):55-63.
47. Vichai V, Kirtikara K. Sulforhodamine B colorimetric assay for cytotoxicity screening. Nature protocols. 2006;1(3):1112-6.
48. Pittenger MF, Mackay AM, Beck SC, Jaiswal RK, Douglas R, Mosca JD, et al. Multilineage potential of adult human mesenchymal stem cells. Science. 1999;284(5411):143-7.

49. Williams IH, Polakis SE. Differentiation of 3T3-L1 fibroblasts to adipocytes. The effect of indomethacin, prostaglandin E1 and cyclic AMP on the process of differentiation. Biochemical and biophysical research communications. 1977;77(1):175-86.
50. Abràmoff MD, Magalhães PJ, Ram SJ. Image processing with ImageJ. Biophotonics international. 2004;11(7):36-42.
51. Chen HH, Decot V, Ouyang JP, Stoltz JF, Bensoussan D, de Isla NG. In vitro initial expansion of mesenchymal stem cells is influenced by the culture parameters used in the isolation process. Biomed Mater Eng. 2009;19(4-5):301-9.
52. Sotiropoulou PA, Perez SA, Salagianni M, Baxevanis CN, Papamichail M. Characterization of the optimal culture conditions for clinical scale production of human mesenchymal stem cells. Stem Cells. 2006;24(2):462-71.
53. Zuk PA, Zhu M, Ashjian P, De Ugarte DA, Huang JI, Mizuno H, et al. Human adipose tissue is a source of multipotent stem cells. Molecular biology of the cell. 2002;13(12):4279-95.
54. Miard S, Dombrowski L, Carter S, Boivin L, Picard F. Aging alters PPARgamma in rodent and human adipose tissue by modulating the balance in steroid receptor coactivator-1. Aging cell. 2009;8(4):449-59.
55. Higuchi M, Dusting GJ, Peshavariya H, Jiang F, Hsiao ST, Chan EC, et al. Differentiation of human adipose-derived stem cells into fat involves reactive oxygen species and Forkhead box O1 mediated upregulation of antioxidant enzymes. Stem cells and development. 2013;22(6):878-88.
56. Bergamini C, Moruzzi N, Sblendido A, Lenaz G, Fato R. A water soluble CoQ10 formulation improves intracellular distribution and promotes mitochondrial respiration in cultured cells. PloS one. 2012;7(3):e33712.
57. Miller NJ, Rice-Evans C, Davies MJ, Gopinathan V, Milner A. A novel method for measuring antioxidant capacity and its application to monitoring the antioxidant status in premature neonates. Clin Sci (Lond). 1993;84(4):407-12.
58. Brigelius-Flohe R, Traber MG. Vitamin E: function and metabolism. FASEB J. 1999;13(10):1145-55.
59. Alves H, Mentink A, Le B, van Blitterswijk CA, de Boer J. Effect of antioxidant supplementation on the total yield, oxidative stress levels, and multipotency of bone marrow-derived human mesenchymal stromal cells. Tissue engineering Part A. 2013;19(7-8):928-37.
60. Lim S, Dilley R, Dusting G. Cytoprotection and preconditioning for stem cell therapy. Advances in Regenerative Medicine InTech. 2011:89-118.
61. Boveris A, Oshino N, Chance B. The cellular production of hydrogen peroxide. The Biochemical journal. 1972;128(3):617-30.
62. Wientjes FB, Segal AW. NADPH oxidase and the respiratory burst. Seminars in cell biology. 1995;6(6):357-65.
63. Meier B, Radeke HH, Selle S, Younes M, Sies H, Resch K, et al. Human fibroblasts release reactive oxygen species in response to interleukin-1 or tumour necrosis factor-alpha. The Biochemical journal. 1989;263(2):539-45.
64. Stohs SJ, Bagchi D. Oxidative mechanisms in the toxicity of metal ions. Free radical biology & medicine. 1995;18(2):321-36.

65. Thannickal VJ, Fanburg BL. Reactive oxygen species in cell signaling. American journal of physiology Lung cellular and molecular physiology. 2000;279(6):L1005-28.
66. Rhee SG. Redox signaling: hydrogen peroxide as intracellular messenger. Experimental & molecular medicine. 1999;31(2):53-9.
67. Rhee SG, Bae YS, Lee SR, Kwon J. Hydrogen peroxide: a key messenger that modulates protein phosphorylation through cysteine oxidation. Science's STKE : signal transduction knowledge environment. 2000;2000(53):pe1.
68. Zafari AM, Ushio-Fukai M, Akers M, Yin Q, Shah A, Harrison DG, et al. Role of NADH/NADPH oxidase-derived H2O2 in angiotensin II-induced vascular hypertrophy. Hypertension. 1998;32(3):488-95.
69. Tang QQ, Lane MD. Adipogenesis: from stem cell to adipocyte. Annual review of biochemistry. 2012;81:715-36.
70. Rosen ED. The transcriptional basis of adipocyte development. Prostaglandins Leukot Essent Fatty Acids. 2005;73(1):31-4.
71. Yeh WC, Cao Z, Classon M, McKnight SL. Cascade regulation of terminal adipocyte differentiation by three members of the C/EBP family of leucine zipper proteins. Genes & development. 1995;9(2):168-81.
72. Farmer SR. Regulation of PPARgamma activity during adipogenesis. Int J Obes (Lond). 2005;29 Suppl 1:S13-6.
73. Bost F, Aouadi M, Caron L, Binetruy B. The role of MAPKs in adipocyte differentiation and obesity. Biochimie. 2005;87(1):51-6.
74. Engelman JA, Lisanti MP, Scherer PE. Specific inhibitors of p38 mitogen-activated protein kinase block 3T3-L1 adipogenesis. The Journal of biological chemistry. 1998;273(48):32111-20.
75. Mahadev K, Motoshima H, Wu X, Ruddy JM, Arnold RS, Cheng G, et al. The NAD(P)H oxidase homolog Nox4 modulates insulin-stimulated generation of H2O2 and plays an integral role in insulin signal transduction. Molecular and cellular biology. 2004;24(5):1844-54.
76. Krieger-Brauer HI, Kather H. Human fat cells possess a plasma membrane-bound H2O2-generating system that is activated by insulin via a mechanism bypassing the receptor kinase. The Journal of clinical investigation. 1992;89(3):1006-13.
77. Ohba M, Shibanuma M, Kuroki T, Nose K. Production of hydrogen peroxide by transforming growth factor-beta 1 and its involvement in induction of egr-1 in mouse osteoblastic cells. The Journal of cell biology. 1994;126(4):1079-88.
78. Lo YY, Wong JM, Cruz TF. Reactive oxygen species mediate cytokine activation of c-Jun NH2-terminal kinases. The Journal of biological chemistry. 1996;271(26):15703-7.
79. Schmidt KN, Amstad P, Cerutti P, Baeuerle PA. The roles of hydrogen peroxide and superoxide as messengers in the activation of transcription factor NF-kappa B. Chemistry & biology. 1995;2(1):13-22.
80. Schreck R, Rieber P, Baeuerle PA. Reactive oxygen intermediates as apparently widely used messengers in the activation of the NF-kappa B transcription factor and HIV-1. The EMBO journal. 1991;10(8):2247-58.

81. Berg AH, Lin Y, Lisanti MP, Scherer PE. Adipocyte differentiation induces dynamic changes in NF-kappaB expression and activity. American journal of physiology Endocrinology and metabolism. 2004;287(6):E1178-88.
82. Scott RE, Florine DL, Wille JJ, Jr., Yun K. Coupling of growth arrest and differentiation at a distinct state in the G1 phase of the cell cycle: GD. Proceedings of the National Academy of Sciences of the United States of America. 1982;79(3):845-9.
83. Cornelius P, MacDougald OA, Lane MD. Regulation of adipocyte development. Annu Rev Nutr. 1994;14:99-129.
84. Bernlohr DA, Bolanowski MA, Kelly TJ, Jr., Lane MD. Evidence for an increase in transcription of specific mRNAs during differentiation of 3T3-L1 preadipocytes. The Journal of biological chemistry. 1985;260(9):5563-7.
85. Patel YM, Lane MD. Mitotic clonal expansion during preadipocyte differentiation: calpain-mediated turnover of p27. The Journal of biological chemistry. 2000;275(23):17653-60.
86. Murrell GA, Francis MJ, Bromley L. Modulation of fibroblast proliferation by oxygen free radicals. The Biochemical journal. 1990;265(3):659-65.
87. Burdon RH, Gill V, Rice-Evans C. Cell proliferation and oxidative stress. Free radical research communications. 1989;7(3-6):149-59.
88. Le Belle JE, Orozco NM, Paucar AA, Saxe JP, Mottahedeh J, Pyle AD, et al. Proliferative neural stem cells have high endogenous ROS levels that regulate self-renewal and neurogenesis in a PI3K/Akt-dependant manner. Cell stem cell. 2011;8(1):59-71.
89. Davies KJ. The broad spectrum of responses to oxidants in proliferating cells: a new paradigm for oxidative stress. IUBMB life. 1999;48(1):41-7.
90. Lee H, Lee YJ, Choi H, Ko EH, Kim JW. Reactive oxygen species facilitate adipocyte differentiation by accelerating mitotic clonal expansion. The Journal of biological chemistry. 2009;284(16):10601-9.
91. Wiese AG, Pacifici RE, Davies KJ. Transient adaptation of oxidative stress in mammalian cells. Archives of biochemistry and biophysics. 1995;318(1):231-40.
92. Slater TF, Sawyer B, Straeuli U. Studies on Succinate-Tetrazolium Reductase Systems. Iii. Points of Coupling of Four Different Tetrazolium Salts. Biochimica et biophysica acta. 1963;77:383-93.
93. Giandomenico AR, Cerniglia GE, Biaglow JE, Stevens CW, Koch CJ. The importance of sodium pyruvate in assessing damage produced by hydrogen peroxide. Free radical biology & medicine. 1997;23(3):426-34.
94. Andrae U, Singh J, Ziegler-Skylakakis K. Pyruvate and related alpha-ketoacids protect mammalian cells in culture against hydrogen peroxide-induced cytotoxicity. Toxicology letters. 1985;28(2-3):93-8.
95. Nath KA, Enright H, Nutter L, Fischereder M, Zou JN, Hebbel RP. Effect of pyruvate on oxidant injury to isolated and cellular DNA. Kidney international. 1994;45(1):166-76.
96. O'Donnell-Tormey J, Nathan CF, Lanks K, DeBoer CJ, de la Harpe J. Secretion of pyruvate. An antioxidant defense of mammalian cells. The Journal of experimental medicine. 1987;165(2):500-14.

97. Lee WC, Choi CH, Cha SH, Oh HL, Kim YK. Role of ERK in hydrogen peroxide-induced cell death of human glioma cells. Neurochemical research. 2005;30(2):263-70.
98. van den Berg R, Haenen GR, van den Berg H, Bast A. Transcription factor NF-kappaB as a potential biomarker for oxidative stress. The British journal of nutrition. 2001;86 Suppl 1:S121-7.
99. Suzuki YJ, Packer L. Inhibition of NF-kappa B activation by vitamin E derivatives. Biochemical and biophysical research communications. 1993;193(1):277-83.
100. Turunen M, Olsson J, Dallner G. Metabolism and function of coenzyme Q. Biochimica et biophysica acta. 2004;1660(1-2):171-99.
101. Bucky LP, Percec I. The science of autologous fat grafting: views on current and future approaches to neoadipogenesis. Aesthetic surgery journal / the American Society for Aesthetic Plastic surgery. 2008;28(3):313-21; quiz 22-4.
102. Bentinger M, Brismar K, Dallner G. The antioxidant role of coenzyme Q. Mitochondrion. 2007;7 Suppl:S41-50.
103. Mukai K, Kikuchi S, Urano S. Stopped-flow kinetic study of the regeneration reaction of tocopheroxyl radical by reduced ubiquinone-10 in solution. Biochimica et biophysica acta. 1990;1035(1):77-82.
104. Choi BS, Song HS, Kim HR, Park TW, Kim TD, Cho BJ, et al. Effect of coenzyme Q10 on cutaneous healing in skin-incised mice. Arch Pharm Res. 2009;32(6):907-13.
105. Carmona MC, Lefebvre P, Lefebvre B, Galinier A, Benani A, Jeanson Y, et al. Coadministration of coenzyme Q prevents rosiglitazone-induced adipogenesis in ob/ob mice. Int J Obes (Lond). 2009;33(2):204-11.
106. Witort EJ, Pattarino J, Papucci L, Schiavone N, Donnini M, Lapucci A, et al. Autologous lipofilling: coenzyme Q10 can rescue adipocytes from stress-induced apoptotic death. Plastic and reconstructive surgery. 2007;119(4):1191-9.
107. Bour S, Carmona MC, Galinier A, Caspar-Bauguil S, Van Gaal L, Staels B, et al. Coenzyme Q as an antiadipogenic factor. Antioxidants & redox signaling. 2011;14(3):403-13.
108. Bruggisser R, von Daeniken K, Jundt G, Schaffner W, Tullberg-Reinert H. Interference of plant extracts, phytoestrogens and antioxidants with the MTT tetrazolium assay. Planta medica. 2002;68(5):445-8.
109. Denizot F, Lang R. Rapid colorimetric assay for cell growth and survival. Modifications to the tetrazolium dye procedure giving improved sensitivity and reliability. Journal of immunological methods. 1986;89(2):271-7.
110. Haselsberger K, Peterson DC, Thomas DG, Darling JL. Assay of anticancer drugs in tissue culture: comparison of a tetrazolium-based assay and a protein binding dye assay in short-term cultures derived from human malignant glioma. Anti-cancer drugs. 1996;7(3):331-8.
111. Keepers YP, Pizao PE, Peters GJ, van Ark-Otte J, Winograd B, Pinedo HM. Comparison of the sulforhodamine B protein and tetrazolium (MTT) assays for in vitro chemosensitivity testing. Eur J Cancer. 1991;27(7):897-900.
112. Linnane AW, Eastwood H. Cellular redox poise modulation; the role of coenzyme Q10, gene and metabolic regulation. Mitochondrion. 2004;4(5-6):779-89.

113. Turrens JF. Mitochondrial formation of reactive oxygen species. The Journal of physiology. 2003;552(Pt 2):335-44.
114. Mukhopadhyay P, Rajesh M, Hasko G, Hawkins BJ, Madesh M, Pacher P. Simultaneous detection of apoptosis and mitochondrial superoxide production in live cells by flow cytometry and confocal microscopy. Nature protocols. 2007;2(9):2295-301.
115. Hye Kim J, Gyu Park S, Kim WK, Song SU, Sung JH. Functional regulation of adipose-derived stem cells by PDGF-D. Stem Cells. 2015;33(2):542-56.
116. Hou J, Han ZP, Jing YY, Yang X, Zhang SS, Sun K, et al. Autophagy prevents irradiation injury and maintains stemness through decreasing ROS generation in mesenchymal stem cells. Cell Death Dis. 2013;4:e844.
117. Perez LM, Bernal A, de Lucas B, San Martin N, Mastrangelo A, Garcia A, et al. Altered metabolic and stemness capacity of adipose tissue-derived stem cells from obese mouse and human. PloS one. 2015;10(4):e0123397.
118. Pietila M, Palomaki S, Lehtonen S, Ritamo I, Valmu L, Nystedt J, et al. Mitochondrial function and energy metabolism in umbilical cord blood- and bone marrow-derived mesenchymal stem cells. Stem cells and development. 2012;21(4):575-88.
119. Son Y, Cheong YK, Kim NH, Chung HT, Kang DG, Pae HO. Mitogen-Activated Protein Kinases and Reactive Oxygen Species: How Can ROS Activate MAPK Pathways? J Signal Transduct. 2011;2011:792639.
120. Johnson GL, Lapadat R. Mitogen-activated protein kinase pathways mediated by ERK, JNK, and p38 protein kinases. Science. 2002;298(5600):1911-2.
121. Sano M, Fukuda K, Sato T, Kawaguchi H, Suematsu M, Matsuda S, et al. ERK and p38 MAPK, but not NF-kappaB, are critically involved in reactive oxygen species-mediated induction of IL-6 by angiotensin II in cardiac fibroblasts. Circulation research. 2001;89(8):661-9.
122. Kern PA, Ranganathan S, Li C, Wood L, Ranganathan G. Adipose tissue tumor necrosis factor and interleukin-6 expression in human obesity and insulin resistance. American journal of physiology Endocrinology and metabolism. 2001;280(5):E745-51.
123. Kim DH, Burgess AP, Li M, Tsenovoy PL, Addabbo F, McClung JA, et al. Heme oxygenase-mediated increases in adiponectin decrease fat content and inflammatory cytokines tumor necrosis factor-alpha and interleukin-6 in Zucker rats and reduce adipogenesis in human mesenchymal stem cells. J Pharmacol Exp Ther. 2008;325(3):833-40.
124. Hirosumi J, Tuncman G, Chang L, Gorgun CZ, Uysal KT, Maeda K, et al. A central role for JNK in obesity and insulin resistance. Nature. 2002;420(6913):333-6.
125. Hu J, Roy SK, Shapiro PS, Rodig SR, Reddy SP, Platanias LC, et al. ERK1 and ERK2 activate CCAAAT/enhancer-binding protein-beta-dependent gene transcription in response to interferon-gamma. The Journal of biological chemistry. 2001;276(1):287-97.
126. Bost F, Aouadi M, Caron L, Even P, Belmonte N, Prot M, et al. The extracellular signal-regulated kinase isoform ERK1 is specifically required for in vitro and in vivo adipogenesis. Diabetes. 2005;54(2):402-11.

127. Schroder K, Wandzioch K, Helmcke I, Brandes RP. Nox4 acts as a switch between differentiation and proliferation in preadipocytes. Arteriosclerosis, thrombosis, and vascular biology. 2009;29(2):239-45.
128. Li WG, Miller FJ, Jr., Zhang HJ, Spitz DR, Oberley LW, Weintraub NL. H(2)O(2)-induced O(2) production by a non-phagocytic NAD(P)H oxidase causes oxidant injury. The Journal of biological chemistry. 2001;276(31):29251-6.
129. Hawkins BJ, Madesh M, Kirkpatrick CJ, Fisher AB. Superoxide flux in endothelial cells via the chloride channel-3 mediates intracellular signaling. Molecular biology of the cell. 2007;18(6):2002-12.
130. Ahima RS, Flier JS. Adipose tissue as an endocrine organ. Trends in endocrinology and metabolism: TEM. 2000;11(8):327-32.
131. Greenspan P, Fowler SD. Spectrofluorometric studies of the lipid probe, nile red. Journal of lipid research. 1985;26(7):781-9.
132. Goodman JM. The gregarious lipid droplet. The Journal of biological chemistry. 2008;283(42):28005-9.
133. Gubern A, Barcelo-Torns M, Casas J, Barneda D, Masgrau R, Picatoste F, et al. Lipid droplet biogenesis induced by stress involves triacylglycerol synthesis that depends on group VIA phospholipase A2. The Journal of biological chemistry. 2009;284(9):5697-708.
134. Spector AA, Mathur SN, Kaduce TL, Hyman BT. Lipid nutrition and metabolism of cultured mammalian cells. Progress in lipid research. 1980;19(3-4):155-86.
135. Yao W, Li K, Liao K. Macropinocytosis contributes to the macrophage foam cell formation in RAW264.7 cells. Acta Biochim Biophys Sin (Shanghai). 2009;41(9):773-80.
136. Murphy DJ, Vance J. Mechanisms of lipid-body formation. Trends in biochemical sciences. 1999;24(3):109-15.
137. Kuerschner L, Moessinger C, Thiele C. Imaging of lipid biosynthesis: how a neutral lipid enters lipid droplets. Traffic. 2008;9(3):338-52.
138. Sekiya I, Larson BL, Vuoristo JT, Cui JG, Prockop DJ. Adipogenic differentiation of human adult stem cells from bone marrow stroma (MSCs). J Bone Miner Res. 2004;19(2):256-64.
139. Sugihara H, Yonemitsu N, Miyabara S, Toda S. Proliferation of unilocular fat cells in the primary culture. Journal of lipid research. 1987;28(9):1038-45.
140. Matsumoto T, Kano K, Kondo D, Fukuda N, Iribe Y, Tanaka N, et al. Mature adipocyte-derived dedifferentiated fat cells exhibit multilineage potential. Journal of cellular physiology. 2008;215(1):210-22.
141. Aldridge A, Kouroupis D, Churchman S, English A, Ingham E, Jones E. Assay validation for the assessment of adipogenesis of multipotential stromal cells--a direct comparison of four different methods. Cytotherapy. 2013;15(1):89-101.
142. Wang QA, Tao C, Gupta RK, Scherer PE. Tracking adipogenesis during white adipose tissue development, expansion and regeneration. Nature medicine. 2013;19(10):1338-44.
143. Harms M, Seale P. Brown and beige fat: development, function and therapeutic potential. Nature medicine. 2013;19(10):1252-63.

144. Dixit R, Cyr R. Cell damage and reactive oxygen species production induced by fluorescence microscopy: effect on mitosis and guidelines for non-invasive fluorescence microscopy. Plant J. 2003;36(2):280-90.
145. Lee YH, Chen SY, Wiesner RJ, Huang YF. Simple flow cytometric method used to assess lipid accumulation in fat cells. Journal of lipid research. 2004;45(6):1162-7.
146. Bunnell BA, Flaat M, Gagliardi C, Patel B, Ripoll C. Adipose-derived stem cells: isolation, expansion and differentiation. Methods. 2008;45(2):115-20.
147. Kern S, Eichler H, Stoeve J, Kluter H, Bieback K. Comparative analysis of mesenchymal stem cells from bone marrow, umbilical cord blood, or adipose tissue. Stem Cells. 2006;24(5):1294-301.
148. Pachon-Pena G, Yu G, Tucker A, Wu X, Vendrell J, Bunnell BA, et al. Stromal stem cells from adipose tissue and bone marrow of age-matched female donors display distinct immunophenotypic profiles. Journal of cellular physiology. 2011;226(3):843-51.
149. Shao D, Lazar MA. Peroxisome proliferator activated receptor gamma, CCAAT/enhancer-binding protein alpha, and cell cycle status regulate the commitment to adipocyte differentiation. J Biol Chem. 1997;272(34):21473-8.
150. Cristancho AG, Lazar MA. Forming functional fat: a growing understanding of adipocyte differentiation. Nature reviews Molecular cell biology. 2011;12(11):722-34.
151. Gocze PM, Freeman DA. Factors underlying the variability of lipid droplet fluorescence in MA-10 Leydig tumor cells. Cytometry. 1994;17(2):151-8.
152. Smyth MJ, Wharton W. Differentiation of A31T6 proadipocytes to adipocytes: a flow cytometric analysis. Experimental cell research. 1992;199(1):29-38.
153. Ebert R, Ulmer M, Zeck S, Meissner-Weigl J, Schneider D, Stopper H, et al. Selenium supplementation restores the antioxidative capacity and prevents cell damage in bone marrow stromal cells in vitro. Stem Cells. 2006;24(5):1226-35.
154. Stolzing A, Jones E, McGonagle D, Scutt A. Age-related changes in human bone marrow-derived mesenchymal stem cells: consequences for cell therapies. Mechanisms of ageing and development. 2008;129(3):163-73.
155. Lund P, Pilgaard L, Duroux M, Fink T, Zachar V. Effect of growth media and serum replacements on the proliferation and differentiation of adipose-derived stem cells. Cytotherapy. 2009;11(2):189-97.
156. Le Blanc K, Tammik C, Rosendahl K, Zetterberg E, Ringden O. HLA expression and immunologic properties of differentiated and undifferentiated mesenchymal stem cells. Experimental hematology. 2003;31(10):890-6.
157. Reger RL, Tucker AH, Wolfe MR. Differentiation and characterization of human MSCs. Methods Mol Biol. 2008;449:93-107.
158. Saitoh Y, Xiao L, Mizuno H, Kato S, Aoshima H, Taira H, et al. Novel polyhydroxylated fullerene suppresses intracellular oxidative stress together with repression of intracellular lipid accumulation during the differentiation of OP9 preadipocytes into adipocytes. Free radical research. 2010;44(9):1072-81.
159. Imhoff BR, Hansen JM. Extracellular redox environments regulate adipocyte differentiation. Differentiation; research in biological diversity. 2010;80(1):31-9.

160. Lechpammer S, Epperly MW, Zhou S, Nie S, Glowacki J, Greenberger JS. Adipocyte differentiation in Sod2(-/-) and Sod2(+/+) murine bone marrow stromal cells is associated with low antioxidant pools. Experimental hematology. 2005;33(10):1201-8.
161. Xia Z, Appelkvist EL, DePierre JW, Nassberger L. Tricyclic antidepressant-induced lipidosis in human peripheral monocytes in vitro, as well as in a monocyte-derived cell line, as monitored by spectrofluorimetry and flow cytometry after staining with Nile red. Biochem Pharmacol. 1997;53(10):1521-32.
162. Hyslop PA, Hinshaw DB, Halsey WA, Jr., Schraufstatter IU, Sauerheber RD, Spragg RG, et al. Mechanisms of oxidant-mediated cell injury. The glycolytic and mitochondrial pathways of ADP phosphorylation are major intracellular targets inactivated by hydrogen peroxide. The Journal of biological chemistry. 1988;263(4):1665-75.
163. Le TT, Cheng JX. Single-cell profiling reveals the origin of phenotypic variability in adipogenesis. PloS one. 2009;4(4):e5189.
164. Rosen ED, Spiegelman BM. Adipocytes as regulators of energy balance and glucose homeostasis. Nature. 2006;444(7121):847-53.
165. Wilson-Fritch L, Burkart A, Bell G, Mendelson K, Leszyk J, Nicoloro S, et al. Mitochondrial biogenesis and remodeling during adipogenesis and in response to the insulin sensitizer rosiglitazone. Molecular and cellular biology. 2003;23(3):1085-94.
166. McKay RM, McKay JP, Avery L, Graff JM. C elegans: a model for exploring the genetics of fat storage. Developmental cell. 2003;4(1):131-42.
167. May JM, de Haen C. The insulin-like effect of hydrogen peroxide on pathways of lipid synthesis in rat adipocytes. The Journal of biological chemistry. 1979;254(18):9017-21.
168. Livingston JN, Gurny PA, Lockwood DH. Insulin-like effects of polyamines in fat cells. Mediation by H2O2 formation. The Journal of biological chemistry. 1977;252(2):560-2.
169. Lawrence JC, Jr., Larner J. Activation of glycogen synthase in rat adipocytes by insulin and glucose involves increased glucose transport and phosphorylation. The Journal of biological chemistry. 1978;253(7):2104-13.
170. Hayes GR, Lockwood DH. Role of insulin receptor phosphorylation in the insulinomimetic effects of hydrogen peroxide. Proceedings of the National Academy of Sciences of the United States of America. 1987;84(22):8115-9.
171. Lu HF, Sue CC, Yu CS, Chen SC, Chen GW, Chung JG. Diallyl disulfide (DADS) induced apoptosis undergo caspase-3 activity in human bladder cancer T24 cells. Food Chem Toxicol. 2004;42(10):1543-52.
172. Lee JH, Kim KA, Kwon KB, Kim EK, Lee YR, Song MY, et al. Diallyl disulfide accelerates adipogenesis in 3T3-L1 cells. Int J Mol Med. 2007;20(1):59-64.
173. Gesquiere L, Loreau N, Minnich A, Davignon J, Blache D. Oxidative stress leads to cholesterol accumulation in vascular smooth muscle cells. Free radical biology & medicine. 1999;27(1-2):134-45.

174. Fleischmann M, Iynedjian PB. Regulation of sterol regulatory-element binding protein 1 gene expression in liver: role of insulin and protein kinase B/cAkt. The Biochemical journal. 2000;349(Pt 1):13-7.
175. Salsman S, Felts N, Pye QN, Floyd RA, Hensley K. Induction of Akt phosphorylation in rat primary astrocytes by H2O2 occurs upstream of phosphatidylinositol 3-kinase: no evidence for oxidative inhibition of PTEN. Archives of biochemistry and biophysics. 2001;386(2):275-80.
176. Debacq-Chainiaux F, Erusalimsky JD, Campisi J, Toussaint O. Protocols to detect senescence-associated beta-galactosidase (SA-betagal) activity, a biomarker of senescent cells in culture and in vivo. Nature protocols. 2009;4(12):1798-806.
177. Chen Q, Ames BN. Senescence-like growth arrest induced by hydrogen peroxide in human diploid fibroblast F65 cells. Proceedings of the National Academy of Sciences of the United States of America. 1994;91(10):4130-4.
178. Young DA, Choi YS, Engler AJ, Christman KL. Stimulation of adipogenesis of adult adipose-derived stem cells using substrates that mimic the stiffness of adipose tissue. Biomaterials. 2013;34(34):8581-8.
179. Stamm C, Westphal B, Kleine HD, Petzsch M, Kittner C, Klinge H, et al. Autologous bone-marrow stem-cell transplantation for myocardial regeneration. Lancet. 2003;361(9351):45-6.
180. Wollert KC, Meyer GP, Lotz J, Ringes-Lichtenberg S, Lippolt P, Breidenbach C, et al. Intracoronary autologous bone-marrow cell transfer after myocardial infarction: the BOOST randomised controlled clinical trial. Lancet. 2004;364(9429):141-8.
181. Premer C, Blum A, Bellio MA, Schulman IH, Hurwitz BE, Parker M, et al. Allogeneic Mesenchymal Stem Cells Restore Endothelial Function in Heart Failure by Stimulating Endothelial Progenitor Cells. EBioMedicine. 2015;2(5):467-75.
182. Karantalis V, Hare JM. Use of mesenchymal stem cells for therapy of cardiac disease. Circulation research. 2015;116(8):1413-30.
183. Li JH, Zhang N, Wang JA. Improved anti-apoptotic and anti-remodeling potency of bone marrow mesenchymal stem cells by anoxic pre-conditioning in diabetic cardiomyopathy. J Endocrinol Invest. 2008;31(2):103-10.
184. Li S, Deng Y, Feng J, Ye W. Oxidative preconditioning promotes bone marrow mesenchymal stem cells migration and prevents apoptosis. Cell Biol Int. 2009;33(3):411-8.
185. Pendergrass KD, Boopathy AV, Seshadri G, Maiellaro-Rafferty K, Che PL, Brown ME, et al. Acute preconditioning of cardiac progenitor cells with hydrogen peroxide enhances angiogenic pathways following ischemia-reperfusion injury. Stem cells and development. 2013;22(17):2414-24.
186. Pevsner-Fischer M, Levin S, Zipori D. The origins of mesenchymal stromal cell heterogeneity. Stem Cell Rev. 2011;7(3):560-8.
187. Tremain N, Korkko J, Ibberson D, Kopen GC, DiGirolamo C, Phinney DG. MicroSAGE analysis of 2,353 expressed genes in a single cell-derived colony of undifferentiated human mesenchymal stem cells reveals mRNAs of multiple cell lineages. Stem Cells. 2001;19(5):408-18.

188. Yu HM, Zhi JL, Cui Y, Tang EH, Sun SN, Feng JQ, et al. Role of the JAK-STAT pathway in protection of hydrogen peroxide preconditioning against apoptosis induced by oxidative stress in PC12 cells. Apoptosis. 2006;11(6):931-41.
189. Calzadilla P, Sapochnik D, Cosentino S, Diz V, Dicelio L, Calvo JC, et al. N-acetylcysteine reduces markers of differentiation in 3T3-L1 adipocytes. International journal of molecular sciences. 2011;12(10):6936-51.
190. Rodbell M. Metabolism of Isolated Fat Cells. I. Effects of Hormones on Glucose Metabolism and Lipolysis. The Journal of biological chemistry. 1964;239:375-80.
191. Park SG, Kim JH, Xia Y, Sung JH. Generation of reactive oxygen species in adipose-derived stem cells: friend or foe? Expert opinion on therapeutic targets. 2011;15(11):1297-306.

We each exist for but a short time, and in that time explore but a small part of the whole universe.

- Stephen Hawkings

Chapter 5

The effect of artificial hypoxic conditioning on the viability, phenotype, and adipogenic differentiation of adipose-derived mesenchymal stem/stromal cells

Introduction

In the 18th century, Priestley in a lethal but clear experiment demonstrated the importance of molecular oxygen (O_2) by placing a burning candle in a bell jar alongside an unfortunate mouse. This highlighted the outcome of lack of exposure to O_2 (1). A state in which the level of O_2 is reduced compared to the typical ambient level of O_2 is defined as hypoxia. However, physiological normoxia is hypoxic according to this definition and this hypoxia is essential for the full development of embryos and the generation of an intact cardiovascular system (2-4). The ability to sense and respond to changes in O_2 is essential for the survival of most organisms. The transcription complex called hypoxia-inducible factor (HIF) plays a pivotal role in this process.

In the presence of normoxia, HIF-α is degraded almost as soon as it is made due to the O_2-dependent hydroxylation of specific proline residues (402 and 564) (5-7). Three homologous 2-oxoglutarate-dependent prolyl hydroxylase domain-containing (PHD) dioxygenases PHD1, PHD2, and PHD3 catalyze this prolyl hydroxylation (8). Another 2-oxoglutarate-dependent dioxygenase (FIH-1) catalyzes the formation of a specific hydroxyasparagine (803) leading to decreased binding of HIF-α to the transcriptional co-activator p300 and thus affecting the transcriptional potency of HIF-α (9, 10). The von Hippel-Lindau protein (pVHL) recognizes and binds to the two specific hydroxyproline residues in HIF-α, leading to its ubiquitination and subsequent degradation by the 26S proteasome (5, 11). Conversely, under hypoxic conditions, hydroxylation does not occur, HIF-α escapes degradation, and is therefore free to heterodimerise with the constitutively expressed HIF-β subunit (also called Aryl hydrocarbon nuclear translocator, ARNT). This whole HIF complex translocates to the nucleus. The HIF complex binds to hypoxia response elements (HREs) that are found in numerous genes involved in cell growth and fate, glucose metabolism, and O_2 transport and delivery (12).

Both the prolyl and asparaginyl hydroxylases require α-ketoglutarate (2-oxoglutarate) (9). The cell-permeable 2-oxoglutarate analogue dimethyloxalylglycine (DMOG) competitively inhibits the HIF prolyl and asparaginyl hydroxylases by competing for 2-oxoglutarate and is predicted to also inhibit other members of the class of 2-oxoglutarate-dependent dioxygenases (7, 9). Thus, DMOG can activate the HIF complex and HIF transcriptional cascades through stabilising HIF-α during normoxia.

One of the defining characteristics of stem cells is that they produce all cells that make up the tissues of the body through self-renewal and differentiation. The *in vivo* O_2 concentrations can have a direct effect on stem cell self-renewal and differentiation. Schofield conceptualized the stem cell "niche" in 1978 (13). This term defines the anatomical position, including the cellular and acellular components, in which stem cells reside. One hypothesis is that stem cells reside in hypoxic niches where the physiological O_2 tension is lower than ambient O_2 tension (21% O_2) and thus oxidative stress may be reduced. The niche is said to maintain the proliferative or multipotent capabilities of stem cells while differentiation down specific lineages coincides with the migration of these stem cells out of the niche.

Niches vary in O_2 tension. The adipose tissue niche consists of many cell types including mature adipocytes, fibroblasts, smooth muscle cells, adipose-derived stem/stromal cells (ASCs), endothelial cells, and pericytes. Pericytes are cells that wrap around the endothelial cells of capillaries. The location of ASCs within this environment is not fully understood but literature places the stromal cells in a perivascular location (14). *In vivo* measurements in adipose tissues have shown that O_2 tensions tend to range between 2 and 8% (15, 16). The O_2 tension within the bone marrow has been reported to range from 1 to 7% (17-19) (Figure 5.1).

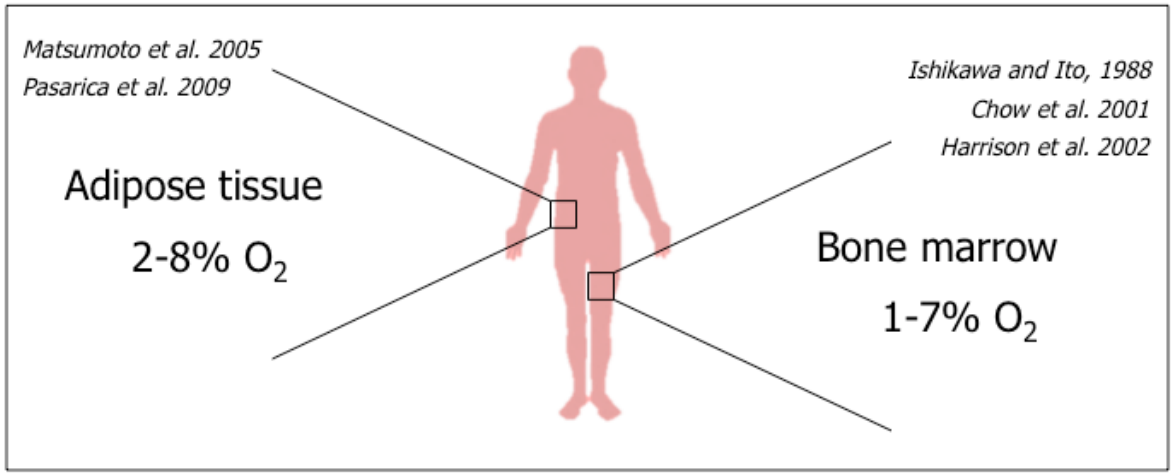

Figure 5.1. Oxygen tensions of stem cell anatomical niches within adipose tissue and bone marrow. The O_2 tension within the bone marrow has been comprehensively studied, mainly in the context of hematopoietic stem cells (HSCs) and ranges from 1 to 7%. *In vivo* measurements in adipose tissues have demonstrated that the O_2 tension ranges between 2 and 8%. Adapted from Mohyeldin *et al.* 2010.

Although it appears that an O_2 gradient affects the fate of specific cells (20), especially during embryonic development, in the context of differentiation the results are often conflicting. Oxygen levels may inhibit the differentiation of certain stem cells, but promote the differentiation of others. Numerous research groups have demonstrated these inconsistent results. Fehrer and colleagues demonstrated that 3% O_2 promoted mesenchymal stromal/stem cells (MSCs) to remain in an undifferentiated state (21). Holzwarth *et al.* (2010) found that at an O_2 tension of 1% there was a lack in differentiation potential, but increasing the O_2 tension to 3% restored the osteogenic potential (22). D'Ippolito and colleagues experimented with O_2 tensions <10% and found that osteogenic differentiation was undetected at 3% (23). Tsai and fellow researchers demonstrated that under hypoxic conditions (1-7%), an increased differentiation potential for all three mesenchyme lineages was observed (24). It was observed that the growth of MSCs in hypoxia enhanced osteogenesis *in vitro* and *in vivo* (25). Kim and colleagues state that hypoxia induced adipocyte differentiation (26). Wagegg and colleagues demonstrated that activation of HIF-1 using 100 μM of DMOG promoted osteogenesis but suppressed adipogenesis (27).

Intriguingly, analysis of the literature shows that when there is stimulation of osteogenesis, there is suppression of adipogenesis and vice-versa (28, 29). Hypoxia modulates the Wnt (wingless-type mouse mammary tumor virus integration site) signaling family. Hypoxia inducible factor-1α enhances Wnt/β-catenin signaling and β-catenin has an inverse relationship with peroxisome proliferator-activated receptor-γ (PPARγ). Thus, several members of the Wnt signaling family have been shown to inhibit early steps of adipogenesis (30). The other side of the coin is that hypoxia increases mitochondrial ROS generation at Complex III, which as Kim and colleagues discovered, enhances adipocyte differentiation (26, 31). The confusion that exists around the role that hypoxia and the stabilisation of HIF-1α play in adipogenic differentiation, as well as a deficit in experimentation with artificial hypoxia in ASC adipogenic differentiation, led to the question: What is the effect of artificial hypoxia (DMOG) on the adipogenic differentiation potential of ASCs? This question was explored in the following section.

Materials and methods

Preparation of adipose-derived stromal cell artificial hypoxic cultures

Human ASCs were isolated as previously described (Chapter 3). Adherent ASCs from four donors (A180313, A220313, A070813, and A270813) from passages four (P4F1) to seven (P7F1) were used to conduct the majority of the artificial hypoxia experiments. The cells were seeded at 5 x 10^3 cells/cm^2 into flasks with α-MEM (Gibco®, Invitrogen Corporation, Carlsbad, California, USA) supplemented with 10% (v/v) fetal bovine serum (FBS; Biochrom AG, Berlin, Germany) and 2% (v/v) penicillin and streptomycin (Pen/Strep; Sigma-Aldrich, St. Louis, MO, USA) and were maintained and expanded under normoxic conditions in an incubator at 37°C with a humidified atmosphere of 20% O_2 containing 5% CO_2. The changing and replenishment of media were carried out every second day until the cells reached ± 80% confluence. Upon commencement of artificial hypoxic experiments, the ASCs were cultured under normoxic conditions in an incubator at 37°C with a humidified atmosphere of 20% O_2 containing 5% CO_2 with the addition of 100 μM of the PHD enzyme inhibitor, DMOG (1.75 mg DMOG/1 ml DMSO; both Sigma-Aldrich, St. Louis, MO, USA) to block O_2-dependent HIF-1α degradation. The DMOG was made up immediately prior to use and added directly to the medium.

Viability of ASCs cultured with dimethyloxalylglycine (DMOG)

Analysis of the current literature revealed that concentrations of 100 μM up to 1 mM of DMOG exhibited no cytotoxicity towards MSCs. However, increasing the DMOG concentration to 5 mM resulted in cytotoxicity (32). Liu and colleagues observed increasing expression of HIF-1α using 100 μM DMOG (32). Thus, for this research a concentration of 100 μM of DMOG was chosen. An assessment of the influence of this concentration of DMOG or vehicle on ASC death was performed using the viability assay, SRB, described in the previous chapter (Chapter 4).

Multi-colour flow-cytometric analysis of immunophenotype under artificial hypoxic conditions

Multi-colour flow cytometry was employed for the immunophenotypic analysis. The cell phenotypes from normoxic and artificial hypoxic cultures were assessed over two passages (±17 days). The cells were trypsinized and centrifuged for 5 minutes at 184 *g*. The supernatant was aspirated and the pellet resuspended in PBS. The cell suspension was incubated with Phycoerythrin-Cyanin 7-conjugated CD34 (CD34-PC7) and Krome orange-conjugated CD45 (CD45-KO) antibodies (Both Beckman Coulter). The cell suspension was also incubated with fluorescein isothiocyanate-conjugated CD73 (CD73-FITC; eBioscience, San Diego, California, USA), Phycoerythrin-Cyanin 5.1-conjugated CD90 (CD90-PC5; Beckman Coulter), and phycoerythrin-conjugated CD105 (CD105-PE; Beckman Coulter) antibodies. The panel of 5 antibodies was incubated for 10 to 15 minutes in the dark at room temperature. The ASCs-antibody mixture was subsequently washed with PBS once to remove any unbound antibodies. The ASC-antibody mixture was then resuspended in PBS. Cells that were not stained with antibodies represented a negative control allowing for the detection of any autofluorescence from the cells. Data was obtained by flow cytometric analysis (Gallios; Beckman Coulter). The unstained cell events were measured within the first decade of single-parameter plots. A minimum of 5 000 events per flow cytometric sample was collected and dead cells, cellular aggregates and debris were excluded from the analysis. The list mode data (LMD) generated was analyzed using Kaluza® Analysis Software 1.2 (Beckman Coulter). In order to keep the settings uniform during the experiments, the flow cytometer was checked before each experiment with Flow-Check™ Fluorospheres (Beckman Coulter) and the voltage was maintained.

Fibroblastoid colony-forming unit assay under artificial hypoxic conditions

The ASCs were serially diluted and seeded onto 100 x 20 mm CELLSTAR® tissue culture dishes (Greiner Bio-One) in triplicate at a final density of 100 cells per dish, which is an average cell density of 1.72 cells/cm^2 (number of cells/growth area). Clonal growth was carried out for 13 days of normoxic culture or artificial hypoxic culture. The colonies were washed twice with PBS and fixed with 4% (v/v) formaldehyde for 60 minutes. After fixation, colonies were washed twice again with PBS and stained with Toluidine Blue O stain (Sigma-Aldrich) and enumerated. The colony sizes consisted of three categories: 0-25 cells, 25-50 cells or >50 cells.

In vitro adipocyte differentiation under artificial hypoxia conditions

Adipose-derived stromal cells were seeded at a density of 5 x 10^3 cells/cm^2 in 6-well plates and cultured using standard growth medium, α-MEM. At confluence, in triplicate, the adherent cells (in the seventh passage) were subjected to adipogenic differentiation *in vitro* under either normoxic or artificial hypoxic conditions. The cells were incubated in adipogenic induction medium consisting of DMEM culture medium (and for clarification only + pyruvate was used in this chapter) supplemented with 1 μM dexamethasone (Sigma-Aldrich), 0.5 mM 3-iosbutyl-methylxanthine (Sigma-Aldrich), 200 μM indomethacin (Sigma-Aldrich), 10 μg/ml human insulin (Sigma-Aldrich), 10% (v/v) FBS and 2% (v/v) Pen/Strep for 14 and 21 days (33). Control medium (used for non-differentiated cells) consisted of DMEM supplemented with 10% (v/v) FBS and 2% (v/v) Pen/Strep. Media were replaced on the 1st and 5th days of culture and the cells were replenished with medium on the 3rd day of culture.

Quantification of adipogenesis under artificial hypoxia conditions using flow cytometry

Induced and non-induced cells were trypsinized and washed using DMEM. In order to obtain a quantitative measure of intracellular lipid accumulation, single cell suspensions were prepared and were simultaneously stained with Nile red (1 μg/ml) and DAPI (5 μg/ml) for 20 minutes at room temperature. Fresh working solutions of DAPI (500 μg/ml) and Nile red (100 μg/ml) were prepared in staining buffer (100 mM Tris; pH 7.4, 150 mM NaCl, 1 mM $CaCl_2$, 0.5 mM $MgCl_2$) and protected from light. The cells were analyzed on a Gallios flow cytometer. Nile Red was excited with a 488 nm laser and yellow-gold fluorescence was detected in FL2 using a 575/30 nm BP filter and deep red fluorescence was detected in FL5

using a 755 nm LP filter. DAPI was excited with a 405 nm laser and fluorescent emissions were detected in FL9 using a 450/40 nm BP filter. The LMD collected from the experiments were analyzed using Kaluza analysis software. The compensation matrix was determined using the dedicated function of the Kaluza software. Any replicate having less than 100 viable cells was excluded.

Statistical analysis

Kaluza statistics files were exported into Microsoft® Excel® for Mac 2011 Version 14.4.4 (140807) for further analysis. Statistics were also performed using GraphPad PRISM 6 Version 6.0d (GraphPad, UK). Data are represented as the mean ± standard error of the mean (SEM). The D'Agostino-Pearson omnibus K2 normality test was utilized to quantify how much a data set deviated from a Gaussian distribution. If the data followed a Gaussian distribution, statistical differences were calculated using the Student's two-tailed t-test for comparison of two independent groups and One–way analysis of variance (One-way ANOVA) followed by Tukey's post hoc test for multiple comparisons. If the data did not follow a Gaussian distribution then a non-parametric statistical method was followed. Statistical differences were calculated using the Mann-Whitney test for comparison of two independent groups. The Kruskal-Wallis test was utilized followed by the Dunn's post test for multiple comparisons. The multiple comparison post tests indicate the significance level of a comparison. Differences were considered significant at $p \leq 0.05$. All of the data presented are the results of three technical repeats.

Results

Effect of dimethyloxalylglycine (DMOG) on ASC viability

In order to investigate the effect of artificial hypoxia on the adipogenic differentiation potential of human ASCs, the optimal concentration of DMOG was determined. Examination of the current literature on DMOG revealed that there is increased expression of HIF-1α with 100 μM, 500 μM and 1 mM DMOG concentrations. These concentrations up to 1 mM were non-toxic to MSCs (32). Following treatment with different concentrations of DMOG, ASC growth was analyzed using the SRB assay. Increased cellular growth was observed after 24 hours. The untreated ASCs and 100 μM DMOG treated-ASC continued to increase in number at 96 hours. Cellular growth was significantly suppressed after 96 hours of incubation with

1000 μM DMOG compared to the untreated control (Figure 5.2). Cell viability was displayed as percentages of the viability at time point 0 hours (100%) (Figure 5.3). Treatment with 100 μM DMOG for 24 hours resulted in a non-significant increase in cell viability due to cell growth to 111.50% ± 9.18% viable cells and treatment with 100 μM DMOG for 96 hours also resulted in a non-significant increase in cell viability due to cell growth to 139.90% ± 9.89% viable cells. Only a concentration of 1000 μM of DMOG for 96 hours resulted in significant (P<0.01) decrease in viability. Treating the ASCs with DMSO vehicle had no effect on cell viability over the 96-hour period. The grey bars in Figure 5.3 demonstrate treatment with the largest volume of DMSO that was used as a vehicle for treatment of the ASCs with the DMOG concentrations. The concentration of 100 μM DMOG was chosen for further experiments.

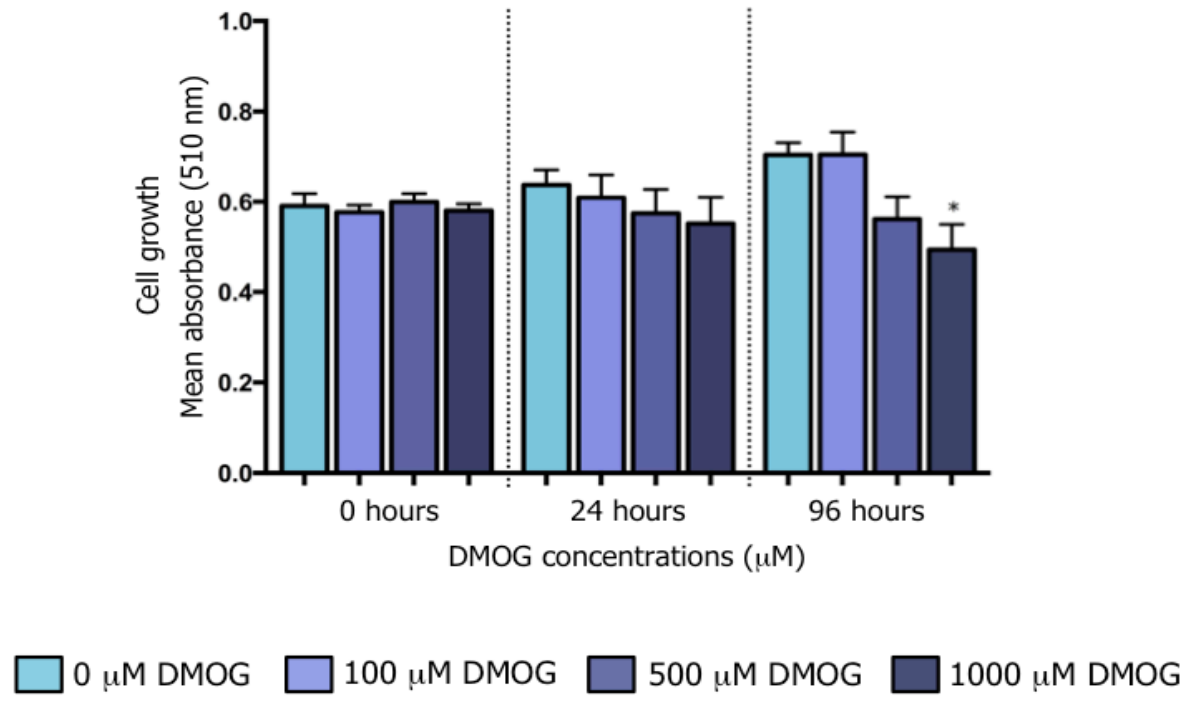

Figure 5.2. Effect of treatment with DMOG on ASC cell growth. Adipose-derived stromal cells were treated with the indicated concentrations of DMOG over 96 hours and assayed at the indicated time points. Cell growth was significantly suppressed after 96 hours of incubation with 1000 μM DMOG. Data represent the mean absorbance ± SEM. Data represents n = 2 biological replicates, repeated twice, each in triplicate. *P<0.05 as compared to the untreated control.

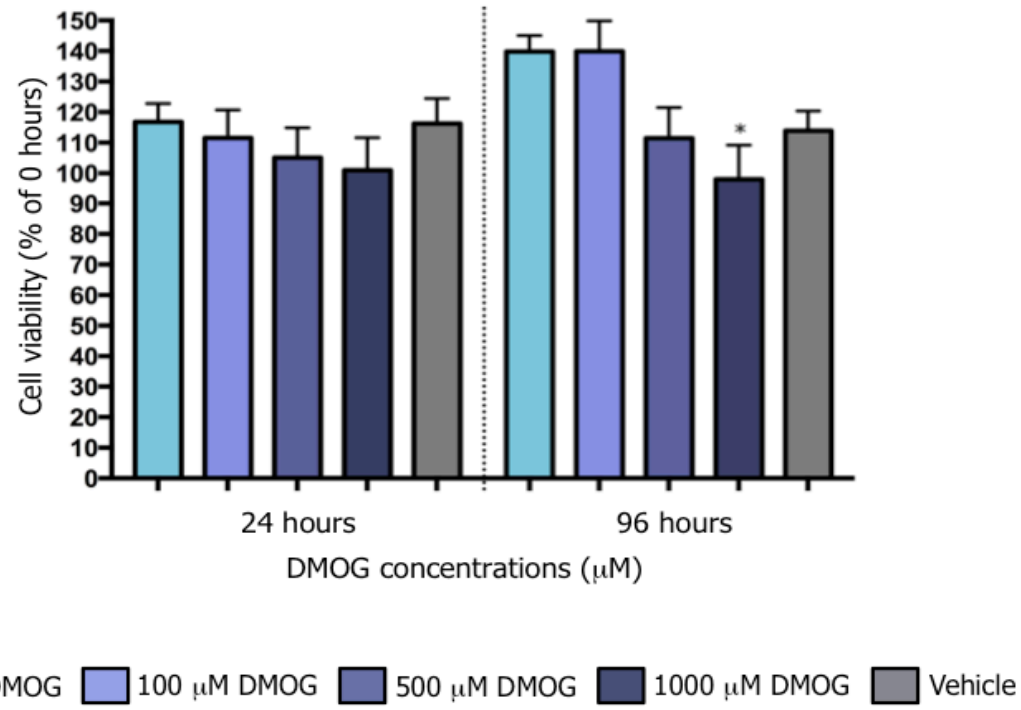

Figure 5.3. The effect of DMOG on ASC viability. Adipose-derived stromal cells were treated with the indicated concentrations of DMOG over 96 hours and assayed at the indicated time points. A concentration of 100 μM of DMOG over the 96-hour period was not toxic to the cells. Data represent the cell viability as a % of the viability at time point 0 hours ± SEM. Data represents n = 2 biological replicates, repeated twice, each in triplicate. *P<0.05 as compared to the untreated control.

Viability of the ASCs while maintained in artificial hypoxic culture was investigated by uptake of the cell viability stain, Propidium iodide (PI) (Figure 5.4). Propidium iodide is only permeable to cells with compromised membrane integrity, thus non-viable cells can be distinguished from viable cells by the fluorescence of PI which binds to DNA in the nucleus. Propidium iodide fluoresces in FL3. The two-parameter plots shown below were gated on an "Intact cells" region (as demonstrated in Chapter 3, Figure 3.12**B** and **D**). A high concentration of hydrogen peroxide (H_2O_2; 100 μM) is not conducive to cell viability and the non-viable and viable regions were set using this condition (5.4**A**). These viable and non-viable regions were maintained throughout the analysis. The viable cells were recognized by a shift in distribution to the left of the non-viable cells and thus a decrease in FL3 fluorescence on the plot (5.4**B**). Criteria set by the International Federation for Adipose

Therapeutics and Science (IFATS) and the International Society for Cellular Therapy (ISCT) state that >90% cell viability criteria should be met for ASCs.

An average of 93.39% ± 1.53% of the intact cells were viable under normoxic conditions before DMOG treatment for culture A180313. Following treatment with 100 μM DMOG 96.83% ± 1.23% were viable over 2 passages for culture A180313. An average of 94.55% ± 1.39% of the intact cells were viable in normoxic conditions before DMOG treatment for culture A220313. Following treatment with 100 μM DMOG 98.71% ± 0.71% were viable over 2 passages for culture A220313. Finally, the viability at the beginning of the artificial hypoxic experiment using culture A270813 was 96.00% ± 3.26% in normoxic conditions and 94.11% ± 0.17% following treatment with DMOG. There were no significant differences between the ratio of non-viable and viable ASCs with and without DMOG treatment. This indicated that DMOG at this concentration had no obvious cytotoxicity on ASCs.

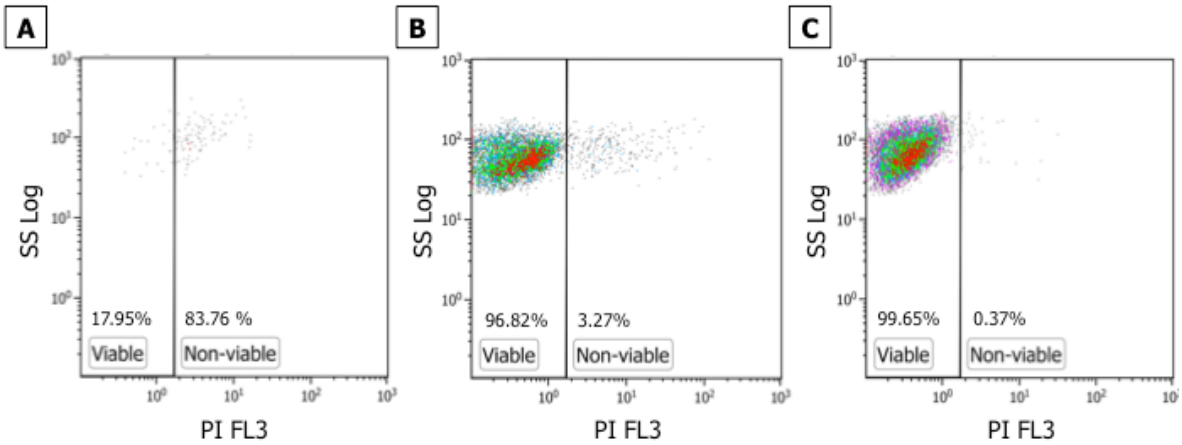

Figure 5.4. Viability of ASCs treated with DMOG as determined by flow cytometry measuring PI uptake. A high concentration of hydrogen peroxide (H_2O_2; 100 μM) is not conducive to cell viability and the non-viable and viable regions were set using this concentration of H_2O_2 (**A**). Cells in the left region indicated the percentage of cells that were viable. The plot in (**B**) indicates the viable and non-viable cells cultured in normoxic conditions. The plot in (**C**) indicates the viable and non-viable cells cultured with 100 μM of DMOG. Treatment with artificial hypoxia did not affect the viability of the cells negatively.

Artificial hypoxic culture maintains adipose-derived stromal cells' *in vitro* characteristics

The effect of 100 μM of DMOG on the cells' *in vitro* characteristics was further elucidated.

Expansion and maintenance of adipose-derived stromal cells cultured under artificial hypoxia

The three different thawed-cryopreserved ASC populations (A180313, A220313, A070813) were cultured comparatively for two passages under normoxia and artificial hypoxia. The images below were taken 3 days after seeding the second passage (Figure 5.5). Treatment with DMOG was initiated at time of seeding. The cells maintained plastic adherence throughout the passages. Visually there were no changes observed in the morphology between the ASCs grown in α-MEM and treated with DMOG compared to the ASCs just grown in α-MEM.

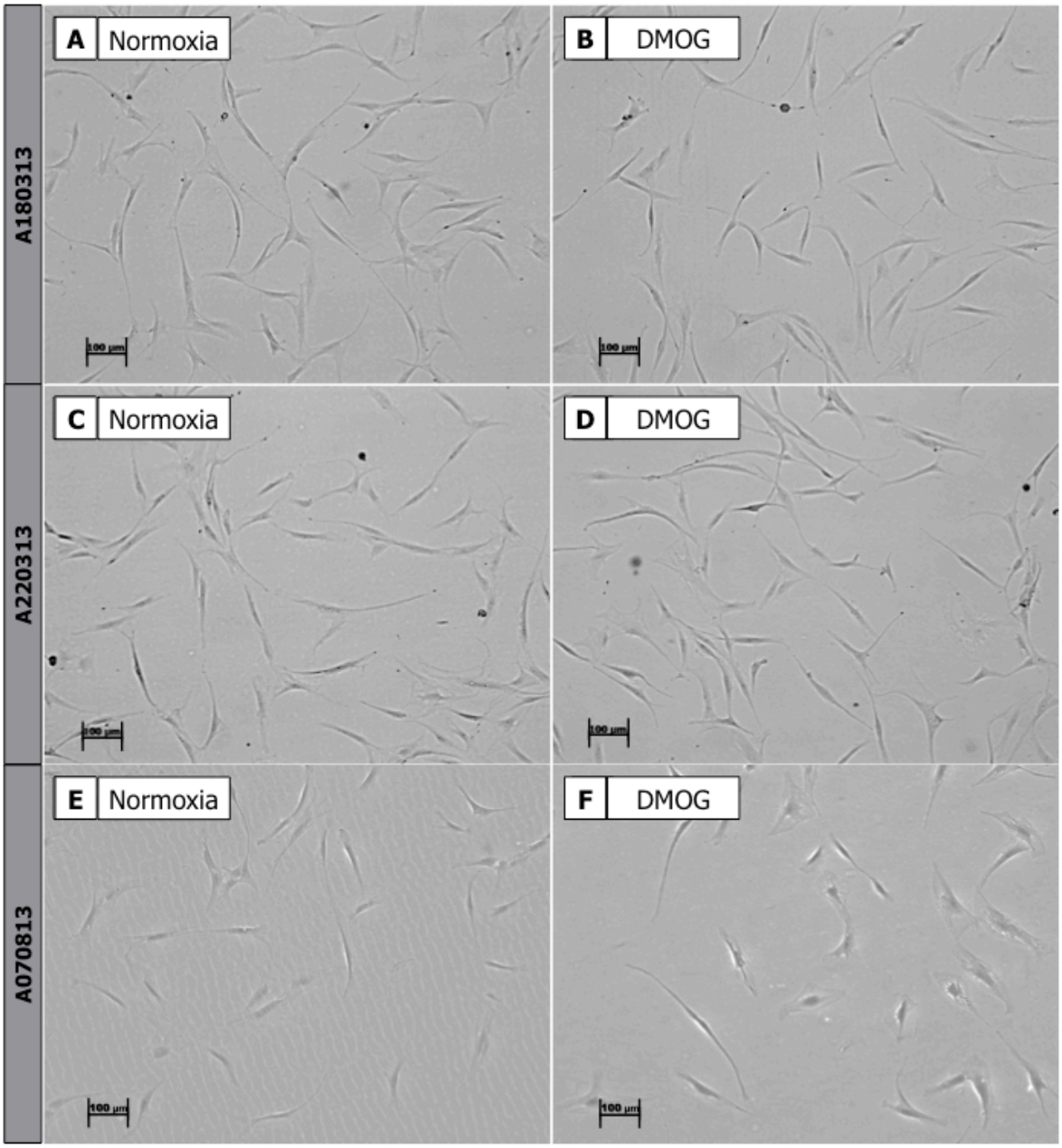

Figure 5.5. Morphology of ASCs cultured in normoxia and artificial hypoxia. The phase contrast microscopy photographs are representative of three different thawed-cryopreserved adherent ASC populations (A180313 P5, A220313 P4, A070813, P4) cultured for two passages under normoxia and artificial hypoxia. The images were taken 3 days after seeding the second passage. The ASCs were grown in standard α-MEM with 20% O_2 and 5% CO_2 (**A, C, E**), and under standard α-MEM with 20% O_2 and 5% CO_2, with the addition of 100 μM DMOG (**B, D, F**). The cultures displayed the typical spindle-shaped cells. No morphological differences with the two different conditions were observed. Original magnification: 5x, scale bars: 100 μm.

Multi-colour flow-cytometric analysis of immunophenotype of adipose derived-stromal cells cultured under artificial hypoxia

The immunophenotype of ASCs from four donor samples was characterized by assessing for the cell surface expression of CD73, CD90, CD105 and the lack of expression of CD34 and CD45. Greater than 95% expression for CD73, CD90 and CD105 is needed and less than 2% of the total population may be positive for CD34 and CD45 for the cells to be considered ASCs (34, 35). The expression of these markers on the cells of both the normoxic and artificial hypoxic cultures was assessed using flow cytometry.

Unstained cell suspensions were used to set gates which were maintained for the stained cell suspensions. Any cell population appearing to the right of the unstained cell population (in the second and greater decades of the four decades) of the single-parameter histogram plots was viewed as positively stained (Figure 5.6). The cells from the four donors cultured under normoxic and artificial hypoxic conditions showed very similar expression of surface markers. There was no significant difference in cell surface expression of the markers mentioned above over the two passages of culture in artificial hypoxia. The ASCs in artificial hypoxia expressed CD73 (98.25% ± 0.17%; average of both passages), CD90 (97.77% ± 0.20%), and CD105 (98.05% ± 0.08%) surface markers whereas the expression of CD34 (0.12% ± 0.06%), and CD45 (0.34% ± 0.04%) surface markers were below the limit of 2% (Table 5.1). The cells treated with DMOG in purple had greater than 95% expression for CD73, CD90 and CD105 and less than 2% expression of CD34 and CD45 (Figure 5.7). Thus, artificially mimicking hypoxic conditions by DMOG treatment did not alter the immunophenotype of the ASCs, reflecting the same ASC profile as observed under normoxic conditions.

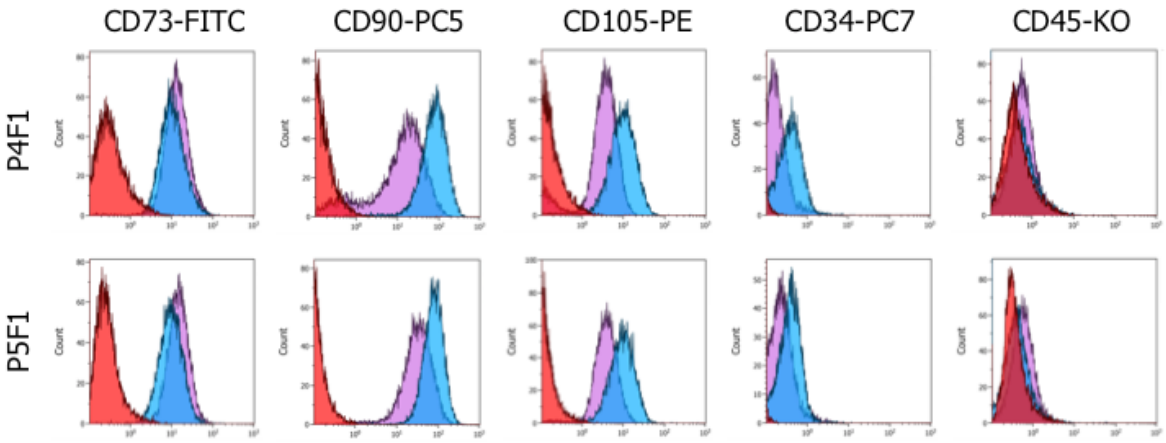

Figure 5.6. Overlay plots for selected surface markers of adherent cells cultured in normoxia and artificial hypoxia *in vitro*. The figure displays histograms of ASCs obtained from flow cytometry. Representative overlay plots for selected surface markers were generated from P4F1 to P5F1 showing positive expression for markers, CD73, CD105, CD90 and the lack of CD34 and CD45 expression. The red histograms represent unstained normoxic cultures, the blue histograms represent untreated normoxic cells stained with antibody, and the purple histograms represent artificial hypoxic cells stained with antibody.

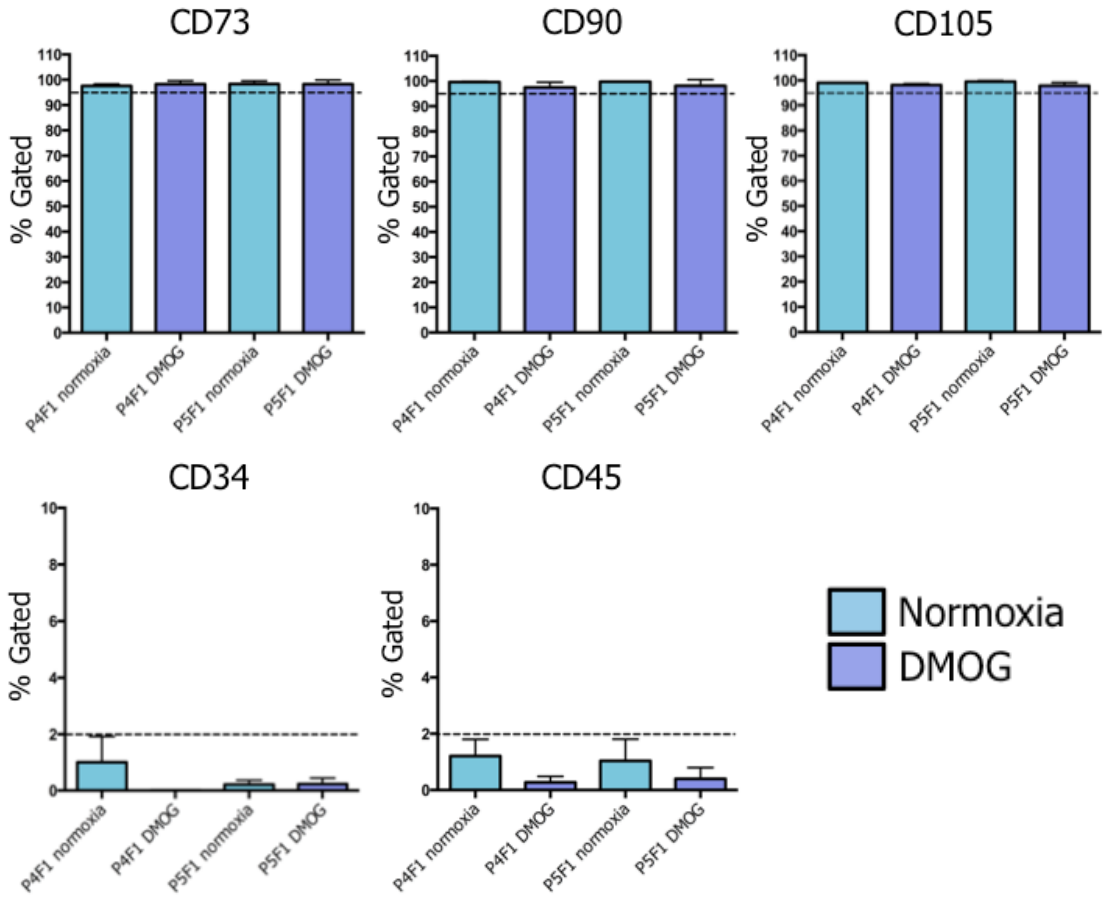

Figure 5.7. Immunophenotypic characterization of the adherent cells cultured in normoxia and artificial hypoxia *in vitro.* Immunophenotype of cells cultured under normoxic conditions and cells treated with 100 μM DMOG over 2 passages. Flow cytometric analysis of cultures A180313, A220313, A070813, and A270813 treated with 100 μM DMOG displayed an overall ASC phenotype. More than 95% cells expressed CD73, CD90 and CD105 (above dotted line) and less than 2% expressed CD34 and CD45 (below the dotted line). Error bars represent SEM. n = 4. No significant differences between cultures and conditions.

Table 5.1. Phenotypic characterization of adipose-derived stromal cells cultured in normoxia and artificial hypoxia *in vitro*.

	Normoxic		DMOG	
Antibody	**P4F1**	**P5F1**	**P4F1**	**P5F1**
CD73-FITC	97.60% ± 0.53%	98.35% ± 1.21%	98.28% ± 0.77%	98.22% ± 0.97%
CD90-PC5	99.60% ± 0.18%	99.72% ± 0.19%	97.42% ± 1.21%	98.12% ± 1.41%
CD105-PE	99.06% ± 0.16%	99.56% ± 0.28%	98.18% ± 0.52%	97.92% ± 0.75%
CD34-PC7	1.02% ± 0.91%	0.21% ± 0.11%	0.01% ± 0.00%	0.23% ± 0.12%
CD45-KO	1.21% ± 0.59%	1.04% ± 0.78%	0.27% ± 0.12%	0.40% ± 0.23%

Data are presented as mean ± SEM. Data represents n = 4. No significant differences between cultures and conditions.

Fibroblastoid colony-forming unit assay

The clonogenic potential of ASC was assessed after 13 days of expansion (Figure 5.8). The tissue culture dishes were seeded with 100 cells and cultured in either normoxic or artificial hypoxic conditions for the 13 days. The tissue culture dishes were stained with Toluidine Blue O to reveal the colonies. The average number of colonies resulting from 100 cells grown under normoxic and artificial hypoxia conditions was 55.11 ± 5.22 and 49.33 ± 1.89 respectively. These two averages were not significantly different from one another. Inter-culture variation was apparent. The A220313 donor culture behaved differently from A180313 and A270813. Culture A180313 resulted in 47.67 ± 6.57 colonies under normoxic conditions and 48.00 ± 3.51 colonies in artificial hypoxic conditions, while culture A220313 resulted in 73.67 ± 2.33 colonies in normoxic conditions and 52.00 ± 4.58 colonies in artificial hypoxic conditions. Culture A270813 resulted in 44.00 ± 4.04 colonies in normoxic conditions and slightly more colonies (48.00 ± 2.00) in artificial hypoxic conditions.

The heterogeneous nature of the ASC populations was noticeable upon further inspection of individual colonies in both normoxic and artificial hypoxic conditions. There was a broad

range of colony sizes, indicative of varied cell growth rates. However, there appeared to be a trend of numerous smaller colonies and fewer large colonies with DMOG treatment for 13 days. The average number of colonies formed consisting of >50 cells was significantly lower, 3.11 ± 1.68, in artificial hypoxic conditions compared to 39.44 ± 4.71 in normoxic conditions (Figure 5.9). The average number of colonies formed consisting of <50 cells was 23.11 ± 4.53 in artificial hypoxic conditions and 7.83 ± 1.10 in normoxic conditions. The number of colonies formed consisting of <50 cells from the 100 seeded cells for A180313 was 24.00 ± 9.18. The number of colonies formed consisting of <50 cells from the 100 seeded cells for A220313 was 21.33 ± 3.38, and the number of colonies formed consisting of <50 cells from the 100 seeded cells for A270813 was 24.00 ± 10.61. Upon examination of the cells within individual colonies, both spindle-shaped and rounded flat cells existed in both conditions. A greater proportion of the A220313 cells treated with DMOG, however, were more rounded in shape. All the cultures treated with DMOG had sparsely situated cells compared to the colonies cultured in normoxic conditions. It was also noted that ASCs treated with DMOG were smaller in size compared to untreated ASCs in normoxic conditions. The frequency of ASCs able to form colonies should be greater than 5% (35). The ASCs treated with 100 μM DMOG displayed a frequency of 6.31% ± 3.40%. Both normoxic untreated ASCs and DMOG-treated ASCs demonstrated a frequency to form colonies greater than 5%. All of the cultures were able to form colonies in both conditions, but great intra-culture and inter-culture variability was observed.

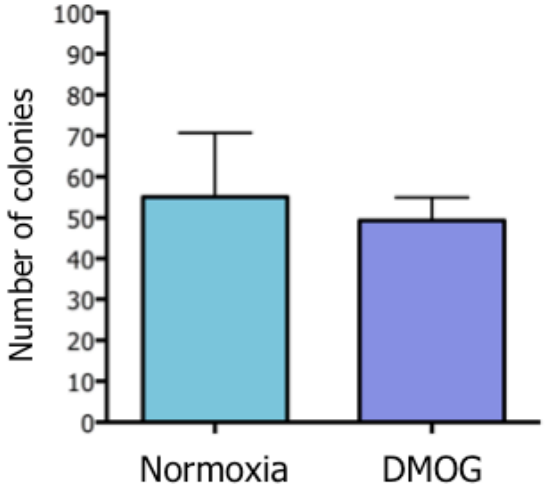

Figure 5.8. The effect of artificial hypoxia on colony forming ability. The graph displays the average number of colonies obtained from 3 donor cultures (A180313, A220313, and A270813) carried out in triplicate following 13 days of culture in normoxia or supplemented with 100 μM DMOG.

The average number of colonies resulting from 100 cells per dish under normoxic conditions was 55.11 ± 5.22. The average number of colonies resulting from 100 cells per dish under artificial hypoxia conditions was 49.33 ± 1.89. The averages were not significantly different.

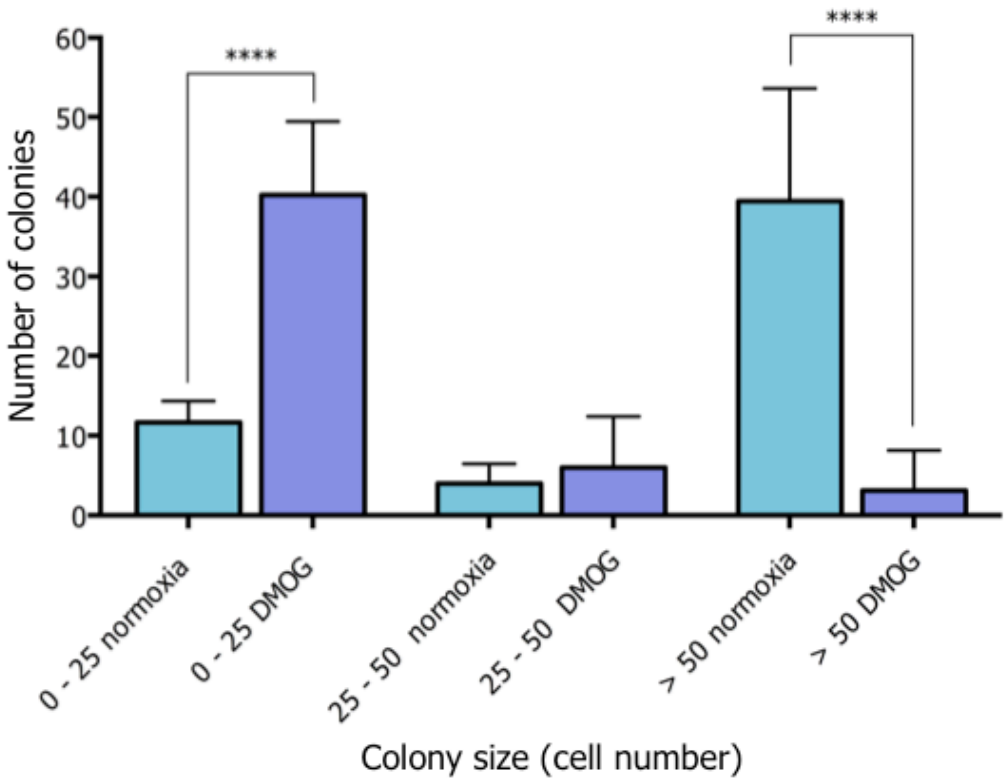

Figure 5.9. The effect of artificial hypoxia on colony forming ability. The size distribution of colonies obtained following 13 days of culture supplemented with 100 μM DMOG after seeding 100 cells per dish. Values are from 55,11 ± 16,17 colonies per plate in normoxic conditions and 49.33 ± 1.89 colonies per plate in artificial hypoxic conditions from three donors (A180313, A220313, and A270813) at passage 5 carried out in triplicate. Values are colony sizes consisting of 0-25 cells, 25-50 cells or ≥50 cells. Compared to the normoxic conditions, DMOG supplemented cultures had more small colonies and fewer large colonies than cells grown under normoxia. ****P<0.0001.

The effect of artificial hypoxia on adipogenic differentiation of adipose-derived stromal cells

ASCs were induced to differentiate into adipocytes using the adipogenic induction cocktail. To evaluate the effect of artificial hypoxia on adipogenesis, differentiation experiments were carried out under both normoxic and artificial hypoxic conditions for 14 and 21 days. Light microscopy revealed that the adipogenic-induced cells cultured in artificial hypoxia did not accumulate lipids to the same extent as adipogenic-induced cells cultured without DMOG

over a 21-day period (Figure 5.10). In artificial hypoxia, all induced cells accumulated a very little number of small lipid droplets, but in untreated adipogenic cultures there was an abundance of lipid droplets that varied greatly in size. The majority of lipid droplets in the untreated adipogenic cultures were significantly larger than those in artificial hypoxia. The nuclei of adipogenic-induced ASCs treated with DMOG moved to peripheral area of the cells while the cytoplasm became more complex 5.10**B**. Analysis of untreated adipogenic-induced ASCs revealed the typical more rounded morphology observed during adipogenic differentiation with numerous lipid droplets of varying sizes 5.10**A**. Quantitative information about lipid accumulation was needed and the cells were stained with Nile red and subjected to flow cytometric analysis.

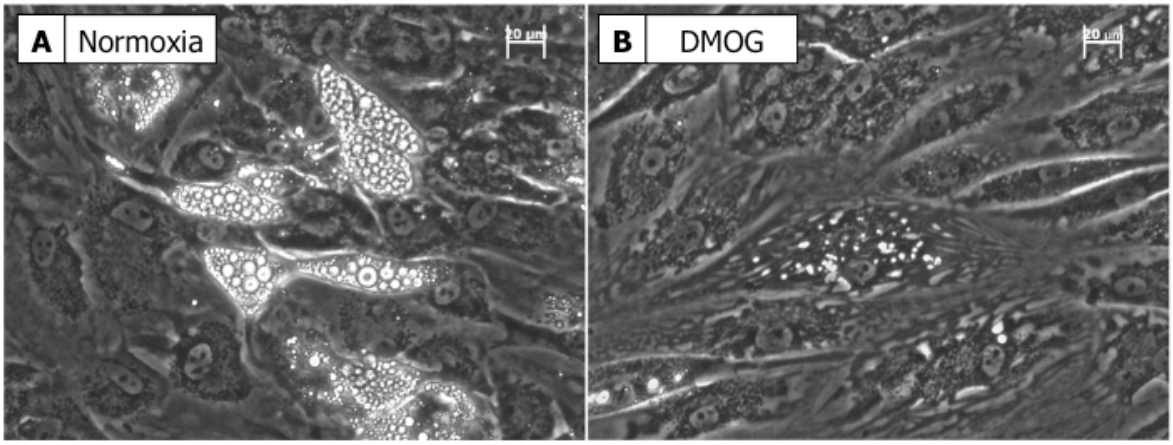

Figure 5.10. Effect of DMOG on the morphological changes of ASCs undergoing adipogenesis. The phase contrast microscopy photographs are of adipogenic-induced cells (**A**) and adipogenic-induced cells treated with 100 µM DMOG (**B**). Images were taken 14 days following adipogenic induction. Cells grown in adipogenic induction medium supplemented with 100 µM DMOG did not accrue lipids to the same extent as adipogenic differentiation in normoxic conditions. Very few tiny lipid droplets, if any, formed. The cytoplasm of the induced cells with DMOG appeared to be very complex compared to the induced cells in normoxic conditions. Donor sample: A220313 P7F1. Original magnification: 20x, scale bars: 20 µm.

Flow cytometric analysis of the accumulation of lipid droplets based on Nile red positive staining at day 14 of adipogenic induction

At day 14 of adipogenic induction, Nile red and DAPI staining were used to quantify lipid accumulation flow cytometrically. The ASCs grown in DMEM served as a gating control (Figure 5.11). The regions were set using day 14 of adipogenic differentiation in normoxic conditions and these regions were kept for analysis with DMOG supplementation. These regions were also kept for analysis of day 21 adipogenic differentiation for the same culture. Only viable ASCs were used in the analysis. Dead cells or cells undergoing necrosis have damaged cell membranes that were more permeable to DAPI. Fluorescent emissions of DAPI were detected in FL9, thus if the FL9 fluorescence intensity increased, the cell membrane was compromised and these cells were also counted as non-viable. Cell debris and non-viable cells, which are represented by low forward- and high side-scatter were gated out for analysis.

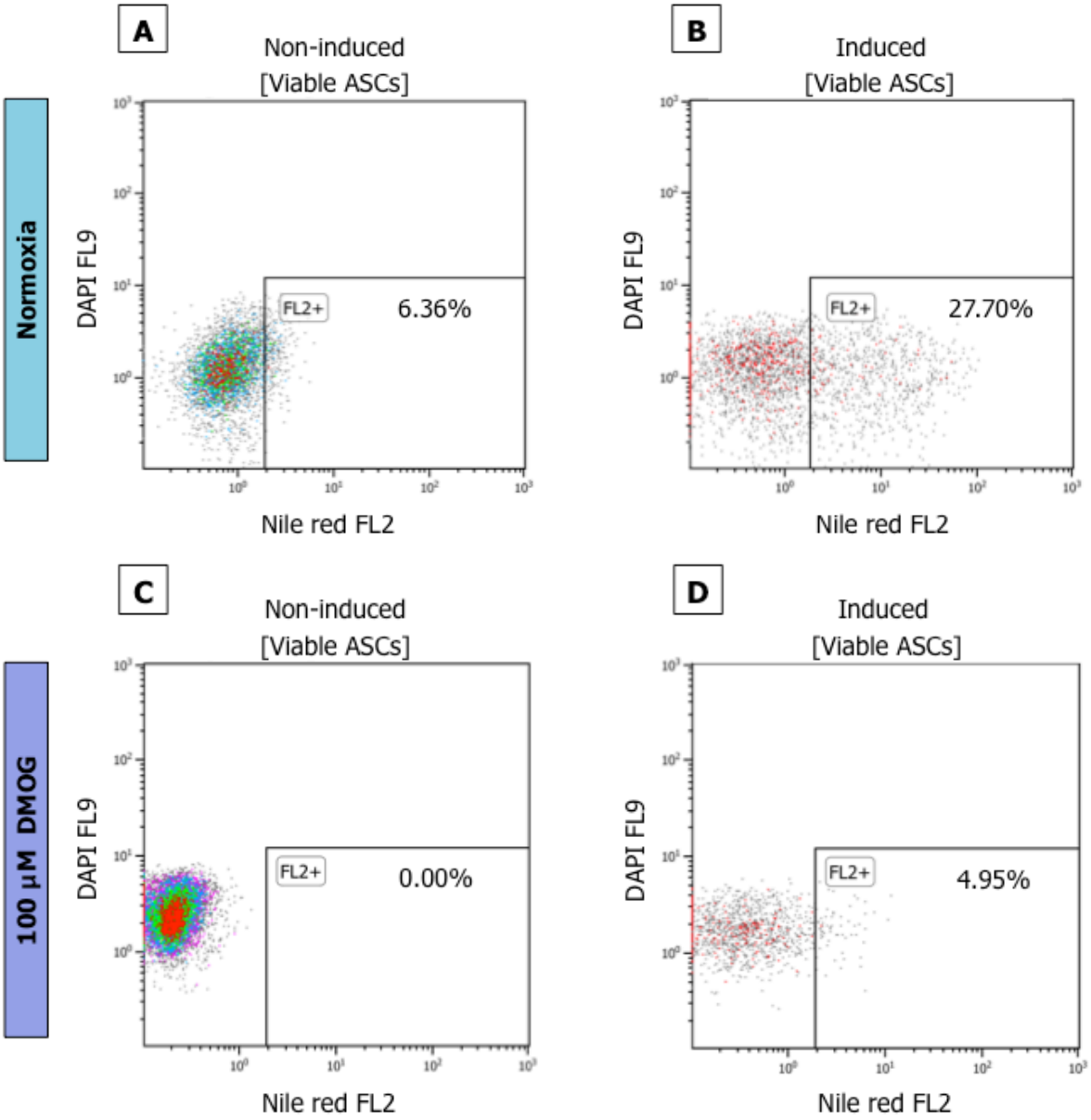

Figure 5.11. Strategy for flow cytometric analysis of adipogenesis. Representative two-parameter plots of DAPI and Nile red fluorescence. Regions were set according to the yellow-gold fluorescence of the non-induced Nile red stained ASCs at day 14 (**A**). These regions were used as gating controls to monitor the increase in yellow-gold fluorescence emitted by the Nile red stained adipogenic-induced ASCs (**B**). The rectangular regions indicate the percentage of events/cells that had accumulated lipids after Nile red staining. The differentiation potential varied between donor samples cultured in normoxia or treated with 100 µM of DMOG as observed in the rectangular region of B compared to the rectangular region in D. These are the results of ASCs grown in DMEM (Non-induced; **A**), adipogenic induction medium (**B**), DMEM treated with 100 µM of DMOG (Non-induced; **C**), and adipogenic induction medium with 100 µM of DMOG (**D**).

Visually, it appeared that treating adipogenic-differentiating cells with DMOG inhibited adipogenesis. It was observed following quantification of lipid accumulation by flow cytometry at day 14 of adipogenic induction that the adipose cocktail supplemented with DMOG did not have any affect on adipogenic differentiation compared to standard adipogenic differentiation. The mean percentage of adipogenic induced cells cultured in artificial hypoxia that upon staining with Nile red were positive for an increase in FL2 fluorescence was 11.81% ± 4.29%. This was not statistically different compared to the 17.24% ± 3.20% of Nile red positive cells cultured in normoxic adipogenic conditions (Figure 5.12). The following graph indicates the percentage of cells that emit yellow-gold fluorescence after Nile red staining after 14 days of induction. The mean fluorescence intensity (MFI) of the adipogenic-induced cells treated with DMOG was 1.73 ± 0.05 and the MFI of the adipogenic-induced cells in normoxia was 2.43 ± 0.33. These two fluorescence intensities were not significantly different.

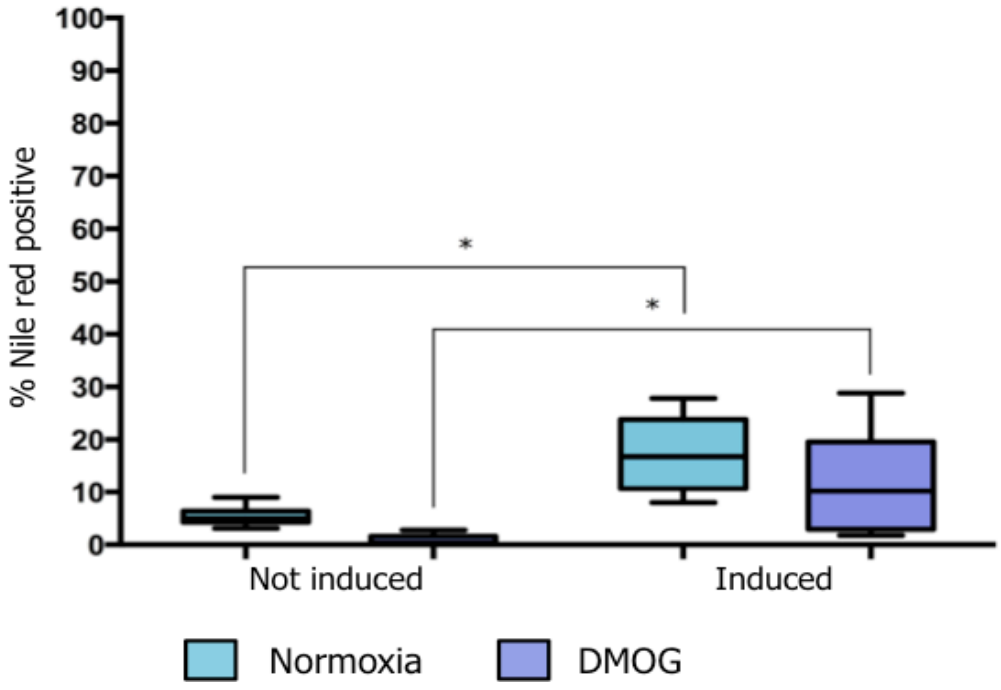

Figure 5.12. Percentage of cells that emit yellow-gold fluorescence after Nile red staining following 14 days of adipogenic induction. This graph indicates the percentage of cells that emit yellow-gold fluorescence after Nile red staining of early-passage, P7, thawed-cryopreserved ASCs at 14 days after adipogenic induction. The box of the box whisker plot extends from the 25th percentile to the 75th percentile. The line situated in the middle of the box represents the median. The lower whisker is the smallest percentage of cells that emitted yellow-gold fluorescence and the upper whisker is the largest percentage of cells that emitted yellow-gold fluorescence. The addition of DMOG

reduced Nile red staining. n = 2. There was no significant difference between the induced conditions. See Table 5.2 for all significance values.

Table 5.2. Statistical differences relating to Figure 5.12.

		Not induced		Induced	
		Normoxia	100 µM DMOG	Normoxia	100 µM DMOG
Not induced	Normoxia		ns	*	ns
	100 µM DMOG	ns		**	*
Induced	Normoxia	*	**		ns
	100 µM DMOG	ns	*	ns	

The data passed the normality test and the results of the Tukey's multiple comparisons test are represented in the above table. The mean difference is significant at the 0.05 level. *P<0,05 **P<0,01.

Flow cytometric analysis of the accumulation of lipid droplets based on lipid composition at day 14 of adipogenic induction

Nile Red emits yellow-gold fluorescence when dissolved in neutral lipids, while it fluoresces in the deep red spectrum when dissolved in amphipathic lipids such as cell membranes. During pre-adipocyte maturation a larger number of amphipathic lipids are formed upon the merging of the lipid droplets and their increase in size. This causes a correlated increase in deep red fluorescence and sub-populations of increasing lipid content can be determined. Visually, from Figure 5.13, there appears to be a decrease in the brighter deep red sub-populations with DMOG treatment. There was a significant (P<0.01) decrease in the FL2++/FL5+ sub-population that simultaneously emitted yellow-gold and deep red fluorescence upon DMOG treatment of adipogenic-induced cells compared to normoxic adipogenic-induced cells.

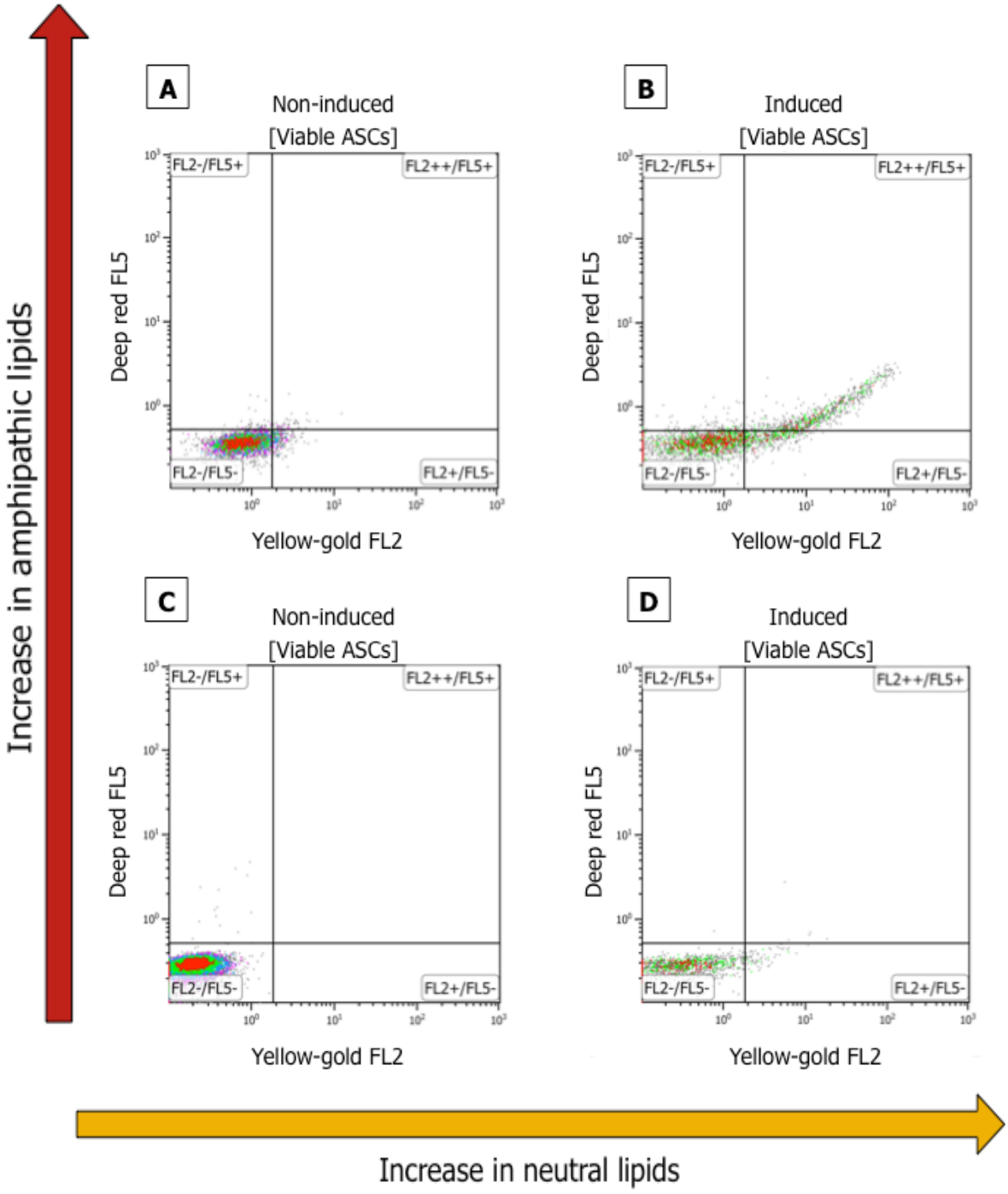

Figure 5.13. Accumulation of lipid droplets based on lipid composition. The x-axis reflected the increase in FL2 yellow-gold fluorescence and y-axis reflected the increase in FL5 deep red fluorescence emitted by cells. The increase in the simultaneous emission of deep red and yellow-gold fluorescence is indicative of the merging of lipid droplets and thus an accumulation of lipid content within the cells. Following standard adipogenic induction, the ASCs became increasingly more fluorescent in both FL2 and FL5 (FL2++/FL5+), as demonstrated in **B**. However, following adipogenic

induction in an artificial hypoxic environment it can be clearly seen that an increase in both FL2 and FL5 fluorescence (FL2++/FL5+) did not occur.

Flow cytometric analysis of the accumulation of lipid droplets based on Nile red positive staining at day 21 of adipogenic induction

ASCs were induced to differentiate into adipocytes under normoxic and artificial hypoxic conditions. After 21 days of culture in adipogenic differentiation medium with or without DMOG, the cells were stained with Nile red for quantification of lipid droplets. All of the non-induced ASCs resulted in low levels of staining, showing the absence of lipid droplets. The cells cultured in differentiation medium in normoxic conditions were positively stained with Nile red, indicating that 34.48% ± 6.88% of the cells had differentiated. The cells cultured in adipogenic differentiation medium in artificial hypoxic conditions demonstrated a reduced percentage (23.91% ± 7.74%) in cells positive for Nile red compared to standard adipogenic-induced cells but this reduction was not significant. There were no significant differences in the MFI of the adipogenic-induced Nile red stained cells under either artificial hypoxia or normoxia. The graph below indicates the percentage of cells that emit yellow gold fluorescence after Nile red staining following 21 days of induction (Figure 5.14). The addition of 100 μM of DMOG thus had no significant effect on adipogenic differentiation of ASCs compared to standard adipogenic differentiation. There was yet again a significant ($P<0.01$) decrease in the FL2++/FL5+ sub-population that simultaneously emitted yellow-gold and deep red fluorescence upon DMOG treatment of adipogenic-induced cells compared to normoxic adipogenic-induced cells.

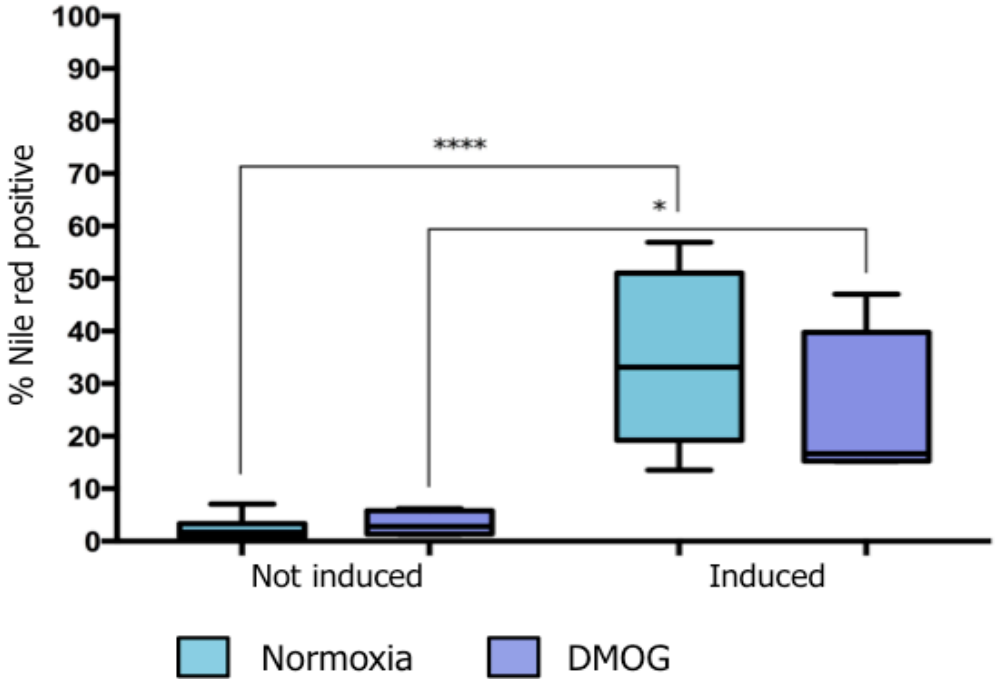

Figure 5.14. Percentage of cells that emit yellow-gold fluorescence after Nile red staining following 21 days of adipogenic induction. This graph indicates the percentage of cells that emit yellow-gold fluorescence after Nile red staining of early-passage, P8, P9 and P12, thawed-cryopreserved ASCs at 21 days after adipogenic induction. n = 2. There was no significant difference between the induced conditions. See Table 5.3 for all significance values.

Table 5.3. Statistical differences relating to Figure 5.14.

		Not induced		Induced	
		Normoxia	100 µM DMOG	Normoxia	100 µM DMOG
Not induced	Normoxia		ns	****	*
	100 µM DMOG	ns		***	*
Induced	Normoxia	****	***		ns
	100 µM DMOG	*	*	ns	

The data passed the normality test and the results of the Tukey's multiple comparisons test are represented in the above table. The mean difference is significant at the 0.05 level. $^{*}P<0.05$; $^{***}P<0.001$; $^{****}P<0.0001$.

Table 5.4. The % positive cells and MFI of non-induced and induced ASCs grown under normoxic and artificial hypoxic conditions that emitted yellow-gold fluorescence after staining with Nile red.

	% Nile red positive				MFI			
	Normoxia		DMOG		Normoxia		DMOG	
	Not induced	Induced	Not induced	Induced	Not induced	Induced	Not induced	Induced
Day 14	5.38% ± 0.80%	17.24% ± 3.20%	0.79% ± 0.45%	11.81% ± 4.29%	1.37 ± 0.03	2.43 ± 0.33	1.36 ± 0.03	1.73 ± 0.05
Day 21	2.43% ± 0.68%	34.48% ± 6.88%	3.36% ± 0.90%	23.91% ± 7.74%	1.34 ± 0.46	2.48 ± 0.23	1.43 ± 0.03	2.16 ± 0.12

Discussion

Human ASCs and bone-marrow-derived MSCs can be expanded to large numbers and have the ability to differentiate into cells of mesenchymal origin, for example, bone, cartilage, adipose, and muscle (33). The mechanisms underlying the commitment of these stromal/stem cells to a given differentiation lineage *in vivo* are not very clear. However, *in vitro*, it is known that for stromal cells to undergo lineage conversion the addition of selected chemicals, nutrients and growth factors is needed. The *in vitro* adipogenic differentiation protocol has been well established, utilizing dexamethasone, indomethacin, 3-isobutyl-1-methylxanthine, and insulin (36). Stem cells receive instructions from their niche. Cellular differentiation involves transcriptional responses due to stimulation from the environmental cues. Thus, it could be plausible that O_2 may modulate different differentiation pathways. The majority of *in vitro* differentiation experiments take place at an O_2 concentration (21%) that corresponds to that of ambient air. It is often over-looked that this concentration of O_2 far exceeds the physiological O_2 concentrations and is as such not adapted to *in vivo* niche scenarios. In this research, it was investigated whether the responses of ASCs during artificial hypoxia were compatible with changes associated with adipogenesis under normoxic conditions.

Effect of DMOG on ASC viability

Packer and Fuehr were the first to report in 1977 that low O_2 concentrations prolonged growth in culture of cells from a fibroblast cell line (37). What followed was attention

towards the role that O_2 played in cell culture and the cellular responses to hypoxia. At the centre of O_2 sensing and adaption to limited O_2 in cells was the transcription factor HIF (38). Investigators next identified the HIF hydroxylases, PHDs, and the O_2-dependent ability of these PHDs to posttranslationally modify HIF-α subunit (39). Current research indicates that a hydroxylase enzyme-ferrous iron (Fe^{2+}) complex forms and binds to 2-oxoglutarate, which is followed by binding to the HIF subunit. The binding of molecular O_2, or dioxygen, to this whole complex results in the hydroxylation of HIF and the oxidative decarboxylation of 2-oxoglutarate to give succinate and CO_2. Hydroxylation leads to the degradation of the HIF subunit. The increased understanding of O_2 sensing led to the creation of pharmacological manipulation of HIF in a dish. A 2-oxoglutarate-dependent dioxygenase PHD inhibitor, DMOG can be utilized to mimic the reduced hydroxylase activity in hypoxia.

Human ASCs with self-renewal and differentiation capabilities reside in poorly perfused niches and are therefore presumably hypoxic. Elvidge and colleagues revealed concordance in gene expression patterns induced by hypoxia and DMOG. This study underlined a similar mode of action for both hypoxia and DMOG and demonstrates that DMOG is an appropriate pharmacological manipulator of hypoxia (40). The effect of pharmacologic stabilization of HIF-1α with DMOG on ASC viability *in vitro* was investigated. Analysis of the current literature revealed that concentrations of 100 μM up to 1 mM of DMOG exhibited no cytotoxicity towards MSCs. However, increasing the DMOG concentration to 5 mM resulted in cytotoxicity (32). Liu and colleagues observed increasing expression of HIF-1α using 100 μM, 500 μM and 1 mM DMOG (32). Howard *et al*. examined the stabilization of HIF-1α at 10 μM, 100 μM and 1 mM concentrations of DMOG. They found that the effect of 100 μM of DMOG matched the effect of hypoxia the closest (41). Rey and colleagues deemed 100 μM DMOG in DMSO appropriate as a hypoxic mimic in bone-marrow-derived angiogenic cells (BMDACs). Ding and fellow researchers investigated concentrations of 200 μM, 500 μM, and 1 mM DMOG on cytotoxicity and found that there were no significant differences between the death ratio of cells with or without exposure to DMOG (42). An assessment of the influence of this concentration of DMOG or vehicle on ASC viability was performed using the SRB assay.

A concentration of 100 μM of DMOG did not affect cell growth and the addition of the vehicle, DMSO, also did not influence cell viability. Even over two passages, 100 μM DMOG

did not affect cell viability compared to untreated controls. The results indicated that DMOG at this concentration had no obvious cytotoxicity to the ASCs. Thus for this research a concentration of 100 μM of DMOG was chosen. Researchers have previously determined the influence of DMOG on ASC proliferation, by treating the cells with different concentrations of DMOG and measuring proliferation with cell proliferation and cytotoxicity assays such as Cell Counting Kit-8 (CCK-8). This kit is a colorimetric assay for the determination of cell viability in cell proliferation and cytotoxicity. Ding and colleagues found that ASC proliferation was significantly suppressed by 500 μM and 1 mM DMOG, but not by 200 μM DMOG after 48 and 72 hours of incubation. The hypoxia-mimetic agents, desferrioxamine (DFO) and cobalt chloride ($CoCl_2$), are said to inhibit umbilical cord-derived MSC proliferation by influencing the cell cycle (43). On the other hand, MSCs from mice cultured at 5% O_2 proliferated more *in vitro* and had higher DNA values compared to MSCs cultured at 21% O_2.

Adipose derived-stromal cell morphology under artificial hypoxia

The ASCs were grown in standard growth medium, α-MEM, or growth medium treated with 100 μM of DMOG over two passages. A number of studies have contradicting results regarding the morphology of MSCs grown in hypoxia or with hypoxia mimetics. Mesenchymal stromal/stem cells and ASCs contain two main morphologically distinct cells: spindle-shaped cells and flattened more rounded cells as described in Chapter 3 (44). Ren and colleagues looked at the morphology of cells grown in 8% O_2 and with the hypoxia mimetic, $CoCl_2$ until 70-80% confluence. Growth in 8% O_2 resulted in a decrease in the spindle-shaped cells, and the proportion of flat rounded cells greatly increased. On the other hand, treatment with $CoCl_2$ resulted in small spindle-like cells with almost complete disappearance of the flat rounded cells (45). Holzwarth and colleagues looked at the morphology of MSCs in both normoxic and hypoxic conditions over 3 weeks. One donor sample cultured in 1% O_2 did not exhibit any distinct morphological changes compared to normoxia, but the second donor sample died after a week of exposure to 1% O_2 (22). They have suggested that this outcome could be due to donor-specific genetics. The study by Zeng and colleagues, mentioned in the above section, used $CoCl_2$ and DFO and assessed the effect on morphology. Following treatment, with both of the hypoxia mimetic agents, the spindle-like cells elongated and cell-to-cell contacts diminished (43). In the study presented herein both spindle-shaped and the flatter more round cells were observed in the cultures treated with 100 μM of DMOG. There were no differences in morphology observed between ASCs

cultured in normoxia or treated with DMOG throughout the two passages. Death of a whole culture treated with DMOG did not occur, although donor-specific differences were observed.

Multi-colour flow-cytometric analysis of immunophenotype of adipose-derived stromal cells grown under conditions of artificial hypoxia

The immunophenotype of ASCs is characterized by the expression of CD73 (also known as ecto-5'-nucleotidase), CD90 (a membrane glycoprotein, also called Thy-1), and CD105 (Endoglin; a proliferation-associated protein) as well as the lack of expression of CD34 (hematopoietic progenitor marker) and CD45 (hematopoietic marker). The criteria required for MSCs and ASCs regarding immunophenotype is ≥95% of the cells must express CD73, CD90, and CD105 and ≤2% of the total population may be positive for CD34 and CD45.

Positive staining in normoxic conditions was established by comparison to unstained samples. This staining was then compared to the positive staining in artificial hypoxic conditions. Overlay plots for all the selected surface markers were generated. The percentage of cells staining positive for CD73, CD90, and CD105 surface markers was >95% as recommended. ASCs cultured in artificial hypoxia also lacked the expression of CD34 and CD45. Thus it appears that artificial hypoxia does not have an effect on the immunophenotype of ASCs. Figure 5.7 reveals a decrease in the number of cells expressing CD34 and CD45 with DMOG treatment. It is not significant in this study but previous research suggests that hypoxic conditions decreased the number of cells that expressed hematopoietic markers (46). According to Holzwarth and colleagues, 1% O_2 did not alter the phenotype of MSCs compared to 20% O_2 following 14 days of culture (22). Thus the consensus appears to be that artificial hypoxic conditions do not alter the classical CD73+CD90+CD105+CD34-CD45- ASC phenotype, but may reduce hematopoietic marker expression.

In vivo models have shown that MSCs' beneficial effects tend to be immunomodulatory and through paracrine and autocrine signaling. Transplanting MSCs into ischemic tissues, tissues with a lack in blood supply and thus a deficiency in oxygen, is said to enhance their tissue repair potential due to increased viability as well as to modulate their signaling (47). Interest has peaked in hypoxic research due to the finding that exposure to hypoxia, and even hypoxia mimetics, upregulates the expression of receptors for stromal-derived factor-1 (SDF-

1), such as CXCR4 and CXCR7 (48, 49). These receptors are said to be involved in enhancing MSC migration, adhesion and survival. Ischemia is proposed to be one of the areas to greatly benefit from MSC tissue regenerative capacities and wound healing. Hypoxia and the SDF-1 receptors could be an area of further research in our group.

Fibroblastoid colony-forming unit assay

Terminally differentiated cells are replaced following cell death through the proliferation of progenitor or stem cells. The CFU-F assay is used to define the number of progenitor cells. Adult stromal cells are characterized by a number of properties one of which is the ability to form colonies from single cells (35, 50). The plastic-adherent ASCs were plated in triplicate at 100 cells per dish. At 13 days, the tissue culture dishes were washed with PBS and stained with Toluidine Blue O for colony enumeration. Bourin and colleagues consider a group of >50 cells to be a colony. The frequency of ASCs able to form colonies should be greater than 5%. Both normoxic untreated ASCs and DMOG-treated ASCs demonstrated a frequency to form colonies greater than 5%.

Heterogeneous morphology is known to occur commonly in ASC populations. Mets and Verdonk used cloning experiments and microscopy to distinguish between two different cell types, spindle-shaped cells and what they call epithelial-like cells, which are more squamous in shape (51). Colter, Sekiya and Prockop noted the two cell types: spindle-shaped cells and large flat cells. They also identified a third morphologically distict cell in early colonies that were very small and round. These cells would undergo rapid self-renewal (44). The following year Sekiya and colleagues classified the spindle-shaped MSCs into three categories: thin spindle-shaped cells; wider, spindle-shaped cells; and still wider, spindle-shaped cells (52). ASCs plated at a standard seeding density of 5 x 10^3 cells/cm^2 and treated with 100 μM DMOG for donor culture A220313 at P4F1 displayed both the spindle-shaped cells as well as the more squamous cells seen in normoxic conditions. Seeding the same donor culture ASCs (A220313 but at P3F1) at an average cell density of 1.72 cells/cm^2 (100 cells) and treating the cells with 100 μM DMOG for 13 days, appeared to give rise to colonies consisting of a small number of cells that were for the majority small, more squamous-shaped and sparsely distributed. Previously published results suggest that these small cells have favoured clonogenic ability (53). The discrepancy in cell number within a colony between our results and the literature could be due to the difference between the use of hypoxia and artificial

hypoxia. Tamama *et al*. discovered that the hypoxia-mediated increase of MSC colony formation was not dependent HIF-1α, HIF-2α, and HIF-1β (54). Treatment with DMOG in normoxic conditions stabilizes HIF, therefore, perhaps clonogenicity is in response to HIF-independent mechanisms. Stem cells are said to reside in low oxygen niches (16), and this may protect them from some degree of oxidative damage during aerobic metabolism. Ezachi *et al.* found that 3 - 5% O_2 maintained pluripotency with no effect on proliferation, while reducing the O_2 tension to 1% maintained pluripotency, but significantly reduced proliferation. In the context of the niche, the conservation of stemness and low telomere shortening of the stem cells would be ideal for maintenance of the tissue (55).

Effect of artificial hypoxia on adipogenic differentiation of adipose-derived stromal cells

Oxygen is a crucial regulator during embryonic development; thus, it is likely that it is an important regulator in other aspects of development, such as differentiation of stromal cells. An interesting fact is that around 1%, possibly 1.5%, of the human genome is regulated by hypoxia (56). Cultures grown under standard conditions (21% O_2) are exposed to significantly higher concentrations of O_2 than physiological concentrations. Interest in hypoxia and stem cells arose when evidence suggested that hypoxia maintained embryonic stem cells in an undifferentiated state but normoxic conditions caused the cells to spontaneously differentiate (55). Research has shown that hematopoietic stem cells (HSCs) remain in a quiescent state under hypoxic conditions (57). It has been suggested that physiologically low oxygen concentrations favour stemness over differentiation of stromal cells (23).

Adipogenic differentiation is one of three main differentiation pathways used to characterize ASCs. The presence of low O_2 concentrations *in vivo*, within adipose tissue, motivated our investigation into the adipogenic differentiation capacity of ASCs under artificial hypoxic and normoxic conditions. In order to initiate differentiation, ASCs were treated with standard adipogenic medium. The accumulation of intracellular lipid was detected by Nile red staining and flow cytometry. All of the cultures induced to undergo adipogenic differentiation in normoxic conditions were able to differentiate down the adipose lineage over a period of both 14 and 21 days. Following adipogenic induction in normoxia, the morphology of the ASCs undertook the typical changes observed normally with adipogenic differentiation. The

spindle-shaped cells became more oval and acquired small lipid droplets, which grew in both size and number over the differentiation period. Adipogenic differentiation was comparatively carried out under artificial hypoxic conditions. These cells from the same cultures, visually, had a limited ability to differentiate. The majority of the DMOG-treated adipogenic differentiated cells did not contain lipid droplets; however the cells in Figure 5.10 contained a few unidentified vacuoles. The cytoplasm was very complex compared to the adipogenic-differentiated cells cultured in normoxia.

Low oxygen concentrations are an important aspect of the proposed MSC niche. D'Ippolito and colleagues cultured MSCs in low oxygen concentrations (3% O_2) as well as ambient O_2 concentration (21%). They demonstrated that this low concentration of O_2 inhibited osteoblastic differentiation and embryonic stem cell markers were upregulated and maintained throughout the culture period. They propose that MSCs self-renew while situated in areas of low O_2 concentration in the bone marrow, but tend to differentiate toward osteoblasts when they are located closer to blood vessels and thus exposed to higher O_2 concentrations (23). Cicione *et al*. demonstrated that hypoxia (1% O_2) resulted in complete inhibition of adipogenic differentiation of MSCs. Differentiation into the other two lineages, bone and cartilage, was also inhibited (58). Holzwarth and colleagues also showed that the ability of MSCs to differentiate into adipocytes was impaired at 1% O_2. At 1% O_2 osteogenesis was inhibited completely. An increase in O_2 concentration to 3% restored osteogenesis (22). Yun and colleagues state that hypoxia (0.01% or 2%) as well as $CoCl_2$ and DFO inhibited the conversion of 3T3-L1 preadipocytes into adipocytes upon addition of adipogenic medium. This was found to be due to hypoxic-inhibition of peroxisome proliferator-activated receptor (PPAR)γ-2 (59). Another study found that hypoxia (1% O_2) suppresses adipogenesis of MSCs in a HIF-1-dependent manner (27).

These results suggest that low oxygen concentrations maintain stromal cells in a less differentiated state. However, contradictory results involving adipogenic differentiation using low O_2 concentrations have been published. Grayson *et al*. found that long-term three-dimensional (3D) cultures under hypoxic (2%) conditions increased adipogenic differentiation. An O_2 concentration of 2% significantly increased lipid accumulation in ASCs compared to 20% and 5% O_2 according to Kim and colleagues (26). Valorani *et al*. cultured adipogenic induced MSCs in 2% hypoxia for 3 weeks and found that adipogenic differentiation was inhibited, however, pre-conditioning the MSCs with 2% hypoxia for 10

days prior adipogenic induction resulted in an increase in adipogenesis (60). Mylotte and fellow researchers used 0.5% hypoxia and found that adipogenic differentiation potential was maintained in rat MSCs; however, Oil red O photometric quantification demonstrated that adipogenesis was decreased compared to normoxic controls (61).

As described, there are those studies that claim hypoxia promotes adipogenic differentiation and others that suggest that hypoxia suppresses, but there are also studies that mention hypoxia has no effect on adipogenic differentiation. Tsai and colleagues reported that hypoxia maintained MSC tri-lineage differentiation capabilities (24). Another study demonstrated that hypoxia (2%) also maintained the MSCs' differentiation abilities (62). Mesenchymal stromal cells were subjected to 1.5% O_2 for 24 hours before adipogenic differentiation and following 21 days the cells maintained adipogenic differentiation (63).

Regarding the adipogenesis results in this study, adipogenic differentiation took place at day 14 and at day 21 of induction, and although it appeared that this potential was reduced there were no significant differences compared to normoxic induced cultures at these two time points. This is likely due to the number of biological replicates used. There was a significant decrease in the simultaneous emission of yellow-gold and deep red fluorescence (FL2++/FL5+), indicative of larger droplets, following Nile red staining at 14 and 21 days upon comparison to this sub-population in normoxic induced cells. It has been shown previously that the lipid droplets that form are small in size compared to the lipid droplets that form under normoxia (64). An observation by Fink *et al*. was that upon exposure to 1% O_2 during adipogenic differentiation, the formation of the adipocyte phenotype with lipid droplets occurred. An interesting finding was that despite lipid accumulation, there was a lack in adipocyte-specific transcription patterns (64). It will be worth exploring whether the ASCs induced with adipogenic differentiation and treated with 100 μM DMOG display a similar transcription pattern. Ren *et al*. looked at the expression of octamer-binding transcription factor 4 (Oct4), a marker for undifferentiated cells. This factor was inhibited under 8% O_2, but following adipocyte differentiation in normoxic culture or with hypoxia-mimetic agents, $CoCl_2$ and DFX, it was still expressed in MSCs. They explain that differing results in MSC differentiation may be due to differing effects between hypoxia and hypoxia-mimetics on MSC differentiation (45). It appears that HIF-1 is an important mechanism for the inhibition of adipogenic differentiation by hypoxia (65). There are, however, mechanisms

for hypoxic gene regulation that do not require hydroxylation or are HIF-1 independent (66). There is still much to be discovered in the arena of adipose differentiation.

The contradictory results can also possibly be explained by the type of culture used, such as 3D design or monolayer, differences in culture conditions, such as medium used, glucose and serum supplementation, the method and period of adipogenic differentiation. The O_2 concentrations used, the time points evaluated, chronic or pre-conditioning with hypoxia, as well as the assortment of stromal cells used; the different tissues sources (bone marrow, adipose tissue, umbilical cord) and even the different species involved, could have an influence on the outcome. Perhaps different sub-populations within the ASC/MSC population, which are more primitive or have greater plasticity exist, and conditioning the cells with hypoxia or hypoxia-mimetics selects for these sub-populations differently. Finally, the detection method, such as histochemical staining, flow cytometric quantification or gene expression quantification, could also have an effect on the sensitivity of the results.

Conclusion

Oxygen is an effective signaling molecule that is gaining increasing recognition for its role in determining the fate of stem cells. Simon and Keith revealed that O_2 is imperative in embryonic development and in regulating stem cell behavior (67). It appears from the literature that oxygen tensions of approximately 1% O_2 maintain the earliest progenitor cells when culturing HSCs and increasing the oxygen tension to approximately 5% leads to hematopoiesis (57, 68). The stem cell niche is said to maintain the proliferative or multipotent capabilities of stem cells, and differentiation down specific lineages coincides with the migration of these stem cells out of the niche. Niches vary in O_2 tension. The O_2 tension within the bone marrow has been extensively studied and ranges from 1 to 7%. *In vivo* measurements in adipose tissue have shown that the O_2 tension tends to range between 2% and 8%. The confusion that exists about the role that hypoxia and the stabilization of HIF-1α play in adipogenic differentiation, as well as a deficit in experimentation with DMOG in ASC adipogenic differentiation, led to the question of what effect artificial hypoxia would have on the adipogenic differentiation potential of ASCs? The O_2 tension that is equivalent to a known concentration of DMOG could not be found in literature.

Fatty acid metabolism requires mitochondrial respiration. It was proposed that hypoxia would limit fatty acid usage and the formation of any additional adipose tissue (67). High O_2 tension can be toxic, due to the transfer of electrons to O_2 leading to excessive oxidative stress and damage to DNA, protein, and lipids. Thus it was suspected that hypoxia might decrease the accumulation of reactive oxygen species (ROS). It was considered that the decrease in oxygen and ROS that occurs with hypoxia may decrease/inhibit adipogenic differentiation. In light of these facts, the hypothesis that hypoxia would inhibit adipogenesis arose. Instead of low O_2 concentrations, the hypoxia mimetic and HIF stabilizer, DMOG was used. Adipose derived-stromal cells were induced to differentiate into adipocytes under normoxic and artificial hypoxic conditions. The involvement of artificial hypoxia in ASC adipogenic differentiation is not well understood.

The addition of DMOG, resulted in a clear trend towards the reduction in adipogenesis over the 14 and 21-day induction periods. Some of the experiments did not result in statistically significant differences. This is likely to change as the number of replicates is increased beyond two. Thus, it was tentatively concluded for the present study that the treatment of adipogenic differentiating cells with 100 μM of DMOG had no effect compared to standard adipogenic differentiation. A role for HIF-independent regulation of adipogenic differentiation is also plausible. There are several limitations to the present study. Firstly, this study only analyzed the effects of the hypoxia mimetic, DMOG, on ASCs. The effects of low O_2 concentration (physiological hypoxia) were not assessed. The O_2 concentration equivalent to 100 μM of DMOG is unknown. Lastly, more biological replicates are required. Future research needs to assess the effect of DMOG on HIF-1α stabilization using Western blotting. Complimentary studies on gene expression both for HIF-regulated genes and genes implicated in adipogenesis will need to be carried out in future studies. The conflicting results in the literature regarding the regulation of adipogenesis by hypoxia underscores the importance for future research to assess the effects of both hypoxia and artificial hypoxia on adipogenesis at a gene and protein level.

References

1. Priestley JH, W. Observations on different kinds of air. Phil Trans. 1772;62:147-264.
2. Iyer NV, Kotch LE, Agani F, Leung SW, Laughner E, Wenger RH, et al. Cellular and developmental control of O2 homeostasis by hypoxia-inducible factor 1 alpha. Genes & development. 1998;12(2):149-62.
3. Ryan HE, Lo J, Johnson RS. HIF-1 alpha is required for solid tumor formation and embryonic vascularization. The EMBO journal. 1998;17(11):3005-15.
4. Morriss GM, New DA. Effect of oxygen concentration on morphogenesis of cranial neural folds and neural crest in cultured rat embryos. Journal of embryology and experimental morphology. 1979;54:17-35.
5. Ivan M, Kondo K, Yang H, Kim W, Valiando J, Ohh M, et al. HIFalpha targeted for VHL-mediated destruction by proline hydroxylation: implications for O2 sensing. Science. 2001;292(5516):464-8.
6. Yu F, White SB, Zhao Q, Lee FS. HIF-1alpha binding to VHL is regulated by stimulus-sensitive proline hydroxylation. Proceedings of the National Academy of Sciences of the United States of America. 2001;98(17):9630-5.
7. Jaakkola P, Mole DR, Tian YM, Wilson MI, Gielbert J, Gaskell SJ, et al. Targeting of HIF-alpha to the von Hippel-Lindau ubiquitylation complex by O2-regulated prolyl hydroxylation. Science. 2001;292(5516):468-72.
8. Bruick RK, McKnight SL. A conserved family of prolyl-4-hydroxylases that modify HIF. Science. 2001;294(5545):1337-40.
9. Lando D, Peet DJ, Gorman JJ, Whelan DA, Whitelaw ML, Bruick RK. FIH-1 is an asparaginyl hydroxylase enzyme that regulates the transcriptional activity of hypoxia-inducible factor. Genes & development. 2002;16(12):1466-71.
10. Lando D, Peet DJ, Whelan DA, Gorman JJ, Whitelaw ML. Asparagine hydroxylation of the HIF transactivation domain a hypoxic switch. Science. 2002;295(5556):858-61.
11. Maxwell PH, Wiesener MS, Chang GW, Clifford SC, Vaux EC, Cockman ME, et al. The tumour suppressor protein VHL targets hypoxia-inducible factors for oxygen-dependent proteolysis. Nature. 1999;399(6733):271-5.
12. Lando D, Gorman JJ, Whitelaw ML, Peet DJ. Oxygen-dependent regulation of hypoxia-inducible factors by prolyl and asparaginyl hydroxylation. Eur J Biochem. 2003;270(5):781-90.
13. Schofield R. The relationship between the spleen colony-forming cell and the haemopoietic stem cell. Blood cells. 1978;4(1-2):7-25.
14. Jiang Y, Jo AY, Graff JM. SnapShot: adipocyte life cycle. Cell. 2012;150(1):234- e2.
15. Pasarica M, Sereda OR, Redman LM, Albarado DC, Hymel DT, Roan LE, et al. Reduced adipose tissue oxygenation in human obesity: evidence for rarefaction, macrophage chemotaxis, and inflammation without an angiogenic response. Diabetes. 2009;58(3):718-25.
16. Matsumoto A, Matsumoto S, Sowers AL, Koscielniak JW, Trigg NJ, Kuppusamy P, et al. Absolute oxygen tension (pO(2)) in murine fatty and muscle tissue as determined by EPR. Magn Reson Med. 2005;54(6):1530-5.

17. Harrison JS, Rameshwar P, Chang V, Bandari P. Oxygen saturation in the bone marrow of healthy volunteers. Blood. 2002;99(1):394.
18. Ishikawa Y, Ito T. Kinetics of hemopoietic stem cells in a hypoxic culture. European journal of haematology. 1988;40(2):126-9.
19. Chow DC, Wenning LA, Miller WM, Papoutsakis ET. Modeling pO(2) distributions in the bone marrow hematopoietic compartment. II. Modified Kroghian models. Biophysical journal. 2001;81(2):685-96.
20. Genbacev O, Zhou Y, Ludlow JW, Fisher SJ. Regulation of human placental development by oxygen tension. Science. 1997;277(5332):1669-72.
21. Fehrer C, Brunauer R, Laschober G, Unterluggauer H, Reitinger S, Kloss F, et al. Reduced oxygen tension attenuates differentiation capacity of human mesenchymal stem cells and prolongs their lifespan. Aging cell. 2007;6(6):745-57.
22. Holzwarth C, Vaegler M, Gieseke F, Pfister SM, Handgretinger R, Kerst G, et al. Low physiologic oxygen tensions reduce proliferation and differentiation of human multipotent mesenchymal stromal cells. BMC cell biology. 2010;11:11.
23. D'Ippolito G, Diabira S, Howard GA, Roos BA, Schiller PC. Low oxygen tension inhibits osteogenic differentiation and enhances stemness of human MIAMI cells. Bone. 2006;39(3):513-22.
24. Tsai CC, Chen YJ, Yew TL, Chen LL, Wang JY, Chiu CH, et al. Hypoxia inhibits senescence and maintains mesenchymal stem cell properties through down-regulation of E2A-p21 by HIF-TWIST. Blood. 2011;117(2):459-69.
25. Lennon DP, Edmison JM, Caplan AI. Cultivation of rat marrow-derived mesenchymal stem cells in reduced oxygen tension: effects on in vitro and in vivo osteochondrogenesis. Journal of cellular physiology. 2001;187(3):345-55.
26. Kim JH, Kim SH, Song SY, Kim WS, Song SU, Yi T, et al. Hypoxia induces adipocyte differentiation of adipose-derived stem cells by triggering reactive oxygen species generation. Cell Biol Int. 2014;38(1):32-40.
27. Wagegg M, Gaber T, Lohanatha FL, Hahne M, Strehl C, Fangradt M, et al. Hypoxia promotes osteogenesis but suppresses adipogenesis of human mesenchymal stromal cells in a hypoxia-inducible factor-1 dependent manner. PloS one. 2012;7(9):e46483.
28. Beresford JN, Bennett JH, Devlin C, Leboy PS, Owen ME. Evidence for an inverse relationship between the differentiation of adipocytic and osteogenic cells in rat marrow stromal cell cultures. Journal of cell science. 1992;102 (Pt 2):341-51.
29. Dorheim MA, Sullivan M, Dandapani V, Wu X, Hudson J, Segarini PR, et al. Osteoblastic gene expression during adipogenesis in hematopoietic supporting murine bone marrow stromal cells. Journal of cellular physiology. 1993;154(2):317-28.
30. Ross SE, Hemati N, Longo KA, Bennett CN, Lucas PC, Erickson RL, et al. Inhibition of adipogenesis by Wnt signaling. Science. 2000;289(5481):950-3.
31. Chandel NS, McClintock DS, Feliciano CE, Wood TM, Melendez JA, Rodriguez AM, et al. Reactive oxygen species generated at mitochondrial complex III stabilize hypoxia-inducible factor-1alpha during hypoxia: a mechanism of O2 sensing. The Journal of biological chemistry. 2000;275(33):25130-8.

32. Liu XB, Wang JA, Ogle ME, Wei L. Prolyl hydroxylase inhibitor dimethyloxalylglycine enhances mesenchymal stem cell survival. Journal of cellular biochemistry. 2009;106(5):903-11.
33. Pittenger MF, Mackay AM, Beck SC, Jaiswal RK, Douglas R, Mosca JD, et al. Multilineage potential of adult human mesenchymal stem cells. Science. 1999;284(5411):143-7.
34. Dominici M, Le Blanc K, Mueller I, Slaper-Cortenbach I, Marini F, Krause D, et al. Minimal criteria for defining multipotent mesenchymal stromal cells. The International Society for Cellular Therapy position statement. Cytotherapy. 2006;8(4):315-7.
35. Bourin P, Bunnell BA, Casteilla L, Dominici M, Katz AJ, March KL, et al. Stromal cells from the adipose tissue-derived stromal vascular fraction and culture expanded adipose tissue-derived stromal/stem cells: a joint statement of the International Federation for Adipose Therapeutics and Science (IFATS) and the International Society for Cellular Therapy (ISCT). Cytotherapy. 2013;15(6):641-8.
36. Janderova L, McNeil M, Murrell AN, Mynatt RL, Smith SR. Human mesenchymal stem cells as an in vitro model for human adipogenesis. Obes Res. 2003;11(1):65-74.
37. Packer L, Fuehr K. Low oxygen concentration extends the lifespan of cultured human diploid cells. Nature. 1977;267(5610):423-5.
38. Semenza GL. HIF-1, O(2), and the 3 PHDs: how animal cells signal hypoxia to the nucleus. Cell. 2001;107(1):1-3.
39. Epstein AC, Gleadle JM, McNeill LA, Hewitson KS, O'Rourke J, Mole DR, et al. C. elegans EGL-9 and mammalian homologs define a family of dioxygenases that regulate HIF by prolyl hydroxylation. Cell. 2001;107(1):43-54.
40. Elvidge GP, Glenny L, Appelhoff RJ, Ratcliffe PJ, Ragoussis J, Gleadle JM. Concordant regulation of gene expression by hypoxia and 2-oxoglutarate-dependent dioxygenase inhibition: the role of HIF-1alpha, HIF-2alpha, and other pathways. The Journal of biological chemistry. 2006;281(22):15215-26.
41. Howard LS, Crosby A, Vaughan P, Sobolewski A, Southwood M, Foster ML, et al. Distinct responses to hypoxia in subpopulations of distal pulmonary artery cells contribute to pulmonary vascular remodeling in emphysema. Pulm Circ. 2012;2(2):241-9.
42. Ding H, Gao YS, Wang Y, Hu C, Sun Y, Zhang C. Dimethyloxaloylglycine increases the bone healing capacity of adipose-derived stem cells by promoting osteogenic differentiation and angiogenic potential. Stem cells and development. 2014;23(9):990-1000.
43. Zeng HL, Zhong Q, Qin YL, Bu QQ, Han XA, Jia HT, et al. Hypoxia-mimetic agents inhibit proliferation and alter the morphology of human umbilical cord-derived mesenchymal stem cells. BMC cell biology. 2011;12:32.
44. Colter DC, Sekiya I, Prockop DJ. Identification of a subpopulation of rapidly self-renewing and multipotential adult stem cells in colonies of human marrow stromal cells. Proceedings of the National Academy of Sciences of the United States of America. 2001;98(14):7841-5.

45. Ren H, Cao Y, Zhao Q, Li J, Zhou C, Liao L, et al. Proliferation and differentiation of bone marrow stromal cells under hypoxic conditions. Biochemical and biophysical research communications. 2006;347(1):12-21.
46. Buravkova LB, Anokhina EB. Effect of hypoxia on stromal precursors from rat bone marrow at the early stage of culturing. Bull Exp Biol Med. 2007;143(4):411-3.
47. Hu X, Yu SP, Fraser JL, Lu Z, Ogle ME, Wang JA, et al. Transplantation of hypoxia-preconditioned mesenchymal stem cells improves infarcted heart function via enhanced survival of implanted cells and angiogenesis. The Journal of thoracic and cardiovascular surgery. 2008;135(4):799-808.
48. Hung SC, Pochampally RR, Hsu SC, Sanchez C, Chen SC, Spees J, et al. Short-term exposure of multipotent stromal cells to low oxygen increases their expression of CX3CR1 and CXCR4 and their engraftment in vivo. PloS one. 2007;2(5):e416.
49. Liu H, Xue W, Ge G, Luo X, Li Y, Xiang H, et al. Hypoxic preconditioning advances CXCR4 and CXCR7 expression by activating HIF-1alpha in MSCs. Biochemical and biophysical research communications. 2010;401(4):509-15.
50. Friedenstein AJ, Gorskaja JF, Kulagina NN. Fibroblast precursors in normal and irradiated mouse hematopoietic organs. Experimental hematology. 1976;4(5):267-74.
51. Mets T, Verdonk G. In vitro aging of human bone marrow derived stromal cells. Mechanisms of ageing and development. 1981;16(1):81-9.
52. Sekiya I, Larson BL, Smith JR, Pochampally R, Cui JG, Prockop DJ. Expansion of human adult stem cells from bone marrow stroma: conditions that maximize the yields of early progenitors and evaluate their quality. Stem Cells. 2002;20(6):530-41.
53. Dos Santos F, Andrade PZ, Boura JS, Abecasis MM, da Silva CL, Cabral JM. Ex vivo expansion of human mesenchymal stem cells: a more effective cell proliferation kinetics and metabolism under hypoxia. Journal of cellular physiology. 2010;223(1):27-35.
54. Tamama K, Kawasaki H, Kerpedjieva SS, Guan J, Ganju RK, Sen CK. Differential roles of hypoxia inducible factor subunits in multipotential stromal cells under hypoxic condition. Journal of cellular biochemistry. 2011;112(3):804-17.
55. Ezashi T, Das P, Roberts RM. Low O2 tensions and the prevention of differentiation of hES cells. Proceedings of the National Academy of Sciences of the United States of America. 2005;102(13):4783-8.
56. Hill RP, Marie-Egyptienne DT, Hedley DW. Cancer stem cells, hypoxia and metastasis. Semin Radiat Oncol. 2009;19(2):106-11.
57. Cipolleschi MG, Dello Sbarba P, Olivotto M. The role of hypoxia in the maintenance of hematopoietic stem cells. Blood. 1993;82(7):2031-7.
58. Cicione C, Muinos-Lopez E, Hermida-Gomez T, Fuentes-Boquete I, Diaz-Prado S, Blanco FJ. Effects of severe hypoxia on bone marrow mesenchymal stem cells differentiation potential. Stem Cells Int. 2013;2013:232896.
59. Yun Z, Maecker HL, Johnson RS, Giaccia AJ. Inhibition of PPAR gamma 2 gene expression by the HIF-1-regulated gene DEC1/Stra13: a mechanism for regulation of adipogenesis by hypoxia. Developmental cell. 2002;2(3):331-41.
60. Valorani MG, Montelatici E, Germani A, Biddle A, D'Alessandro D, Strollo R, et al. Pre-culturing human adipose tissue mesenchymal stem cells under hypoxia increases

their adipogenic and osteogenic differentiation potentials. Cell proliferation. 2012;45(3):225-38.

61. Mylotte LA, Duffy AM, Murphy M, O'Brien T, Samali A, Barry F, et al. Metabolic flexibility permits mesenchymal stem cell survival in an ischemic environment. Stem Cells. 2008;26(5):1325-36.
62. Grayson WL, Zhao F, Bunnell B, Ma T. Hypoxia enhances proliferation and tissue formation of human mesenchymal stem cells. Biochemical and biophysical research communications. 2007;358(3):948-53.
63. Martin-Rendon E, Hale SJ, Ryan D, Baban D, Forde SP, Roubelakis M, et al. Transcriptional profiling of human cord blood CD133+ and cultured bone marrow mesenchymal stem cells in response to hypoxia. Stem Cells. 2007;25(4):1003-12.
64. Fink T, Abildtrup L, Fogd K, Abdallah BM, Kassem M, Ebbesen P, et al. Induction of adipocyte-like phenotype in human mesenchymal stem cells by hypoxia. Stem Cells. 2004;22(7):1346-55.
65. Lin Q, Lee YJ, Yun Z. Differentiation arrest by hypoxia. The Journal of biological chemistry. 2006;281(41):30678-83.
66. Lee CY, Yeh TL, Hughes BT, Espenshade PJ. Regulation of the Sre1 hypoxic transcription factor by oxygen-dependent control of DNA binding. Molecular cell. 2011;44(2):225-34.
67. Simon MC, Keith B. The role of oxygen availability in embryonic development and stem cell function. Nature reviews Molecular cell biology. 2008;9(4):285-96.
68. Mostafa SS, Miller WM, Papoutsakis ET. Oxygen tension influences the differentiation, maturation and apoptosis of human megakaryocytes. British journal of haematology. 2000;111(3):879-89.

We shall not cease from exploration, and the end of all our exploring will be to arrive where we started and know the place for the first time.

- T.S. Elliot

Chapter 6

Overview and general conclusions

Oxygen and adipose tissue; from stem cell origin, signaling, to a source of stress

The stem cell niche was conceptualized in 1978 (1). It defines the anatomical position and the cellular and acellular components in which stem cells reside. Adipose tissue is of mesenchymal origin and is comprised of many cell types, including mature adipocytes, fibroblasts, smooth muscle cells, endothelial cells, pericytes, and adipose-derived stromal cells (ASCs) with a small percentage (<0.1%) of true stem cells, which are found within the stromal vascular fraction (SVF) (2). In 1964, Rodbell treated adipose tissue with collagenase and found that fat cells and the SVF, upon centrifugation, could be released from adipose tissue fragments (3). In 2001, Zuk and colleagues identified that the stromal cells in adipose tissue had self-renewal capabilities and multipotent differentiation potential (4). Since then, ASCs have been given a great deal of attention. Adipose tissue-derived stromal cells have demonstrated potential for regenerative strategies. Successful cell-based therapy is the main goal. Ideally we want to translate the information gained through molecular and cellular-based research to the clinic. Knowledge of the way these stromal cells respond to their environment *in vitro* and *in vivo* is crucial for successful therapy. Adipose-derived stromal cells play important roles in physiological turnover of adipose tissue as well as hyperplasia during obesity.

Obesity and its comorbidities, including type II diabetes, have reached alarming levels both locally and abroad. This has led to an increase into the investigation of the biology of adipose tissue. The *in vitro* characteristics of the ASCs were investigated. The cells displayed adherence to plastic under standard culture conditions. The ASCs expressed the classical MSC CD73+CD90+CD105+CD34-CD45- phenotype proposed by Dominici *et al*. The ASCs demonstrated colony forming ability as well as the *in vitro* differentiation into the osteogenic, adipogenic, and chondrogenic lineages (2, 5). It was noted that great intra- and inter-variability within and between donor cultures were observed. Reiterating what many researchers have discovered previously, this population of stromal cells is heterogeneous in

nature. Heterogeneity arises in part from the donor tissue location (adipose tissue depot), the lack of standardization in isolation and expansion methods, the health and weight of the donor, possibly the sex of the donor, and the underlying genetics of the donor. In order to minimize this heterogeneity in this study, ASCs had to adhere to the criteria set by Bourin and colleagues, donor tissue location was kept constant and the same isolation and expansion techniques were used throughout. It was important to first identify that the cells were in fact ASCs in order to answer the objectives of the entire study. The cell populations described herein presented characteristics that enabled their classification as ASCs.

This dissertation focused on the *in vitro* effect of reactive oxygen species (ROS) and artificial hypoxia (dimethyloxalylglycine; DMOG) on the adipogenic differentiation capability of ASCs in the hope of understanding how adipogenesis is influenced during inflammation or settings requiring stem cell therapy. The development of effective therapeutics for obesity has been hindered by gaps in our understanding of all the molecular mechanisms underlying adipogenesis. A detailed cell model of the process of adipogenesis is needed to identify key molecular targets for therapeutic development. Adipose-derived stromal cells have proven to be an effective model. Much remains to be understood about ASCs from a physiological perspective, but improvement in the understanding of stromal cell biology, and evaluation of white adipose tissue (WAT) expansion and differentiation, is underway.

Obesity and diabetes are metabolic disorders that are induced by an increase in body fat, and are associated with oxidative and inflammatory stress. Inflammation is associated with the generation of ROS and the accumulation of ROS leads to oxidative stress. Investigations into adipocyte biology have revealed that adipogenesis is sensitive to redox changes. Recent evidence indicates that ROS constitute an important cellular mechanism for signal transduction (6). Reactive oxygen species are thought to interact with a number of pathways affecting the transcription machinery required for stromal cell differentiation (7). The interaction between mitochondria, oxidative stress and the role of antioxidants in these pathways, as well as the reported changes in antioxidant capacity in WAT during obesity, led to the aim of this study, namely to investigate the effect of oxidative stress on the adipogenic differentiation potential of ASCs.

Initially there was no effect noted during exposure of ASCs, cultured in α-MEM and DMEM with pyruvate, to high H_2O_2 concentrations, in the cell viability experiments. This result was

unexpected since high concentrations should have a detrimental effect on cell viability. Only once pyruvate was removed from the culture medium and treated with H_2O_2 did the higher concentrations have an observable effect on cell viability. It was determined that the H_2O_2 had been eliminated by the antioxidant pyruvate in the culture medium. This is an important observation for stromal cell culture experimentation because ASCs are usually cultured in media with pyruvate. It demonstrates the importance of experimental design and knowledge of the components of culture media. The ROS scavenging effect of pyruvate was confirmed with the intracellular ROS detection assay, MitoSOX™ red. The increase in intracellular ROS with the addition of exogenous ROS (H_2O_2) was also confirmed.

ASCs were induced to differentiate into adipocytes using an adipogenic-inducing cocktail with or without the antioxidant, pyruvate. The adipogenic-induced ASCs were treated with Trolox, CoQ10, H_2O_2 or a combination of both pro-oxidant and antioxidant for 14 and 21 days. Pre-conditioning with the pro-oxidant for 24 hours before the adipogenic induction period of 14 and 21 days was also examined. The effects on adipogenic differentiation were quantitatively assessed using flow cytometry and the emission profiles of Nile Red. It was demonstrated that the removal of pyruvate from the adipogenic induction medium enhanced adipogenic differentiation compared to the standard adipogenic induction medium. The addition of exogenous ROS to adipogenic-induced ASCs further increased adipose differentiation. It was also observed that H_2O_2 added to non-induced ASCs grown in medium without pyruvate caused substantial lipid accumulation. Scavengers, such as Trolox and CoQ10, attenuated the increase in ROS and thus a decrease in adipogenic differentiation was seen. Pre-conditioning with pro-oxidant could either increase or decrease adipogenic differentiation depending on the concentration of pro-oxidant. The results of this study indicate that higher levels of ROS mediate increased adipocyte differentiation, implicating a self-perpetuating system which may contribute to the pathogenesis of obesity and affiliated complications.

The stem cell niche is said to maintain the proliferative or multipotent capabilities of stem cells, and differentiation down specific lineages coincides with the migration of these stem cells out of the niche (8). Niches vary in O_2 tension. *In vivo* measurements in adipose tissue have demonstrated that the O_2 tension tends to range between 2% and 8% (9, 10). The confusion that exists about the role that hypoxia and the stabilization of HIF-1α may play in adipogenic differentiation, as well as a deficit in experimentation with artificial hypoxia in ASC adipogenic differentiation, led to the study on the effect of artificial hypoxia on the

adipogenic differentiation potential of ASCs. Oxygen-dependent HIF-1α degradation was blocked using the prolyl hydroxylase domain (PHD) enzyme inhibitor, DMOG. This hypoxia mimetic was added to ASCs that were induced to differentiate into adipocytes in response to adipogenic induction medium. Adipogenic differentiation was once again quantified using flow cytometry and the emission profiles of Nile red. It was observed that treatment of adipogenic-induced ASCs with DMOG had no significant effect on adipogenesis. Both studies revealed that flow cytometry is a powerful technique that can monitor total cell lipid content and in real time. This technique aided in the quantitative detection of adipogenesis and the cell sub-populations that made up this differentiation process.

Obesity appears to be associated with multiple types of stress. Obesity and type II diabetes have been associated with disorders of the mitochondrial electron transport chain, oxidative stress, lipoperoxides and impairments in antioxidant defenses (11, 12). The transcription factor peroxisome proliferator-activated receptor-γ (PPARγ), which is mainly expressed in adipose tissue, plays an important role in mitochondrial biogenesis (13). The mitochondria generate most of the endogenous ROS. The production of ROS is increased by leakage of electrons from the electron transport chain, during inhibition of oxidative phosphorylation or following excessive caloric intake (14). With regard to emotional stress, activating a neural stress-response network induces the secretion of glucocorticoids. Glucocorticoids increase the desire for food, induce polydipsia and increase circulating insulin (15). This promotes food intake and, if not controlled, obesity. It has been suggested that hypoxic stress underlies dysregulation in the production of adipocytokines in obesity (16). Scientific evidence emphasizes the importance of investigating the relationships between these stresses and obesity in order for clinical translation to be realized.

Park and colleagues stated that whether ROS is harmful or beneficial is primarily a question of dosage (17). The results of this study confirm this statement. It appears that this could also be the case with oxygen concentrations. The study emphasizes the importance of redox metabolism in adipose tissue biology. Although the work in this dissertation has focused predominantly on the effect of H_2O_2 and artificial hypoxia in determining ASC adipogenic differentiation, it is important to establish how all the various aspects of the ASC niche may interact to bring about either stemness or selection for a specific differentiation pathway.

Future work

A greater understanding of stromal cell biology is the key to the appropriate utilization of ASCs for cell-based therapeutic purposes. Factors influencing stromal/stem cell fate could include nutrients (serum, glucose) and cytokines. Any compounds which could reduce adipogenesis could provide an opportunity to protect overweight people from these metabolic diseases of lifestyle and their comorbidities. It may be cumbersome to probe large sample numbers of non-induced and adipogenic induced ASCs with many different compounds for the discovery of possible pro- or anti-adipogenic effects. A high-throughput screening model has been proposed for the identification of novel pharmacotherapeutic compounds for the treatment of obesity. This model would incorporate semi-automated rapid screening of large numbers of compounds using adipogenic assays and imaging. Computational models such as Bayesian networks or systems biology approaches could also be beneficial in determining effective anti- and pro-adipogenic factors. A Bayesian network pictorially displays the probabilistic relationships between different variables and thus could help identify novel interactions/relationships between variables involved in obesity. A systems biology approach looks at the complexity of biological systems and instead of focusing on the effects of compounds on individual targets, the focus is on biomolecular networks as a whole.

Human stromal cells are a convenient model for the study of human adipogenesis Contrasting results in this dissertation, due to the heterogeneity of the population of ASCs, demonstrates the importance of using large donor sample populations. Future studies will incorporate both quantitative gene expression and more donor ASC cultures. Quantitative gene expression would confirm adipogenic differentiation versus lipogenesis. Complimentary studies on gene expression both for HIF-regulated genes and genes implicated in adipogenesis will need to be carried out in future studies. Future research needs to assess the effect of DMOG on HIF-1α stabilization using Western blotting. The conflicting results in the literature regarding the regulation of adipogenesis by hypoxia underscores the importance for future research to assess the effects of both hypoxia and artificial hypoxia on adipogenesis at a gene and protein level. Efforts to optimize the differentiation of ASCs in the presence of various pharmacological compounds that impact signaling systems known to

be important in adipocyte differentiation and deconstructing the ASCs on genetic, epigenetic and molecular levels can ensure their utmost applications in clinical settings.

References

1. Schofield R. The relationship between the spleen colony-forming cell and the haemopoietic stem cell. Blood cells. 1978;4(1-2):7-25.
2. Bourin P, Bunnell BA, Casteilla L, Dominici M, Katz AJ, March KL, et al. Stromal cells from the adipose tissue-derived stromal vascular fraction and culture expanded adipose tissue-derived stromal/stem cells: a joint statement of the International Federation for Adipose Therapeutics and Science (IFATS) and the International Society for Cellular Therapy (ISCT). Cytotherapy. 2013;15(6):641-8.
3. Rodbell M. Metabolism of Isolated Fat Cells. I. Effects of Hormones on Glucose Metabolism and Lipolysis. The Journal of biological chemistry. 1964;239:375-80.
4. Zuk PA, Zhu M, Mizuno H, Huang J, Futrell JW, Katz AJ, et al. Multilineage cells from human adipose tissue: implications for cell-based therapies. Tissue engineering. 2001;7(2):211-28.
5. Dominici M, Le Blanc K, Mueller I, Slaper-Cortenbach I, Marini F, Krause D, et al. Minimal criteria for defining multipotent mesenchymal stromal cells. The International Society for Cellular Therapy position statement. Cytotherapy. 2006;8(4):315-7.
6. D'Autreaux B, Toledano MB. ROS as signalling molecules: mechanisms that generate specificity in ROS homeostasis. Nature reviews Molecular cell biology. 2007;8(10):813-24.
7. Atashi F, Modarressi A, Pepper MS. The role of reactive oxygen species in mesenchymal stem cell adipogenic and osteogenic differentiation: a review. Stem cells and development. 2015;24(10):1150-63.
8. Watt FM, Hogan BL. Out of Eden: stem cells and their niches. Science. 2000;287(5457):1427-30.
9. Pasarica M, Sereda OR, Redman LM, Albarado DC, Hymel DT, Roan LE, et al. Reduced adipose tissue oxygenation in human obesity: evidence for rarefaction, macrophage chemotaxis, and inflammation without an angiogenic response. Diabetes. 2009;58(3):718-25.
10. Matsumoto A, Matsumoto S, Sowers AL, Koscielniak JW, Trigg NJ, Kuppusamy P, et al. Absolute oxygen tension (pO(2)) in murine fatty and muscle tissue as determined by EPR. Magn Reson Med. 2005;54(6):1530-5.
11. Li J, Romestaing C, Han X, Li Y, Hao X, Wu Y, et al. Cardiolipin remodeling by ALCAT1 links oxidative stress and mitochondrial dysfunction to obesity. Cell metabolism. 2010;12(2):154-65.
12. Yuzefovych LV, Musiyenko SI, Wilson GL, Rachek LI. Mitochondrial DNA damage and dysfunction, and oxidative stress are associated with endoplasmic reticulum stress, protein degradation and apoptosis in high fat diet-induced insulin resistance mice. PloS one. 2013;8(1):e54059.

13. Medina-Gomez G, Gray S, Vidal-Puig A. Adipogenesis and lipotoxicity: role of peroxisome proliferator-activated receptor gamma (PPARgamma) and PPARgammacoactivator-1 (PGC1). Public Health Nutr. 2007;10(10A):1132-7.
14. Wallace DC. A mitochondrial paradigm of metabolic and degenerative diseases, aging, and cancer: a dawn for evolutionary medicine. Annu Rev Genet. 2005;39:359-407.
15. Dallman MF, Pecoraro NC, la Fleur SE. Chronic stress and comfort foods: self-medication and abdominal obesity. Brain Behav Immun. 2005;19(4):275-80.
16. Hosogai N, Fukuhara A, Oshima K, Miyata Y, Tanaka S, Segawa K, et al. Adipose tissue hypoxia in obesity and its impact on adipocytokine dysregulation. Diabetes. 2007;56(4):901-11.
17. Park SG, Kim JH, Xia Y, Sung JH. Generation of reactive oxygen species in adipose-derived stem cells: friend or foe? Expert opinion on therapeutic targets. 2011;15(11):1297-306.

Appendix A: Health Sciences MSc committee approval and ethics approval

UNIVERSITEIT VAN PRETORIA
UNIVERSITY OF PRETORIA
YUNIBESITHI YA PRETORIA

Faculty of Health Sciences
Fakulteit van Gesondheidswetenskappe

Prof Riana Cockeran
Chair: MSc Committee
School of Medicine
Dr Savage Rd, Private Bag x323, Pretoria, 0001
Tel.: (012) 319-2624 Fax: (012) 323-0732
E-mail: riana.cockeran@up.ac.za

05 June 2013

Prof MS Pepper
Department of Medical Immunology
Faculty of Health Sciences

Dear Prof Pepper,

Ms D de Villiers, Student no 2724076, MSc Committee submission

Thank you for submitting the ethics approval to the MSc Committee.

Student name	Ms D de Villiers	**Student number**	27240976
Name of study leader	Prof M Pepper		
Department	Immunology		
Title of MSc	The effect of oxidative stress and hypoxic conditioning on mesenchymal stem cell differentiation		
Date of first submission	November 2012		
May 2014	• Thank you for submitting a copy of the ethics approval letter		
Decision	This **protocol** has been **approved**. **Ethics approval** obtained The internal and external examiners can be nominated and required documents submitted 6 months prior to submission of the dissertation.		

Yours sincerely
Prof Riana Cockeran
Chair: MSc Committee

Department of Immunology
University of Pretoria
PRETORIA 0002
Republic of South Africa

Tel: Number +27 (0)12 319 2624
Fax: Number +27 (0)12 323 0732

Email address riana.cockeran@up.ac.za
www.up.ac.za

The Research Ethics Committee, Faculty Health Sciences, University of Pretoria complies with ICH-GCP guidelines and has US Federal wide Assurance.
- FWA 00002567, Approved dd 22 May 2002 and Expires 20 Oct 2016.
- IRB 0000 2235 IORG0001762 Approved dd 13/04/2011 and Expires 13/04/2014.

UNIVERSITEIT VAN PRETORIA
UNIVERSITY OF PRETORIA
YUNIBESITHI YA PRETORIA

Faculty of Health Sciences Research Ethics Committee

30/01/2014

Approval Certificate
New Application

Ethics Reference No.: 422/2013

Title The effect of oxidative stress and hypoxic conditioning on mesenchymal stem cell differentiation

Dear Ms Danielle de Villiers

The **New Application** as supported by documents specified in your cover letter for your research received on the 13/11/2013, was approved by the Faculty of Health Sciences Research Ethics Committee on the 29/01/2014.

Please note the following about your ethics approval:
- Ethics Approval is valid for 3 years
- Please remember to use your protocol number (**422/2013**) on any documents or correspondence with the Research Ethics Committee regarding your research.
- Please note that the Research Ethics Committee may ask further questions, seek additional information, require further modification, or monitor the conduct of your research.

Ethics approval is subject to the following:
- The ethics approval is conditional on the receipt of 6 monthly written Progress Reports, and
- The ethics approval is conditional on the research being conducted as stipulated by the details of all documents submitted to the Committee. In the event that a further need arises to change who the investigators are, the methods or any other aspect, such changes must be submitted as an Amendment for approval by the Committee.

We wish you the best with your research.

Yours sincerely

Dr R Sommers; MBChB; MMed (Int); MPharMed.
Deputy Chairperson of the Faculty of Health Sciences Research Ethics Committee, University of Pretoria

The Faculty of Health Sciences Research Ethics Committee complies with the SA National Act 61 of 2003 as it pertains to health research and the United States Code of Federal Regulations Title 45 and 46. This committee abides by the ethical norms and principles for research, established by the Declaration of Helsinki, the South African Medical Research Council Guidelines as well as the Guidelines for Ethical Research: Principles Structures and Processes 2004 (Department of Health).

♦ Tel:012-3541330 ♦ Fax:012-3541367 Fax2Email: 0866515924 ♦ E-Mail: fhsethics@up.ac.za
♦ Web: //www.healthethics-up.co.za ♦ H W Snyman Bld (South) Level 2-34 ♦ Private Bag x 323, Arcadia, Pta, S.A., 0007

The Research Ethics Committee, Faculty Health Sciences, University of Pretoria complies with ICH-GCP guidelines and has US Federal wide Assurance.

* **FWA** 00002567, Approved dd 22 May 2002 and Expires 20 Oct 2016.
* **IRB** 0000 2235 IORG0001762 Approved dd 13/04/2011 and Expires 13/04/2014.

Universiteit van Pretoria
University of Pretoria

Faculty of Health Sciences Research Ethics Committee
Fakulteit Gesondheidswetenskappe Navorsingsetiekkomitee
DATE: 30/01/2013

AMENDMENT	• Permission to obtain adipose tissue from which mesenchymal stem cells (MSCs) will be isolated and used for *in vitro* investigation of the effect of light activation, reactive oxygen species (ROS), and hypoxic culture conditions; • New informed consent forms for obtaining consent to use adipose tissue to be used in above stated experiments, and • Permission to obtain adipose tissues from patients in the private sector collected at the Life Brooklyn Day Hospital, by Prof. ZF Annandale.
PROTOCOL NO.	**218/2010**
PROTOCOL TITLE	Isolation of mesenchymal stem cells from human tissues.
INVESTIGATOR	**Principal Investigator:** Prof. MS Pepper
SUBINVESTIGATOR	Dr. Marnie Potgieter, Ms. Karlien Kallmeyer, Ms. Fiona van Vollenstee
SUPERVISOR	Prof. MS Pepper **E-Mail:**michael.pepper@up.ac.za
DEPARTMENT	**Dept:** Immunology **Phone:**Secretary: 012-319-2621 **Fax:**012-323-0732**E-Mail:**michael.pepper@up.ac.za **Cell:** 072-209-6324
STUDY DEGREE	MSc: Ms. Kallmeyer and Ms. Van Vollenstee fionavanvollenstee@gmail.com
SPONSOR	None
MEETING DATE	**30/01/2013**

The Amendments
- Permission to obtain adipose tissue from which mesenchymal stem cells (MSCs) will be isolated and used for in vitro investigation of the effect of light activation, reactive oxygen species (ROS), and hypoxic culture conditions;
- New informed consent forms for obtaining consent to use adipose tissue to be used in above stated experiments, and
- Permission to obtain adipose tissues from patients in the private sector collected at the Life Brooklyn Day Hospital, by Prof. ZF Annandale.

were approved on 30/01/2013 by a properly constituted meeting of the Ethics Committee.

Members of the Research Ethics Committee:

Prof RSK Apatu	MBChB (Legon,UG); PhD (Cantab); PGDip International Research Ethics (UCT)
Prof M J Bester	(female)BSc (Chemistry and Biochemistry); BSc (Hons)(Biochemistry); MSc(Biochemistry); PhD (Medical Biochemistry)
Mrs N Briers	(female) BSc (Stell); BSc Hons (Pretoria); MSc (Pretoria); DHETP (Pretoria)
Dr IK Dada	BSc.HB; MB ChB (UNZA); MA Appl. Pop. Research (EXON) ; MPH (UP)
Prof R Delport	(female)BA et Scien, B Curationis (Hons) (Intensive care Nursing), M Sc (Physiology), PhD (Medicine), M Ed Computer Assisted Education

Prof MM Ehlers	(female) BSc (Agric) Microbiology (Pret); BSc (Agric) Hons Microbiology (Pret); MSc (Agric) Microbiology (Pret); PhD Microbiology (Pret); Post Doctoral Fellow (Pret)
Dr R Leech	(female) B.Art et Scien; BA Cur; BA (Hons); M (ECI); PhD Nursing Science
Mr SB Masombuka	BA (Communication Science) UNISA; Certificate in Health Research Ethics Course (B compliant cc)
Dr MP Mathebula	(female)Deputy CEO: Steve Biko Academic Hospital; MBCHB, PDM, HM
Prof A Nienaber	(female) BA(Hons)(Wits); LLB; LLM; LLD(UP); PhD; Dipl.Datametrics(UNISA) – Legal advisor
Mrs MC Nzeku	(female) BSc(NUL); MSc(Biochem)(UCL, UK) – Community representative
Prof L M Ntlhe	MbChB (Natal) FCS (SA)
Dr SAS Olorunju	BSc (Hons). Stats (Ahmadu Bello University –Nigeria); MSc (Applied Statistics (UKC United Kingdom); PhD (Ahmadu Bello University – Nigeria)
Snr Sr J Phatoli	(female) BCur(Eet.A); BTec(Oncology Nursing Science) – Nursing representative
Dr R Reynders	MBChB (Prêt), FCPaed (CMSA) MRCPCH (Lon) Cert Med. Onc (CMSA)
Dr T Rossouw	(female) MBChB (cum laude); M.Phil (Applied Ethics) (cum laude), MPH (Biostatistics and Epidemiology (cum laude), D.Phil
Dr L Schoeman	(female) B.Pharm, BA(Hons)(Psych), PhD – **Deputy Chairperson**
Mr Y Sikweyiya	MPH; SARETI Fellowship in Research Ethics; SARETI ERCTP; BSc(Health Promotion)Postgraduate Dip (Health Promotion) – Community representative
Dr R Sommers	(female) MBChB; MMed(Int); MPharmMed – **Deputy Chairperson**
Dr GP Stevens	LLB, LLM, LLD.
Prof L Sykes	(female) BSc, BDS, MDent (Pros)
Prof TJP Swart	BChD, MSc (Odont), MChD (Oral Path), PGCHE – School of Dentistry representative
Prof C W van Staden	MBChB; MMed (Psych); MD; FCPsych; FTCL; UPLM - **Chairperson**

DR R SOMMERS; MBChB; MMed(Int); MPharmMed.
Deputy Chairperson of the Faculty of Health Sciences Research Ethics Committee
University of Pretoria

♦Tel: 012-3541677
♦Web: www.healthethics-up.co.za
♦ Private Bag x 323, Arcadia, Pta, S.A., 0007
♦Fax: 0866516047
♦H W Snyman Bld (South) Level 2, Rm 2.33
♦E-Mail: deepeka.behari@up.ac.za

Appendix B: Informed consent form

PATIENT INFORMATION LEAFLET AND INFORMED CONSENT FORM

(Each patient must receive, read and understand this document before the start of the study)

STUDY TITLE: The isolation, characterisation and differentiation of mesenchymal stem cells from umbilical cord blood, Wharton's jelly and adipose tissue

Sub title: *Investigation of the effect of light activation, reactive oxygen species (ROS) and hypoxic culture conditions on mesenchymal stem cells in culture*

Dear Patient/Participant: _____

INTRODUCTION

You are invited to participate in a research study that is being carried out by the Department of Immunology at the University of Pretoria. This information leaflet is to help you to decide if you would like to participate. Before you agree to take part in this study you should fully understand what is involved. No selection criteria will be applied. Any donor will be eligible to participate (donate tissue). If you have any questions, which are not fully explained in this leaflet, do not hesitate to ask the investigator. You should not agree to take part unless you are completely happy about all the procedures involved. Your personal health will not be compromised at all by the procedures. These procedures have already been discussed with your doctor before hand.

THE PURPOSE OF THE STUDY

Researchers at the University of Pretoria would like to investigate the healing properties of adult stem cells for possible future application, in regenerative medicine. These adult stem cells, found in **fat (adipose tissue)**, could potentially be used to cure patients with various kinds of injuries or diseases. In order to use these cells to cure humans in the future, researchers must first study their behaviour and growth, in tissue cultures or animal models. The collection of adult stem cells does not make use of any unethical procedures.

HOW IS ADIPOSE TISSUE COLLECTED

During various normal plastic surgery operations, adipose tissue (fat) will be aspirated (sucked out), and discarded. This adipose tissue according to the surgical doctor does not serve a purpose to the patient's physique anymore. This discarded fat could serve a very important purpose to researchers in the field of regenerative medicine.

No additional fat will be collected, only the fat that the doctor would normally discard. The fat will be collected in the form of lipoaspirate (from liposuction).

There will be no added risks or discomfort with the collection of the adipose tissue other than normally associated with the specific procedure the patient will experience during normal operative procedures.

WHAT IS EXPECTED

Consent should be given by you (the patient) to the researchers to receive your discarded fat from your doctor. The consent will also allow the researchers to grow, differentiate and study the isolated stem cells from the fat tissue under different conditions in culture (laboratory experiments).

CONFIDENTIALITY

No personal information will be collected from you, the participant. Each participant will be assigned a specific code and this code will be the only information that the researchers will have. So no one will be able to identify you. Research reports and articles in scientific journals will not include any information that may identify you.

It might however be important for the doctors or researchers involved in this study to convey medical information to medical personnel or appropriate Research Ethics Committees. In such a case, you hereby authorise your investigator to release your medical records to regulatory health authorities or an appropriate Research Ethics Committee. These records will only be utilised by them in order for them to carry out their obligations toward this study, while always acting in your best interest.

ETHICAL APPROVAL

The protocol involved for this study as well as addendums to the protocol was submitted to the Research Ethics Committee. This study has received written approval from the Research Ethics Committee of the Faculty of Health Sciences at the University of Pretoria. The study is structured in accordance with the Declaration of Helsinki, which deals with the recommendations of guiding doctors in biomedical research involving humans.

RIGHTS OF THE PARTICIPANT

Your participation in this study is entirely voluntary and you can refuse to participate or withdraw consent at any time without stating any reason. Your withdrawal will not affect your access to medical care or the quality of medical care that you will receive. Your participation or withdrawal from the study would not affect you in any way.

FINANCIAL GAIN OR LOSS

There will be no financial gain or loss to your account, should you participate or withdraw from the study. This research could potentially lead to future profitable treatments. However, you will not have access to these profits. There will be no additional financial costs for you to participate in the study.

The participant has no legal remedy and will not share in any financial gain that may be derived from the study

INFORMATION AND CONTACT PERSON

If at any time you would like to find out more information or have any questions regarding the study, please do not hesitate to contact the researchers.
Ms. D de Villiers: 082 366 5663
Dr. M Potgieter: 083 996 0078
Prof. MS Pepper: 012 420 3845 or 012 420 5317

INFORMED CONSENT

I confirm that the person asking my consent to take part in this study has told me about the nature, process, risks, discomforts and benefits of the study. I have also received, read and understood the above written information (Information Leaflet and Informed Consent) regarding the study. I am aware that the results of the study, including personal details, will be anonymously processed into research reports. I am participating willingly. I have had time to ask questions and have no objection to participate in the study. I understand that there is no penalty should I wish to discontinue with the study and my withdrawal will not affect my access to medical care or the quality of medical care I will receive.

I have received a copy of this informed consent agreement.

Participant full names (print):_____

Participant signature:_____ Date:_____

Investigator full names (print):_____

Investigator signature:_____ Date:_____

Witness full names (print):_____

Witness signature:_____ Date: _____

Witness full names (print):_____

Witness signature:_____ Date: _____

You hereby give the researchers permission to perform routine HIV, hepatitis B and hepatitis C tests on your adipose tissue sample since it is important for our work that we only work with tissue that are negative for these infections. If the researchers detect HIV or hepatitis B or C in the tissue sample, the codified sample details will be sent to _____, who will notify you. If you do not wish us to test your tissue for HIV or hepatitis B or hepatitis C, or if you do not wish to know the results of these tests, we will not be able to include you in the study. In the case of an HIV, hepatitis B or C positive result, you will be counselled and treated by qualified medical personnel.

Patient signature: _____

INFORMED CONSENT

I confirm that the person asking my consent to take part in this study has told me about the nature, process, risks, discomforts and benefits of the study. I have also received, read and understood the above written information (Information Leaflet and Informed Consent) regarding the study. I am aware that the results of the study, including personal details, will be anonymously processed into research reports. I am participating willingly. I have had time to ask questions and have no objection to participate in the study. I understand that there is no penalty should I wish to discontinue with the study and my withdrawal will not affect my access to medical care or the quality of medical care I will receive.

I have received a copy of this informed consent agreement.

Participant full names (print):_____

Participant signature:_____ Date:_____

Investigator full names (print):_____

Investigator signature:_____ Date:_____

Witness full names (print):_____

Witness signature:_____ Date: _____

Witness full names (print):_____

Witness signature:_____ Date: _____

You hereby give the researchers permission to perform routine HIV, hepatitis B and hepatitis C tests on your adipose tissue sample since it is important for our work that we only work with tissue that are negative for these infections. If the researchers detect HIV or hepatitis B or C in the tissue sample, the codified sample details will be sent to _____, who will notify you. If you do not wish us to test your tissue for HIV or hepatitis B or hepatitis C, or if you do not wish to know the results of these tests, we will not be able to include you in the study. In the case of an HIV, hepatitis B or C positive result, you will be counselled and treated by qualified medical personnel.

Patient signature: _____

Appendix C: Media formulation comparison

α-MEM				DMEM + pyruvate				DMEM – pyruvate			
Components	**Molecular Weight**	**Concentration (mg/L)**	**mM**	**Components**	**Molecular Weight**	**Concentration (mg/L)**	**mM**	**Components**	**Molecular Weight**	**Concentration (mg/L)**	**mM**
Amino Acids				**Amino Acids**				**Amino Acids**			
L-Alanine	89.0	25.0	0.28089887								
Glycine	75.0	50.0	0.6666667	Glycine	75.0	30.0	0.4	Glycine	75.0	30.0	0.4
L-Alanyl-L-Glutamine	217.0	406.0	1.8709677	L-Alanyl-Glutamine	217.0	862.0	3.9723501				
L-Arginine hydrochloride	211.0	105.0	0.49763033	L-Arginine hydrochloride	211.0	84.0	0.39810428	L-Arginine hydrochloride	211.0	84.0	0.39810428
L-Asparagine-H2O	132.0	50.0	0.37878788								
L-Aspartic acid	133.0	30.0	0.22556391								
L-Cysteine hydrochloride-	176.0	100.0	0.5681818								
L-Cystine	240.0	24.0	0.1	L-Cystine	313.0	48.0	0.15335463	L-Cystine 2HCl	313.0	63.0	0.20127796
L-Glutamic Acid	147.0	75.0	0.5102041					L-Glutamine	146.0	584.0	4.0
L-Histidine	155.0	31.0	0.2	L-Histidine hydrochloride-	210.0	42.0	0.2	L-Histidine hydrochloride-	210.0	42.0	0.2
L-Isoleucine	131.0	52.4	0.4	L-Isoleucine	131.0	105.0	0.8015267	L-Isoleucine	131.0	105.0	0.8015267
L-Leucine	131.0	52.4	0.4	L-Leucine	131.0	105.0	0.8015267	L-Leucine	131.0	105.0	0.8015267
L-Lysine	146.0	58.0	0.39726028	L-Lysine hydrochloride	183.0	146.0	0.7978142	L-Lysine hydrochloride	183.0	146.0	0.7978142
L-Methionine	149.0	15.0	0.10067114	L-Methionine	149.0	30.0	0.20134228	L-Methionine	149.0	30.0	0.20134228
L-Phenylalanine	165.0	32.0	0.19393939	L-Phenylalanine	165.0	66.0	0.4	L-Phenylalanine	165.0	66.0	0.4
L-Proline	115.0	40.0	0.3478261								
L-Serine	105.0	25.0	0.23809524	L-Serine	105.0	42.0	0.4	L-Serine	105.0	42.0	0.4
L-Threonine	119.0	48.0	0.40336135	L-Threonine	119.0	95.0	0.79831934	L-Threonine	119.0	95.0	0.79831934
L-Tryptophan	204.0	10.0	0.04901961	L-Tryptophan	204.0	16.0	0.078431375	L-Tryptophan	204.0	16.0	0.078431375
L-Tyrosine	181.0	36.0	0.19889502	L-Tyrosine disodium salt	261.0	104.0	0.39846742	L-Tyrosine disodium salt	261.0	104.0	0.39846742
L-Valine	117.0	46.0	0.3931624	L-Valine	117.0	94.0	0.8034188	L-Valine	117.0	94.0	0.8034188
Vitamins				**Vitamins**				**Vitamins**			
Ascorbic Acid	176.0	50.0	0.2840909								
Biotin	244.0	0.1	4.0983607E-4								
Choline chloride	140.0	1.0	0.007142857	Choline chloride	140.0	4.0	0.028571429	Choline chloride	140.0	4.0	0.028571429
D-Calcium pantothenate	477.0	1.0	0.002096436	D-Calcium pantothenate	477.0	4.0	0.008385744	D-Calcium pantothenate	477.0	4.0	0.008385744
Folic Acid	441.0	1.0	0.0022675737	Folic Acid	441.0	4.0	0.009070295	Folic Acid	441.0	4.0	0.009070295
Niacinamide	122.0	1.0	0.008196721	Niacinamide	122.0	4.0	0.032786883	Niacinamide	122.0	4.0	0.032786883
Pyridoxal hydrochloride	204.0	1.0	0.004901961	Pyridoxine hydrochloride	206.0	4.0	0.019417476	Pyridoxine hydrochloride	206.0	4.0	0.019417476
Riboflavin	376.0	0.1	2.6595744E-4	Riboflavin	376.0	0.4	0.0010638298	Riboflavin	376.0	0.4	0.0010638298
Thiamine hydrochloride	337.0	1.0	0.002967359	Thiamine hydrochloride	337.0	4.0	0.011869436	Thiamine hydrochloride	337.0	4.0	0.011869436
Vitamin B12	1355.0	1.36	0.0010036901								
i-Inositol	180.0	2.0	0.011111111	i-Inositol	180.0	7.2	0.04	i-Inositol	180.0	7.2	0.04
Inorganic Salts				**Inorganic Salts**				**Inorganic Salts**			
Calcium Chloride (CaCl2-2H2O)	147.0	264.0	1.7959183	Calcium Chloride (CaCl2) (anhyd.)	111.0	200.0	1.8018018	Calcium Chloride (CaCl2) (anhyd.)	111.0	200.0	1.8018018
				Ferric Nitrate (Fe(NO3)3"9H2O	404.0	0.1	2.4752476E-4	Ferric Nitrate (Fe(NO3)3"9H2O	404.0	0.1	2.4752476E-4
Magnesium Sulfate (MgSO4-	246.0	200.0	0.8130081	Magnesium Sulfate (MgSO4)	120.0	97.67	0.8139166	Magnesium Sulfate (MgSO4)	120.0	97.67	0.8139166
Potassium Chloride (KCl)	75.0	400.0	5.3333335	Potassium Chloride (KCl)	75.0	400.0	5.3333335	Potassium Chloride (KCl)	75.0	400.0	5.3333335
Sodium Bicarbonate	84.0	2200.0	26.190475	Sodium Bicarbonate	84.0	3700.0	44.04762	Sodium Bicarbonate	84.0	3700.0	44.04762
Sodium Chloride (NaCl)	58.0	6800.0	117.24138	Sodium Chloride (NaCl)	58.0	6400.0	110.344826	Sodium Chloride (NaCl)	58.0	6400.0	110.344826
Sodium Phosphate	156.0	158.0	1.0128205	Sodium Phosphate	138.0	125.0	0.9057971	Sodium Phosphate	138.0	125.0	0.9057971
Other Components				**Other Components**				**Other Components**			
D-Glucose (Dextrose)	180.0	1000.0	5.5555553	D-Glucose (Dextrose)	180.0	4500.0	25.0	D-Glucose (Dextrose)	180.0	4500.0	25.0
Phenol Red	376.4	10.0	0.026567481	Phenol Red	376.4	15.0	0.039851222	Phenol Red	376.4	15.0	0.039851222
Sodium Pyruvate	110.0	110.0	1.0	Sodium Pyruvate	110.0	110.0	1.0				
Lipoic Acid	206.0	0.2	9.708738E-4								